



Swansea University
Prifysgol Abertawe



Swansea University E-Theses

Ion structure determination using novel time-of-flight techniques and mass-analysed ion kinetic energy spectrometry.

Williams, Jonathan Paul

How to cite:

Williams, Jonathan Paul (2000) *Ion structure determination using novel time-of-flight techniques and mass-analysed ion kinetic energy spectrometry..* thesis, Swansea University.
<http://cronfa.swan.ac.uk/Record/cronfa42653>

Use policy:

This item is brought to you by Swansea University. Any person downloading material is agreeing to abide by the terms of the repository licence: copies of full text items may be used or reproduced in any format or medium, without prior permission for personal research or study, educational or non-commercial purposes only. The copyright for any work remains with the original author unless otherwise specified. The full-text must not be sold in any format or medium without the formal permission of the copyright holder. Permission for multiple reproductions should be obtained from the original author.

Authors are personally responsible for adhering to copyright and publisher restrictions when uploading content to the repository.

Please link to the metadata record in the Swansea University repository, Cronfa (link given in the citation reference above.)

<http://www.swansea.ac.uk/library/researchsupport/ris-support/>

Ion Structure Determination Using Novel Time-of-Flight Techniques And Mass-Analysed Ion Kinetic Energy Spectrometry

by

Jonathan Paul Williams B.Sc.(Hons)

A thesis submitted in fulfilment of the requirements for the degree of

DOCTOR of PHILOSOPHY

at

The University of Wales Swansea

January 2000

ProQuest Number: 10805429

All rights reserved

INFORMATION TO ALL USERS

The quality of this reproduction is dependent upon the quality of the copy submitted.

In the unlikely event that the author did not send a complete manuscript and there are missing pages, these will be noted. Also, if material had to be removed, a note will indicate the deletion.



ProQuest 10805429

Published by ProQuest LLC (2018). Copyright of the Dissertation is held by the Author.

All rights reserved.

This work is protected against unauthorized copying under Title 17, United States Code
Microform Edition © ProQuest LLC.

ProQuest LLC.
789 East Eisenhower Parkway
P.O. Box 1346
Ann Arbor, MI 48106 – 1346

DECLARATION

This work has not previously been accepted in substance for any degree and is not being concurrently submitted in candidature for any degree.

STATEMENT 1

This thesis is the result of my own investigations, except where otherwise stated.

Other sources are acknowledged by footnotes giving explicit references. A bibliography is appended.

Signature of Candidate
J.P.Williams

Date

Signature of Supervisor
A.G.Brenton

Date

STATEMENT 2

I hereby give consent for my thesis, if accepted, to be available for photocopying and for inter-library loan, and for the title and summary to be made available to outside organisations

Signature of Candidate
J.P.Williams

Date

Summary

Mass spectrometry is a powerful analytical technique that possesses the capability of molecular characterisation of complex mixtures. The technique has been the method afforded in this study for the characterisation of such mixtures of industrial relevance.

The last decade has seen an important revival of one area in particular, time-of-flight mass spectrometry, which has had a significant impact on the field of mass spectrometry. This has been largely due to two recently developed ionisation methods, namely electrospray and matrix-assisted laser desorption ionisation.

These ionisation methods have led to the development of novel time-of-flight mass spectrometer designs by commercial manufacture's, which take advantage of the theoretically unlimited mass range and the acquisition of a full mass spectrum every injection pulse of ions. Matrix-assisted laser desorption and electrospray ionisation have been interfaced to two novel time-of-flight mass analysers, the 'Autospec' oa-ToF, a hybrid sector orthogonal-acceleration time-of-flight instrument and the 'LCT', a liquid chromatograph time-of-flight instrument, manufactured by Micromass U.K., Ltd respectively. They have been successfully used to investigate and fully characterise complex systems of industrial significance.

The 'Autospec' oa-ToF was used for high-energy collision induced dissociation experiments. The high sensitivity of the time-of-flight analyser was very powerful in the detection of product ions produced from various synthetic polymer precursor ions. The detailed structural information produced will be shown to fully characterise the polystyrene samples studied.

An expanding area of mass spectrometry is electrospray ionisation used with orthogonal acceleration time-of-flight. The two methods when used in reflectron mode have significantly removed early limitations on resolution that time-of-flight mass analysers initially possessed. Sampling the electrosprayed ions orthogonally results in an increased duty cycle, which can be advantageous if fast chromatography is required. Evaluation of the LCT instrument, will be shown to provide mass resolution of the order of 5000 at full-width half maximum, mass accuracies of the order of 5ppm, full scan sensitivity equal to that of a quadrupole instrument in single ion monitoring mode and the detection of singly charged ions greater than m/z 10000.

The research unit at Swansea University allowed the opportunity to investigate ion structural problems on an instrument built in house of BEE geometry. The energy released upon metastable fragmentation, leading to the formation of $C_3H_3^+$ ions formed in some simple organic molecules yield peak shapes of a composite nature. The selection of ions from the translational energy-release distribution produced, have been investigated by consecutive reactions and will be shown to fully characterise isomeric ion structures.

Dedication

For my grandfather and grandmother who died prior to and during my studies respectively. Their love, friendship, generosity and total support during my life could never have been repaid and will never be forgotten. Thanks for your guidance. Also to my best friends, my parents. Two unique individuals who deserve only the best things that life affords them.

Acknowledgements

I would initially like to thank EPSRC and ICI for funding this research. My sincere gratitude goes to Professor Dai Games for allowing me to do research at Swansea in a well renowned mass spectrometric laboratory.

I acknowledge the help received from members of the mass spec team at ICI Wilton (Middlesbrough), Mike, Mark, Richy and my directors of study Dr Tony Jackson and Professor Jim Scrivens. On a personal level, I wish to show my total appreciation to Professor Scrivens for helpful discussions and support during my research period.

Many thanks go to members of the MSRU team at Swansea. Brian and Des for their help when parts needed frequent replacement on the mass spec and to Chris, Matt and Dave for help with computing and ToF related queries.

My sincere appreciation goes to my supervisor Professor Gareth Brenton for his excellent tuition and total support, not just relating to mass spec but life in general. Your discussions have been taken on board and will surely be beneficial to myself in the future, thanks.

Without the help and influences of my family, the hopefully privileged position I will soon be in would not have been possible.

My grandparents, for so long the backbone of such a wonderful family, were unknowingly to them, one of the biggest influences on me returning to further education. I just want to say a big thanks and wish you were still here today. The problems they had to face during their life, particularly the latter, was not what they deserved. Its fair to say on behalf of all the family, what you gave us was so much appreciated.

The biggest thank you of all goes to two very special people, my parents. Their unselfishness, love and friendship all of my life has been never ending and sometimes I wonder how you put up with me! Its sad the way things turned out, but I hope you both have the perfect health and happiness this century.

Glossary of abbreviations

A	amp
APCI	atmospheric pressure chemical ionisation
API	atmospheric pressure ionisation
ASMS	American society for mass spectrometry
B	magnetic field strength
CE	capillary electrophoresis
CEC	capillary electrochromatography
CI	chemical ionisation
CID	collision induced dissociation
CZE	capillary zone electrophoresis
Da	dalton
DC	direct current
e	electronic charge
E_{app}	ESA voltage
EI	electron impact
ESA	electrostatic analyser
ESI	electrospray ionisation
FAB	fast atom bombardment
FD	field desorption
FFR	field free region
ω	frequency of rf voltage
FWHM	full-width half maximum
GC	gas chromatography
KE	kinetic energy
LC	liquid chromatography
LCT	liquid chromatograph-time-of-flight
LD	laser desorption
LoD	limit of detection
LSI	liquid secondary ionisation
LSIMS	liquid secondary ionisation mass spectrometry
m	mass

m/z	mass-to-charge ratio
MALDI	matrix assisted laser desorption ionisation
MCP	micro channel plate
MIKES	mass-analysed ion kinetic energy spectrometry
MS/MS	tandem mass spectrometry
oa	orthogonal accelerator
PBMA	polybutyl methacrylate
PC	personal computer
PEG	polyethylene glycol
PDMS	polydimethyl siloxane
PMMA	polymethyl methacrylate
ppb	parts per billion
ppm	parts per million
ppt	parts per trillion
PS	polystyrene
R	centrifugal force
rf	radio frequency
RSD	relative standard deviation
S/N	signal-to-noise ratio
SEC	size exclusion chromatography
SEM	secondary electron emission
SFC	supercritical fluid chromatography
SIM	single ion monitoring
SIMS	secondary ionisation mass spectrometry
SIS	superconductor-insulator-superconductor
TIC	total ion current
ToF	time-of-flight
TOFMS	time-of-flight mass spectrometry (mass spectrometer)
v	velocity
V	volt
V_{acc}	acceleration voltage
V_p	orthogonal accelerator voltage
z	number of electronic charges

Table of contents

Title	i
Declaration	ii
Summary	iii
Dedication	iv
Acknowledgements	v
Glossary of abbreviations	vi

Chapter 1: Introduction

1.1	Introduction and thesis scope	2
1.2	Historical account of mass spectrometry	4
1.2.1	What is mass spectrometry?	5
1.3	Ionisation methods	6
1.4	Mass analysers	8
1.4.1	Sector instruments	8
1.4.1.1	Magnetic sector	8
1.4.1.2	Electric sector	10
1.4.1.3	Double-focusing instruments	11
1.4.1.4	Resolution of sector mass analysers	12
1.4.2	Quadrupole mass analyser	13
1.4.2.1	Resolution of quadrupole mass analysers	16
1.4.3	Time-of-flight mass analysers	16
1.4.3.1	Principles of TOFMS	17
1.4.3.2	Types of ToF mass analysers	18
1.4.3.2.1	Linear TOFMS	18
1.4.3.2.2	Reflectron TOFMS	19
1.4.3.2.3	Resolution of ToF mass analysers	20
1.5	Ion detectors	22
1.5.1	The Faraday cup	22
1.5.2	Electron multiplier	23
1.5.2.1	Discrete dynode electron multiplier	23
1.5.2.2	Continuous dynode electron multiplier	23
1.6	References	25

Chapter 2: An evaluation of a novel orthogonal acceleration Time-of-Flight mass spectrometer

Section A: Electrospray ionisation mechanism, instrument design and theoretical considerations of the LCT

2.1	Aim	29
2.1.1	Introduction	29
2.2	Detailed description of the LCT	30

2.2.1	Introduction	30
2.2.1.1	Atmospheric pressure ionisation	31
2.2.1.2	Electrospray ionisation	32
2.2.1.3	Mechanism and theory of the electrospray ionisation process	33
2.2.1.4	Dole: Singlet ion in droplet theory	36
2.2.1.5	Iribarne and Thomson: Ion evaporation theory	37
2.2.2	'Z-spray' ionisation source and sample introduction	37
2.2.3	Ion guide interface to the ToF mass analyser	40
2.2.3.1	Radio frequency only ion guides	41
2.2.3.2	Hexapole interface voltages	43
2.2.4	Orthogonal acceleration source	44
2.2.4.1	Introduction	44
2.2.4.2	Application of orthogonal acceleration in the LCT	47
2.2.4.3	The orthogonal accelerator employed in the LCT	48
2.2.5	Reflectron ion mirror	50
2.2.6	Ion detection system	52
2.2.6.1	Introduction	52
2.2.6.2	Micro channel plate	52
2.2.7	Vacuum system of the LCT	54

Section B: Results of the performance characteristics of the LCT

2.3	Investigation of the performance characteristics of the LCT mass spectrometer	
2.3.1	Introduction	57
2.3.2	Mass range characteristics of TOFMS	57
2.3.2.1	Introduction	57
2.3.2.2	Mass range of the LCT	58
2.3.3	Calibration	66
2.3.3.1	Introduction	66
2.3.3.2	Calibration procedure	66
2.3.4	Investigation of the mass resolution performance	70
2.3.4.1	Introduction	70
2.3.4.2	Resolution of the LCT	71
2.3.5	Determination of limit of detection	74
2.3.5.1	Aim	74
2.3.5.2	Quantitative analysis	74
2.3.5.3	Repeatability	76
2.3.5.4	Data interpretation	77
2.3.5.5	Limit of detection of DMPA	78
2.3.5.5.1	Aim	78
2.3.5.5.2	Single ion monitoring	78
2.3.6	LCMS sensitivity	96
2.3.6.1	Aim	96
2.3.6.2	Introduction	96
2.3.6.3	Alkyl phenol ethoxylates	96

2.3.7	Exact mass measurement of synthetic polymer and functional fluid additives	
2.3.7.1	Aim	102
2.3.7.1.1	Introduction	102
2.3.7.2	Investigation of the factors affecting mass measurement accuracy	105
2.3.7.3	The role of additives in plastics	107
2.3.7.4	ESI oa-ToF of pure polymer additives	109
2.3.7.5	Optimum source and instrumental voltage conditions	109
2.3.7.6	Exact mass data acquisition	111
2.3.8	In source cone voltage fragmentation	125
2.4	Summary	128
2.5	Conclusion	128
2.6	References	130
	Appendix	136

Chapter 3: End group determination of some polystyrene polymers by means of Matrix assisted laser desorption ionisation-collision induced dissociation orthogonal acceleration TOFMS

3.1	Aim	146
3.2	Development and principles of MALDI	146
3.2.1	MALDI TOFMS	148
3.2.2	The application of MALDI TOFMS to synthetic polymers	150
3.2.3	Molecular weight characterisation of polymers	152
3.2.4	Size exclusion chromatography	153
3.2.5	Polystyrene polymerisation	154
3.2.6	Ionisation mechanism of synthetic polymers	157
3.3	MALDI-CID of Polystyrene	158
3.3.1	Introduction	158
3.4	Experimental	160
3.4.1	Polymer synthesis	160
3.4.2	Instrumentation	162
3.4.2.1	The 'Autospec 5000' oa-TOFMS	162
3.4.3	Sample preparation	166
3.5	Results and discussion	167
3.6	Conclusion	186
3.7	References	188

Chapter 4: Studies of consecutive reactions to distinguish isomeric C₃H₃⁺ ions formed in some simple organic molecules

4.1	Aim	193
4.2	Introduction	193
4.2.1	C ₃ H ₃ ⁺ ion identification	196
4.2.2	Consecutive reaction studies	199
4.2.2.1	Energetics of consecutive reactions	200

4.3	Experimental	205
4.3.1	Instrumentation	205
4.3.2	Calibration	208
4.3.3	Sample preparation	211
4.4	Results and discussion	212
4.4.1	Toluene	220
4.4.2	n-Hexane	223
4.4.3	Propene	226
4.5	Conclusion	229
4.6	References	231
	Appendix	233

Chapter 1

Introduction

1.0 Introduction

1.1 Introduction and thesis scope

Mass spectrometry has become the technique of choice for many problems in the characterisation of complex mixtures. The high sensitivity, versatility and rapid scan speeds that can be obtained have made the partnership of mass spectrometry with separation science approaches a very successful one. Mass spectrometry development continues to advance at a rapid rate. Newer ionisation techniques such as electrospray ionisation (ESI) and matrix-assisted laser desorption ionisation (MALDI) have come to dominate the field and to extend the applicability of the approach. Improvements in analyser design, together with ESI and MALDI, has importantly led to the reintroduction of ToF mass analysers.

Mass spectrometry information is used in a variety of applications, ranging from giving molecular weight data to providing detailed ion structural information. This work covers the major impact provided by some of these new approaches as well as studying the fundamental structural information that can be obtained from mass spectrometric experiments.

A thorough detailed examination of a new instrument (LCT, Micromass, U.K. Ltd) is undertaken. This orthogonal-acceleration (oa) ToF ESI based analyser is compared with existing ESI quadrupole instrumentation. In establishing the parameters of the instrument, clear indication is given, via practical examples, of the importance of the technical advances to problems of current industrial relevance. The first part of the evaluation concentrates on instrumental design characteristics and a fundamental

discussion of the ESI process. The second part discusses the performance characteristics of the instrument, demonstrated using a number of practical analysis problems. A detailed comparison with existing methods is made and an evaluation of the importance of the instrumental improvements presented.

The oa-ToF approach has also found to have great utility as a second mass analyser when used in conjunction with a magnetic sector instrument. Here, in the conventional tandem mass spectrometry product ion experiment, the first mass analyser is used to select an ion of interest. This ion is then collisionally excited and the resulting product ions are detected using the second mass analyser. The oa-ToF approach presents significant advances over quadrupole or magnetic sectors in this type of experiment. The high sensitivity, the very fast acquisition rates and increased mass range provides practical improvements.

The pulsed nature of the oa-ToF analyser makes it ideal for MALDI experiments. The use of MALDI as an ionisation source coupled with a double focusing magnetic sector to select ions of interest presents a very effective partnership to an oa-ToF analyser. This enables high-energy collision induced dissociation (CID) product ion spectra to be obtained with high sensitivity on precursor ions of significant molecular weight. These spectra can be, in the case of synthetic polymers, be interpreted to provide detailed structural information. Some examples of this approach in the study of polystyrene oligomers is presented.

Ion structural studies of a more fundamental nature have also been made in order to probe the detailed information that can be obtained in tandem mass spectrometry

experiments. A detailed examination of the various possible structures of $C_3H_3^+$ has been made and conclusions regarding the information provided by the mass spectrometry experiments made.

1.2 Historical account of mass spectrometry

In 1886 Goldstein [1] discovered positive rays, which were later analysed by Wien [2] in a magnetic field. Wien concluded that these positive rays were deflected less and in the opposite direction to cathode rays in a magnetic field and that the rays held a positive charge. It was not until some years later however, that Thomson [3] interested in these positive rays, constructed a 'parabolic mass spectrograph'. It was using this instrument that he produced a mass spectrum which demonstrated the existence of two stable isotopes of neon, resulting in the birth of mass spectrometry. It was probably never imagined that one century later the ability to mass measure molecules in the mega dalton mass range would at all be possible [4]. However, present day mass spectrometry offers this possibility through ESI and MALDI coupled with, in general, ToF instrumentation.

The former ionisation method relies heavily on multiple charging of the molecule, which was not unknown at the turn of the century. Thomson [3] obtained mass spectra which was observed to contain some multiply charged ions formed from some simple gases such as O_2 , N_2 , CO and CO_2 .

Significant advances in the field of mass spectrometry were provided for by Dempster in 1918 [5] who developed the first magnetic sector instrument and by Aston [6] who constructed the first mass spectrometer which provided velocity focusing of the ions.

Aston developed an instrument in which these positive rays were first subjected to an electric field and then a magnetic field. It was found that positive rays with the same mass-to-charge (m/z) ratio, but with varying velocity could be focused at the same point on the detector. This was a major achievement at that time and set the foundations for which future double-focussing instruments were based. However, Dempster and Astons' efforts would not have been made possible if it was not for the pioneering work of Thomson. For it was he who was responsible for the discovery of the electron, one of the basic building blocks of all atoms and the measurement of its m/z ratio. He is therefore regarded by many as the 'father of mass spectrometry' [7].

1.2.1 What is mass spectrometry?

A simple definition could explain mass spectrometry: *a physical analytical technique that separates gas phase ions according to their m/z ratio and detects them.*

The creation of a charge on the molecule under investigation is brought about through ionisation. Once the sample molecules have been ionised, they need to be separated or resolved by a mass analyser. Upon separation the ions need to be detected, which results in a mass spectrum, ultimately providing molecular weight and depending on the method of analysis, structural information characteristic of the sample molecule. Therefore, the overall basic requirements of a mass spectrometer are simplified in Figure 1.01.

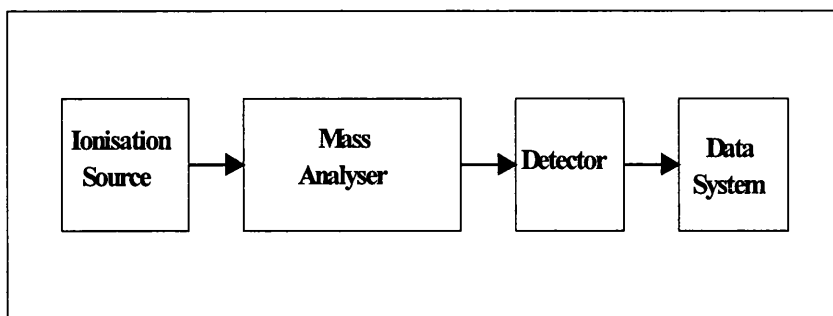


Figure 1.01: Schematic of the basic components of a mass spectrometer

1.3 Ionisation methods [10-14]

1.3.1 Electron impact (EI)

Prior to the successful development of new ionisation techniques of the late 1980's, electron impact (EI) played an important role as one of the main ionisation methods used. (A comprehensive discussion for the ESI and MALDI techniques can be found in Chapters two and three respectively). EI is restricted to compounds of a volatile nature unlike the other two methods and therefore only has a limited mass range of around m/z 1500. The technique can only be used in the positive ionisation mode and is generally termed a 'hard' ionisation method, since a high degree of fragmentation is induced through excess energy being imparted to the gaseous sample molecules upon impact. The technique however, is simple to use and does not suffer frequent source contamination problems inherent with ESI and MALDI.

The electron impact source was developed by Dempster [8] and improved by Nier [9] where gaseous sample molecules interact with a beam of electrons emitted from a

heated filament. A simple schematic of the source is shown in Figure 1.02. Once the gaseous sample molecules cross the electron beam path an electron is displaced from the neutral molecule and the sample becomes ionised, resulting in the formation of a radical cation. Electrons emitted from the filament, are generally accelerated through an electric potential of 70V. It has been well established that this voltage provides an ion transmission maximum and was therefore kept constant at this voltage throughout the study in Chapter four.

After ionisation, the ions need to be separated and sufficiently resolved from one another. Only sector, quadrupole and ToF instruments will be discussed here, since these were the only instruments used during this study. ToF will be discussed in more detail since the majority of the work made use of ToF instrumentation.

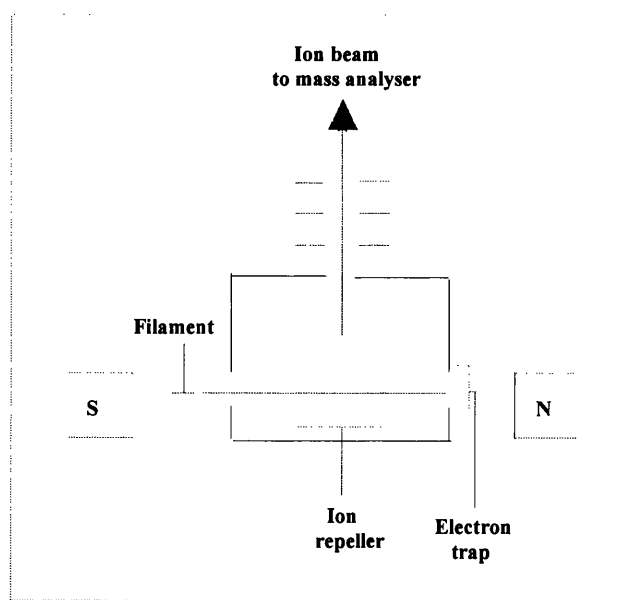


Figure 1.02: Simple schematic of an electron impact source

1.4 Mass analysers [10-14]

1.4.1 Sector instruments

The sector mass analyser can be described as the ‘classical’ method of mass analysis, since it has been in existence since the birth of mass spectrometry. However, its use in modern day mass spectrometric investigations has been somewhat overshadowed by quadrupole and ToF instruments. It does however provide high mass resolution for singly charged ions in comparison with the two former techniques and therefore still has a tremendous amount to offer.

1.4.1.1 Magnetic sector

A schematic diagram illustrating the principle of a single focussing mass spectrometer is shown in Figure 1.03. Ions of mass m , with electronic charge e (z charges) and velocity v are accelerated through a voltage V_{acc} from the ion source. The potential energy lost is equal to the kinetic energy gained and thus:

$$\frac{mv^2}{2} = zeV_{acc} \quad (\text{Eq}^n.1)$$

An ion beam therefore, exiting the source can be separated according to their m/z ratios using the magnetic sector. Ions entering the magnetic field experience a force, of strength B , in a direction perpendicular to their original direction of motion. This force will be equal to $Bzev$, which causes the ions to follow a circular path. This force is equal to the centrifugal force where:

$$\frac{mv^2}{R} = Bzev \quad (\text{Eq}^n.2)$$

Where R equals the radius of curvature of the magnet. Manipulation of these two equations yields:

$$\frac{m}{z} = \frac{R^2 B^2 e}{2V_{\text{acc}}} \quad (\text{Eq}^n.3)$$

The radius of curvature of an ions trajectory is therefore dependent upon its momentum. Thus, the magnetic sector can be classed as a momentum-to-charge analyser. Thus, by scanning the magnetic field or varying V_{acc} allows ions of various m/z ratios to reach the detector, resulting in a mass spectrum.

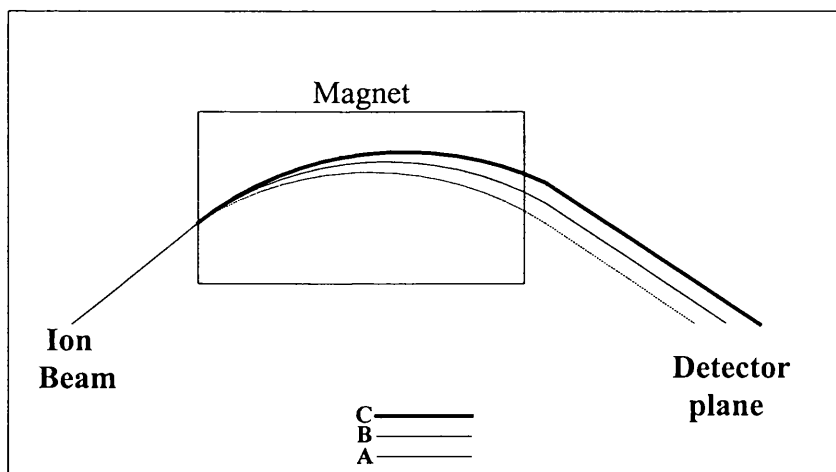


Figure 1.03: Schematic of a single-focussing magnetic sector mass analyser, illustrating that small mass ions, **A**, are deflected to greater extent than ions of higher mass, **B** and **C** in a magnetic field

1.4.1.2 Electric sector

The electric sector contains two cylindrical parallel plates of opposite potential but of equal magnitude. A schematic is shown in Figure 1.04. Ions moving in an electric field suffer a force perpendicular to their ion motion. Thus, the centrifugal force acting on ions in an electric field, is given by:

$$\frac{mv^2}{R} = zeE_{app} = \frac{zeV_{app}}{2d} \quad (\text{Eq}^n.4)$$

Where E_{app} is the electric field applied across the ESA (electrostatic analyser) plates and d is the half gap width of ESA. Substitution of equation 4 into equation 1 yields:

$$R = \frac{2V_{acc}}{E} \quad (\text{Eq}^n.5)$$

Thus, in an electric sector the ion trajectory depends on the acceleration and ESA voltages only. Electric sectors therefore separate ions according to varying energy-to-charge ratios. For instance, ions of the same mass possessing different energies on entry into the electric sector will be brought to focus at separate points on a focal plane beyond the electric sector.

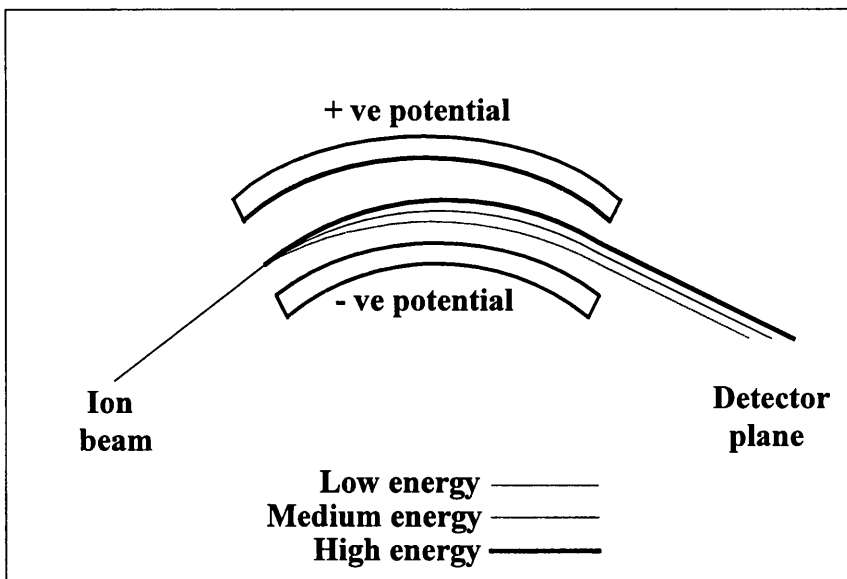


Figure 1.04: Schematic of operation of an electric sector analyser, illustrating that low energy ions are deflected more in an electric field than higher energy ions

1.4.1.3 Double-focussing instruments

The mass resolution of single focussing instruments is limited by the spread in kinetic energy and the angular divergence of the ion beam as it leaves the ion source. However, this resolution limitation can be overcome by a combination of a magnetic sector and electric sector. This geometry ultimately results in a substantial increase in resolution and sensitivity. This combination provides direction and energy focussing simultaneously. The point of double focussing is achieved when the direction and velocity curves crossover.

1.4.1.4

Resolution of sector mass analysers

The definition of resolution for sector mass analysers is $m/\Delta m$ which is the difference between two masses that can be separated divided by the mass number of the mass obtained. Peaks are defined to be separated sufficiently down to a 10% valley. This means that the height of the valley is 10% of the height of the peaks, with each peak contributing to 5% of the valley, see Figure 1.05.

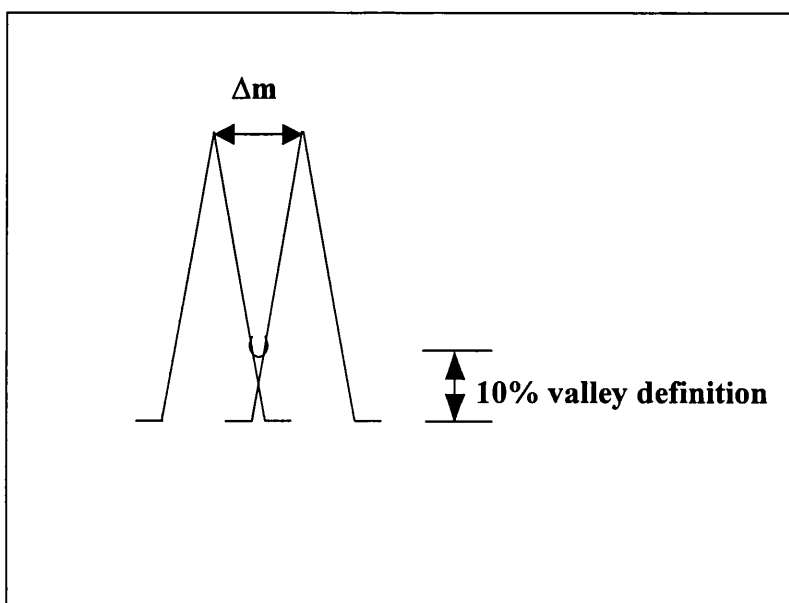


Figure 1.05: Schematic illustrating the 10% valley definition

For this type of analyser, some of the advantages and disadvantages can be listed as:

Advantages

- High mass accuracy (double focus)
- High resolution, $> 100,000$
- Reproducible mass spectra
- Mass range $\sim m/z 15000$

Disadvantages

- Expensive
- Not suited to pulsed ionisation methods, unless used in conjunction with an oa-ToF

1.4.2 Quadrupole mass analyser [10-16]

This mass filter was developed by Paul and co-workers in 1950's [15]. The operating principle of the quadrupole is different from the sector instruments described previously, due to the fact that ion focussing is not carried out nor is a magnet used. This analyser is called a mass filter, since it uses an alternating quadrupolar electric field to filter out masses other than those of interest. A quadrupole analyser is constructed from four equally spaced parallel rods of either hyperbolic or cylindrical cross section.

A voltage consisting of a DC component, U and a rf component, $V_0 \cos \omega t$ is applied to opposite pairs of rods, see Figure 1.06.

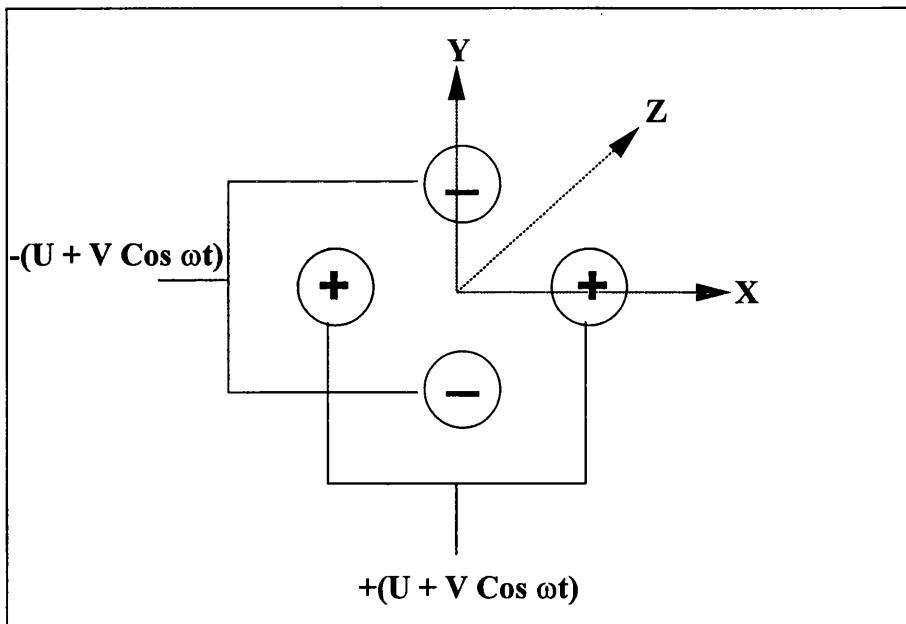


Figure 1.06: Schematic of a quadrupole mass analyser showing the applied potentials to the four parallel rods

The rods are separated by a distance of $2r_0$. A small acceleration voltage, typically of 10-20V is used to accelerate ions from the source into the centre of the quadrupole, along the z-axis. The alternating electric field applied between the two pairs of poles will cause ions to oscillate in the x and y directions. Some ions of a particular m/z ratio will have a stable trajectory, pass through the filter and reach the detector. Other ions of different m/z ratio will have an unstable oscillatory movement, impact on the rods and be lost in the filter.

Ion motion in a quadrupole filter is complex and is described using a set of equations known as the Mathieu equations. A detailed derivation however is beyond the scope of this brief introduction. The oscillation of an ion is governed by several factors, the distance between the rods, ω the frequency of the rf voltage and the m/z ratio of the

ion itself. For ions to have a stable trajectory and reach the detector conditions a and q described by equations 6 and 7 have to be met:

$$a = \frac{8eU}{mr_o^2\omega^2} \quad (\text{Eq}^n.6)$$

and

$$q = \frac{4eV_o}{mr_o^2\omega^2} \quad (\text{Eq}^n.7)$$

Thus, $a/q = 2U/V_o$. This can be illustrated with a stability diagram which shows the relationship between a and q and the condition for stable oscillations.

It can be seen from Figure 1.07, that an ion of mass m_1 will reach the detector, but an ion of mass m_2 will become unstable, hit one of the rods and be lost in the system. A mass spectrum can be obtained by varying U , the DC voltage and V_o , the rf amplitude voltage whilst keeping the U/V_o ratio constant. The recorded mass is proportional to V_o so that a linear increase of V_o provides an easily calibrated linear mass scale.

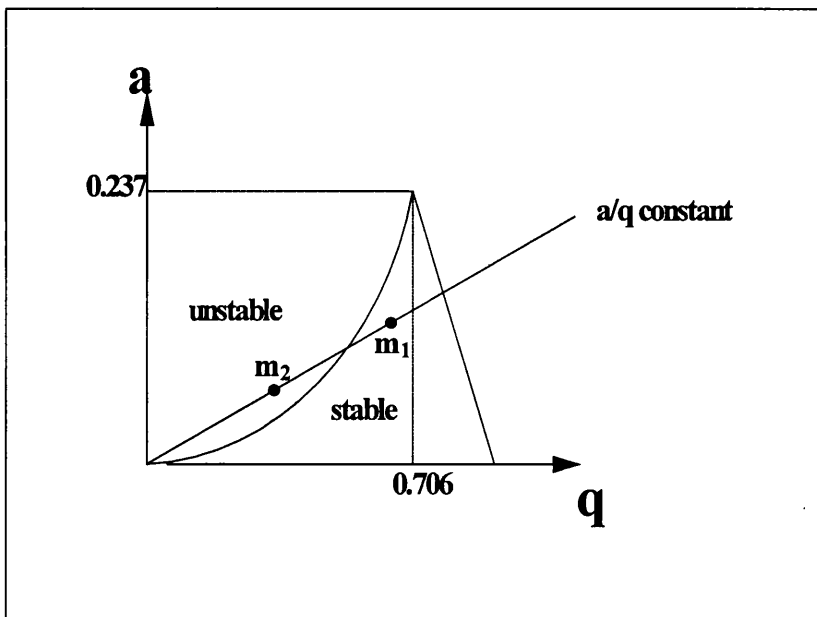


Figure 1.07: Simplified stability diagram for a quadrupole mass analyser

1.4.2.1 Resolution of quadrupole mass analysers

Resolution of quadrupole instruments is usually defined as unit mass resolution. This means that each mass can be separated from the next integer mass. Resolution is at its highest when the scan line, shown in Figure 1.07 approaches the apex of the stability region. Thus, as the mass increases the resolving power increases. However, this leads to a reduction in ion transmission.

Some of the advantages and disadvantages for this type of mass analyser can be summarised as follows:

Advantages

- Small and compact
- Inexpensive
- Reproducible mass spectra

Disadvantages

- Limited resolution
- Limited mass range < 4000
- Not suited with pulsed ionisation methods

1.4.3 ToF mass analysers [17-25]

TOFMS it would seem, reading through the literature, to be a relatively new separation technique due to the vast amount of publications in the last decade. This though is not the case. TOFMS has seen a massive resurgence due to highly sophisticated electronics, computers and ionisation methods developed over the last ten years.

The first proposal for a TOFMS dates back to 1946 through the work of Stephens [26]. It was not until two years later that the first experimental account of the instrument called the ‘Ion Velocitron’ was reported by Cameron and Eggers [27]. However, it was the design of Wiley and McLaren [28] in 1955 that the first TOFMS became commercially available by the Bendix Corporation and later by CVC Products (Rochester, New York). The instrument though was seen to have both low resolution and sensitivity and never used widely and was displaced by magnetic sector and quadrupole instruments, which possessed higher resolution and sensitivity.

1.4.3.1 Principles of TOFMS

TOFMS is a relatively simple mass spectrometric technique and as the name suggests, the separation of ions is dependent on their flight times in a field-free drift tube. The ToF experiment relies on the fact that ions are created at the same point and at the same time in the presence of an electric field. Ideally, all ions will enter the drift region with the same kinetic energy (KE), i.e.

$$KE = \frac{mv^2}{2} = zeV_{acc} \quad (\text{Eq}^n.8)$$

Thus, ions will be accelerated to different velocities depending on their m/z ratio. The velocities of ions, which ideally have the same kinetic energies as they enter the drift region, are dependent on mass:

$$v = (2zeV_{acc} / m)^{1/2} \quad (\text{Eq}^n.9)$$

Therefore, the time taken to traverse the drift region, of length D, is given by:

$$t = D \times (m / 2zeV_{acc})^{1/2} \quad (\text{Eq}^n.10)$$

The arrival time of the ions, therefore can be converted directly to a mass spectrum, where:

$$m/z = 2zeV_{acc} (t / D)^2 \quad (\text{Eq}^n.11)$$

Thus, small mass ions, which will attain a higher velocity, will reach the detector before higher mass ions, which will attain a lower velocity.

The maximum achievable resolution, as mentioned previously for early TOFMS, was rather poor. Resolution was initially limited since isobaric ions accelerated from the ion source are subject to initial temporal, spatial and energy distributions. If these distributions are not successfully minimised there will be a time lag for isobaric ions arriving at the detector, which seriously degrades resolution. To overcome the spatial distribution a dual stage source was devised [28], which still plays an important role in modern day ToF instrumentation.

Energy resolution can be achieved by use of a reflectron, which effectively doubles the flight path of the ions, resulting in an order of magnitude increase in resolution.

1.4.3.2 Types of ToF mass analysers

1.4.3.2.1 Linear ToFMS

ToF requires a well defined starting point in time and space and is therefore immediately compatible with pulsed ionisation sources. However, TOFMS is not

solely restricted to these type of methods. The development of orthogonal acceleration, see section 2.2.4, has paved the way for ToF to be used with ionisation methods that are of a continuous nature.

The linear TOF configuration can be seen in Figure 1.08. This particular type consists of two acceleration fields and provides focussing of the ions, i.e. ions of the same mass, but formed at different locations within the ion source will arrive at the detector at the same time. By varying the electric fields, the position of the space focus can be altered and the detector should be placed here. This will ultimately achieve longer flight times compared to a single field ion source resulting in a resolution enhancement for linear TOFMS. Improved ion beam collimation within the source also results in increased resolution.

1.4.3.2.2 Reflectron TOFMS [29]

Positioning the detector at the space focus in linear TOFMS has a resolution of around 1000. The resolution can be increased by an order of magnitude by use of a reflectron for ionisation techniques with a large energy distribution, see section 2.2.5. This corrects for the energy distribution of the ions as they enter the drift tube and the increased flight path effectively allows better separation of the ions. A simple schematic is shown in Figure 1.09. Thus, for isobaric ions those with the lowest energy will not penetrate the reflectron as much as ions with a higher energy. The residence time for the latter ions is much greater but will 'catch up' with their identical mass, after being re-accelerated from the reflectron, at the detector. Thus, the

flight time for ions, in an instrument employing a dual stage source and a single stage reflectron is given by:

$$t = (m / 2zeV_{acc})^{1/2} \times [L_1 + L_2 + 4d] \quad (\text{Eq}^n.12)$$

where, L_1 and L_2 are the drift lengths prior to and after reflection and d is the penetration depth of the reflectron.

1.4.3.2.3 Resolution of TOF mass analysers

The resolution of a ToF instrument is defined as:

$$R = m / \Delta m = t / 2\Delta t$$

Where m is the mass of the ion, Δm is the full width half maximum (FWHM) spread in the ion packet mass, t is the arrival time at the detector of the ions and Δt is the FWHM temporal width of the ion packet.

Some of the advantages and disadvantages can be listed as:

Advantages

- Speed
- Suited to pulsed techniques
- High sensitivity
- Theoretically, has an unlimited mass range

Disadvantages

- Requires fast digitisers
- Data system must contain sufficient memory to store a tremendous amount of generated mass spectra

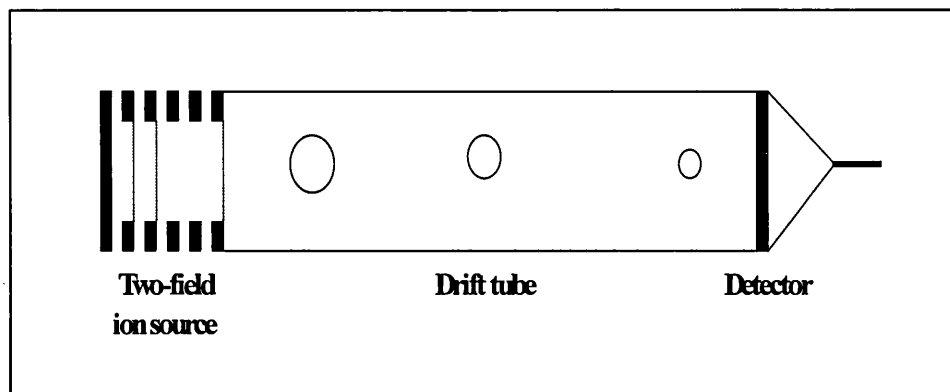


Figure 1.08: Schematic of a linear ToF mass analyser. Small high velocity ions are shown to reach the detector before larger lower velocity ions

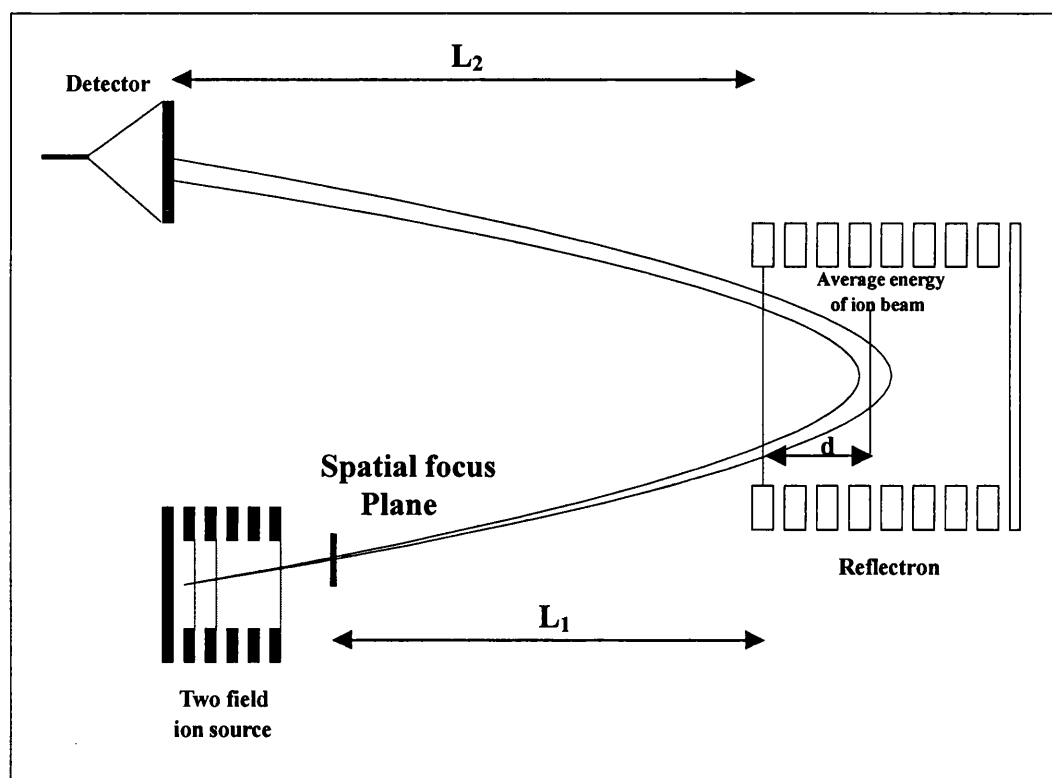


Figure 1.09: Schematic of a reflectron mass analyser. Isobaric ions that attain different energies after acceleration from the source, will arrive at the detector at the same time. The ion with the highest energy will penetrate the reflectron deepest and therefore spend longer in the reflectron than the low energy ion

1.5 Ion Detectors [10-14]

In mass spectrometry ions are usually detected by techniques based on secondary electron emission (SEM) that make use of electron multipliers or micro channel plate (MCP) detectors that amplify the signal intensity typically by 10^5 - 10^7 for single ion detection. The detection of ions can be classified into two groups:

- A. those which detect ions successively at one point, called point ion detectors and
- B. those which detect ions at the same time along a focal plane, called multi point detectors.

Types of point ion detectors are:

1.5.1 The Faraday cup

Here a metal cup is positioned in the path of high velocity incoming ions. Ions which strike the cup transfer their charge to the cup resulting in a flow of electrons that in turn creates a current. The surface of the cup is usually coated with BeO, GaP or CsSb, and an ion striking the surface induces several electrons to be ejected. The emitted electrons induce a current in the cup and provides a small amplification of signal when an ion strikes the cup. This type of detector is incompatible with ToF because of its very long time constant typically 0.1 to 1 sec, but is ideal when monitoring a high intensity signal greater than $\sim 10^{-11}$ A. This basic set up was put to use when trying to detect a beam around different sections of the instrument

employed in Chapter four. The ion current was measured by a picoammeter (Keithley Instruments Inc., Ohio, USA).

1.5.2 Electron multiplier

1.5.2.1 Discrete dynode electron multiplier

As the name suggests this type of detector is made from a series of between 12-20 dynodes. The dynodes are coated or made entirely from an electron emissive material and when an ion strikes the first dynode a shower of electrons are emitted. These secondary electrons are accelerated towards the second and subsequent dynodes where the process repeats itself causing a rapid amplification of the electron current. Depending on the number of dynodes and the type of dynode material the initial ion current can be amplified upto 10^6 to 10^7 times, referred to as the gain. This type of detector was employed in the instrument described in Chapter four. These devices have usable lifetimes ranging from months to years depending on usage. However, they can dramatically fail if a vacuum accident or electrical discharge across the device occurs.

1.5.2.2 Continuous dynode electron multiplier

This type of detector is also known as a channel multiplier or channeltron. The device is horn shaped and constructed from glass with the inside coated with a semiconducting electron emissive material that has a high electrical resistance. A

potential difference is applied across both ends, so that the potential varies linearly across the tube. An ion beam striking the tube causes the emission of secondary electrons which then pass along the tube creating an electron cascade effect. The gain can be adjusted by varying the potential, typically between 1-3 kV.

The second class of detectors are called multi-point ion detectors and are most familiar with ToF instrumentation. An example of this type of detector is discussed in section 2.2.6.

1.6 References

1. E Goldstein, *Berl.Ber.*, 39 (1886) 691.
2. W Wien, *Verhanal.Phys.Ges*, 17 (1898).
3. JJ Thomson, in '*Rays of positive electricity and their application to chemical analysis*', Longmans Green, London 1913.
4. DC Schriemer, L Li, *Anal.Chem.*, 68 (1996) 2721.
5. AJ Dempster, *Phys. Rev.*, 11 (1918) 316.
6. FW Aston, *Philos.Mag.*, 38 (1919) 707.
7. IW Griffiths, *Rapid Commun.Mass Spectrom.*, 11 (1997) 2.
8. AJ Dempster, *Phys.Rev.*, 18 (1921) 415.
9. AO Nier, *Rev.Sci.Instrum.*, 18 (1947) 398.
10. JR Chapman, in '*Practical organic mass spectrometry*', 2nd edition, Wiley and Sons, 1993.
11. E De Hoffmann, J Charette, V Stroobant, in '*Mass spectrometry: Principles and applications*', Wiley and Sons, 1996.
12. DM Desiderio, in '*Mass spectrometry: Clinical and biomedical applications*', Volume 2, Plenum Press, New York, 1994.
13. G Siuzdak, in '*Mass spectrometry for biotechnology*', Academic Press, 1996.
14. AE Ashcroft, in '*Ionisation methods in organic mass spectrometry*', The royal society of chemistry, 1997.
15. W Paul, HP Reinhard, U von Zahn, *Z.Phys.*, 152 (1958) 143.
16. PH Dawson, in '*Quadrupole mass spectrometry and its applications*', Elsevier, New York, 1976.
17. X Tang, R Beavis, W Ens, F Lafortune, B Schueler, KG Standing, *Int.J.Mass Spectrom.Ion Processes*, 85 (1988) 43.

18. RJ Cotter, *Biomedical and Environmental Mass Spectrometry*, 18 (1989) 513.
19. RJ Cotter, *Anal. Chem.*, July, 445A (1999).
20. RJ Cotter, in *'Time of flight mass spectrometry: Instrumentation and applications in biological research'*, American Chemical Society, 1997.
21. M Guilhaus, *J. Mass Spectrom.*, 30 (1995) 1519.
22. ML Vestal, in *'Selected topics in mass spectrometry in the biomolecular sciences'*, Kluwer Academic Publishers, 1997.
23. C Weickhardt, F Moritz, J Grotmeyer, *Mass Spectrom. Reviews*, 15 (1996) 139.
24. U Boesl, R Weinkauf, C Weickhardt, EW Schlag, *Int. J. Mass Spectrom. Ion Processes*, 131 (1994) 87.
25. IV Chernushevich, W Ens, KG Standing, *Anal. Chem.*, July, 452A (1999).
26. WE Stephens, *Phys. Rev.*, 69 (1946) 691.
27. AE Cameron, DF Eggers, *Rev. Sci. Instrum.*, 19 (1948) 605.
28. WC Wiley, IH McLaren, *Rev. Sci. Instrum.*, 26 (1955) 1150.
29. BA Mamyrin, VJ Katatajev, DV Shmikk, VA Zugulin, *Soviet Phys. JETP*, 37 (1973) 45.

Chapter 2

An evaluation of a novel orthogonal acceleration Time-of-Flight mass spectrometer

Section A

**ESI mechanism, instrument design and
theoretical considerations of the LCT**

2.1 Aim

Evaluation of impact of novel oa-ToF technology in the qualitative and quantitative characterisation of complex mixtures of industrial significance.

2.1.1 Introduction

Mass spectrometric techniques are widely used in industry to characterise the, often complex, mixtures that are produced. The interfacing of mass spectrometry to various separation science approaches has led to the development of an extremely powerful technique. In recent years commercial, environmental and legislative pressures have led to the need for more sensitivity. The introduction of newer products based on higher molecular weight components have also led to the need to extend the mass range of the mass spectrometric detection systems.

The development of ESI and MALDI has provided the ability to produce ions from complex mixtures of wide mass ranges and the combination of these techniques with ToF analysers has greatly extended the applicability of mass spectrometry to modern industrial problem solving.

In order to evaluate the potential impact of these new approaches, an evaluation was made of a recently developed instrument, the LCT (liquid chromatograph-ToF). This instrument combines ESI with an oa-ToF analyser and promises to provide significant technical improvements over the commonly used ESI quadrupole instruments.

In order to objectively evaluate the instruments performance, measurements including, sensitivity, mass resolution, mass range and mass accuracy were determined and compared with those obtained using conventional ESI quadrupole systems. The limitations of mass measurement on a quadrupole instrument are well characterised and documented in the literature and therefore not investigated during the study (see section 2.3.7 [72]). Limit of detection experiments carried out on the quadrupole instrument were carried out independently [1].

2.2 Detailed description of the LCT Mass Spectrometer

2.2.1 Introduction

The design of the instrument is at the forefront of modern day time-of-flight mass spectrometry using atmospheric pressure ionization (API) techniques. It is also very compact in size and designed to be user friendly. Instrument control, data acquisition and data processing is controlled through a Pentium II 450 MHz PC running Masslynx NT software (version 3) which is written in Microsoft conforming code.

A schematic showing the insides of the instrument is shown in Figure 2.01.

2.2.1.1 Atmospheric Pressure Ionization

The LCT makes use of two API techniques. These are atmospheric pressure chemical ionisation (APCI) and electrospray ionisation (ESI). Results for this thesis made use only of ESI using a newly designed source trademarked 'Z Spray™'. The ESI process will be described in some detail here.

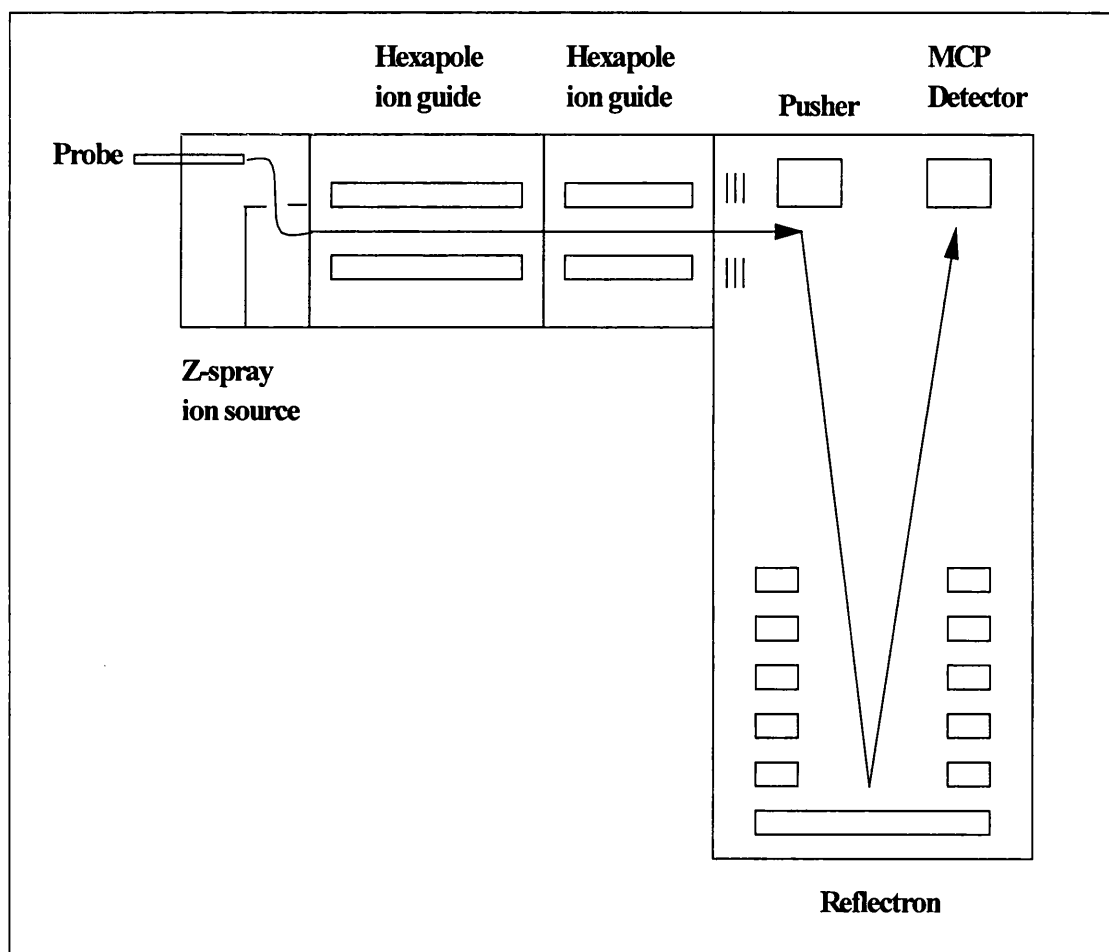


Figure 2.01: Schematic of the LCT

2.2.1.2 Electrospray ionisation

The electrospray process for the production of ions from non-volatile samples is not new. The process seems to date from experiments by Zeleny [2] at the turn of the turn of the century. The process however did not develop and lay dormant for a number of years until Dole *et al.* [3] generated gas phase ions of polystyrene macromolecules.

Since these early developments the ESI process has seen rapid growth in many areas of research over the last decade due to further pioneering work by Fenn *et al.* [4]. Their work was initially presented at the 1987 ASMS meeting which demonstrated the ability to multiply charge poly(ethylene glycol)s with masses in excess of 20000 Da. The rest they say is history!

Electrospray has truly transformed the mass spectrometric field due to its ease of accessibility, low cost and the successful interfacing to various types of mass analysers. It can also achieve an extraordinary mass range of $\sim 3 \times 10^6$ daltons due to its ability to multiply charge very large macromolecules. ESI was first interfaced and commercialised on quadrupole mass spectrometers [4-7]. Since then successful interfacing has also been achieved on magnetic sector instruments [8-11], quadrupole ion traps [12-13] and Fourier transform [14-16].

The first ESI-ToF instrument was reported in 1991 by Boyle *et al.* [17], where low energy ions were accumulated in a storage region before extraction pulses were

applied prior to mass analysis. The instrument however possessed a poor duty cycle and suffered low mass resolution.

Orthogonal acceleration and the use of the reflectron has made ToF once again a force to be reckoned with. Building on the initial concepts of Dodonov *et al.* [18] the number of publications making use of API techniques combined with TOFMS has sharply risen during the 1990's.

2.2.1.3 Mechanism and theory of the electrospray ionisation process

Electrospray in simple terms is a method by which ions present in solution can be successfully transferred into the gas phase. Although proposals have been made, no definite mechanism for the process has been reached. For the successful production of gas phase ions from analyte ions in solution, there is in general two requirements:

- A. the ability to produce charged droplets at atmospheric pressure.
- B. a decrease in the size of the charged droplets formed through solvent evaporation, leading finally to gas phase ions.

Generation of an electrospray is usually carried by applying a potential of around 3-4 kV to a stainless steel capillary from which a solution containing the analyte of interest exits at a rate typically of the order of 10-150 $\mu\text{L min}^{-1}$. A nebulising gas,

If the instrument, for example, is set up for positive electrospray ionisation mode, the stainless steel capillary will become the positive electrode. Positive ions in the solution at the tip of the capillary will move to the surface of the solution and the negative ions will move away from the surface, toward the capillary.

The separation of ions at the surface of the solution caused by electrostatic forces coupled with surface tension forces at the meniscus cause the liquid emanating from the capillary to expand forming a liquid cone, referred to as the 'Taylor cone' [19]. The drifting of charged ions at the surface of the solution was proposed by Kebarle *et al.* [20] and has been called the 'electrophoretic mechanism'.

The electric field created at the tip of the capillary, (E_c), which has a radius, r_c , located a distance, d , from the counter electrode leading into the mass spectrometer can be calculated using the equation:

$$E_c = 2V_c / [r_c \ln (4d/r_c)]$$

Where V_c is the potential in volts applied to the capillary.

The formation of a continuous flow of ions will lead to the breaking of the Taylor cone, releasing ions into the mass spectrometer, ultimately leading in an observed

mass spectrum. The onset of instability in the Taylor cone, leading to an Electrospray [21] is given by:

$$E_{on} \approx [2 \chi \cos \theta / (\epsilon_0 r_c)]^{1/2}$$

ϵ_0 = permittivity of free space

$\theta \sim 49^\circ$

χ = surface tension

E_{on} = instability in the Taylor cone

Combination of the two equations leads to a relationship for the capillary onset voltage (V_{on}) where:

$$V_{on} = 2 \times 10^5 (\chi r_c)^{1/2} \ln (4d/r_c)$$

which estimates the voltage needed to be applied to the capillary that supports the electrospray process.

A solvent therefore, with a surface tension such as water, would find difficulty forming a Taylor cone compared to solvent systems such methanol and acetonitrile which have lower surface tensions. In the case of water, higher voltages would have to be applied to the stainless steel capillary compared to methanol and acetonitrile to form an electrospray process. This though could come as a disadvantage, mainly due to the higher possibility of arcing at the capillary tip. This in turn would lead to a loss in signal.

The size of the initial droplets formed will depend on the solvent and the flow rate being utilised in the system.

The formation of gas phase ions from small pre-formed highly charged droplets is the whole essence behind the electrospray process. The mechanism by which this proceeds, as mentioned earlier, is still somewhat unclear.

When a potential has been applied to the capillary, the solvent exiting the capillary becomes charged and dispersed by Coulomb forces into a spray of charged droplets. The applied potential drives the droplets towards the end of the capillary with the assistance of a sheath gas, typically nitrogen.

There are currently two theories on how a charged droplet enters the gas phase for mass spectrometric analysis as a charged ion:

2.2.1.4 Dole [3]: Single Ion in Droplet Theory (SIDT)

As the charged droplets emerge from the capillary, desolvation occurs in the heated capillary causing the radius of curvature of the droplets formed to decrease thus increasing the charge density at the droplet surface. The droplets rapidly decrease in size through evaporation until the so called 'Rayleigh limit' [22] is reached, at which point the repulsive Coulombic forces are of the same order as the surface tension of the droplet. This causes droplet offspring due to 'Coulomb explosion'. The offspring

in turn continue to evaporate until they explode, until finally only one analyte molecule is left. Once the last of the solvent has been removed and providing the analyte and not the solvent retains the charge a sample ion will be observed.

2.2.1.5 Iribarne and Thomson [23,24]: Ion Evaporation Theory

Similarly, along the lines of Dole, evaporation of solvent from the pre-formed droplets increases the charge density at the droplet surface. Again the Rayleigh limit is reached when coulombic repulsion is of the same order of the surface tension of the droplet. Coulomb explosion again occurs over and over until the repulsive forces within the offspring daughter droplets are so great that the analyte ions are desorbed by field induction (due to surface charge density) into the gas phase. Ejection of ions is therefore proposed to occur via repulsion of forces of the charged ion and forces already present in the droplet.

2.2.2 'Z SprayTM', Ionisation source and sample introduction

For electrospray ionisation the formation of ions takes place outside the vacuum system of the instrument. The analyte of interest which is dissolved in a suitable solvent, is introduced into the 'Z-spray' ionisation source through a stainless steel capillary, which runs through the centre of a probe, at a flow rate of between 10-150 μ L/min. Application of a high voltage, typically 3500V to the end of the capillary,

causes the solvent containing the analyte of interest exiting the capillary, to form a spray of highly charged droplets. A compressed nitrogen gas supply (100 psi, 7 bar) is connected to the mass spectrometer. This nitrogen which has a flow rate of approximately 75 Lhr^{-1} passes down the probe, around the outside of the capillary. The nitrogen aids the solvent containing the analyte of interest to form a spray as it leaves the end of the electrically charged capillary and also provides focusing of the spray beyond the sampling cone. The delivery of nitrogen at this point is called the nebuliser gas. This aerosol spray then enters the 'Z-Spray' ion source which is maintained at a temperature of 100°C . The charged droplets that have been formed are subject to rapid evaporation of the solvent, with ions of the compound of interest being formed. Nitrogen desolvation gas, also known as drying gas, which has a flow rate of approximately 620 Lhr^{-1} , is used to assist the evaporation of the solvent. A desolvation temperature of around $150^{\circ}\text{-}200^{\circ}\text{C}$ was commonly used. These charged droplets are then extracted at a right angle from the spray into the sampling cone orifice which has a voltage of between 20 and 40 volts applied, which affects the degree of fragmentation. The ions then enter the ion block region of the source.

Figure 2.02 shows a schematic diagram of the 'Z-Spray' ion source.

After prolonged use contamination may occur from involatile compounds and buffers. These tend to collect at the orifice of the sampling cone and the baffle indicated in Figure 2.02, ahead of the spray. This leads to a reduction in sensitivity and the sampling cone and baffle require periodic cleaning in an ultrasonic bath, with acetonitrile and methanol. Gaining access to the sampling cone and baffle for cleaning purposes, is straightforward and poses no problem. The vacuum in the instrument is

maintained whilst removing the required parts for cleaning by closing the isolation valve marked on Figure 2.02. The design of the 'Z-spray' ion source allows easy access for cleaning purposes and is a major improvement compared to other instruments used in this investigation, for example, the Platform II (Micromass Ltd.,UK) and Quattro (Micromass U.K. Ltd.,) where cleaning is more tedious.

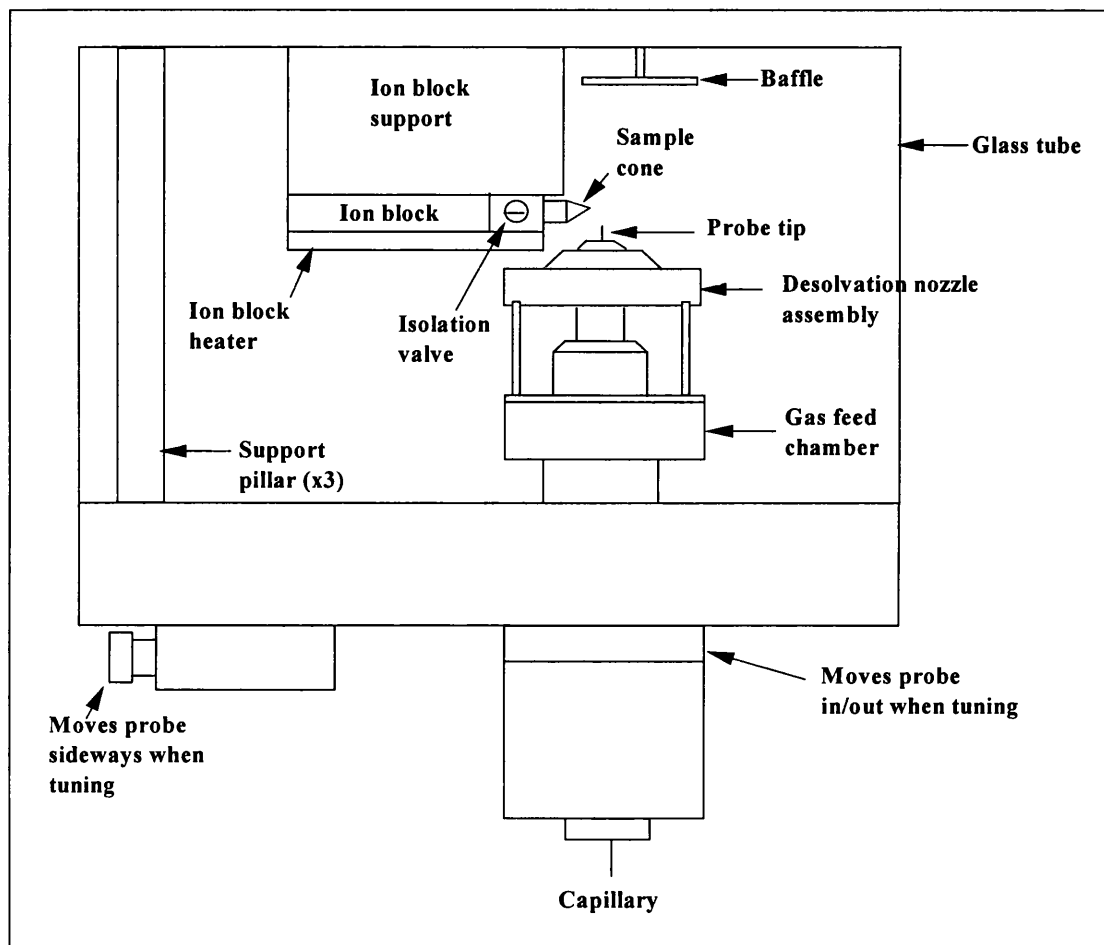


Figure 2.02: Schematic of the 'Z-Spray' ion source

2.2.3 Ion Guide Interface to the Time-of-Flight Mass Analyser

Ions which have entered the ion block region from the source are then subject to an extraction cone voltage of 7-12 volts, (refer to Figure 2.02). The ion block region is maintained at a pressure of approximately 1mbar. The extracted ions then enter the first region of the mass spectrometer, (refer to Figure 2.01), where ions are introduced into the first hexapole ion guide which uses only rf voltages to transfer the ions towards the ToF analyser. The hexapole lens consists of six circular rods arranged in a hexagonal pattern. The rods are charged alternately positive and negative using only rf voltages applied to all six rods. The ions are then transmitted to the second region of the mass spectrometer, (refer to Figure 2.01). Here a second hexapole ion guide is employed again employing rf-only voltages, to transfer the ions.

These ions are then guided into the TOF analyser, the third region of the instrument which has a pressure $\leq 1 \times 10^{-6}$ mbar (refer to Figure 2.01). For the successful transfer of the ion beam to the orthogonal region acceleration region, also known as the 'pusher' region, in the ToF analyser various ion optical voltages have to be tuned.

A fast rising (~ 10 nsec risetime) voltage, V_p is applied to the pusher which pulses a portion of the continuous ion beam in a direction orthogonal to the incoming ion beam axis. These ions then pass down the ToF tube to a reflectron and return towards the detector region (refer to Figure 2.01) and are detected by a micro channel plate (MCP) detector.

2.2.3.1 Radio frequency (RF) only ion guides

Ion optical devices based on symmetrical arrangements of parallel rods such as, quadrupoles, hexapoles and octapoles can be used as ion guides to transfer and collimate an ion beam. To transmit ions, independent of mass, rf-only voltages are required to be applied to the rods. They are commonly referred to as multipoles lenses. Multipoles are precisely engineered devices and have $2p$ electrodes ($p = 2,3,4\dots$) where p is the number of pairs of poles [25]. Multipoles using rf voltages only, play an important role in guiding and confining the ion beam from one part of the mass spectrometer to another.

The use of a quadrupole as an ion guide operating in the rf only mode has been applied to triple quadrupole ($Q_1q_2Q_3$) mass spectrometers where the central quadrupole (q_2) acts as an ion guide [26-28] for collision induced fragments. This quadrupole is used as a collision cell when filled with gas at a suitable pressure, to conduct low-energy collision induced dissociation (CID) experiments. Quadrupoles have also been used in multistage hybrid mass spectrometers [29-32] and in this and the $Q_1q_2Q_3$ design the rf-only quadrupole is used to collimate the ion beam, which has low kinetic energy, usually below 100eV. A thorough investigation of the transmission and collimation of ion beams using rf-only mode of operation in a quadrupole has been carried out by Dawson and Fulford [28].

The transmission and confinement of ion beams in an octapole operating in the rf-only mode was researched over two decades ago by Teloy and Gerlich [33].

Both research and commercial mass analysers have employed multipole lenses of some sort, to guide and transfer ions in the rf-only mode of operation [34-40]. They are usually employed on low energy ion beams and have been used in conjunction with a buffer gas that collisionally focuses the ions towards the central axis of the multipole. The buffer gas acts to damp the radial velocities of the ions, while the rf field constrains them close to the axis of the multipole [41] and is referred to collisional focusing. The technique employed is based on ideas of Douglas and French [42].

Investigative studies by Hagg and Szabo [25] suggest that the use of a hexapole or octapole as an ion guide, is better suited for ion beam collimation and transmission in the rf-only mode, than a quadrupole. The order, p , of the multipole lens is a measure of the effectiveness of ion transmission through the ion guide. The higher the order, the sharper the field boundary is near to the rods resulting in better ion containment. The choice of the multipole for the ion guide will depend on the application, specifically influenced by the ion energy and initial ion velocity.

To successfully transfer ions produced in the ion source to the ToF analyser in the LCT, two hexapole ion guides were used to guide and collimate the ion beam.

As the hexapoles are operated in the rf-only or total ion transmission mode, there is no mass separation and the hexapole acts as a powerful focusing lens. However, depending on ion energy, rf frequency and the rf voltage applied to the hexapole lenses, there is in practice a low mass cut-off. Low mass ions will oscillate to a higher

extent than higher mass ions, and if the voltage is too high, the ions will collide with the rods instead of being transmitted [43].

2.2.3.2 Hexapole interface voltages

Initial studies involved compounds with molecular weight lower than m/z of 1000. It was noticed that the rf lens voltage had a major influence on ion transmission. Results showed that when a rf voltage of between 400-500 volts was applied to the lens assembly no low mass ions (lower than $\sim m/z$ 100) were observed in the mass spectrum. In order to observe low mass ions, the rf voltage amplitude needs to be lowered.

When high mass work was being carried out in the range of $m/z > 1500$ the rf voltage was increased from 100 volts to usually 200 or 300 volts.

Thus, careful consideration of the applied rf voltage, which in our investigation was molecular weight dependent, should take place prior to data acquisition.

2.2.4 Orthogonal Acceleration source

2.2.4.1 Introduction

The growing interest in ToF mass spectrometry over the last decade owes much to the production of ion beams from pulsed laser ion sources. These sources are ideally suited for the ToF technique, which require a pulsed source of ions with a well defined starting point in time and space.

ToF instruments coupled to continuous ionisation sources such as EI, chemical ionisation (CI), and more recent API do not immediately form a suitable partnership due to their 'continuous' nature and their initial spatial, temporal and energy dispersions of the ions prior to entering the ToF drift tube. [44-45].

The spatial dispersion arises from the different positions of the ions, within the source, before they are pulsed into the ToF region. Temporal dispersion occurs due to the creation of ions at different times within the source and due to the 'turnaround' time for ions initially travelling away from the exit grids. The energy dispersion is due to the Maxwell-Boltzmann distribution, since the ions formed in the source move with velocities that are dependent on temperature and mass.

These initial dispersions cause the instrument to suffer poor resolution because of the range of flight times for isobaric ions. Thus, fitting a ToF instrument with a source that continuously produces ions does not provide such a straightforward partnership as with a pulsed source.

Addressing these initial dispersions apparent with continuous ionisation sources with the intention of increasing the resolution of the instrument whilst maintaining the sensitivity advantage of ToF mass analysers has to be made prior to ToF analysis. In the 1950's Wiley and McLaren [44] devised a pulsed dual stage ion source with dimensions and voltages optimized for overcoming these initial dispersions. Their initial ideas and concepts set the foundation on which 'orthogonal accelerator' designs of modern ToF mass spectrometers are presently based.

Wiley and McLaren introduced a concept known as 'time-lag focusing' in order to overcome the initial energy distribution in their dual stage ion source. Here, there is a delay between the ionisation and acceleration of ions. The method did improve mass resolution but the simultaneous focusing of spatial and energy distributions was not achieved to a high degree. A disadvantage of time-lag focusing is that it is mass dependent, so only a small mass range can be sampled at any one time.

Lubman *et al.* [46] have developed an ESI ion trap/ToF instrument which has been used to store ions in a RF quadrupole ion trap before being pulsed as a packet into the ToF analyser. The energy spread of the ions is reduced in the trap through collisional cooling when helium gas is supplied to the trap. The instrument however offers only moderate resolution of 1500 full-width at half maximum (FWHM).

Wollnik *et al.* [47-48] have also employed pulsed extraction on their ToF instrument which has been fitted with an EI source. The ions are pulsed as packets into the ToF

analyser which contains a gridless reflectron. The concept of a gridless reflectron although giving increased ion transmission has poorer performance in terms of mass resolving power compared to a conventional grided reflectron [49]. Mass resolution of around 3000 (FWHM) was obtained on this type of instrument. A disadvantage of the gridless design is that the field equipotentials in the reflectron, particularly at the entrance are curved, and may be the reason why greater mass resolving power was not reported.

The coupling of continuous ionisation sources with ToF mass spectrometers utilising the methods mentioned above have not gained the success which orthogonal acceleration [50-54] has achieved. As this is a method which effectively eliminates the initial kinetic energy distribution or more precisely the velocity distribution along the ToF axis (y-axis). It pulses sections of the ion beam from a continuous ion beam into the ToF analyser and improves mass resolution and the effective duty cycle when compared to other designs. This particular method of gating the ions was employed in the LCT. Duty cycle, mass resolution and abundance sensitivity are all increased through the coupling of orthogonal acceleration sources [50-54], together with the employment of collisionally cooled rf only ion transfer multipoles [42], to ToF instruments utilizing continuous ionisation sources.

2.2.4.2 Application of orthogonal acceleration in the LCT

The formation of ions within the atmospheric pressure 'Z- spray' source is continuous. An extraction voltage is applied to the ion block region (refer to Figure 2.02) which accelerates the ions into the rf ion guide region of the mass spectrometer. After traversing the two ion guide regions the ions are focused and steered into the orthogonal or pusher region (see Figure 2.01) through a series of lenses.

The orthogonal accelerator, is essentially an electrode and a series of grids which pulses a portion of the continuous ion beam at a right angle (see Figure 2.03) to the main ion beam axis (x-axis).

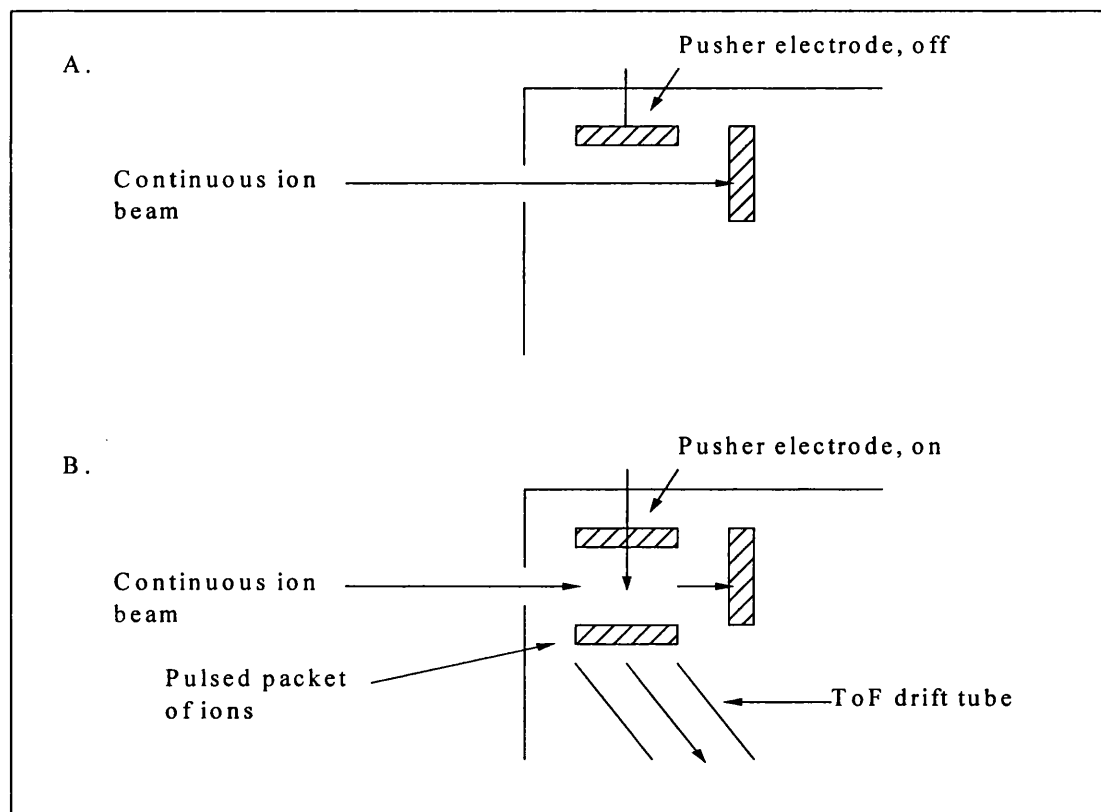


Figure 2.03: Illustration of the pusher [55].

When the pusher electrode is switched off (refer to Figure 2.03) the ion beam fills the orthogonal accelerator region.

Once a potential has been applied to the pusher electrode, which lasts approximately $10\mu\text{s}$, a portion of the main beam is pulsed along the y-axis.

The time-of-flight of the ions is measured from the time the pulse was applied to the orthogonal accelerator, to the time ions reach the detector.

2.2.4.3 The orthogonal accelerator employed in the LCT

The orthogonal accelerator used in the LCT is a dual stage pusher as shown in Figure 2.04. The design of the orthogonal acceleration source is based on principles and ideas of Wiley and McLaren [44].

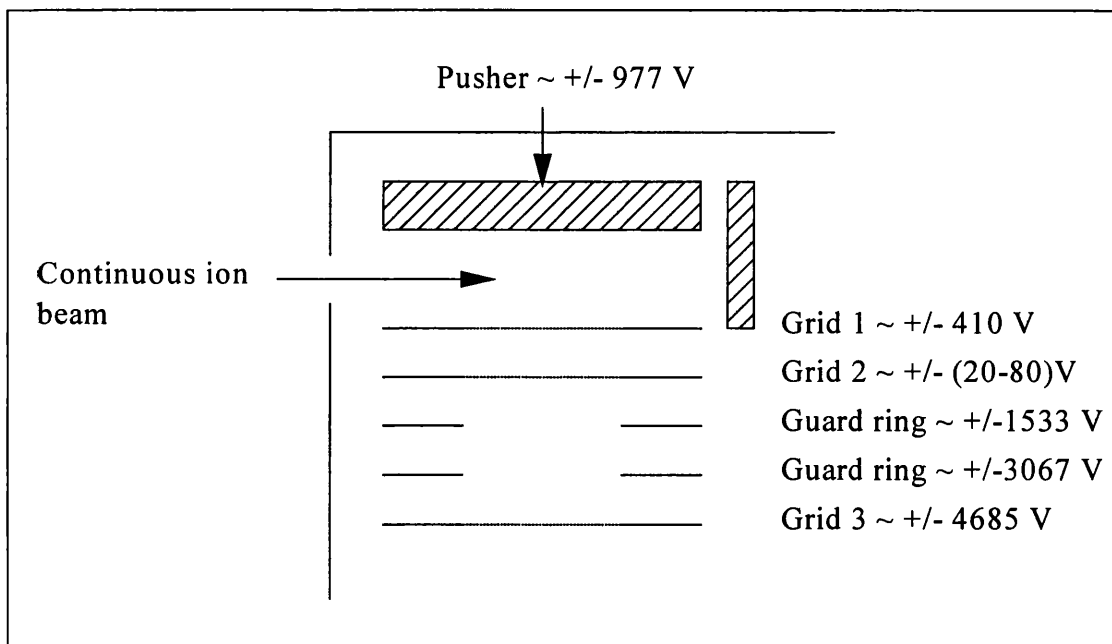


Figure 2.04: Schematic of the orthogonal accelerator showing its voltages

The orthogonal accelerator has two modes of operation, 'fill-up' mode and 'push-out' mode. During 'fill-up' mode the pusher plate and the first grid are at set at zero potential. During 'push-out' mode the voltages applied to each electrode have to be precisely set to certain calculated values to achieve simultaneous space and time focusing and are given in Figure 2.04. The ratio of the filling time of the pusher region, which is dependent on the velocity of the incoming ions, and the time between pulsing, which is dependent on the m/z of the heaviest ions under investigation, defines the duty cycle [56]. The duty cycle for the LCT is estimated to be 20% [57]. The exact dimensions of the orthogonal accelerator are unknown because the manufacturer has not supplied this technical information. The pusher voltage is approximately +/- 977 volts with a risetime of ~ 10 nsecs and a duration around 10 μ secs. The pusher can be operated at a maximum repetition rate of up to 20kHz, therefore 20,000 spectra/s can be collected and summed. This corresponds to a full mass spectrum being recorded by the MCP ~ every 50 μ secs.

The ions traverse the orthogonal accelerator region through a linear electric field and accelerated orthogonally through three transmission grids into the ToF drift region with a final acceleration voltage of +/- 4685 volts plus ~ 60% of the pusher pulse voltage, therefore acquiring a final voltage of ~ +/- 5300 volts. The ions travel down the ToF drift tube until they are reflected by an ion mirror which serves to correct for the energy spread of isobaric ions. Once reflected the ions are detected by an MCP detector. The total effective distance the ions travel from the orthogonal acceleration region to the detector is estimated to be ~ 1.19 metres [57].

2.2.5 Reflectron ion mirror

Situated at the other end of the flight tube, away from the orthogonal accelerator, (see figure 2.01) is a device called a reflectron or ion mirror. It makes use of a retarding electric field to reflect ions that have been pulsed from the orthogonal accelerator. The ions travel back through the reflectron towards the micro channel plate (MCP) detector which is placed on the same plane as the orthogonal accelerator.

The device itself is based on ideas and principles of Mamyrin *et al.* [58] which was used to provide energy focusing, particularly when ions have a large energy distribution.

The reflectron employed in the LCT is constructed from a series of ring shaped electrodes, with the first and last electrodes being grided. The name given to this type of reflectron is termed single-stage, as it has one linear field.

The reflectron compensates for an initial kinetic energy distribution of the ions in the flight tube after they have been pulsed by the orthogonal accelerator. In circumstances where the energy spread is large the resolving power would be very poor without such a device. When the energy distribution is small the reflectron has little influence except that it effectively doubles the path length compared to a linear ToF of similar dimensions.

The underlying physical principle on which a reflectron operates is simple. Consider two ions of equal mass, but with different velocities that have been pulsed by the orthogonal accelerator. The ion with the greatest velocity (energy) will travel faster and reach the reflectron first. This ion will penetrate the repelling electric field to a greater depth than the slower ion. It will therefore spend a longer time in the reflectron.

By carefully considering the potential applied to the ring electrodes the slower ion will turn around and exit the reflectron before the more energetic ion. The more energetic ion catches up with the slower ion in the field-free region beyond the reflectron and the detector is placed here. This is termed energy focusing and provides a substantial increase in mass resolution for ToF instruments when a large energy spread is involved, for example, laser desorption.

When data is being acquired on the LCT the first electrode of the reflectron is set at the same potential as the final grid on the orthogonal accelerator, this is +/- 4685 volts. The other electrodes provide a linear retarding field gradient and the maximum potential supplied to the back of the reflectron is + 1800 volts or - 1802 volts depending on which ionisation mode the acquisition is being performed under.

2.2.6 Ion detection system

2.2.6.1 Introduction

In mass spectrometry ions of interest are usually detected by techniques based on secondary electron emission (SEM) making use of electron multipliers or micro channel plates (MCP) detectors which amplify the signal typically by 10^5 - 10^7 for single ion detection. These type of detection systems are ideally suited to mass spectrometers such as quadrupoles, sectors and ToF.

The detection of ions can further be broken down into two groups, those which detect ions successively at one point, called point ion detectors and those which detect ions at the same time along a focal plane, called multi point detectors. The LCT made use of a multi point detector called a micro channel plate (MCP).

2.2.6.2 Micro Channel Plate (MCP)

MCP's are the key detection element used in TOFMS. The sub-nano second temporal response time, high gain, high dynamic range and low noise characteristics have made them the preferred detector in all TOFMS applications.

The MCP is composed of an array of 10^4 to 10^7 capillary type electron multipliers parallel in position to each other. Each channel has a diameter in the range of 10-

25µm and are approximately 40-100 times greater in length than their diameter. The inner surface of each channel is coated with PbO glass which readily emits secondary electrons when struck by incident ions. A potential difference is placed across the MCP to cause electrons to accelerate from one side to the other. The top surface, the cathode, is held at a negative voltage and the bottom surface, the anode, is held at a positive voltage. Thus, having a negative charge, the electrons within the MCP accelerate towards the anode.

Amplification of the signal for a single MCP is typically 10^3 to 10^4 . To maximise the amplification, the first electron emission should occur as close to the channel entrance as possible. For this reason, MCP channels are usually placed at an angle.

Performance and efficiency is also greatly improved by stacking two MCP's on top of each other. The name given to this kind of setup is the 'chevron design' and was used in the LCT. The MCP's are placed on top of one another but with the channels tilted in opposite directions. The shower of electrons from one MCP will enter the channels of the other at an angle, thus improving overall efficiency. The overall gain of a chevron MCP is typically 10^6 - 10^8 .

Modern mass spectrometry is an important technique for the study of biological and polymer macromolecules in the thousand kilo or more dalton mass range. The detectors mentioned above have very low efficiency at very high m/z values.

At these high masses, the incident ions have insufficient velocity to impart enough energy to an electron, on collision, to provide secondary electron emission (SEM).

Several research groups [59-61] have looked at detection methods that extend the mass range capabilities beyond that obtained with MCP's and electron multipliers. One recent design is based on the use of a low temperature particle detector. These cryogenically cooled superconductor-insulator-superconductor (SIS) tunnel junction detector offer 100% detection efficiency for all macromolecular ions. Cryogenic detectors measure the thermal energy deposited by the ions on impact and thus have a sensitivity that is largely mass independent.

It is well documented that ToF instruments have an unlimited mass range. One limiting factor being the currently employed detectors response. The current upper mass limit of ToF instruments could well be extended by the use of cryogenic detectors in the future. Some disadvantages though in using these type of detectors is that they are relatively large in size compared to the MCP's, they operate at very low temperature and have very small apertures.

2.2.7 Vacuum system of the LCT

The vacuum system of the instrument is shown in a simplified schematic in Figure 2.05. It makes use of three turbomolecular pumps. The first pump is an EXT 250 H1 model (pump 1, in Figure 2.05) which provides fine pumping with a capacity of 250 L

s^{-1} to the first hexapole region. The second (pump 2, in Figure 2.05) and third pumps (pump 3, in Figure 2.05) are EXT 70 models which provide a pumping capacity of $70 L s^{-1}$ to the second hexapole region and the time-of-flight analyser, respectively. The backing lines for the three turbomolecular pumps are all connected to a rotary pump E2M28 model which provides rough pumping for the ion source and turbomolecular pumps backing. All pumps were manufactured by Edwards High Vacuum, Crawley, UK.

Monitoring the pressure inside the instrument is made through readings taken from a Pirani Gauge and Penning Gauge. The former measures the pressure in the ion source, for rough pumping, which was typically around 1×10^{-1} mbar and the latter measures the pressure in the time-of-flight analyser, for the turbomolecular pumping, which was typically as stated previously $< 1 \times 10^{-6}$ mbar.

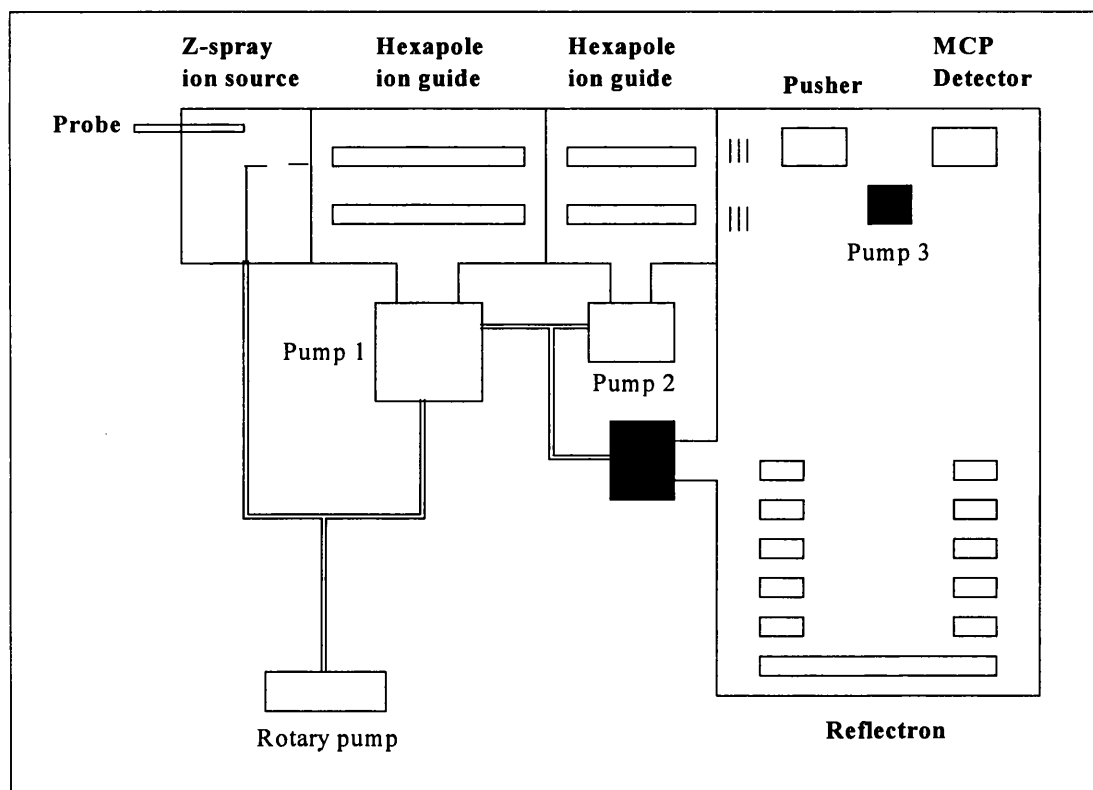


Figure 2.05: Schematic showing position of turbomolecular pumps in the LCT

Section B

Performance characteristics of the LCT

2.3 Investigation of the Performance Characteristics of the LCT Mass Spectrometer

2.3.1 Introduction

Initial experiments on the LCT were aimed at determining the best instrumental settings for achieving high sensitivity and mass measurement accuracy, particularly those concerning the ToF analyser. No operation manuals accompanied the LCT, therefore operating parameters had to be established.

2.3.2 Mass range characteristics of TOFMS

2.3.2.1 Introduction

One of the main advantages of TOFMS is its theoretical unlimited mass range capability. However, in practice the mass range will be limited by the performance of the ionisation technique, the detector employed and the amount of memory that is available to store the vast amount of acquired data that ToF instruments achieve.

The detector sensitivity is less for high mass ions than for low mass ions, since the high mass ions have correspondingly lower velocities, (see section 2.2.6.2).

2.3.2.2 Mass range of the LCT

The first phase of the investigation involved a study to determine the mass range in positive electrospray ionisation mode of a mixture of sodium iodide and caesium iodide salts (BDH Chemicals, England).

A solution of sodium iodide was prepared at a concentration of $2\mu\text{g}/\mu\text{L}$ in 50:50 (isopropyl alcohol) IPA:H₂O. Caesium iodide was added to this solution at a concentration of $0.05\mu\text{g}/\mu\text{L}$. Thus, in positive electrospray ionisation mode, a spectrum of monoisotopic $[\text{Na}(\text{NaI})_n]^+$ singly-charged cluster ions are observed. A little amount of caesium iodide is added to the solution to supply the m/z 132.9 ions in the gap between m/z 22.9 and m/z 172.9.

The NaI and CsI mixture in solution was introduced into the source part of the mass spectrometer directly by means of a $1000\mu\text{L}$ Hamilton (Hamilton Bonaduz AG, Switzerland) gas tight syringe and a Harvard Apparatus (South Natick, MA, USA) Model 22 syringe pump. The flow rate of the solution was kept constant at $50\mu\text{L}/\text{min}$.

The LCT is a highly automated instrument and tuning is carried out entirely through the data system. On infusion of the salt mixture solution the instrument is tuned to give optimum performance before data was acquired.

Optimisation involves tuning source, hexapole transfer voltages and ToF analyser settings. The ToF analyser settings allows the selection of a flight time to be entered.

The flight time then determines the repetition rate of the orthogonal accelerator, which

pulses a packet of incoming ions at a right angle to their initial trajectory prior to entering the orthogonal accelerator. The flight time was varied between 50 μ s and 140 μ s in steps of 10 μ s, which corresponds to a pusher frequency of \sim 20-5 kHz, and the observed mass range noted.

The electrospray source conditions were: capillary voltage of 3500V, sample cone voltage of 30V, extraction cone voltage of 3V, source temperature of 100°C and desolvation temperature of 150°C. The only parameters that were changed during the study, after optimisation of the first acquisition, was extraction cone voltage which was varied between 3-10V and rf lens voltage which was varied between 100-350V.

Data acquisition was performed in the continuum mode and was used throughout the study. In this mode, data is stored for every scan acquired. A scan time of 1s and an interscan time (time between a scan finishing and the next one starting) of 0.1s was selected. Three hundred scans were collected in total. The following table (table 1) and graph (Figure 2.06) show the flight time, t plotted against the observed and theoretical masses for ions acquiring approximately 60% of the pusher potential.

Flight time (μs)	Observed m/z	Theoretical m/z
50	1704	1804
60	2470	2597
70	3379	3535
80	4450	4617
90	5625	5844
100	6982	7215
110	8445	8730
120	10050	10389
130	11800	12193
140	13500	14141

Table 1

The theoretical m/z ratio is calculated from the simple ToF equation, where:

$$t = D \times [(m / (2 z e V_{acc}))^{1/2}]$$

t = time

D = distance travelled by the ions

m = mass

z = number of charges

e = electronic charge

V_{acc} = acceleration voltage

The effective distance travelled by the ions from the time they are pulsed until the time they are detected is ~ 1.19 metres. The acceleration voltage the ions obtain on exiting the orthogonal accelerator is constant and kept at 4685V. These ions however gain an additional percentage of the voltage applied to the pusher plate of the orthogonal accelerator. Therefore, the final voltage the ions obtain on entry to the ToF drift tube is approximately 5300V, which is about 60% of the pusher plate voltage [57].

Thus, for example, if the user sets a flight time of 50µs then the theoretical m/z ratio would be m/z 1804.

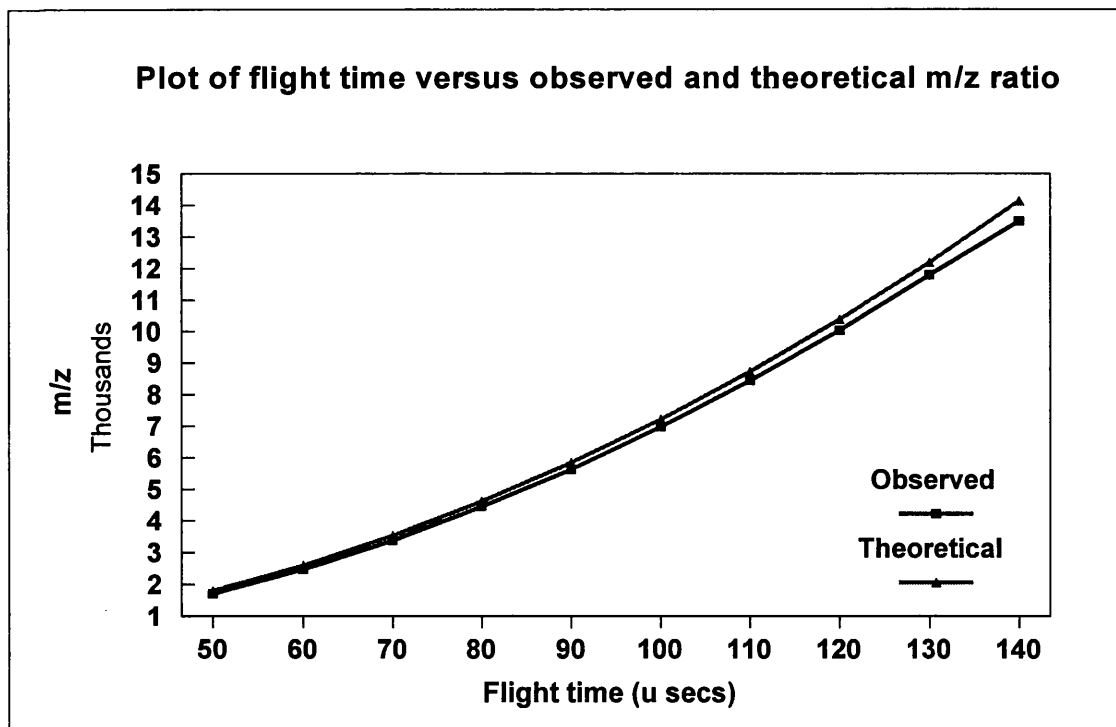


Figure 2.06: Plot of flight time, t against m/z for observed mass and theoretically calculated masses for ions acquiring approximately 60% of the pusher potential.

A mass spectrum obtained from injection of the sodium iodide and caesium iodide mixture (discussed previously), acquired on the LCT is shown in Figure 2.07 (top). As can be seen from the uncalibrated mass spectrum, in which the y-axis has been expanded, singly charged ions approaching m/z 13000 are readily detected by the MCP on the LCT.

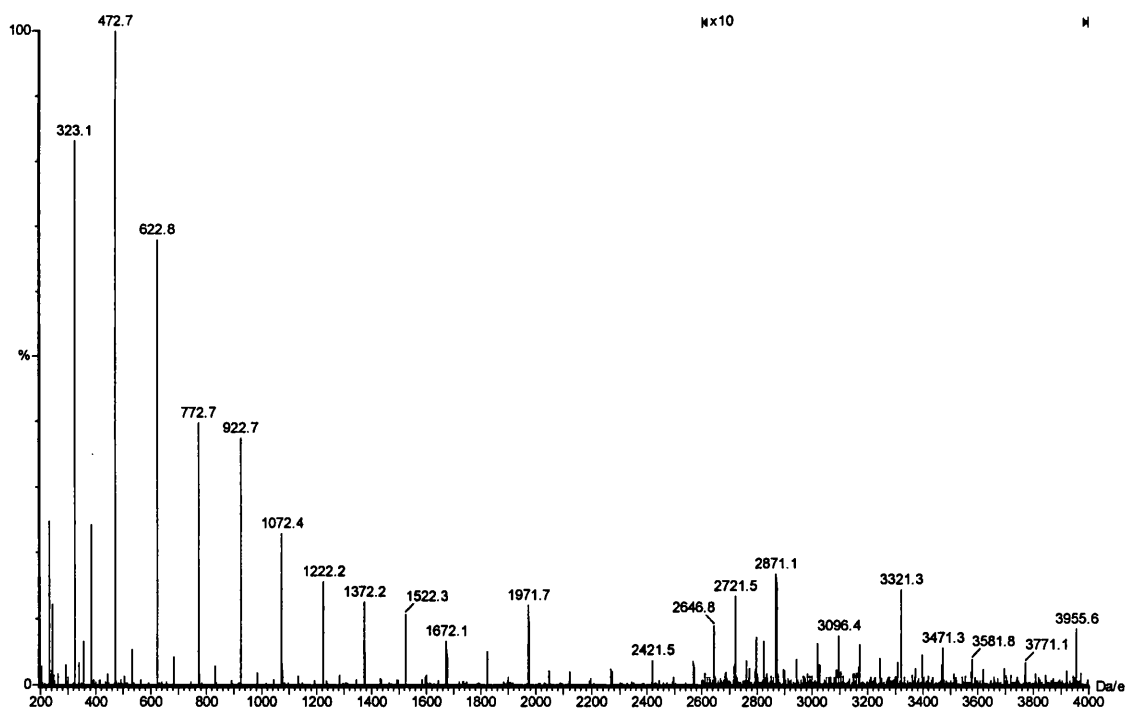
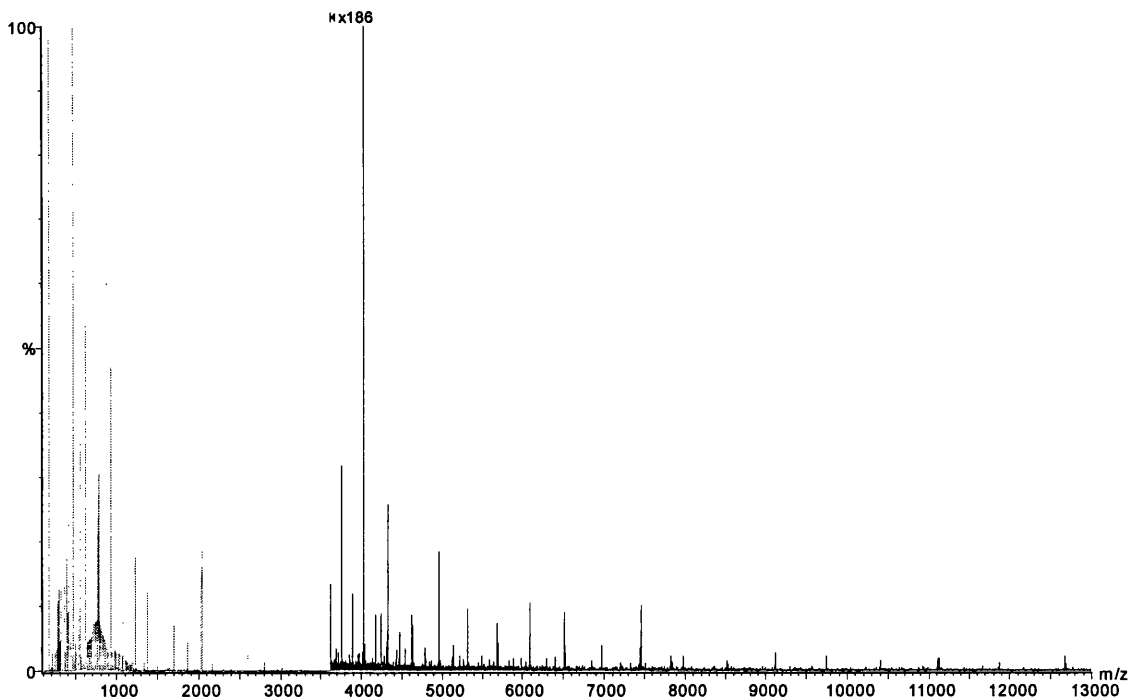


Figure 2.07 : Mass spectrum of a NaI/CsI mixture, showing mass range capability of LCT (top) and Quattro II (bottom)

The detection of singly charged ions observed on the LCT is over three times greater than that obtained on a quadrupole instrument. The comparison is shown in Figure 2.07. The highest achievable mass range for singly charged ions obtained on a quadrupole (Quattro II) is shown in Figure 2.07 (bottom). This spectrum shows $[\text{Na}(\text{NaI})_n]^+$ clusters observed up to $m/z \sim 4000$. Optimum operating conditions for the Quattro are discussed below:

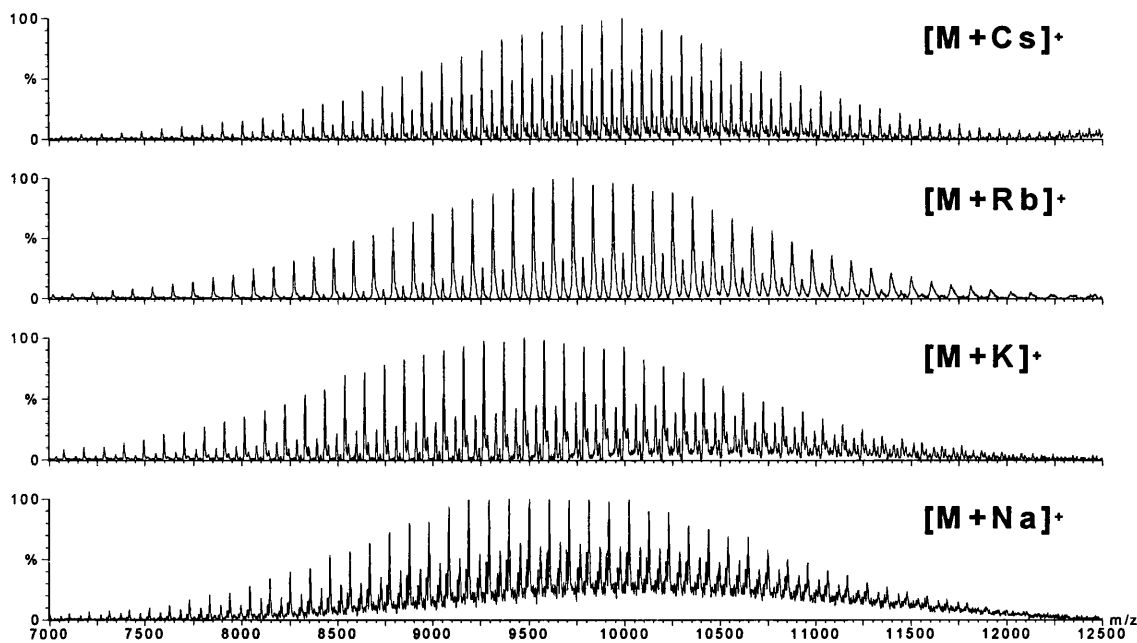
A NaI solution was made to concentration of 10 ppm in IPA:H₂O (50:50). This solution was then injected via a 20 μL loop injector into a MeOH:H₂O (50:50) solvent flowing at 20 $\mu\text{L min}^{-1}$ into the ESI source.

ESI conditions were, capillary voltage of 3500V, sample cone voltage of 40V and source temperature of 70°C. Data acquisition was performed in continuum mode over a mass range of m/z 200-4000, with a scan time of 8s with an interscan time of 0.01s. The number of points per dalton was set at 8.

The extended mass range capability of the LCT as shown in Figure 2.07, means that the instrument can be used to study systems of far greater complexity and molecular weight than quadrupole based systems.

An example, which demonstrates this fact, is given by the study of synthetic polymer distributions [62]. In these systems the molecular weight distribution and mass accuracy of individual oligomeric species are very important parameters to be determined. These

ESI spectra of PS 9850 on LCT



ESI spectra of PS 3050 on Quattro

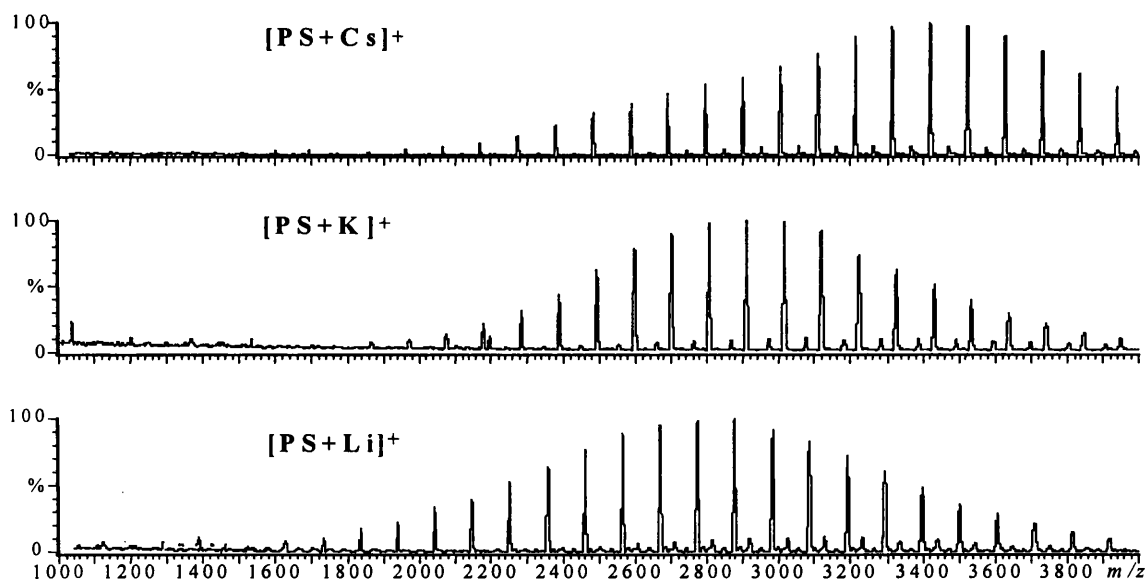


Figure 2.08: Mass spectra obtained on the LCT and Quattro instruments illustrating the greater extended mass range achievable with the LCT

systems have a large number of components covering a wide mass range and a high dynamic. Significant success has been obtained in the study of these particular systems using MALDI-ToF and it is interesting to compare these results with those obtained using ESI. Interfacing ESI with quadrupole mass analysers however does not provide a high enough mass range especially since many of these synthetic systems form singly charged ions in ESI. There are experimental difficulties in obtaining these polymeric distributions, which are mainly associated with choice of solvents and cations used to aid ionisation efficiency.

Figure 2.08 shows the limited mass range of the Quattro II, quadrupole mass analyser and the extended mass range of the LCT [62].

These polystyrene standards were dissolved in 50:50 (DMF:THF) to concentration of 10mg/mL. The alkali metal salts were dissolved in 50:50 (DMF:THF) to a concentration of 10mg/mL. The two solutions were then mixed at a ratio of 9:1 (Polystyrene:salt). This solution was then injected via a 20 μ L loop injection into a stream of 50:50 (DMF:THF) flowing at a rate of 30 μ L/min into the ESI source.

The average molecular weight distribution detected on the Quattro instrument increases with increasing cation size. This difference is also apparent on the LCT. It is known [62] that when the cone voltage is increased, the clustered adduct ions observed in the LCT spectra are reduced, thus affecting the overall spectrum distribution.

2.3.3 Calibration

2.3.3.1 Introduction

Whatever analytical instrument is used for experimental studies, the need for calibration is paramount prior to data analysis. Therefore, the LCT was properly calibrated to give the best mass accuracy measurements prior to acquiring data. Calibration required a suitable sample calibrant that gave a series of ions covering the mass range of interest. A suitable calibrant used for the LCT was found to be a mixture of NaI and CsI, (since it can be easily removed from the source) prepared at the same concentration as discussed previously in section 2.3.2.2. Upon calibration the mixture in solution is introduced into the source region of the mass spectrometer either by direct infusion or by means of a loop injection.

2.3.3.2 Calibration procedure

A mass spectrum of the halide salt mixture in solution was provided by direct infusion at a rate of 30 μ L/min is shown in Figure 2.09, with the same apparatus employed in section 2.3.2.2. Calibration data was acquired typically over a mass range of m/z 100-1000 with a scan time of 1s and an interscan time of 0.1s.

Electrospray source conditions were: capillary voltage of 3500V, sample cone voltage of 10V, source temperature of 100°C and desolvation temperature of 150°C.

The rf lens voltage was set at 200V and the flight time of ions entered as 75 μ s, which corresponds to a pusher frequency of \sim 15kHz.

When the sample is injected via a loop injection a 'peak' arises in the total ion chromatogram (TIC) where each point on the peak gives a mass spectrum. When the sample is directly infused no peak is observed, normally just an horizontal line, where each point on the line gives a separate mass scan.

The acquired uncalibrated mass spectrum of the halide mixture, is then matched against a table of known masses of the peaks in the reference compound which is stored as a reference file in the computer software. Each peak in the reference file is then matched to the corresponding peak in the uncalibrated acquired mass spectrum.

The mass differences between the reference compound and the calibrant are used as calibration points through which a calibration curve is drawn. The vertical distance of each calibration point to the curve is also calculated. This represents the residual mass error after calibration and the lower the residual values are the better.

Once an acceptable calibration has been performed, ie. to within 0.1 Da for nominal mass and to within 3 mDa for accurate mass the data is saved as a calibration file and applied for future acquisitions. A calibration report is then produced, see Figure 2.10.

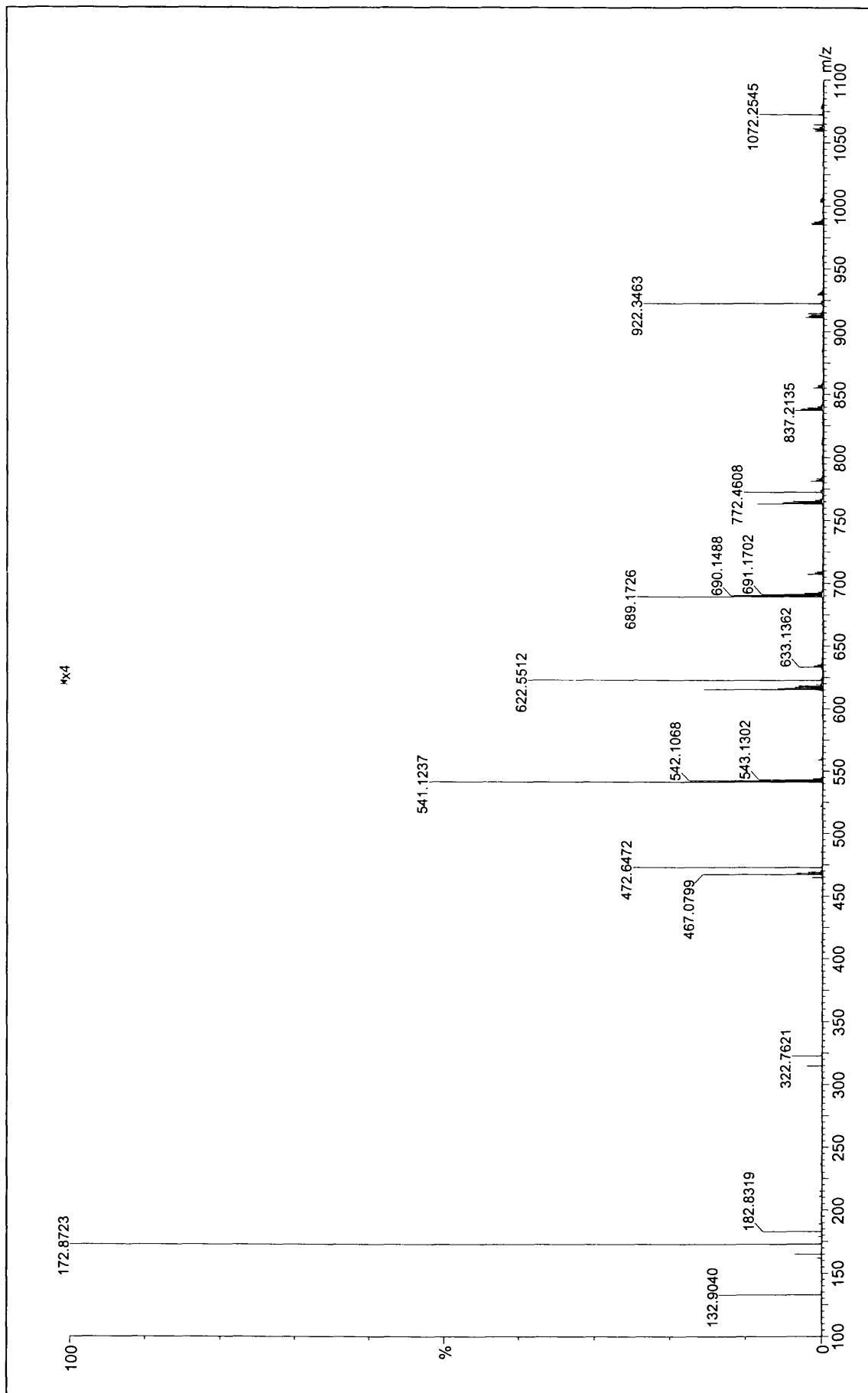


Figure 2.09: Mass spectrum of NaI/CsI mixture

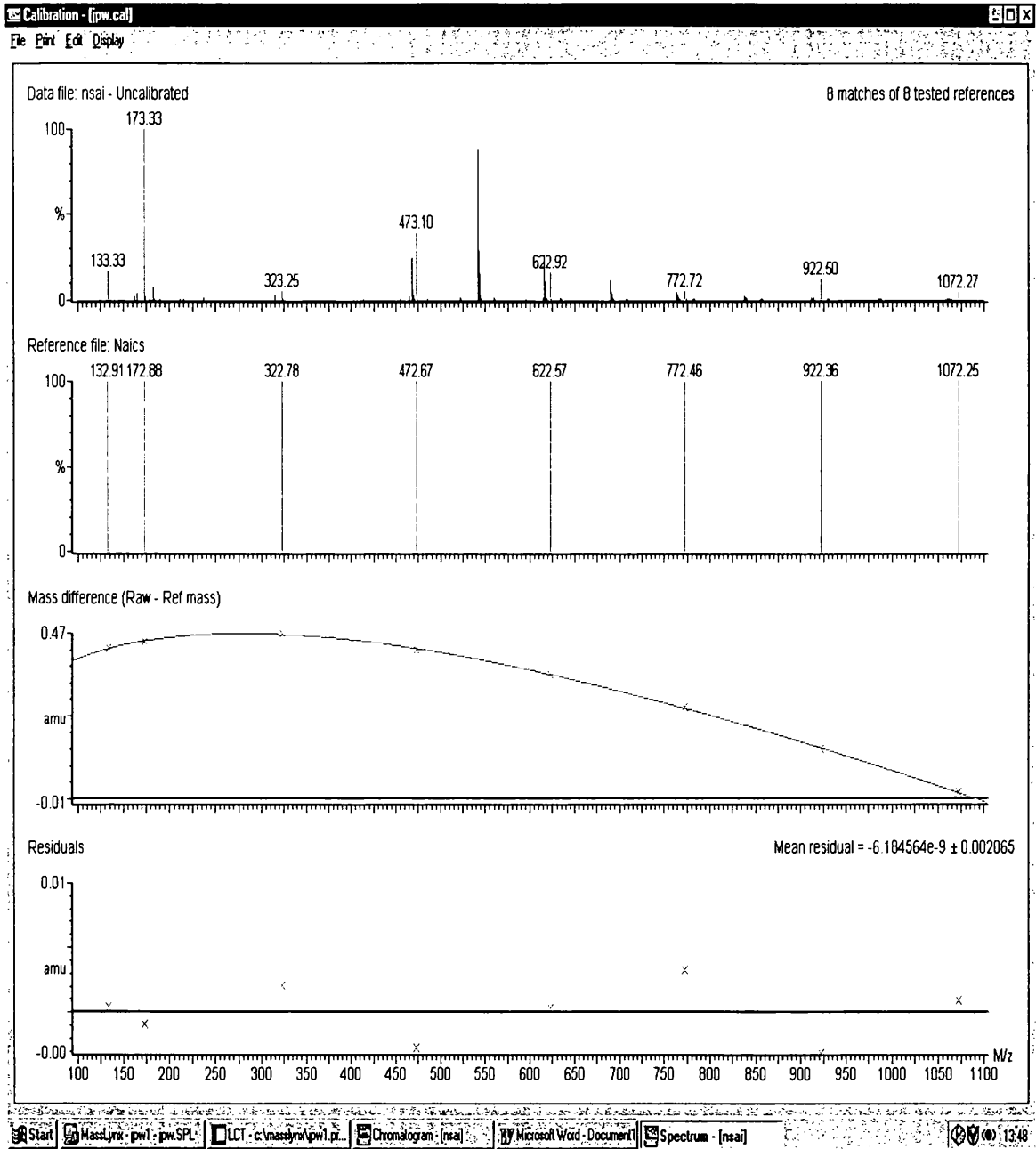


Figure 2.10: Calibration report

If, however instrumental voltages were altered with regard to the voltages of the saved calibration file, a new calibration file would have to be set up otherwise inaccuracies in mass measurement accuracy would result.

2.3.4 Investigation of the Mass Resolution Performance

2.3.4.1 Introduction

Generally, resolution is limited by the initial, spatial and energy dispersions in the y-direction (direction of orthogonal pulse), as discussed previously in section 2.2.4.

Ions that have different spatial positions in the y-direction in the orthogonal accelerator can be focused onto a point just outside the accelerator, providing spatial focusing. At this point the spatial spread is decreased but the energy spread is dominant.

Optimisation of resolution in the reflecting geometry mode, as in the LCT, can be achieved by placing the space focus point just beyond the accelerator, by careful choice of voltages applied to the accelerator. This point then serves as the object plane for the reflectron. At this plane there will be a range of energies, due to the energy spread of the ions gained during acceleration. This energy spread though is overcome by the single-stage reflectron employed in the LCT, which provides first order space focusing.

2.3.4.2 Resolution of the LCT

A peptide known as Melittin, a bee sting extract (MW 2844.754 Daltons), was used to measure the resolution of the instrument. Melittin was directly infused at a rate of 20 μ L/min into the source region of the mass spectrometer at a concentration of 10ppm in 50:50 acetonitrile:water and 0.2% formic acid. The acquisition was performed in positive electrospray ionisation mode.

Electrospray source conditions were: capillary voltage of 3500V, sample cone voltage of 60V, extraction cone voltage of 3V, source temperature of 100 $^{\circ}$ C and desolvation temperature of 150 $^{\circ}$ C. The rf lens voltage was set at 300V and the flight time of ions entered as 50 μ s, which corresponds to a pusher frequency of 20 kHz.

Data was acquired over a mass range of m/z 200-1000 with a scan time of 1s and an interscan time of 0.1s. Three hundred scans were acquired in total.

A characteristic feature of electrospray is its ability to form multiply charged ions. Resolution of the LCT was performed on the multiply charged ions $[M + 3H]^{3+}$, $[M + 4H]^{4+}$, $[M + 5H]^{5+}$. An example of the resolution of the quadruply charged ion is shown in Figure 2.11 (top) and corresponds to m/z 712.18. The calculation of resolution for this ion and the other ions in different charge states, was mass divided by the peak width at half height and found to be ~ 5450 . This resolution can clearly be seen to be sufficient to distinguish separate isotopic peaks that differ by ~ 0.3 Da for this peptide.

The resolution obtained on the LCT can be seen to be far greater than that obtained on the quadrupole instrument (Quattro II). Quadrupole instruments provide unit resolution. The resolution of the quadruply charged ion of melittin obtained on the quadrupole is shown in Figure 2.11 (bottom). Both spectra show an expanded region of the quadruply charged ion.

To obtain maximum resolution on the quadrupole instrument, the following parameters were set, where the mass range of m/z 650-850 was scanned. Capillary voltage 3500V, sample cone voltage 40V and source temperature of 70°C. The mass range was scanned in continuum mode with a scan time of 1s and interscan time of 0.01s. The number of points per dalton was set at 16. The sample solution solvent and carrier solvent was the same as the experimental conditions performed on the LCT.

Although the mass accuracy of quadrupole instrumentation has been well documented to be < 10 ppm, it has been shown that the ability to resolve and mass measure isotopic distributions of < 1 Dalton for the quadruply charged ion of Mellitin can not compete with the LCT.

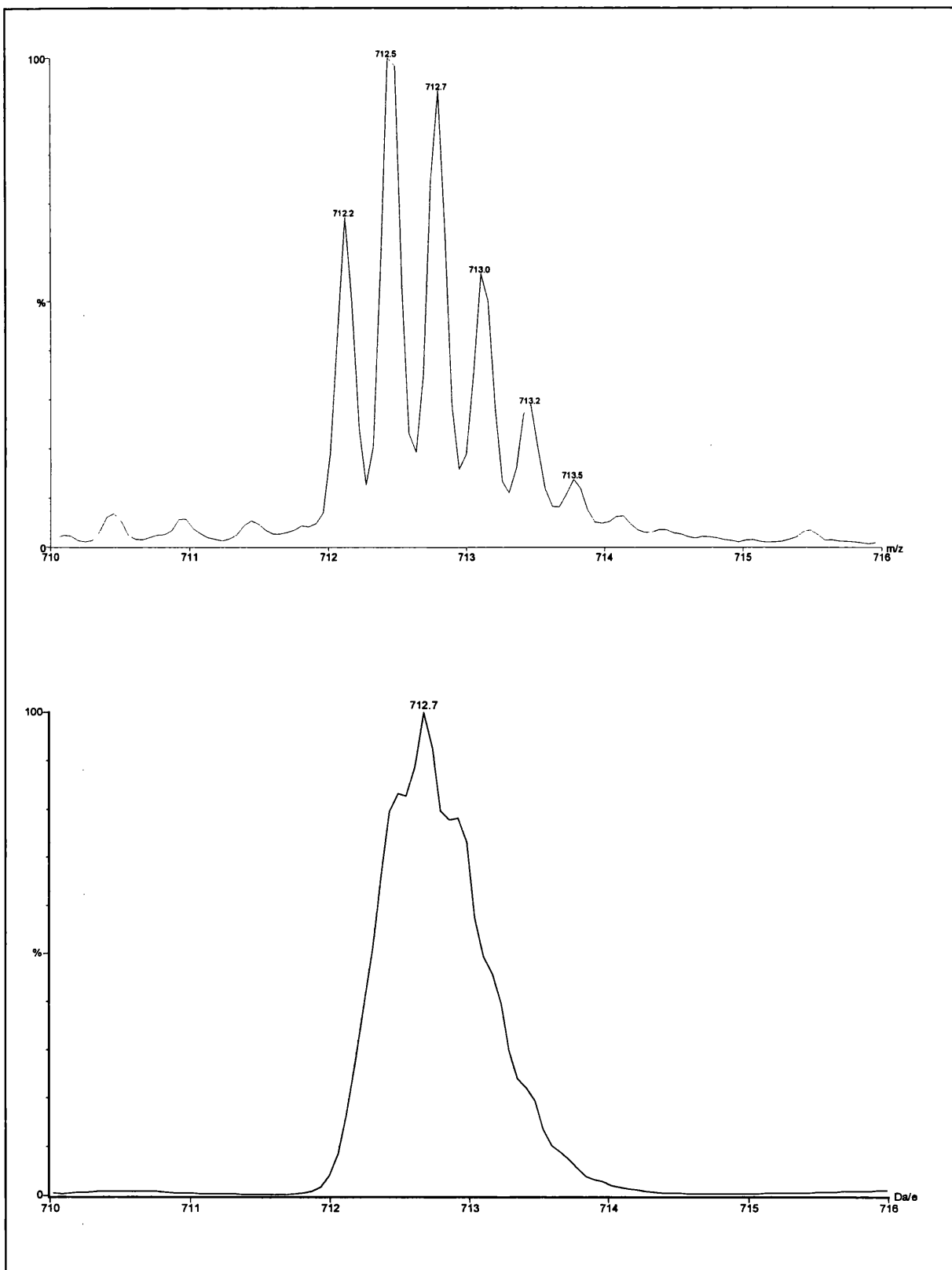


Figure 2.11: Comparison of resolution of $[M+4H]^{4+}$ of Melittin obtained on LCT (top) and Quattro II (bottom)

2.3.5 Determination of Limit of Detection (LoD)

2.3.5.1 Aim

The objective of this section was the determination of the lower limit of detection for Dimethylol propionic acid (DMPA), a polymer additive used in food contact applications.

2.3.5.2 Quantitative analysis

There is not one single universally accepted definition that clearly defines the limit of detection (LoD). Generally, it is regarded as the smallest amount of analyte that can be measured or detected with 'reasonable confidence' above the level of baseline noise. It is up to the analyst to decide what is 'reasonable confidence' through the use of statistical methods.

The application of mass spectrometry provides a suitable analytical method to quantitatively determine a particular molecular species in either organic or inorganic matrices. The LoD is especially important in trace analysis, particularly when the analyst has to decide whether a contaminant is present below or above a legalised limit. In these circumstances the LoD should be approximately an order of magnitude lower than the legalised limit.

Several standards of known concentration, containing the analyte of interest are introduced into the mass spectrometer and the MCP's response recorded as a function

of run time. The response is shown in the form of a peak, in what is called 'The Total Ion Chromatogram' (TIC). The peak area for a given response was determined using the 'integrate' icon from the MassLynx software. The MCP's response for the average area of a sample blank is subtracted from the average area calculated for the sample, which is injected between three and five times. Once the average peak area response is obtained a calibration curve relating the 'Average peak area' versus 'sample concentration' can be produced.

Microsoft Excel was used to construct a 'line of best fit' by means of linear regression which takes the form:

$$y = mx + c$$

where,

m = slope of the curve

c = intercept on the y-axis

An estimate of how well the experimental data points fit a straight line is then given by the correlation coefficient, r^2 through the Microsoft software. A perfect correlation between the plotted x and y values would result in r^2 being equal to 1.

For this study the LoD was calculated by two methods:

Method I: where, the analyte signal : baseline noise is 3:1 and

Method II: where, $L_d = y_b + kS_b$

Here, L_d is the lowest detectable signal, y_b is the blank or baseline signal (intercept), S_b is the standard deviation of the blank values over the range of interest and the

multiple factor k generally equals 3 which was recommended by Kaiser [63] and the American Analytical Methods Committee [64].

2.3.5.3 Repeatability

To demonstrate the repeatability and hence the precision of the integrated areas, a sample of known concentration within the calibration range was injected into the mass spectrometer at least fifteen times to ascertain the percentage relative standard deviation (% RSD).

The repeatability is the closeness of the peak integrated areas between successive results obtained with the same method under the same conditions, that is, the same operator, at the same time on the same instrument.

The % RSD takes the form:

$$\% \text{ RSD} = \frac{\text{standard deviation}}{\text{mean}} \times 100 \%$$

The European Union [65] have drawn up recommendations for the precision of an analytical method and is shown in the table 2 below:

Concentration	% RSD
1 ppm	16
100 ppb	23
10 ppb	32
1 ppb	45

Table: 2

A simple definition for the precision of the fifteen replicate injections would be ‘the closeness of a series of replicate measurements to each other’.

2.3.5.4 Data interpretation

Quantitative measurements are subject to errors. These errors can be random or systematic errors.

Random errors are known to affect the precision or reproducibility of an experiment. This is shown for example, when replicate injections of the same sample are injected but have varying results (varying integrated areas see section 2.3.5.5.3(i)). The imprecise measurements therefore affect the repeatability of the result.

Systematic errors cause the results of replicate measurements to deviate from the true value of the quantity being measured. These errors are said to affect the accuracy of experimental measurements. These errors however would not be observed in the replicate injection study since a ‘true value’ is not known.

Another source of error is due to contamination caused by previously injected samples and termed the ‘carry-over error’. This type of error can be considered a systematic error since its dependent on the test method parameters and depends solely on the concentration of the previous sample.

2.3.5.5 LoD of DMPA

2.7.3.5.1 Aim

To quantitatively determine the LoD in full scan mode for DMPA on the LCT compared to the LoD in the single ion monitoring (SIM) regime on a quadrupole instrument (Platform II, Micromass).

2.3.5.5.2 Single Ion Monitoring (SIM)

An ideal mass spectrometer would sample every ion produced, all of the time. This, though in practical terms, is not possible for a quadrupole instrument.

The acquisition and recording of a single ion current at a selected m/z value is referred to as single ion monitoring (SIM). In SIM mode all other ions are excluded from the analysis and a major improvement in sensitivity over scanning the whole spectrum is observed, since the mass spectrometer will monitor the selected ion 100% of the time. No time is wasted making measurements of the baseline noise between peaks or measuring ions that are not relevant to the analysis.

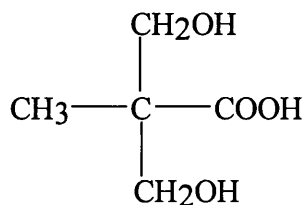
Thus, detection limits in full scan mode on a quadrupole are approximately two orders of magnitude greater than in SIM mode since the instrument spends a limited amount of time at each m/z value during scanning. The LoD level in SIM mode can be achieved in full scan mode by recording all the ions over the full mass range all of the time. Thus, the ions have to be recorded simultaneously which is not possible with a quadrupole instrument.

ToF instruments coupled with a MCP detector and a TDC have the ability to record all the ions over the full mass range for every pulse of ions supplied by the orthogonal accelerator.

It was therefore hoped that the LoD in full scan mode for DMPA on the LCT was equal to that in SIM mode on the quadrupole instrument.

2.3.5.5.3 LoD of DMPA in full scan mode

DMPA, of molecular weight 134, is a monomer used in the manufacture of certain plastic materials, which are intended to come into contact with foodstuffs. Its structure is shown below:



After the plastic product manufacture, the DMPA can remain in the product and could migrate into foodstuffs which come into contact with the food packaging plastic. This could serve as a health risk to humans unless it is carefully monitored since it could be directly or indirectly consumed into the human body.

The additives therefore, that are used for food packaging plastics are well regulated in most countries due to the possibility of health risk. The possibility of migration through the plastic depends on the type of plastic, diffusion properties of the additive, storage temperature and contact time between the plastic and the food.

The manufacturer of the plastic packaging must be made aware of the actual amount the additives migrate into the food. Thus, certain testing and criteria have to be met.

Schwope [66] discusses techniques to study the migration of plastic additives. Migration testing is not directly carried out on the food since it would be problematic to separate and quantitatively measure low concentrations of additives. Therefore, solvents such as distilled water, aqueous acetic acid and aqueous ethanol are used as food simulants.

To meet the criteria set by the European Standards Committee the analysis of DMPA should be quantitatively determined in the concentration range 10 ppb – 100 ppb.

Thus, the LoD of DMPA in,

- (i) 95% aqueous Ethanol
- (ii) 10% aqueous Ethanol
- (iii) 3% acetic acid

was determined.

(i) DMPA (95% aqueous Ethanol)

ESI was carried out in negative ionisation mode. Optimum instrumental conditions were as follows:

Electrospray source conditions were capillary voltage of 3500 V, sample cone voltage of 20V, extraction cone voltage of 7 V, source temperature of 100°C and desolvation temperature of 150°C.

The sample solution was introduced via a 10µL rheodyne loop injection into a stream of 90% ethanol + 10% H₂O + 0.03% NH₃ solvent flowing into the ESI source at a rate of 50µL min⁻¹. A small amount of NH₃ was added to the solution since it promotes the deprotonation of acidic compounds.

The rf lens voltage was set at 100 V and the orthogonal accelerator operated with a frequency of between 10-15 kHz. Data acquisition was performed in continuum mode with a scan time of 1s and an interscan time of 0.1s. Mass spectra was acquired over a range m/z 90-140.

Figure 2.12 shows a typical example of a TIC trace obtained when a blank and 5 sample injections were made at the 100ppb concentration level, which was also the adopted method for analysing all other samples during the study. Figure 2.13 shows the mass spectra obtained over the concentration range of interest, 10-100 ppb. The mass spectra obtained for this sample and all other samples studied during the LoD

investigation was provided by selecting the area under one of the sample response peaks from the TIC in Figure 2.12 and subtracting the response from the blank. This is done manually through the MassLynx software.

The LoD was determined for m/z 133 which corresponds to $[M-H]^-$ the deprotonated molecule.

Data was acquired over the mass range m/z 90-140 since in-source fragmentation produced a large ion signal at m/z 89 due to loss of CO_2 from the deprotonated molecule. The signal for this ion totally suppressed all other ion signals, so a different scan range was used. By decreasing the cone voltage to 3V, it was hoped that this would decrease in-source fragmentation, this though did not prove significant since ion suppression from m/z 89 was still apparent.

The molecular ion m/z 133 was chosen for the following reasons; specificity, higher mass produced lower interference from background ions.

As the concentration is increased it is quite evident from the mass spectra that the $[M-H]^-$ signal becomes more intense. At the lowest concentration level, 10 ppb, m/z 133 is observed together with a tremendous amount of background signal.

The signal at m/z 113 cannot be assigned to be coming from the analyte nor to any solvent clusters that may have formed. It seems highly likely that this ion is present from the previous acquisition, where CO_2 neutral was lost from the deprotonated 2,6-DFBA (m/z 158) molecule. A thorough clean of the source region with 50:50

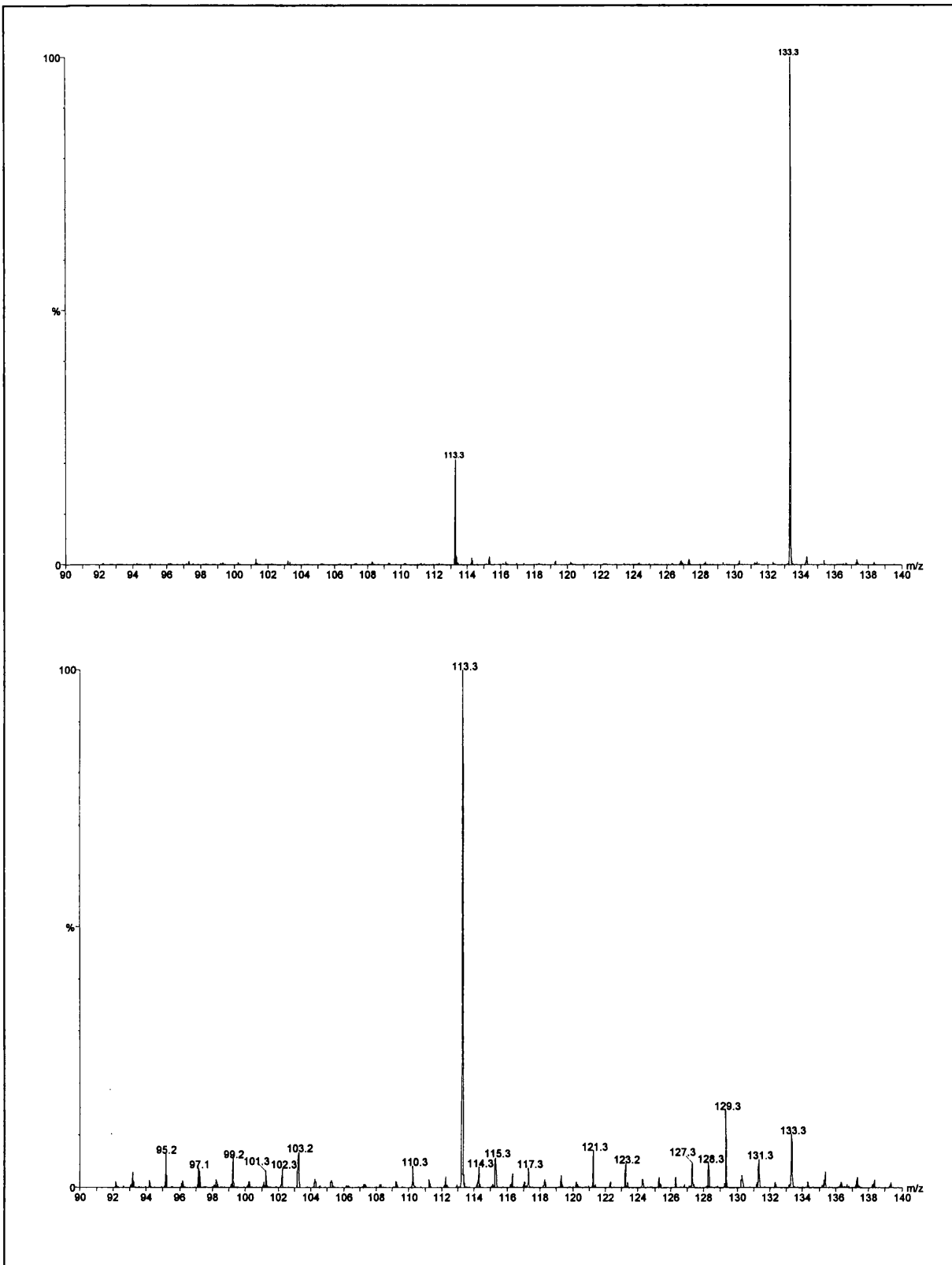


Figure 2.13: Mass spectra at 100 ppb (top) and 10 ppb (bottom) of DMPA (95% aq. EtOH)

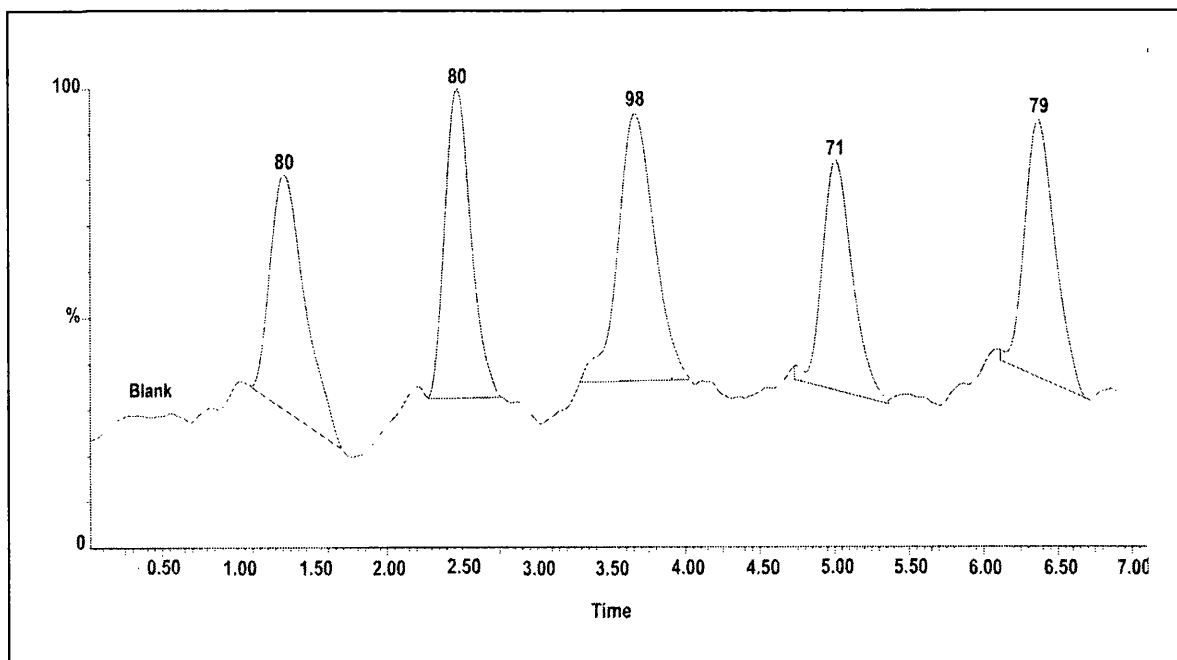


Figure 2.12: TIC from 5 sample injections of 100ppb DMPA (95% aq. EtOH)

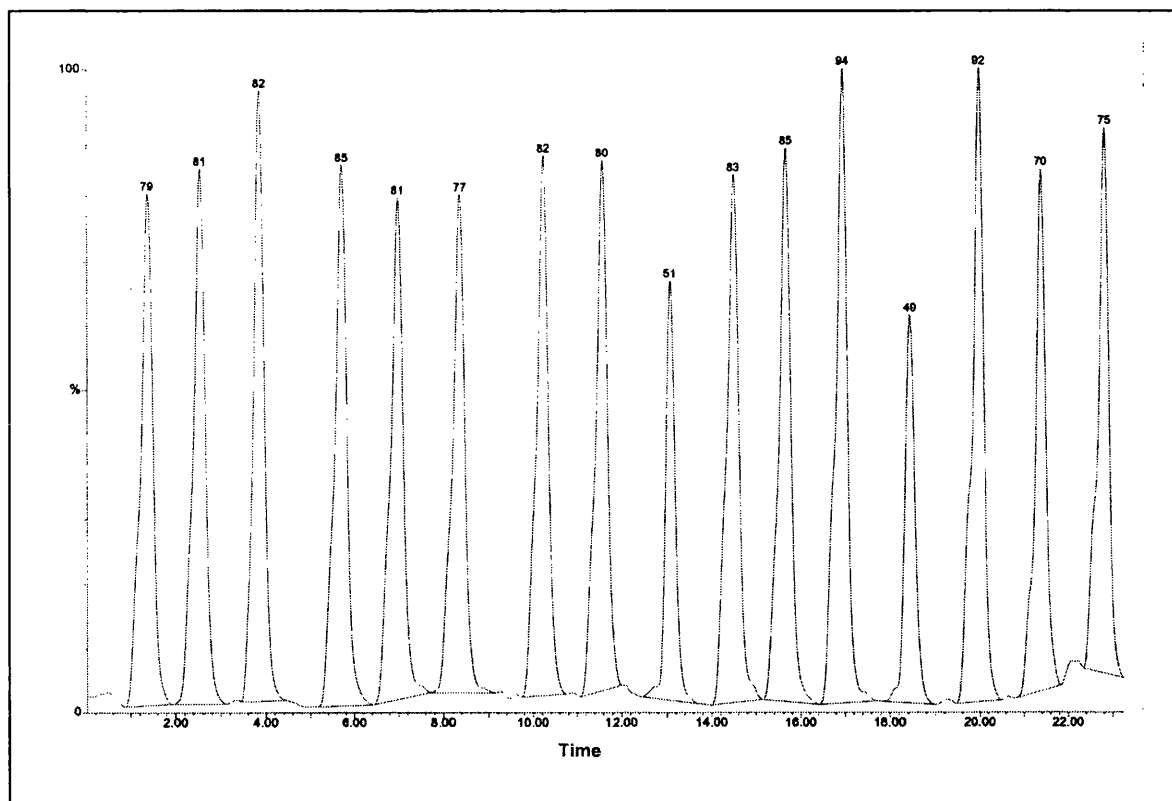


Figure 2.15 : Repeatability study of multiple injections for 100ppb DMPA (95% aq. EtOH)

acetonitrile:H₂O did not prove effective as the ion could still be observed in the mass spectra. The ion at m/z 113 although of greater intensity than [M-H]⁻ at low concentration, did not suppress the [M-H]⁻ signal in the respect that a suitable LoD could not be achieved.

Table 3 below shows the concentration and average area of sample minus average area of blank:

Concentration (ppb)	Area
10	8
25	20
50	39
100	80.6

Table:3

A calibration curve was constructed from this data and is shown in Figure 2.14. The response across the desired range was linear with a regression coefficient of 0.99. The LoD determined by method I where the signal:baseline noise was 3:1 was found to be 10 ppb.

The LoD determined by method II where $L_d = y_b + 3S_b$ was found to be ~ 2.5 ppb. Here, $y_b = -0.4$ and the standard deviation of the blank = 0.6.

A repeatability study was also performed to ascertain the % RSD of 15 replicate injections at the 100 ppb concentration level. Figure 2.15 shows a typical example of the repeatability of the test method which was also carried out on all other LoD

samples. From the chromatogram two peak areas were low and eliminated from the calculation. The reason for this low integrated area compared to the other values can be explained as follows. Occasionally, when the pneumatically assisted rheodyne injector was pressed to inject the sample, from the load position, it would turn to the inject position but almost instantaneously return to the load position, which suggests that some but not all of the sample was being loaded. This was a fault of the instrument that was rectified later. The % RSD was found to be 7 %. If, the two low peak-areas were therefore included in the % RSD calculation the error would have been much greater and not a true reflection of the repeatability study, since a systematic error was introduced by the system.

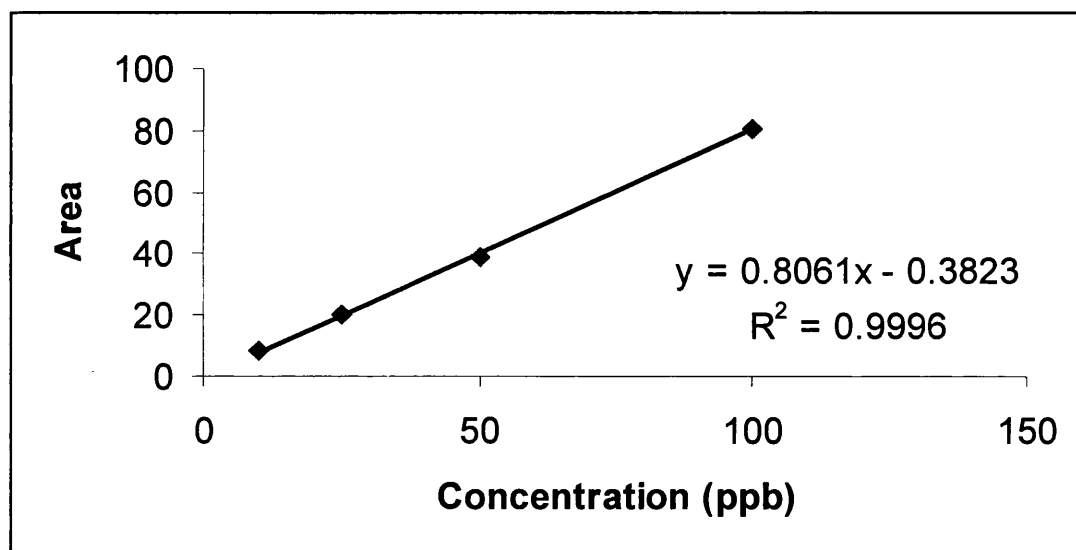


Figure 2.14: Calibration curve for DMPA (95% aq. EtOH)

(ii) DMPA (10% aqueous Ethanol)

ESI was carried out in negative ionisation mode. Optimum conditions were as follows:

Electrospray source conditions were capillary cone voltage of 3500V, sample cone voltage of 20V, extraction cone voltage of 9V, source temperature of 100°C and a desolvation temperature of 150°C.

A 10µL aliquot of sample solution was injected into a stream of 90% EtOH + 10% H₂O + 0.03% NH₃ by means of a rheodyne loop injector. The flow rate of the carrier solvent was set at 100µL min⁻¹.

The rf lens voltage was set at 100V and the orthogonal accelerator operated at a frequency between 10-15 kHz. Data acquisition was performed in continuum mode with a scan time of 1s and an interscan delay of 0.1s. Mass spectra was acquired over a range m/z 90-140.

For this experiment the stainless steel capillary inside the probe was changed together with the PEEK tubing leading from the rheodyne injector to the ESI probe to avoid all possible contamination from the previous sample.

Figure 2.16 shows the mass spectra obtained over the concentration range of 5-100 ppb. The LoD was determined for m/z 133, corresponding to [M-H]⁻. At the lowest concentration of 5 ppb it can be seen that the background signals are significantly

greater than mass spectra obtained with higher concentration, which is to be expected.

The mass spectra show characteristic ions which could take the form:

m/z	Inference
133	$[M-H]^-$
117	$[M-OH]^-$
97	$[M-H-2(H_2O)]^-$

The origin of the ion at m/z 129 remains unclear, one likely possibility is that it is a background signal (contaminant) already present in the source region. The mass spectra here was acquired over a mass range of m/z 90-140, since an intense ion again at m/z 89 totally suppressed all other ion signals.

Table 4 below shows the concentration and average area of sample minus average area of blank:

Concentration (ppb)	Area
5	4
25	10
50	19
100	40

Table:4

A calibration curve was constructed from this data and is shown in Figure 2.17. The response across the desired range was shown to be linear with a regression coefficient of 0.99.

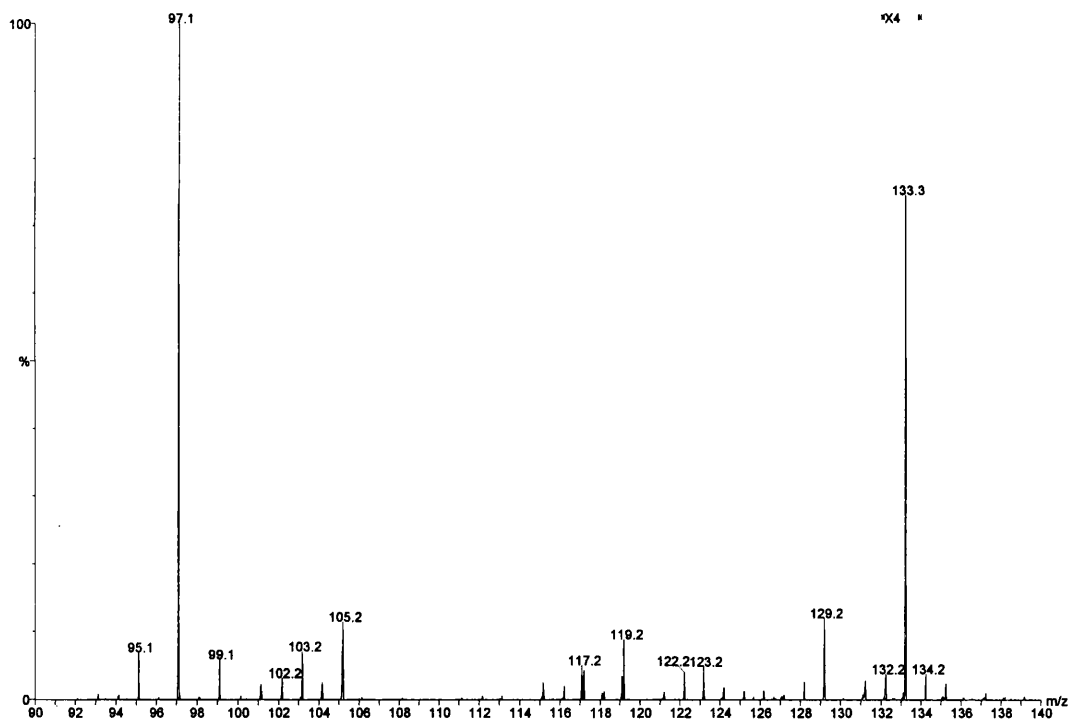


Figure 2.16: Mass spectra at 100 ppb (top) and 5 ppb (bottom) of DMPA (10% aq. EtOH)

The LoD determined by method I was found to be 5 ppb. The LoD determined by method II was found to be ~ 8 ppb since $y_b = 1.0$ and the standard deviation in the blank over the calibration range was found to be 0.91.

The % RSD of 15 replicate injections at the 100 ppb level was found to be 10 %.

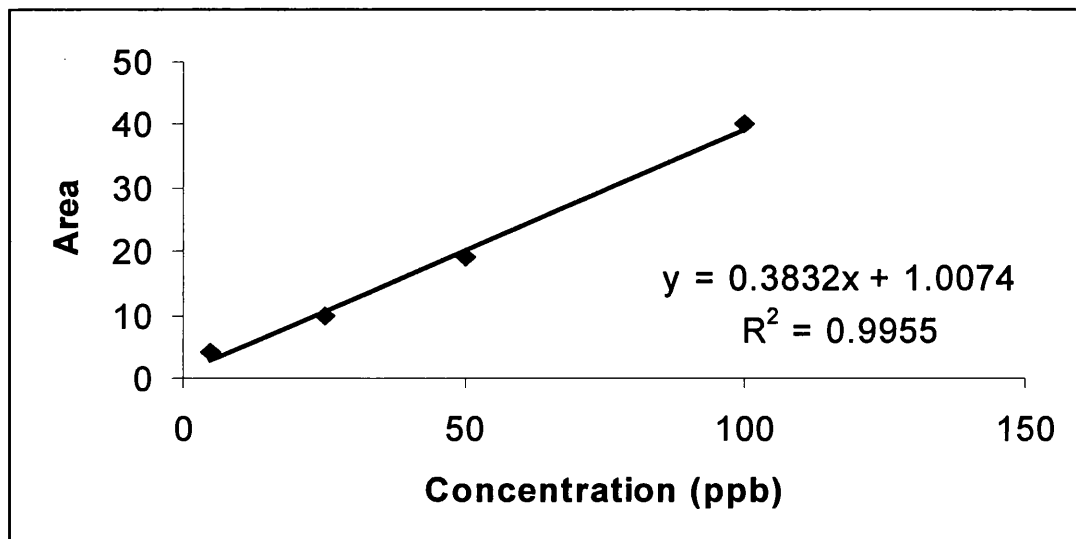


Figure 2.17: Calibration curve for DMPA (10% aq.EtOH)

(iii) DMPA (3% acetic acid)

ESI was carried out in negative ionisation mode. Optimum conditions were as follows:

Electrospray source conditions were: capillary voltage of 3500V, sample cone voltage 35V, extraction cone voltage 9V, source temperature of 100°C and desolvation temperature of 200°C.

A 10 μ L aliquot of sample solution was introduced into the mass spectrometer by means of a rheodyne injection. The sample was injected into a solvent stream of 90% ethanol + 10% H₂O + 0.03% NH₃ solution flowing at a rate of 20 μ L min⁻¹.

The rf lens voltage was set at 100V and the orthogonal accelerator operated at a frequency between 10-15 kHz. Data was acquired in continuum mode with a scan time of 1s and an interscan time of 0.1s. Mass spectra was acquired over a range m/z 75-140.

Figure 2.18 shows the acquired mass spectra over the range 300-1000 ppb. The LoD was determined for m/z 133 which corresponds to [M-H]⁻.

The concentration level required by the European Standards Committee for the LoD of DMPA could not be reached in 3% acetic acid solution. An ion at m/z 119 totally suppressed the signal for [M-H]⁻ which was used to determine the LoD. Competing analytes, impurities, and cluster ions that cause signal suppression is one of the fundamental limitations of electrospray ionisation. The mass spectra show characteristic ions which could possibly take the form:

m/z	Inference
133	[M-H] ⁻
119	[2(CH ₃ COOH)-H] ⁻
103	[2(CH ₃ COOH)-OH] ⁻
89	[M-H-CO ₂] ⁻

The signal at m/z 119 is likely to evolve from loss of a proton from a preformed acetic acid cluster. The ion at m/z 103 is likely to be formed from loss of a hydroxyl group from the acetic acid cluster. A small signal is shown in the spectra obtained at a concentration of 300 ppb, at m/z 89. This probably corresponds to the loss of CO₂ from [M-H]⁻. To obtain a LoD that is required by the European Standards Committee, attempts were made to break up the acetic acid cluster ion that had formed at m/z 119, since it totally suppressed the signal for [M-H]⁻ which was used for calculation of the LoD.

The desolvation gas was initially increased from the usual setting of 660 L/hr to 700 L/hr with the intention of evaporating the solvent quicker. The desolvation temperature was altered over the range 150^oC-250^oC and the flow rate was changed between 10-120 μL min⁻¹. The cone voltage was increased to over 150 volts but none of these significant changes however proved worthwhile and the required LoD could not be reached.

Table 5 below shows the concentration and average area of sample minus average area of blank:

Concentration (ppb)	Area
300	7.2
500	19.2
600	22.2
800	37.8
1000	50

Table:5

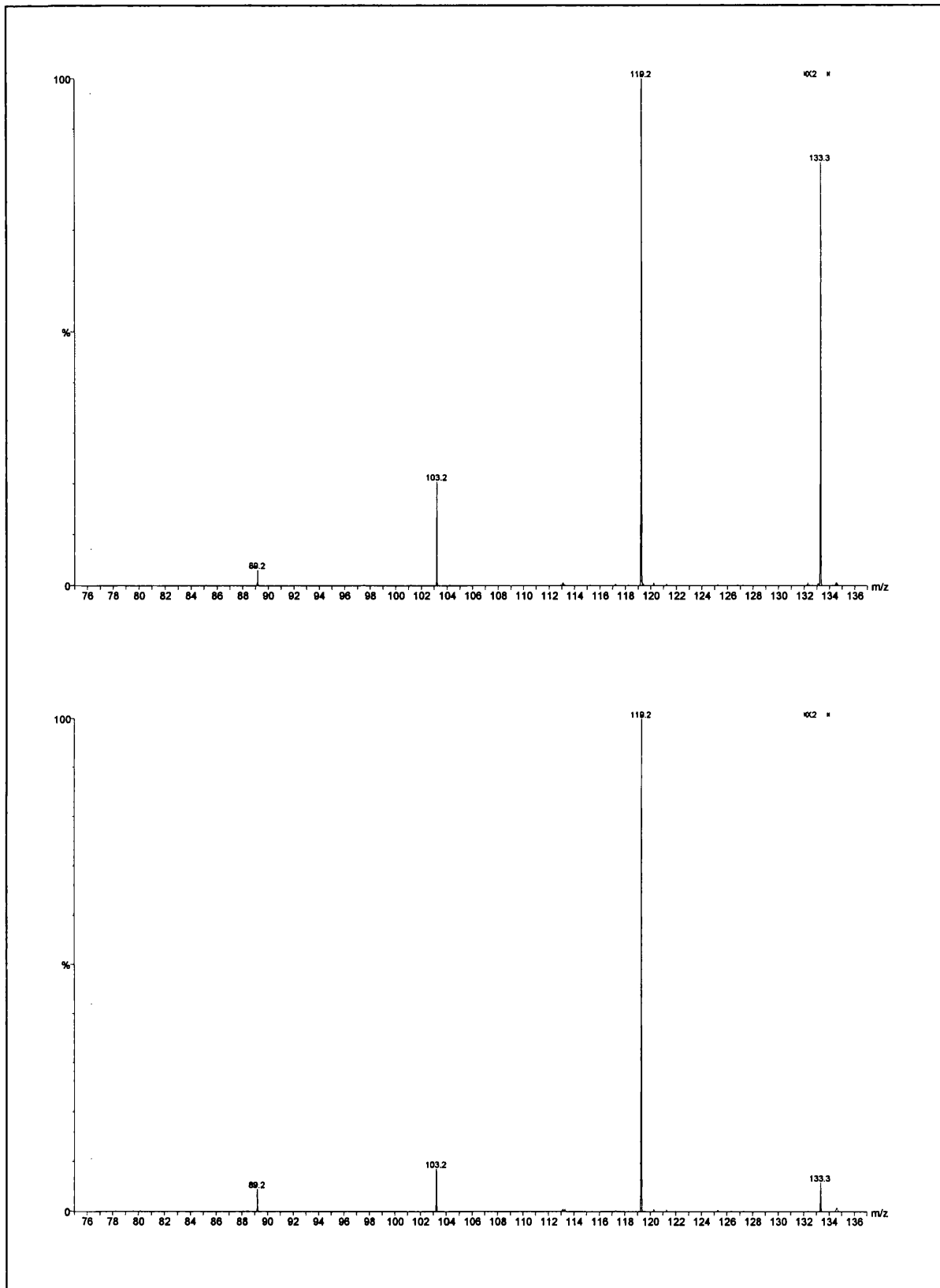


Figure 2.18: Mass spectra at 1000 ppb (top) and 300 ppb (bottom) of DMPA (3% acetic acid)

A calibration curve was constructed from this data and is shown in Figure 2.19. The response across this range was found to be linear with a regression coefficient of 0.99.

The LoD could only be determined by method I which was found to be 300 ppb, since a high negative intercept value made it impossible to calculate the LoD by method II.

The % RSD of 15 replicate injections at the 1000 ppb level was found to be 16 %.

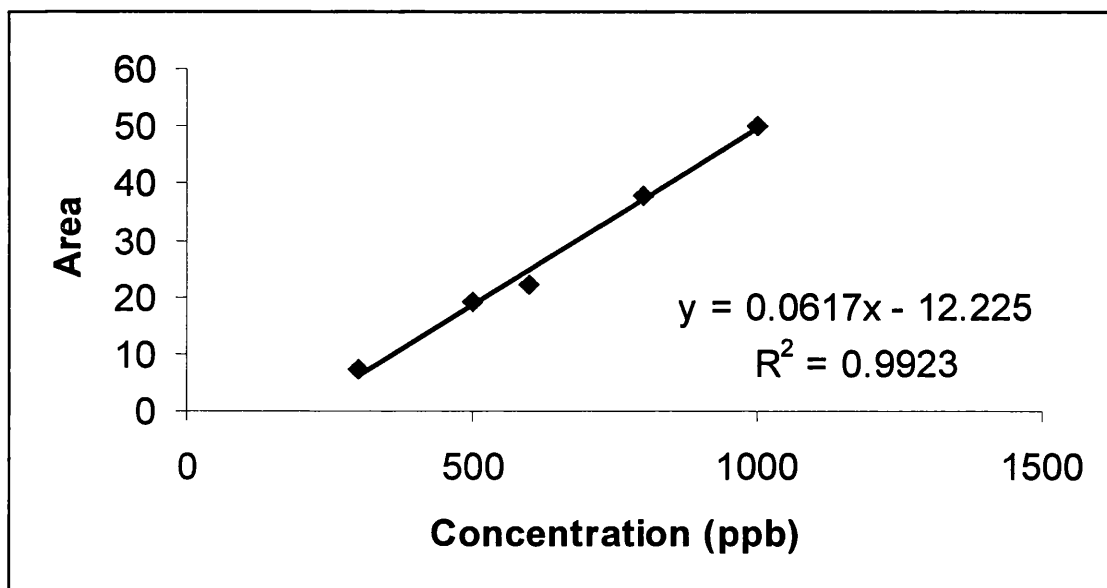


Figure 2.19: Calibration curve for DMPA (3% acetic acid)

The following table (6) shows the LoD results obtained for DMPA on the LCT and Platform II instruments. The LoD experiments were carried out independently on the Platform II instrument [1].

	LCT (LoD)	Platform II (LoD)
DMPA (95% aq.EtOH)	~ 2.5-10 ppb	< 10 ppb
DMPA (10% aq.EtOH)	~ 5-8 ppb	< 10 ppb
DMPA (3% acetic acid)	~ 300 ppb	< 10 ppb

Table: 6

The results show that the LCT LoD (full scan mode) to be < 10 ppb which is approximately the same level to that in SIM mode on the Platform II for DMPA in 95% aq.EtOH and 10% aq.EtOH.

The LoD for the sample in 3% acetic acid however showed to be approximately thirty times less sensitive in the SIM mode.

A possible reason for this could be due to ion signal suppression of $[M-H]^-$ from an acetic acid cluster of the form $[2CH_3COOH-H]^-$ occurring at m/z 119. This ion at m/z 119 totally reduced the area of the deprotonated sample peak so much that it affected the quantitative analysis of the sample in full scan mode.

Problems with cluster formation in the acetic acid medium were probably related to the mobile phase used. Acetic acid media is not suited to the electrospray process in negative ionisation mode.

2.3.6 LCMS sensitivity

2.3.6.1 Aim

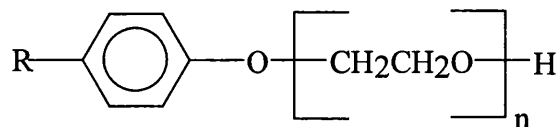
The objective of this section was to compare the LCMS performance of the LCT in comparison with a quadrupole mass analyser, the Platform II. An alkylphenol ethoxylate was used to compare the separation efficiency [67].

2.3.6.2 Introduction

Conventional scanning mass spectrometers such as the quadrupole, used as detectors for separation science, are reaching their fundamental limits when the mass spectral range of interest has to be scanned at a rate exceeding 1 scan/s. ToF technology however offers high scan rates and the LCT is capable of acquiring typically 20000 scans/s and recording 10 spectra/s. Properties such as high speed and high mass range capabilities of ToF instruments make them well suited to high speed chromatographic separations over scanning instruments. Peak widths in separation techniques such as capillary electrophoresis (CE) and capillary electrochromatography (CEC) are of the order of a few milli seconds and scanning instruments have great difficulty in obtaining sufficient data points across such narrow peaks to aid characterisation.

2.3.6.3 Alkylphenol ethoxylates

Alkylphenol ethoxylates (APE's), of structure shown below, are a group of surface active agents that are produced on a mass scale (million ton scale) worldwide.



They find widespread industrial and household use as washing and cleaning agents since they are but one ingredient in surfactant and detergent formulations. It is therefore by no means unusual to find them ending up in municipal wastewaters and rivers, where they constitute a major environmental pollutant.

native biodegradable
 Their biodegradable products are known to affect the glands that secrete hormones directly into the bloodstream, such as pituitary and thyroid of fish [68].

One such biodegradable product, 4-nonyl phenol an estrogenic agonist is thought to be involved in the feminization of male fish in some U.K. rivers [68].

Therefore, the characterisation of this type of compound class is important for regulatory and environmental issues.

A reverse-phase gradient LC separation of the nonyl phenoxy polyethylene glycol (R=nonyl, n=10 and has an average molecular weight distribution of 660) was performed using a HP 1050 Chromatograph (Hewlett Packard Ltd., Stockport, U.K.). The nonyl phenoxy polyethylene glycol was dissolved in methanol to an initial concentration of 1 ppm. This was diluted for analysis and injected via a 20 μ L loop injection into a stream of methanol flowing at a rate of 1mL/min. This flow rate was split 50:1 (waste:ESI

source) using a post column split (Accurate post-column splitting device, Presearch U.K. Ltd). Mass spectra was acquired in positive ionisation mode.

Figure 2.20 shows the TIC traces obtained from injection of sample diluted to a concentration of 200ppb on the Platform II (top) and 40ppb on the LCT (bottom).

A suitable well resolved separation could not be achieved on the Platform at the 40ppb level. Over the elution period of 10-25 minutes the LCT TIC shows peaks that are more well defined and clearly resolved than the Platform instrument. The individual peaks correspond to the number of oligomers present on the nonyl phenoethoxylate. The LCT trace clearly resolves up to 18 components.

The oligomers detected on the Platform are wider and poorly shaped and this is evident over the whole chromatogram. This could be due to the apex of the peak being missed by the quadrupole as it slowly scans the mass range of interest as well as the significantly inferior signal-to-noise ratio.

The nonyl phenoethoxylate has a molecular weight distribution around m/z 660. The mass difference for each oligomer is 44 units which corresponds to the ethoxylate chain. Typical partial mass spectra associated with some peaks obtained in the TIC of the LCT are shown in Figure 2.21. The LCT has shown to provide a more efficient, better resolved separation from much lower levels of analyte concentration.

The high data acquisition rate of the LCT and increased sensitivity makes the use of oa-ToF technology very attractive for the separation sciences. This would be even

more noticeable for separation science approaches such as CE and CEC where much lower sample loadings are commonly used and where peak widths are significantly lower.

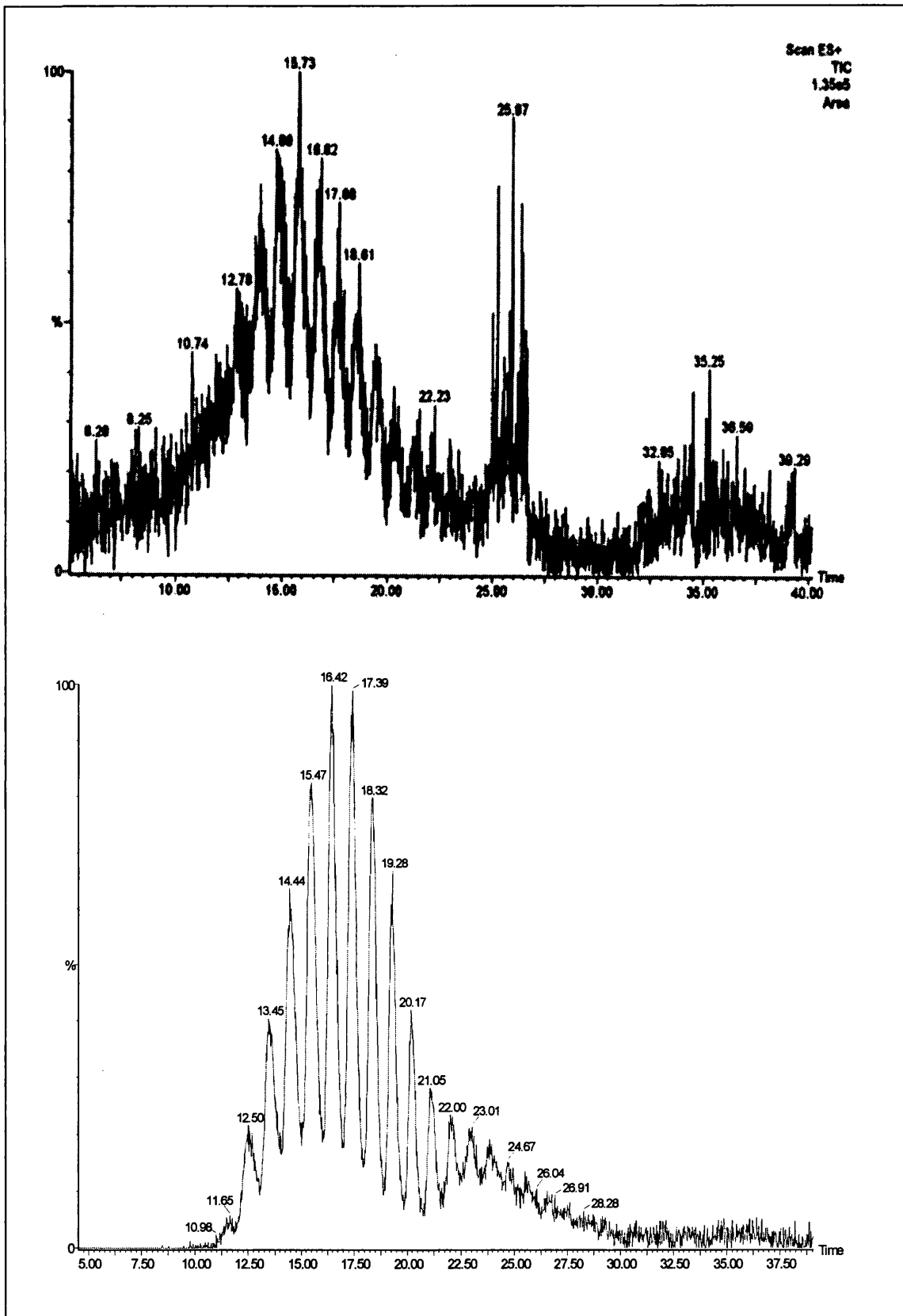


Figure 2.20: Comparison of total ion chromatograms for the Platform II (top) and LCT (bottom)

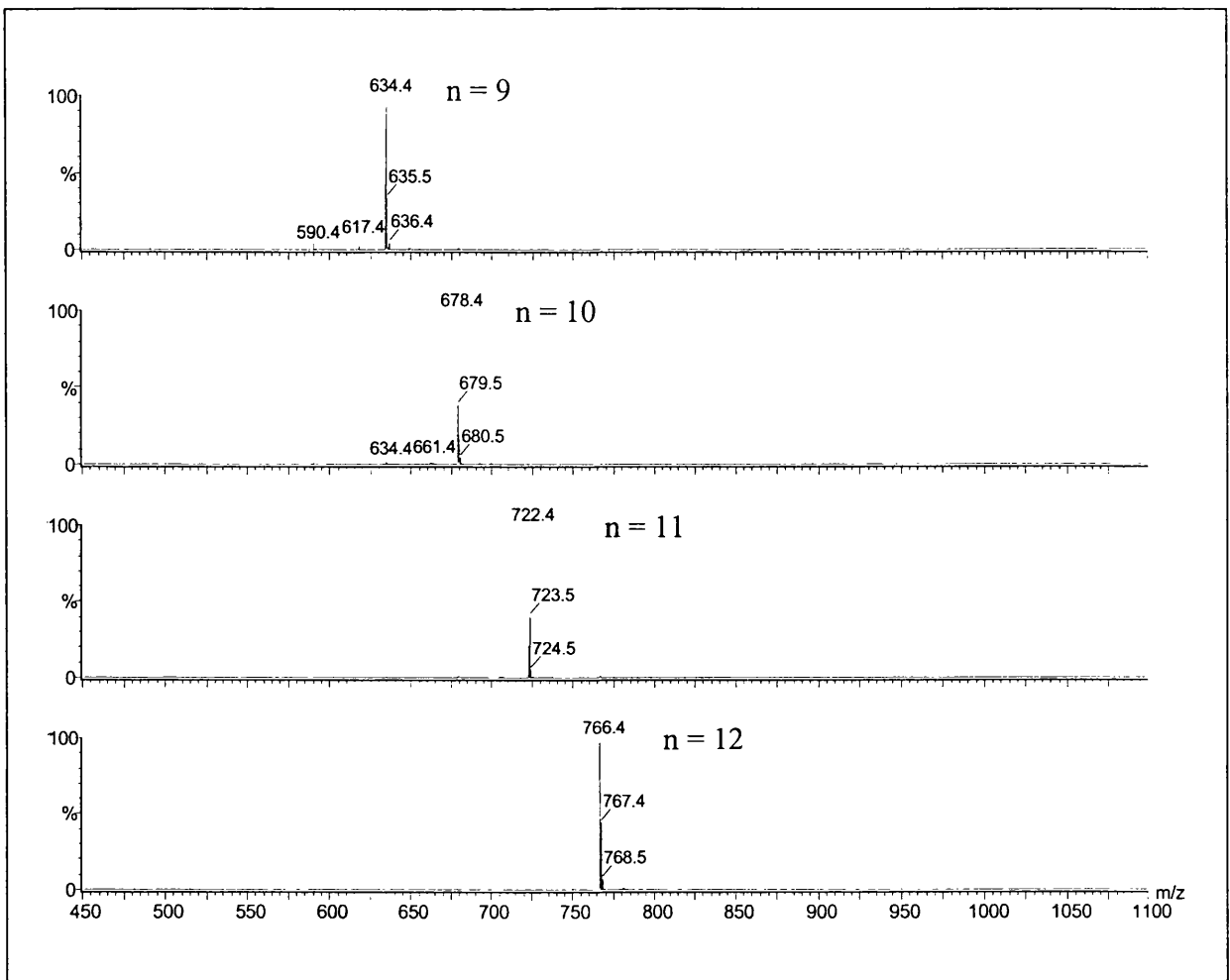


Figure 2.21: Positive ion electrospray mass spectra of some separated nonyl phenolethoxylate oligomers obtained using the LCT. Each oligomer has become ammoniated.



2.3.7 Exact mass measurement of synthetic polymer and functional fluid additives

2.3.7.1 Aim

The objective of this section was to investigate the mass accuracy performance of the LCT. Ten additives contained in either synthetic polymer or functional fluid (lubricant) formulations were studied.

2.3.7.1.1 Introduction

Mass accuracy is defined as 'the measurement of the closeness of the mass of a given measurement to the true mass of the substance' [69]. Exact mass measurement refers to the accuracy of the mass measured to within a specified accuracy. Typically, results of < 10 ppm are presented here. Accurate mass refers to the measurement of an ion's mass to within a specified error or measurement to within sufficient accuracy to assign an elemental formula to that ion. Therefore, exact mass measurement determination by means of mass spectrometry is used to confirm the elemental composition of various compounds.

Accurate mass measurement has traditionally been performed at high resolution on instruments double focusing sectors [70] and more recently on Fourier transform ion cyclotron resonance (FTICR)[71] mass spectrometers.

Compounds of low molecular weight, typically < 1000 Da can be mass measured with routine accuracy to within 1-5 ppm or less on high resolution instruments.

A disadvantage of using low resolution instruments, such as, quadrupoles and ToF, that made use of EI, FAB and LSI is the high possibility of the presence of interfering ions from background signals which could effect the mass measurement accuracy for the analyte of interest if not properly resolved [72].

However, Roboz *et al.* [73] showed that mass accuracy measurement by FAB on a quadrupole gave an error to within 10 ppm. This mass accuracy error has also been demonstrated by Haddon *et al.* [74] by means of LSI on a quadrupole.

The development of ESI allows cleaner spectra to be observed. The chances of interfering ions from ESI effecting inaccuracies in mass measurement on low resolution instruments, is lower than using EI for example.

It would therefore seem ideal to interface ESI to a sector instrument to obtain greater mass accuracy. The successful interfacing of ESI to sector instruments though is problematic since high voltages have to be used which do not aid the ionisation process.

ESI has been demonstrated to provide mass accuracies on low resolution instruments that gave errors that were comparable to high resolution instruments [72].

Kostiainen *et al.* [75] have demonstrated mass accuracy measurements on a quadrupole instrument in negative ionisation mode on some glucuronide derivatives by ESI to be comparable to measurements made by FAB on a sector instrument. Results showed errors of < 5 ppm.

ToF is generally regarded as a low resolution instrument, but the interfacing of continuous ionisation techniques to an orthogonal acceleration type instrument [76-80] facilitates accurate mass measurement determination which now competes with high resolution instruments.

Bahr and Karas [81] have recently demonstrated that two synthetic isobaric peptides showed mass accuracies of < 5 ppm by means of ESI oa-ToF.

Keough *et al.* [82] have used an oa-ToF hybrid magnetic sector instrument equipped with an EI or FAB source to mass measure product ions from MS/MS experiments on simple molecules such as CO, C₂H₄ and some isobaric residues in peptides. Errors of +/- 25 ppm for masses > 200 Da are routinely achieved. Mass accuracy was limited to masses < 200 Da due to the speed of their TDC.

The use of oa-TOFMS is suitable for fast separation techniques such as capillary electrophoresis (CE), capillary electrochromatography (CEC) and capillary zone electrophoresis (CZE) due to fast acquisition rates and high sensitivity. Peak widths obtained in the TIC for these separation techniques are narrow and need sufficient data points for characterisation. Scanning instruments could therefore not compete as well as ToF instruments which generate more spectra/s and has greater sensitivity.

Exact mass measurement of pharmaceutical compounds using CZE/ oa-TOFMS equipped with an ESI source has been performed by Tetler *et al.* [83]. The exact mass obtained showed an error of < 8 ppm which allowed the confirmation of molecular formula.

Solid phase extraction (SPE)/LC/oa-TOFMS in ESI mode, has also been shown to perform to within a 10 ppm error for the determination of pesticides in surface water by Niessen *et al.* [84].

Accurate end group determination by Nielen [85] has also been demonstrated to show errors < 5 ppm for low molecular weight polymers by ESI oa-TOFMS.

Exact mass measurements of lubricant polymer additives has been determined using a high resolution magnetic sector instrument by means of LSI [86].

There are few reports in the literature for the analysis of polymer additives by means of ESI. Jackson *et al.* [87], has applied ESI and MS/MS to the analysis of such additives on a triple quadrupole mass spectrometer.

Exact mass measurement determination of synthetic polymer and functional fluid additives using ESI oa-TOFMS is not cited in the literature and therefore has been investigated for a variety of such compounds of masses < 1500 Da.

2.3.7.2 Investigation of the factors affecting mass measurement accuracy [88,89]

To investigate the factors that influence the mass accuracy measurement, fundamental equations for ToF instruments, derived from Newtons equations of motion, (see Chapter 1) had to be taken into account.

The equations suggest a calibration law for ToF instruments which allows accurate mass measurement of mass spectra to be performed. The calibration law for time-to-mass conversion is of the form:

$$m^{1/2} = At + B$$

where A and B are constants dependent on the instrument. The term A comes from the parameters for example, such as distance travelled by the ions in the drift regions and the acceleration voltages.

The term B comes from the parameters for example, such as minor electronic delays from detector rise time and jitter from the digitiser.

Thus, high resolution can be achieved in ToF mass spectra by the minimisation of jitter and flight time drift. Flight time drift is caused by drift over time of certain power supplies, for example the orthogonal accelerator.

ToF averages individual mass spectra so that the 'jitter' from electronic devices will also average in to the acquired data. This will lead to signal broadening and have a marked effect on mass measurement accuracy, since resolution will be degraded.

The precision of mass measurement due to a signal being received at the detector can be related to the reliability of identifying the mean distribution of ion arrival times and converting these times to mass. The peak signals in the mass spectrum should ideally be Gaussian shaped so that the data can be centroided (see later) which makes mass measurement values more accurate. Factors responsible for the degradation of mass measurement accuracy are a high signal/noise (S/N) ratio, insufficient data points

generated per peak and the width of the distribution of ion arrival times for one mass, since the ion signal detected by the MCP influences the accuracy of the peak centroid.

2.3.7.3 The role of additives in plastics

Polymer additives have several key functions. They aid processing and finally characterise the formulated commercial product. The additives investigated were chemically different from one another and are added as antiwear agents, antioxidants, UV stabilisers, plasticizers, flame retardents or antifoam agents [90], some of which are discussed below. These type of additives tend to be polar involatile compounds and are added to the formulation at the 0.1-3% weight for weight (w/w) level or lower.

Antioxidants are added to a polymer formulation to slow down oxidation and to slow down the ageing process of the polymer, therefore providing a method of stabilisation. They are usually added to the polymer formulation at a level of 1%. These included Irganox 565, Irganox 1010, Irganox 1076 and Irgafos 168 in the study.

Degradation reactions induced by light and oxygen on plastics can cause chemical and physical damage to the product. Therefore, *light stabilisers* are added to a formulation at a concentration of < 2% and are capable of retarding degradation through light. Tinuvin 327 and Tinuvin 770Df were investigated in the study.

Lubricants are added to a polymer formulation to influence the rheology of the final product in a desired way. They also provide the final product with a smooth finish.

Lubricants are added to formulate rigid PVC for example. Only one additive of this type was investigated, commonly known as 3608.

Plasticizers are added to formulations to improve processibility, flexibility and stretchability of the product. The study included Emkarate 3020, TCP and TXP.

The characterisation of polymer additives by mass spectrometry gained popularity with the introduction of soft ionisation techniques such as FAB [91-93] and LD [94-96] in the 1980's. Ionisation techniques such as EI and CI require the additive to be thermally labile (volatile), whereas FAB and LD can analyse involatile compounds.

The characterisation of polymer additives in polymer formulations is difficult owing to the small amounts present. Chromatographic analysis of polymer extracts therefore, have to be employed due to the complexity of the polymer formulations.

Identification and characterisation of various polymer additives has recently been demonstrated by Langridge-Smith *et al.* [97] by means of a two step laser desorption/laser photoionisation TOFMS (L2MS) and by Davidson *et al.* [98] by means of supercritical fluid chromatography (SFC) with APCI on a quadrupole instrument.

Direct infusion mass spectrometry of some polymer additives was utilised and provided exact mass measurement data which could facilitate initial experimental optimisation of hyphenated separation techniques such as LC/MS, CE/MS or CEC/MS, for future investigative studies.

2.3.7.4 ESI oa-ToF of pure polymer additives

The pure polymer additives studied are shown in Table 7. They consist of four various groups of additives, antioxidants, light stabilisers, plasticizer or lubricant additives.

An example of how the exact mass measurement data acquisition was determined will be comprehensively discussed for Irganox 565 and 3608 which was presented as an unknown. It will be shown how elemental formulas can be calculated from the exact mass measurements made. All other additives investigated followed the same procedure. Therefore, it seemed appropriate to demonstrate the procedure only once. The mass spectrum and exact mass measurement spectrum, which contained the reference compound, for each additive will be shown for clarity in a joining appendix.

Each spectra ~~it should be noted~~ were not necessarily acquired on the same day.

*

2.3.7.5 Optimum source and instrumental voltage conditions

ESI was carried out in positive ionisation mode for every additive studied. Optimum source, transfer and analyser voltages were as follows:

Capillary voltage of 3500V, extraction cone voltage of 8V, sample cone voltage variable between 40V and 100V, source temperature 100°C and desolvation temperature 150°C.

The rf lens voltage was set at either 200V or 300V and the orthogonal accelerator operated with a frequency of 10 kHz.

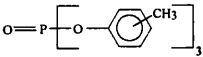
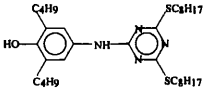
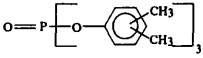
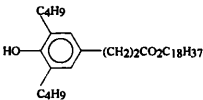
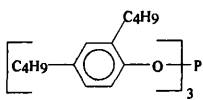
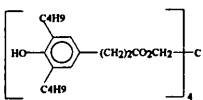
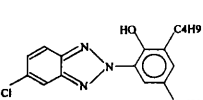
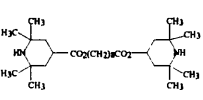
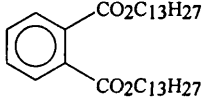
Trivial name	Chemical name	Structure	Elemental Composition	Molecular Weight
TCP	Tricresyl phosphate		$C_{21}H_{21}PO_4$	368
Irganox 565	2,6-di-tert-butyl-4-(4,6-bis(octylthio)-1,3,5-triazin-2-ylamino) phenol		$C_{33}H_{56}OS_2N_4$	588
Durad 220X	Trixylenyl phosphate		$C_{24}H_{27}PO_4$	410
Irganox 1076	Octadecyl-3-(3,5-di-tert-butyl-4-hydroxyphenyl)-propionate		$C_{35}H_{62}O_3$	530
Irgafos 168	Tris (2,4-di-tert-butylphenyl) phosphite		$C_{42}H_{63}PO_3$	646
Irganox 1010	(3-(3,5-di-tert-butyl-4-hydroxyphenyl) propionate)		$C_{73}H_{108}O_{12}$	1176
Tinuvin 327	2,4-di-tert-butyl-6-95-chlorobenzotriazol-2-yl) phenol		$C_{20}H_{24}ON_3Cl$	357
Tinuvin 770Df	Bis (2,2,6,6-tetramethyl-4-piperidyl) sebacete		$C_{28}H_{52}O_4N_2$	480
Emkarate 3020	Ditridecyl phthalate		$C_{34}H_{58}O_4$	530

Table 7: Nomenclature, structure and molecular weight of the polymer additives studied

Data acquisition was performed in the continuum mode, with a scan time of 1s and an inter-scan delay of 0.1s. Mass spectra was acquired over a mass range that covered the mass of the polymer additive being investigated.

These instrumental conditions remained constant except where stated and are fully listed in Table 8 for each additive studied.

2.3.7.6 Exact mass data acquisition

An initial mass spectrum is acquired to determine which ion is to be accurately mass measured. In positive ionisation mode the ions produced are typically a protonated molecular ion, $[M+H]^+$, or ions formed from adduct formation from ammonia, sodium or potassium, i.e. $[M+NH_4]^+$, $[M+Na]^+$ or $[M+K]^+$. For each additive studied, the ion assigned for mass measurement accuracy, together with its monoisotopic mass can be found in Table 9.

The following procedure describes how the exact mass measurement for each of the polymer additives investigated was determined.

After deciding which ion is to be accurately mass measured, the additive in solution was mixed with polyethylene glycol (PEG) which has the chemical structure $[H(CH_2CH_2O)_nOH]$, or Leucine Enkephalin (MW 555) for provision of a 'lock mass', see Table 9. The resulting mass spectrum is mass calibrated with a 'base' calibration, set up prior to the analysis, from a mixture of NaI/CsI salts.

Additive	Sample solvent	Carrier solvent	Flow rate ($\mu\text{L min}^{-1}$)	Cone Voltage (V)	RF lens Voltage (V)	Reference compound	Reference ion	'Lock mass' (m/z)
Irganox 565	DCM	$\text{CH}_3\text{CN}:\text{H}_2\text{O}$ (1:1)	50	50	200	PEG 600	$[\text{PEG}+\text{Na}]^+$	613.3411
Irganox 1010	DCM:MeOH (1:9) + 0.1% Formic acid	MeOH:H ₂ O (1:1)	300	35	150	LEU ENK	$[\text{M}+\text{H}]^+$	556.2771
Emkarate 3020	THF:MeOH (2:8)	MeOH:H ₂ O (1:1)	300	35	150	LEU ENK	$[\text{M}+\text{H}]^+$	556.2771
Irganox 1076	DCM:MeOH (1:9) + 0.1% Formic acid	MeOH:H ₂ O (1:1)	300	35	150	LEU ENK	$[\text{M}+\text{H}]^+$	556.2771
Irgafos 168	DCM:MeOH (1:9)	MeOH:H ₂ O (1:1)	300	35	150	LEU ENK	$[\text{M}+\text{H}]^+$	556.2771
Tinuvin 327	DCM:MeOH (1:9)	MeOH:H ₂ O (1:1)	20	70	200	PEG 600	$[\text{PEG}+\text{H}]^+$	371.2281
Tinuvin 770 Df	MeOH	MeOH	30	75	200	PEG 600	$[\text{PEG}+\text{Na}]^+$	525.2887
TCP	$\text{CH}_3\text{CN}:\text{H}_2\text{O}$ (9:1)	CH_3CN	30	100	200	PEG 400	$[\text{PEG}+\text{Na}]^+$	393.2101
TXP	$\text{CH}_3\text{CN}:\text{H}_2\text{O}$ (9:1)	CH_3CN	50	75	200	PEG 600	$[\text{PEG}+\text{Na}]^+$	437.2363
Unknown	DCM:MeOH (65:35) + 0.1% Formic acid	DCM:MeOH (65:35)	50	50	300	PEG 1000	$[\text{PEG}+\text{Na}]^+$	833.4722

Table 8: Experimental conditions for each additive studied

A 'unique' calibration reference file was also set up which consisted of two PEG ions which sat on either side of the additive ion being accurately mass measured. The acquired mass spectrum over this region is then re-calibrated using this 'unique' reference file. This spectrum is then utilised for the exact mass measurement determination. (Data acquisition for all additives investigated was processed using standard procedures supplied with the MassLynx software).

Initially, background subtraction was performed using a first order polynomial, where a pre-selected percentage of data points that fall below the baseline are eliminated from the spectrum. The peaks obtained in the background subtracted spectrum are then smoothed by application of a 'moving mean' smooth to eliminate any inherent noise. The 'moving mean' takes the mean of the intensities of the acquired data points in the peaks and therefore proceeds to smooth the data. During this study all spectra were smoothed at least twice.

The spectrum of smoothed peaks is then mass centroided to calculate the mass at the peak centre. Only data points which have peak intensities greater than a pre-determined threshold are mass centroided.

In this study the top 80% of the peak was measured, the threshold value was therefore set at 20% on each side of the peak. The threshold value reduces any effects interfering ions may have on the mass spectrum. Therefore, ions of lower intensity than the threshold value are eliminated.

Finally, exact mass measurement was determined using the mean of 5 separate acquisitions, following a 'lock mass' correction which was provided by the highest PEG mass in the unique reference calibration or Leucine Enkephalin. The ion used for

Additive	Concentration (ppm)	Sample:PEG	Ion assignment	Monoisotopic mass
Irganox 565	1	5:1	[M+H] ⁺	589.3974
Irganox 1010	100	n/a	[M+NH ₄] ⁺	1194.8185
Em 3020	100	n/a	[M+H] ⁺	531.4413
Irganox 1076	100	n/a	[M+Na] ⁺	553.4597
Irgafos 168	100	n/a	[M+H] ⁺	647.4593
Tinuvin 327	100	5:1	[M+H] ⁺	358.1686
Tinuvin 770Df	100	1:1	[M+Na] ⁺	503.3825
TCP	100	5:1	[M+H] ⁺	369.1256
TXP	100	5:1	[M+Na] ⁺	433.1545
Unknown	10	10:1	[M+Na] ⁺	809.7363

Table 9 : Sample concentration, mixture ratio and monoisotopic mass of molecular ion mass measured

n/a - since 10 μ L injection made from a Waters 2690 LC system (Waters, Corp., Milford, MA, USA) into the carrier solvent delivered by a Waters 2690 solvent delivery system. Here Leucine Enkephalin was used as 'lock mass' and infused into the mobile phase at a flow rate of 5 μ L/min via a Harvard 22 syringe pump. No 'unique' calibration was applied to this data only the base calibration, which gave residual errors of < 3 mDa.

single mass measurement accuracy can be found in Table 8. Results from the 5 replicate measurements are found in Table 11.

(i) Irganox 565

Irganox 565 is a non-staining, phenolic antioxidant used as a post polymerisation process stabiliser for unsaturated elastomers, such as polybutadiene, polyisoprene and nitrile rubber. It maintains the color properties of the polymer and also been known to be used as an adhesive.

Optimum source, transfer and analyser voltages are discussed in section 2.3.7.5. However, sample cone voltage and rf lens voltage were set at 50V and 200V respectively. Mass spectra was acquired over a mass range of m/z 100-600.

A 1 ppm solution of sample was dissolved in dichloromethane (DCM). This solution was introduced via a 10 μL loop injector (rheodyne) into a stream of 1/1 acetonitrile + water solvent into the ESI source flowing at a rate of 50 μLmin^{-1} . The mass spectrum produced from this infusion is shown in Figure 2.22 (top) which suggests that the sample has become protonated, hence the base peak at m/z 589. This initial spectrum is calibrated by a base calibration, provided by a NaI/CsI salt mixture, prior to analysis.

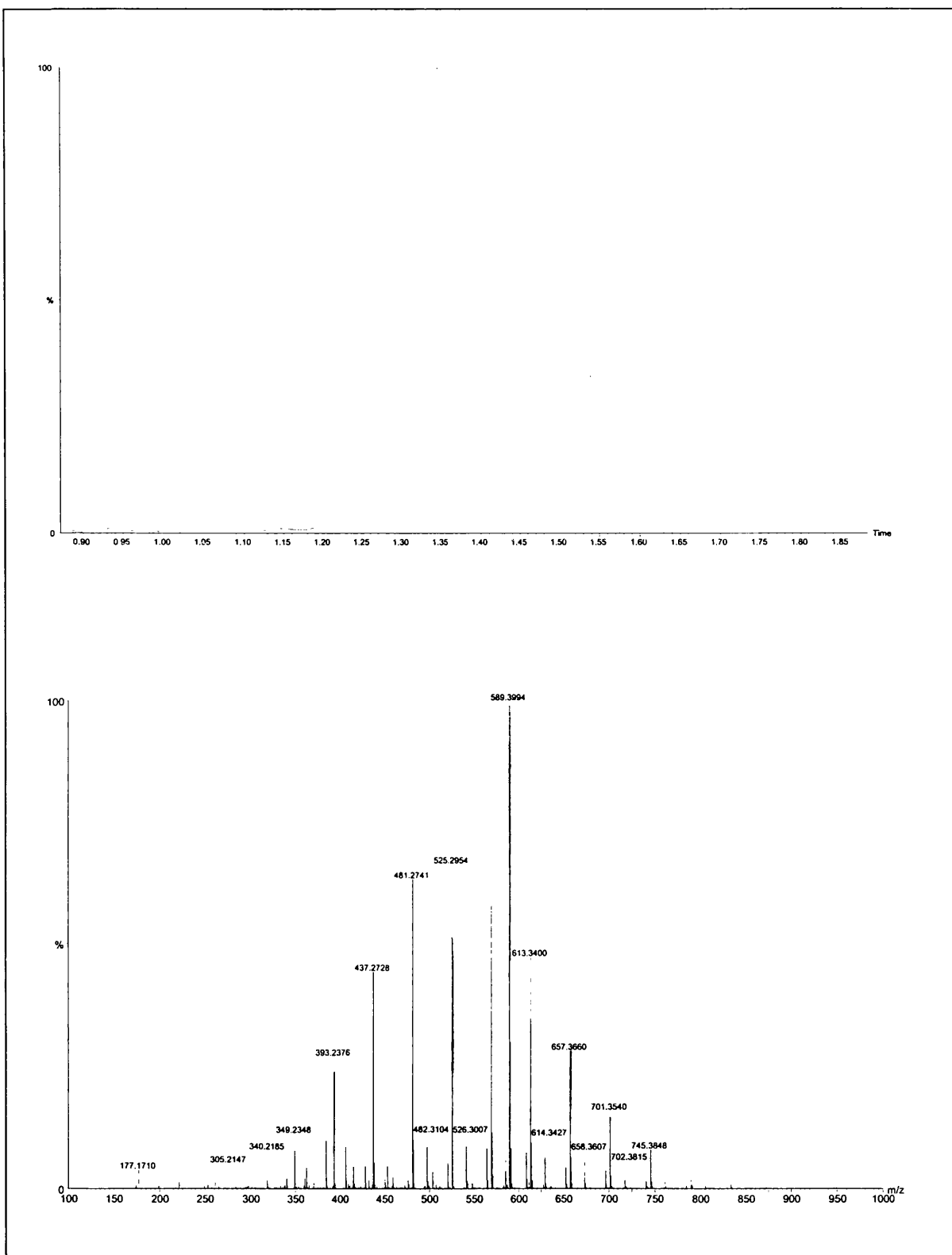


Figure 2.23: Irganox 565 TIC (top) and mass spectrum containing PEG 600 (bottom)

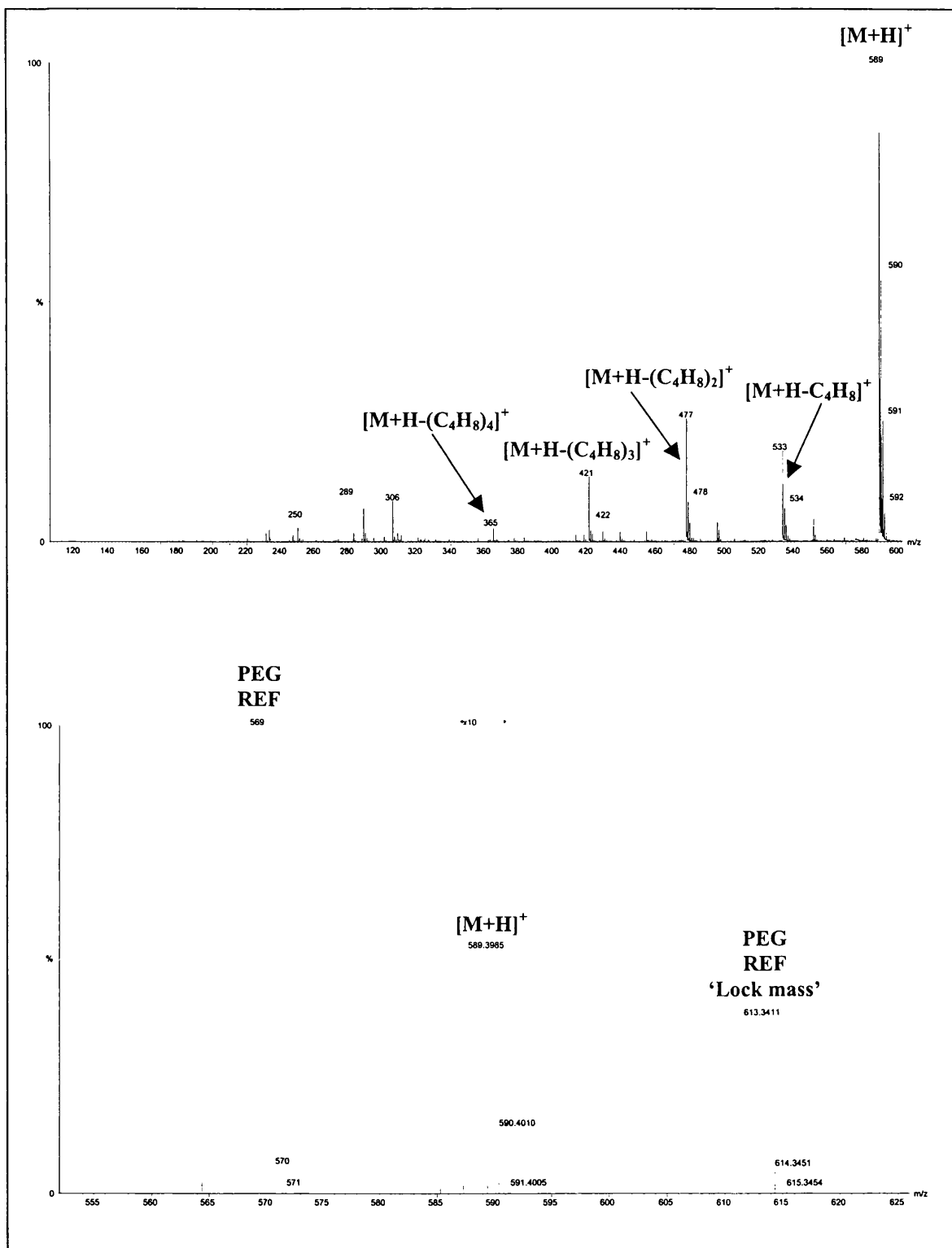


Figure 2.22: Irganox 565 mass spectrum (top) and exact mass measurement spectrum (bottom)

A reference compound PEG 600, which has a distribution of peaks in series, of known masses, was dissolved in MeOH at a concentration of 1ppm and added to the sample solution at a ratio of 1:5 (PEG 600:Irganox 565).

After injection of the mixture (sample + reference) a peak appears in the Total Ion Chromatogram (TIC), shown in Figure 2.23 (top). The peak has been enlarged over the specific elution time of 0.9 and 1.85 minutes. Any point along this peak represents a mass spectrum which is provided by summing the intensities of every ion pulsed from the orthogonal accelerator.

A mass spectrum is produced (see Figure 2.23 (bottom)) from this TIC by subtracting some background signal (prior and after peak elution) from the total area under the peak. A 'unique' calibration reference file is then applied to this mass spectrum where exact mass measurement determination is carried out.

As can be seen from the background subtracted, smoothed and centroided mass spectrum in Figure 2.22 (bottom), the two reference PEG 600 ions that are situated on either side of the $[M+H]^+$ signal, are m/z 569 and m/z 613. These ions correspond to $[H(CH_2CH_2O)_{12}OH.Na]^+$ and $[H(CH_2CH_2O)_{13}OH.Na]^+$ respectively. Accurate masses for $[M+H]^+$ were measured using m/z 613.34112 as a 'lock mass' correction.

The results from 5 replicate analysis of Irganox 565 are summarised in the Table 10 below. The theoretical monoisotopic m/z for $[M+H]^+$ equals 589.3974.

Acquisition N ^o	Measured m/z	Error (mmu)	Error (ppm)
1	589.3985	1.1	1.9
2	589.3928	-4.6	-7.8
3	589.3957	-1.7	-2.9
4	589.4001	2.7	4.6
5	589.3971	-0.3	-0.5
Mean	589.3968	-0.56	-0.94
Standard deviation	0.0028	+/- 2.79	+/- 4.74

Table 10: Results of 5 determinations for Irganox 565

The results show good accuracy and reproducibility. The deviation of the mean from the theoretical m/z value is -0.6 mmu (-0.9 ppm) and the standard deviation for the 5 replicate measurements is +/- 2.8 mmu (4.7 ppm).

(ii) Unknown

The last additive to be accurately mass measured was presented as an unknown to investigate if an accurate empirical formula could be determined from the results obtained. Previous ¹H and ¹³C NMR data had indicated that the additive was an ester derived from an unsaturated long chain aliphatic dicarboxylic acid and a shorter chain aliphatic alcohol.

The additive was dissolved in DCM:MeOH (65:35) to a concentration of 10 ppm. 0.1 % Formic acid was added to the solution to aid ionisation. This solution was injected into a stream of DCM:MeOH (65:35) flowing at a rate of 50 $\mu\text{L min}^{-1}$ into the ESI source. The mass spectrum produced from this injection is shown in Figure 2.24 (top). The base peak in the mass spectrum occurs at m/z 809, a m/z difference of 22 from

m/z 787. The peak at m/z 825 corresponds to an m/z difference of 38 from m/z 787. This suggests that the peaks at m/z 787, 809 and 825 correspond to $[M+H]^+$, $[M+Na]^+$ and $[M+K]^+$. The sodiated base peak was chosen for exact mass measurement since it was the most intense peak in the spectrum.

PEG 1000 was dissolved in MeOH to a concentration of 10 ppm and added to the sample solution at a ratio of 10:1 (Unknown:PEG). The background subtracted, smoothed and centroided mass spectrum of the mixture is shown in Figure 2.24 (bottom). Ions at m/z 789 and m/z 833 correspond to $[H(CH_2CH_2O)_{17}OH.Na]^+$ and $[H(CH_2CH_2O)_{18}OH.Na]^+$ PEG reference ions respectively. Accurate masses for $[M+Na]^+$ were measured using m/z 833.4722 as a 'lock mass' correction. The results from 5 replicate analysis are shown in the table below:

Acquisition N ^o	Measured m/z
1	809.7433
2	809.7413
3	809.7343
4	809.7229
5	809.7443

The selection of $[M+Na]^+$ as the target ion combined with the knowledge of its chemical functionality meant that candidate elemental compositions had to contain 1 sodium atom and 4 oxygen atoms. The first measurement of m/z 809.7433 was used to calculate an empirical formula using commercially available OPUS software (Micromass U.K. Ltd). An error limit of < 15 ppm was entered prior to computation and the following table lists the elemental compositions generated.

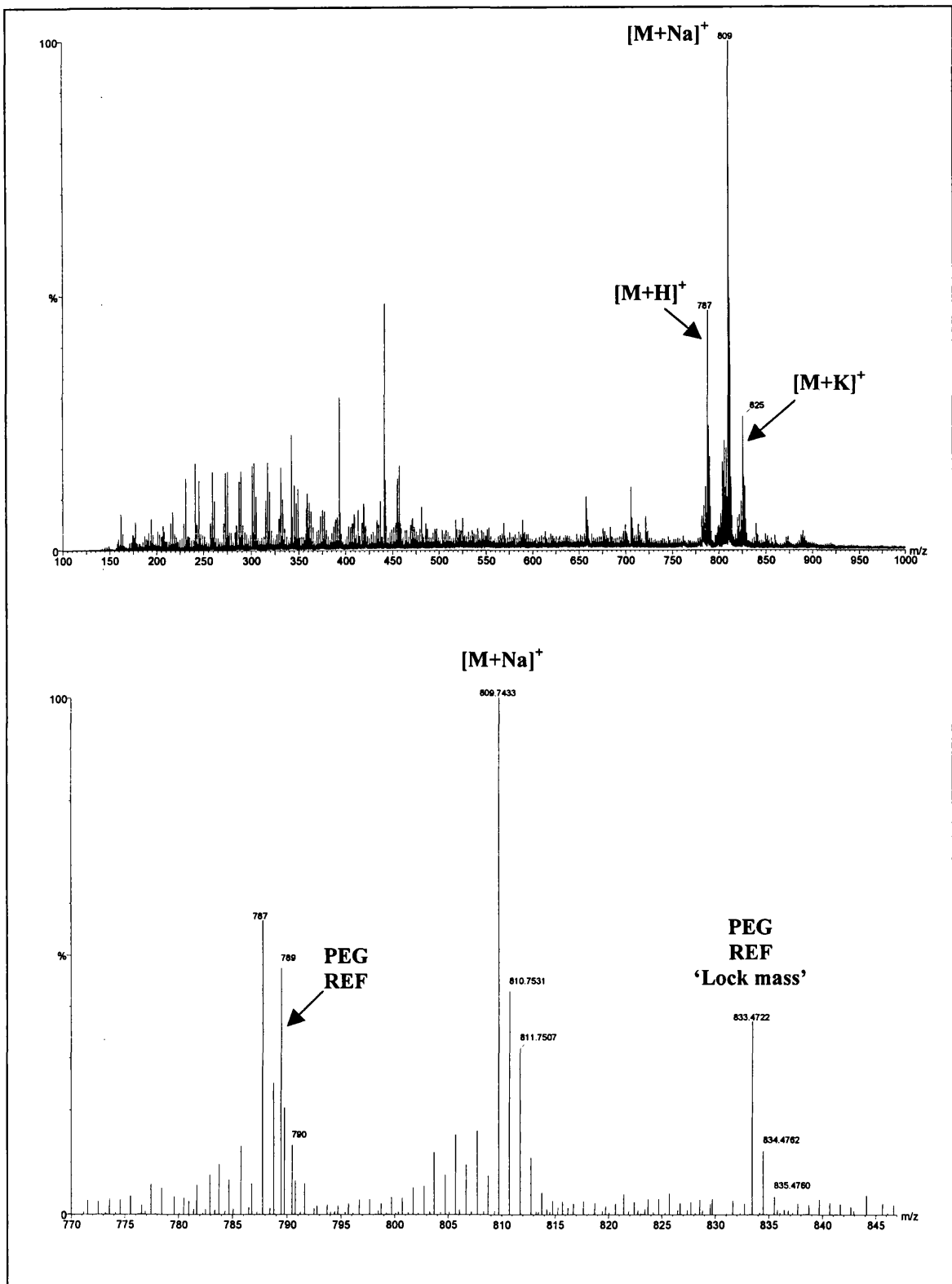
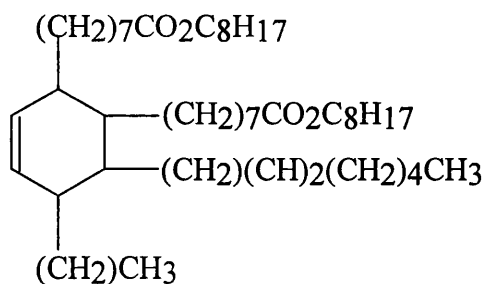


Figure 2.24: Unknown mass spectrum (top) and exact mass measurement spectrum (bottom)

ppm	mmu	Calculated mass	C	H	N	O	P	Na
-5.0	-4.0	809.7393	51	99	2	1	1	1
5.2	4.2	809.7475	51	98	2	3		1
-5.4	-4.3	809.7390	55	96	1	1		1
-7.0	-5.7	809.7376	53	94	4			1
8.5	6.9	809.7502	54	96	3			1
-8.7	-7.0	809.7363	52	98		4		1
8.9	7.2	809.7505	50	99	4		1	1
-9.9	-8.0	809.7353	46	99	4	3	1	1
10.2	8.2	809.7515	56	98		1		1
-10.3	-8.4	809.7349	50	96	3	3		1

From the computed empirical formulas, only one satisfied the mentioned prerequisites and was found to be $C_{52}H_{98}O_4Na$. The theoretical monoisotopic m/z for $[M+Na]^+$ equals 809.7363. The mass measurements obtained were accurate enough to provide the correct elemental composition and showed an average error of 0.9 mmu (1.1 ppm), since the structure of the additive, of molecular weight 786, was shown to be:



This additive has a trivial name of 3608 and is added to lubricant formulations.

Table 11 shows a summary of the exact mass measurement results.

The mass measurements gave impressive results for these classes of compounds. It should be noted that only a simple algorithm was used to calculate the results incorporating only one reference peak. Mass measurements of similar, or better accuracy could be obtained over much wider mass ranges by incorporating more reference peaks and fitting them over the mass range of interest.

Acquis ⁿ N°	Irganox 565	Irganox 1010	Em 3020	Irganox 1076	Irgafos 168	Tinuvin 327	Tinuvin 770Df	TCP	TXP	Unknown
1	589.3985	1194.8184	531.4427	553.4619	647.4610	358.1653	503.3856	369.1285	433.1537	809.7433
2	589.3928	1194.8184	531.4427	553.4619	647.4610	358.1651	503.3753	369.1288	433.1543	809.7413
3	589.3957	1194.8184	531.4427	553.4619	647.4610	358.1684	503.3817	369.1259	433.1541	809.7343
4	589.4001	1194.8184	531.4427	553.4619	647.4610	358.1651	503.3789	369.1248	433.1523	809.7229
5	589.3971	1194.8201	531.4427	553.4619	647.4610	358.1651	503.3772	369.1306	433.1524	809.7443
Mean	589.3968	1194.8187	531.4427	553.4619	647.4610	358.1658	503.3797	369.1277	433.1534	809.7372
Mean Error(mmu)	-0.56	0.24	1.4	2.2	1.7	-2.8	-2.8	2.12	-1.14	0.9
Mean Error (ppm)	-0.94	0.18	2.5	4.0	2.7	-7.8	-5.5	5.74	-2.62	1.1
Appendix	*Fig.2.22	Fig.2.25	Fig.2.26	Fig.2.27	Fig.2.28	Fig.2.29	Fig.2.30	Fig.2.31	Fig.2.32	*Fig.2.33

* Represents results to be found in main body write up

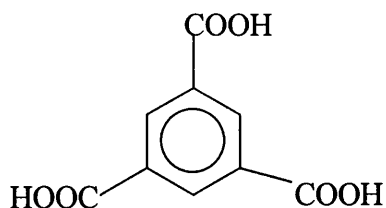
Table 11 : Shows the 5 exact mass measurement results obtained for the 10 polymer additives studied

2.3.8 In source cone voltage fragmentation of low level aryl carboxylic acids [67]

It has been demonstrated in the preceding sections the high sensitivity oa-toF technology possesses, yielding high ion signal-to-noise ratios from low levels of analyte concentration.

Specificity of structural assignment is facilitated if the mass spectra is composed of molecular and fragment ions. The LCT cannot perform MS/MS experiments, however, in source fragmentation can produce significant diagnostic ions. The technique of in-source CID has been applied to a variety of compound classes presented at low level concentrations and used to compare data obtained on the LCT and Platform instruments.

An example of one particular compound class studied was an aromatic carboxylic acid, trimellitic acid (TMA) of molecular weight 210 and structure shown below:



This compound class represents some of the impurities produced during synthesis of terephthalic acid, a major bulk chemical used for the production of polyester materials

and a basic component of polyethylene terephthalate (PET) plastic, which is used to package beverages and household products.

TMA was dissolved to a concentration of 500ppb in methanol for analysis on the LCT and to a concentration of 100ppm in methanol for use on the Platform. The samples were injected via a 10 μ L loop injection into a stream of methanol flowing at a rate of 10 μ L/min into the ESI source. Data acquisition was performed in negative ionisation mode.

Figure 2.33 shows the partial mass spectrum obtained from the LCT (top) produced with a cone voltage of 75V and the mass spectrum obtained on the Platform (bottom).

TMA yields an intense ion at m/z 209 at low cone voltages ($< 25V$), which corresponds to the deprotonated molecular ion $[M-H]^-$. As the cone voltage is increased, carbon dioxide neutrals are eliminated and ions corresponding to $[M-H-(44)_n]^-$, where $n=1-3$, are observed at m/z 165, m/z 121 and m/z 77. As the cone voltage was increased, the relative intensity of these structurally significant diagnostic ions increased.

It has been demonstrated that diagnostic fragment ions produced from in-source CID can be detected with a higher signal-to-noise ratio on the LCT from lower levels of analyte concentration. This procedure will facilitate the characterisation of complex mixtures when applied to separation science from low level sample concentrations and more importantly increase the specificity of structural assignment.

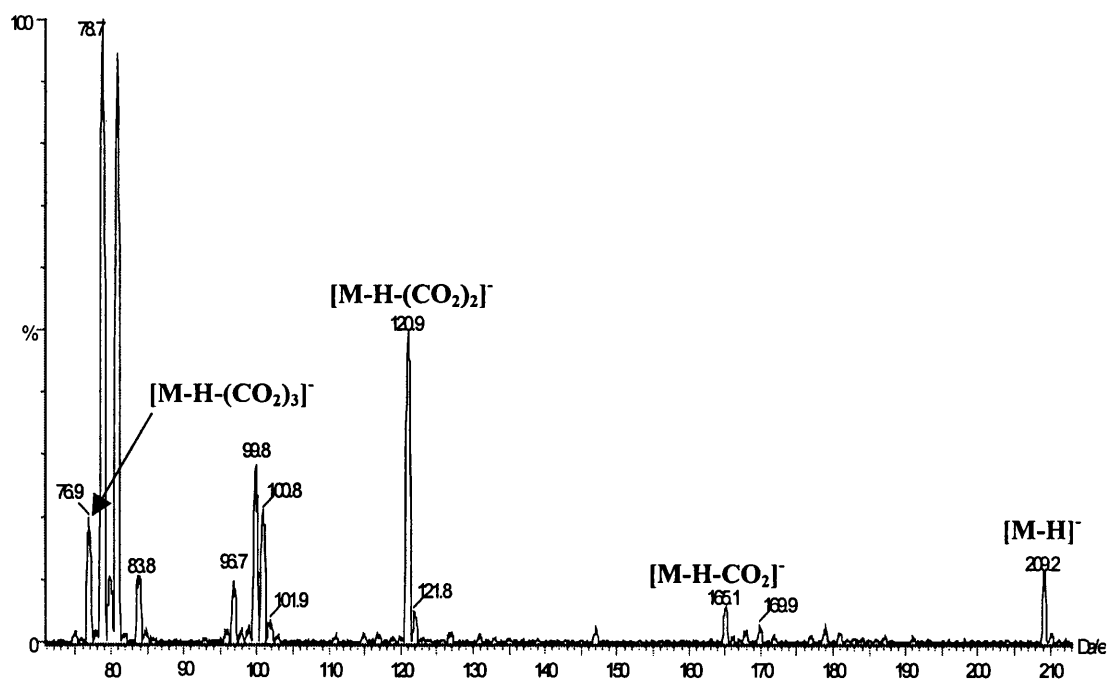
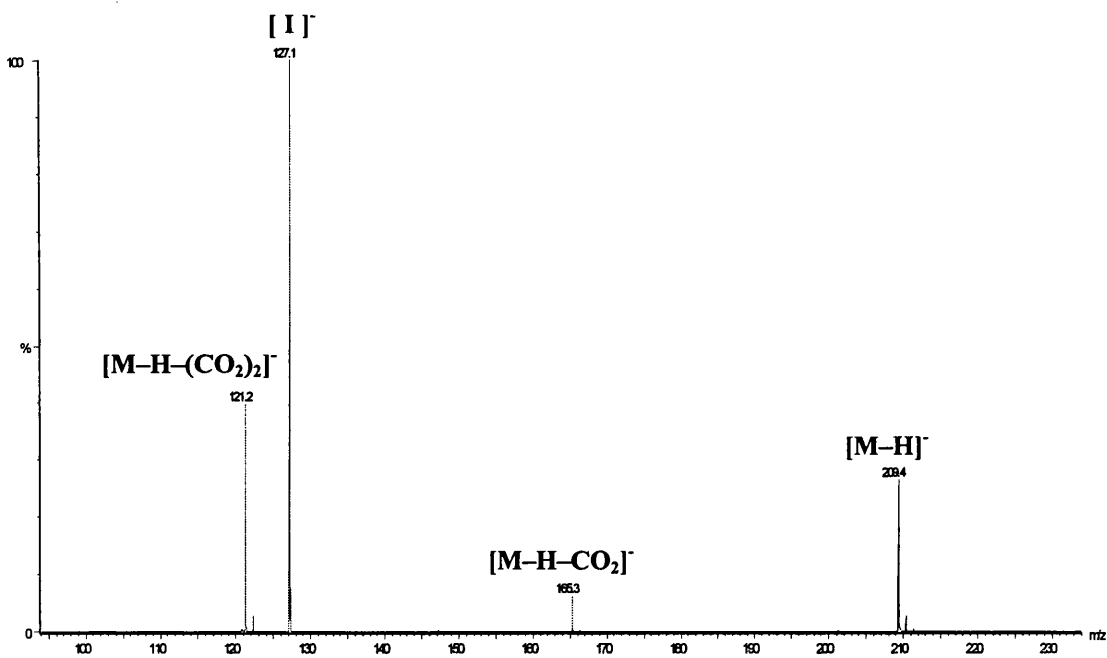


Figure 2.33 : Negative ion electrospray mass spectra obtained following in-source CID of 500ppb of TMA on LCT (top) and 100ppm of TMA on Platform (bottom)

2.4 Summary

The focus of modern industry on more and more complex product formulations, tighter environmental and legislative pressures and an overall increased competitive environment leads to a requirement for more sophisticated measurement science approaches.

Mass spectrometry has, for some years played a central role in the characterisation of these complex systems both alone and in combination with various separation science approaches.

The advent of oa-ToF technology forms an important advance in this area. The combination of increased sensitivity, mass range, mass resolution, scan speed compared with existing instrumentation gives an important edge in a competitive market. The equipment continues to develop at a fast pace and it is clear that this approach will make a significant impact in this area in the coming years.

2.5 Conclusions

Comparisons have been obtained between oa-ToF technology and existing quadrupole instruments. In all cases ESI was used as the ionisation method. The main areas studied were; mass range, mass resolution, sensitivity, scan speed and mass measurement accuracy. The main conclusions are as follows:

1. The useable mass range of the oa-ToF is significantly higher than the quadrupole for singly charged ions. The mass range of the ToF could be significantly increased with improvements in faster digital electronics and improved detector design.
2. The mass resolution obtained on the oa-ToF (~ 5000 FWHM) is significantly better than that obtainable by quadrupole instrumentation. This means that less interference's are observed and that higher mass species can be studied. Rapid advances in ToF development indicate that higher resolution systems are likely in the near future.
3. The combination of very fast data acquisition rates and sensitivity afforded by the oa-ToF makes it an ideal detector for many separation science approaches. The more faster techniques, with lower sample loadings and narrower peaks widths, means that the use of oa-ToF will become increasingly important.
4. The mass measurement accuracy of the oa-ToF gives results, in ESI mode, that are comparable with those obtained traditionally using magnetic sector instruments. The combination of sensitivity, mass resolution and the stability of the mass calibration that oa-ToF affords, means that exact mass measurements are relatively easy to perform.
5. The ease of the approach, the relatively compact deign of the instrument and the facility of computer interfacing and control, all add to the attractiveness of the technique. This enables the instrument to be utilised effectively by non specialists.

2.6 References

1. MJ Taylor, ICI Wilton, Teeside, U.K.
2. J Zeleny, *Phys.Rev.*, 10 (1917) 1.
3. M Dole, LL Mach, RL Hines, RC Mobley, LP Ferguson, MB Alice, *J.Chem.Phys.*, 49 (1968) 2240.
4. JB Fenn, M Mann, CK Meng, SF Wong, CM Whitehouse, *Science*, 246 (1989) 64.
5. JB Fenn, *J.Phys.Chem*, 88 (1984) 4671.
6. JB Fenn, *J.Phys.Chem*, 92 (1988) 546.
7. JB Fenn, CK Meng, M Mann, *Z.Phys.D: At., Mol. Clusters*, 10 (1988) 361.
8. ML Aleksandrov, NL Gall, NV Krasnov, VI Nikolaev, VA Paulenko, VA Shkurou, *Dokl.Akad.Nauk.SSR*, 277 (1984) 379.
9. CK Meng, CN McEwen, BS Larsen, *Rapid Commun.Mass Spectrom.*, 4 (1990) 147.
10. BS Larsen, CN McEwen, *J.Am.Soc.Mass Spectrom.*, 2 (1991) 205.
11. RJ Gallagher, JR Chapman, *Rapid Commun.Mass Spectrom.*, 4 (1990) 369.
12. GJ Van Berkel, GL Glish, SA McLuckey, *Anal.Chem.*, 63 (1990) 1284.
13. AV Mordehai, G Hopfgartner, TG Huggins, JD Henion, *Rapid Commun.Mass Spectrom.*, 6 (1992) 508.
14. KD Henry, ER Williams, BH Wang, FW McLafferty, J Shabanowitz, DF Hunt, *Proc. Natl.Acad.Sci. USA*, 86 (1989) 9075.
15. SA Hofstadler, DA Laude, *Anal.Chem.*, 64 (1992) 572.
16. BE Winger, SA Hofstadler, JE Bruce, HR Udseth, RD Smith, *J.Am.Soc.Mass Spectrom.*, 4 (1993) 566.
17. JE Boyle, CM Whitehouse, JB Fenn, *Rapid Commun. Mass Spectrom.*, 5 (1991) 400.
18. AF Dodonov, IV Chernushevich, TF Dodonova, VV Raznikov, VL Tal'roze, *USSR Patent # 1681340A1*, (Feb.1987).
19. GI Taylor, *Proc.R.Soc.London A*, A280 (1964) 383.

20. P Kebarle, L Tang, *Anal.Chem.*, 65 (1993) 972A.
21. DPH Smith, *IEEE Trans.Ind.Appl.*, IA-22 (1986) 527.
22. Lord Rayleigh, *Philos.Mag.*, 14 (1882) 184.
23. JV Iribarne, BA Thomson, *J.Chem.Phys.*, 64 (1976) 2287.
24. BA Thomson, JV Iribarne, *J.Chem.Phys.*, 71 (1979) 4451.
25. C Hagg, I Szabo, *Int.J.Mass Spectrom.Ion Processes*, 73 (1986) 295.
26. PH Dawson, DJ Douglas, in FW McLafferty (Ed.), *Tandem Mass Spectrometry*, Wiley, New York, 1983, P.125.
27. RA Yost, CG Enke, in FW McLafferty (Ed.), *Tandem Mass Spectrometry*, Wiley, New York, 1983, P.175.
28. PH Dawson, JE Fulford, *Int.J.Mass Spectrom.Ion Processes*, 42 (1892) 195.
29. JH Beynon, FM Harris, BN Green, RH Bateman, *Org. Mass Spectrom.*, 17 (1982) 55.
30. RG Cooks, *Anal. Chem.*, 57 (1985) 823A.
31. GL Glish, SA McLuckey, TY Ridely, RG Cooks, *Int.J.Mass Spectrom.Ion Processes*, 41 (1982) 157.
32. RA Yost, DD Fetterolf, *Mass Spectrom. Rev.*, 2 (1983) 1.
33. E Teloy, D Gerlich, *Chem. Phys.*, 83 (1985) 166.
34. DJ Douglas, JB French, *J.Am.Soc.Mass Spectrom.*, 3 (1992) 398.
35. J Franzen, *Proceedings of the 44th ASMS Conference on Mass Spectrometry and Allied Topics*, Portland, OR, 1996; P1170.
36. CM Whitehouse, E Gulcicek, Multipole Ion Guide for Mass Spectrometry, *Int. Pat. No. WO95/23018* (1995).
37. YL Huang, SH Guan, HS Kim, AG Marshall, *Int.J.Mass Spectrom.Ion Processes*, 152 (1996) 121.
38. AV Tolmachev, IV Chernushevich, AF Dodonov, KG Standing, *Nuclear instruments & methods in physics research section: beam interactions with materials and atoms*, 12 (1997) 112.
39. AN Krutchinsky, AV Loboda, VL Spicer, R Dworschak, W Ens, KG Standing, *Rapid Commun.Mass Spectrom.*, 12 (1998) 508.

40. BA Thomson, *Canadian J of Chem.-revue Canadienne de chimie*, 76 (1998) 499.
41. AN Krutchinsky, IV Chernushevich, V Spicer, W Ens, KG Standing, *J.Am.Soc.Mass Spectrom.*, 9 (1998) 569.
42. DJ Douglas, JB French, *J.Am.Soc.Mass Spectrom.*, 3 (1992) 398.
43. PH Dawson, in 'Quadrupole mass spectrometry and its applications', Elsevier, New York, 1976.
44. WC Wiley, IH McLaren, *Rev.Sci.Int.*, 26 (1955) 1150.
45. G Sanzone, *Rev.Sci.Int.*, 41 (1970) 741.
46. SM Michael, M Chien, DM Lubman, *Rev.Sci.Int.*, 63 (1992) 4277.
47. R Grix, H Gruner, G Li, H Stroh, H Wollnik, *Int.J.Mass Spectrom.Ion Processes*, 93 (1989) 323.
48. RE Tecklenburg, RD McLane, R Grix, CC Sweeley, J Allison, JT Watson, JF Holland, C Enke, H Gruner, H Gotz, H Wollnik, *Proceedings of the 38 th ASMS Conf. On Mass Spectrom. and Allied Topics*, AZ, 1990, 896.
49. X Tang, R Beavis, W Ens, B Schueler, KG Standing, F Lafortune, *Int.J.Mass Spectrom.Ion Processes*, 85 (1988) 43.
50. J Coles, M Guilhaus, *Trends in Anal.Chem.*, 12 (1993) 203.
51. JH Dawson, M Guilhaus, *Rapid Commun.Mass Spectrom.*, 3 (1989) 155.
52. AN Verentchikov, W Ens, KG Standing, *Anal.Chem.*, 66 (1994) 126.
53. RH Bateman, MR Green, G Scott, E Clayton, *Rapid Commun.Mass Spectrom.*, 9 (1995) 1227.
54. AF Dodonov, IV Chernushevich, VV Laiko, *12 th IMSC, Book of abstracts*, 1991, P.153.
55. Back-to-Basics: *Fisons Monographs*
56. IV Chernushevich, W Ens, KG Standing, in 'Electrospray Ionisation: Principles and Practice', Ed. R Cole, 1996.
57. Personal communication with Micromass engineer, John Leslie.
58. BA Mamyrin, VI Karataev, DV Shmikk, *Soviet Physics-Technical Physics*, 16 (1972) 1177.

59. N Booth, *Rapid Commun. Mass Spectrom.*, 11 (1997) 943.
60. GC Hilton, JM Martinis, DA Willman, KD Irwin, LL Dulcie, D Gerber, PM Gillevet, D Twerenbold, *Nature*, 391 (1998) 672.
61. M Frank, CA Mears, SE Labov, WH Benner, D Horn, JM Jaklevic, AT Barfknecht, *Rapid Commun. Mass Spectrom.*, 10 (1996) 1946.
62. WJ Dollard, AT Jackson, JH Scrivens, MJ Deery, KR Jennings, *Proceedings of the 47th ASMS* 1999.
63. H Kaiser, *Anal. Chem.*, 42 (1987) 53A.
64. American Analytical Methods Committee, *Analyst*, 112 (1987) 199.
65. E Prichard in, '*Quality in the analytical Chemistry Laboratory*', 1995, Wiley and Sons, U.K.
66. AD Schwoppe, *Food Chem. Toxicol.*, 25 (1987) 317.
67. MJ Taylor, JP Williams, JH Scrivens, CM Brookes, *Proceedings of the 46th ASMS* 1998.
68. P Dickey, '*Troubling Bubbles*', Washington Toxics Coalition, Seattle, Washington, 1997.
69. R Willoughby, E Sheehan, S Mitrovich, in a '*Global view of LCMS*', Global View Publishing, Pittsburgh, Pennsylvania, 1998.
70. JH Beynon, '*Mass Spectrometry and its applications to organic chemistry*', Elsevier, Amsterdam, 1966.
71. AG Marshall, CL Hendrickson, GS Jackson, *Mass Spectrom. Rev.*, 17 (1998) 1.
72. AN Tyler, E Clayton, BN Green, *Anal. Chem.*, 68 (1996) 3561.
73. J Roboz, JF Holland, MA McDowall, MJ Hillmer, *Rapid Commun. Mass Spectrom.*, 2 (1988) 64.
74. WF Haddon, LA Harden, AE Lieberman, *Proceedings of the 38th ASMS*, 1990, P.122.
75. R Kostianen, J Tuominen, L Luukkanen, J Taskinen, BN Green, *Rapid Commun. Mass Spectrom.*, 11 (1997) 283.
76. JHJ Dawson, M Guilhaus, *Rapid Commun. Mass Spectrom.*, 3 (1993) 155.
77. AN Verentchikov, W Ens, KG Standing, *Anal. Chem.*, 66 (1994) 126.

78. IV Chernushevich, W Ens, KG Standing, '*Electrospray ionisation: Principles and practice*', RB Cole Ed., John Wiley and sons Inc., New York, P.203.
79. HR Morris, T Paxton, A Dell, J Langthorne, M Berg, RS Bordoli, RH Bateman, *Rapid Commun. Mass Spectrom.*, 10 (1996) 889.
80. DH Russell, RD Edmundson, *J. Mass Spectrom.*, 32 (1997) 263.
81. U Bahr, M Karas, *Rapid Commun. Mass Spectrom.*, 13 (1999) 1052.
82. T Keough, MP Lacey, MM Ketcha, RH Bateman, MR Green, *Rapid Commun. Mass Spectrom.*, 11 (1997) 1702.
83. LW Tetler, DR Little, ME Palmer, MR Clench, *Rapid Commun. Mass Spectrom.*, 13 (1999) 256.
84. AC Hogenboom, WMA Niessen, D Little, UA Th. Brinkman, *Rapid Commun. Mass Spectrom.*, 13 (1999) 125.
85. MWF Nielen, *Rapid Commun. Mass Spectrom.*, 13 (1999) 826.
86. JR Donnelly, AH Grange, WC Brumley, S Billets, GW Sovocool, *Anal. Chem.*, 66 (1994) 4416.
87. AT Jackson, A Buzy, KR Jennings, JH Scrivens, *Eur. Mass Spectrom.*, 2 (1996) 115.
88. DH Russell, RD Edmondson, *J. Mass Spectrom.*, 32 (1997) 263.
89. M Guilhaus, *J. Mass Spectrom.*, 30 (1995) 1519.
90. Gachter/Muller: '*Plastic Additives*', Hanser publishers
91. TL Riley, TJ Prater, JL Gerlock, JE DeVries, D Schuetzle, *Anal. Chem.*, 56 (1984) 2145.
92. CL Johlman, CL Wilkins, JD Hogman, TL Donovan, DA Laude Jr, MJ Youssefi, *Anal. Chem.*, 62 (1990) 1167.
93. RP Lattimer, RE Harris, DB Ross, HE Diem, *Rubber Chem. Technol.*, 57 (1984) 1013.
94. B Asamoto, JR Young, RJ Citerin, *Anal. Chem.*, 62 (1990) 61.
95. MP Mawn, RW Linton, SR Bryan, B hagenhoff, U Jurgens, A Benninghoven, *J. Vac. Sci. Technol.*, A9 (1991) 1307.

96. JE Hunt, KR Lykke, MJ Pellin, '*Methods and mechanisms for producing ions from large molecules*', KG Standing Ed., Plenum press, New York, 1991.
97. SJ Wright, MJ Dale, PRR Langridge-Smith, Q Zhan, R Zenobi, *Anal. Chem.*, 68 (1996) 3585.
98. MJ Carrott, DC Jones, G Davidson, *Analyst*, 123 (1998) 1827.

Appendix I (Chapter 2)

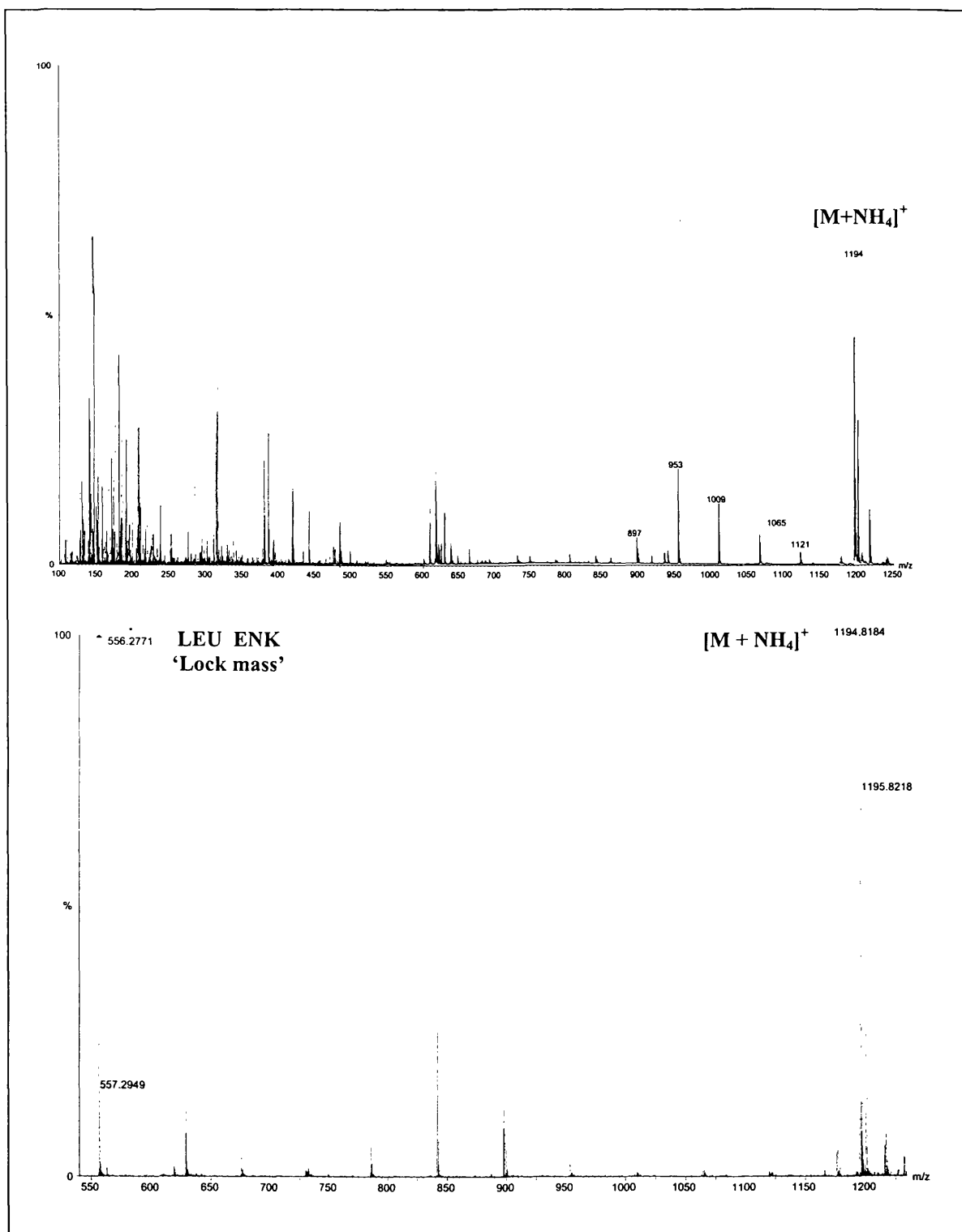


Figure 2.25: Irganox 1010 mass spectrum (top) and exact mass measurement spectrum (bottom)

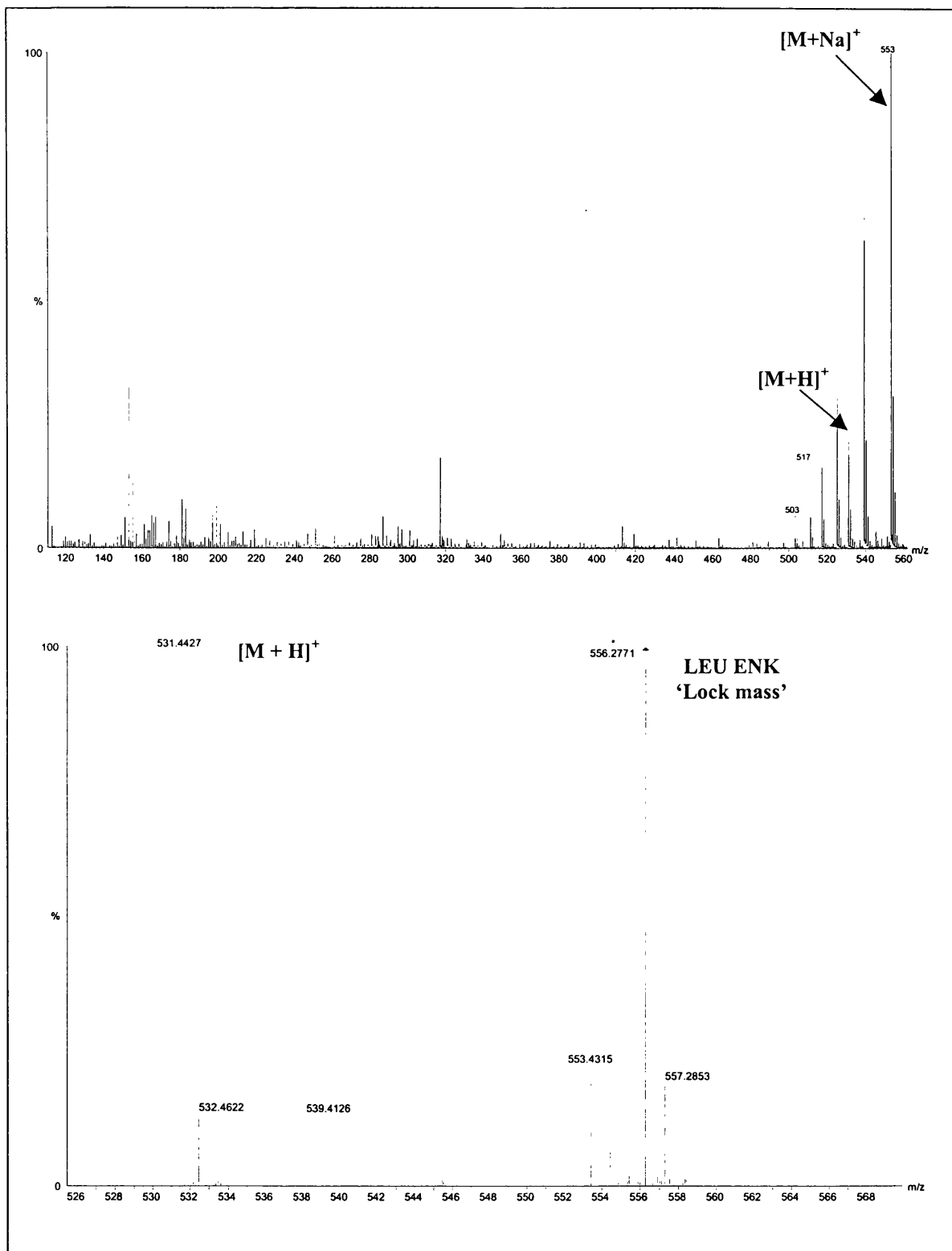


Figure 2.26: Emkarate 3020 mass spectrum (top) and exact mass measurement spectrum (bottom)

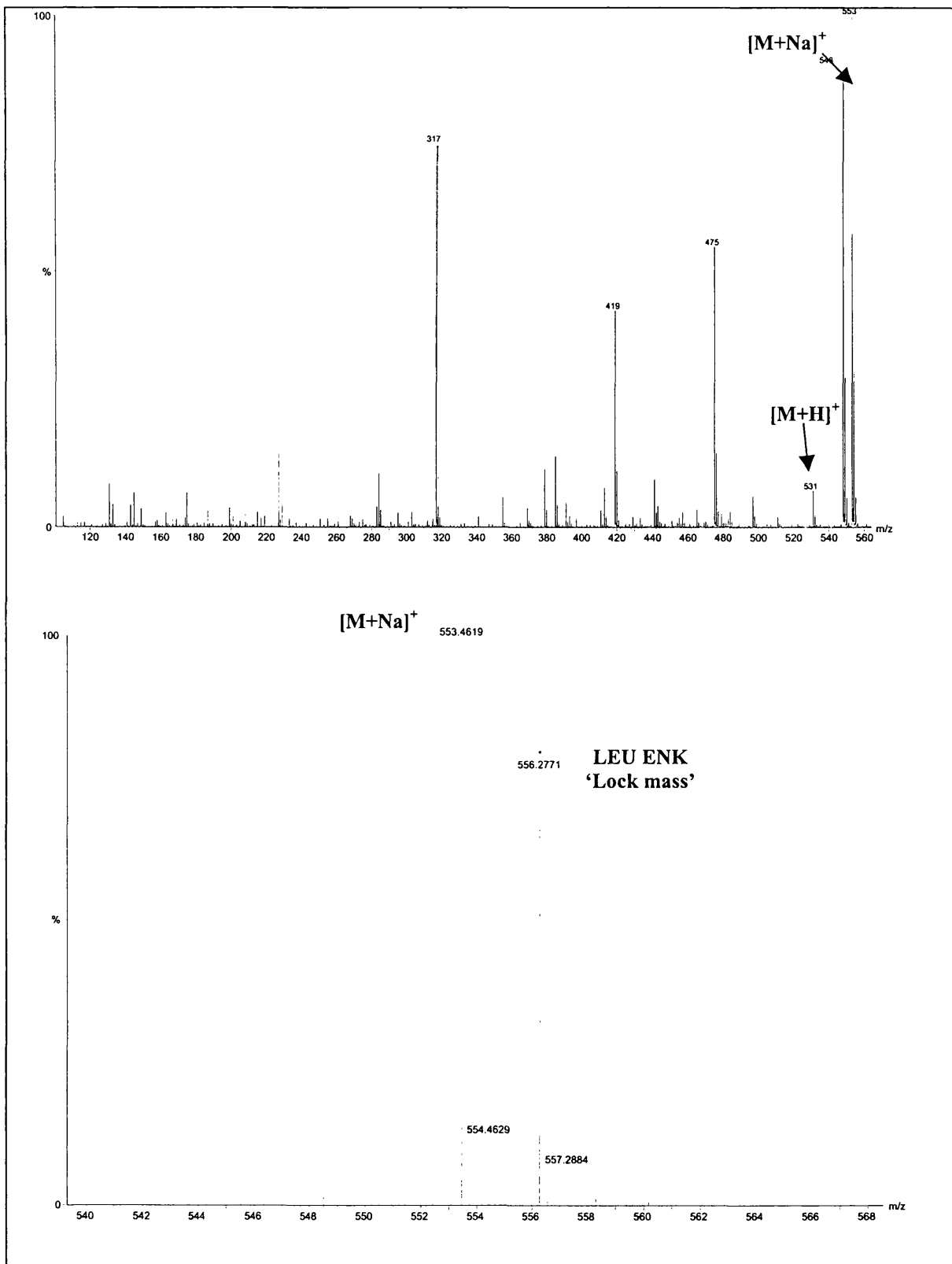


Figure 2.27: Irganox 1076 mass spectrum (top) and exact mass measurement spectrum (bottom)

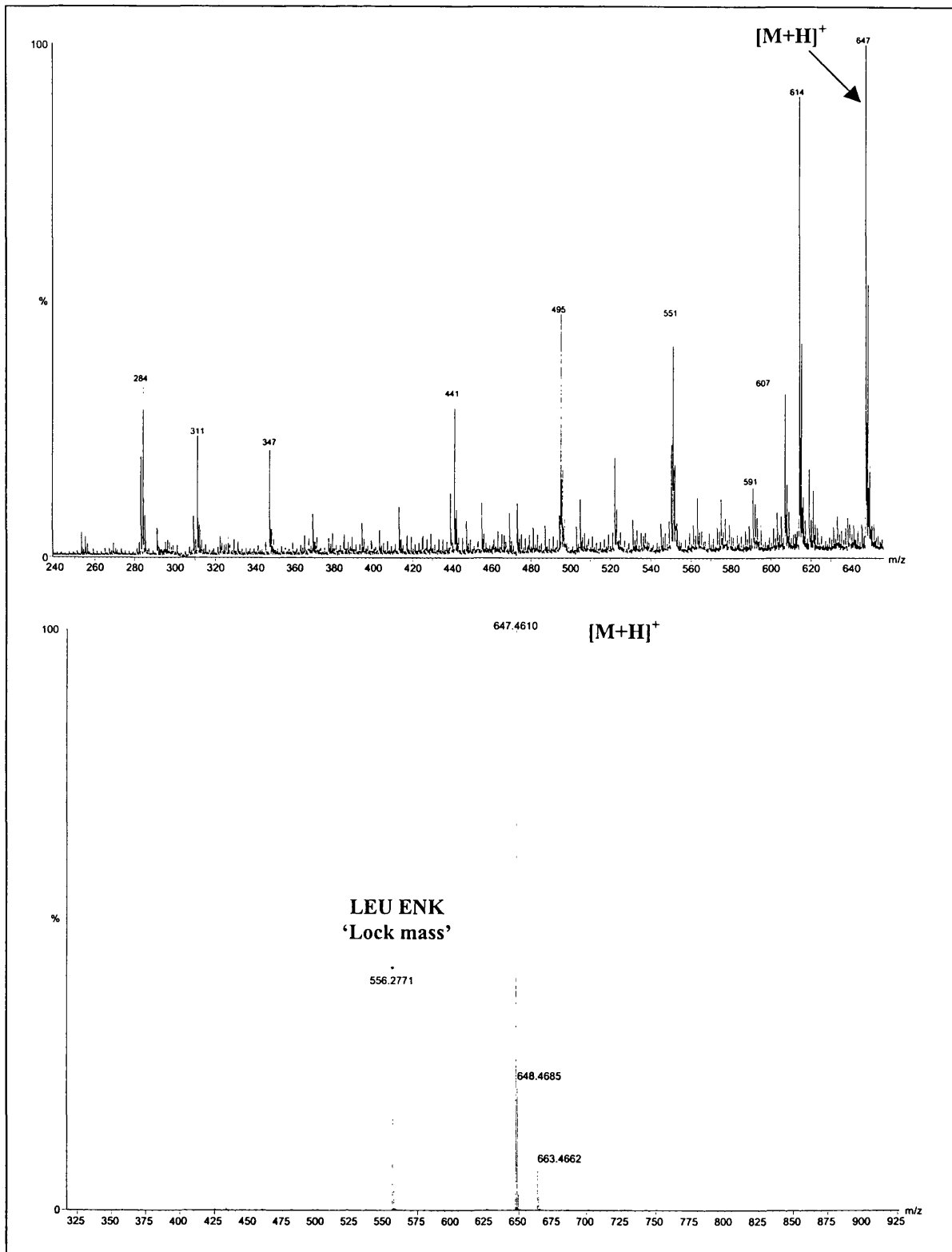


Figure 2.28: Irgafos 168 mass spectrum (top) and exact mass measurement spectrum (bottom)

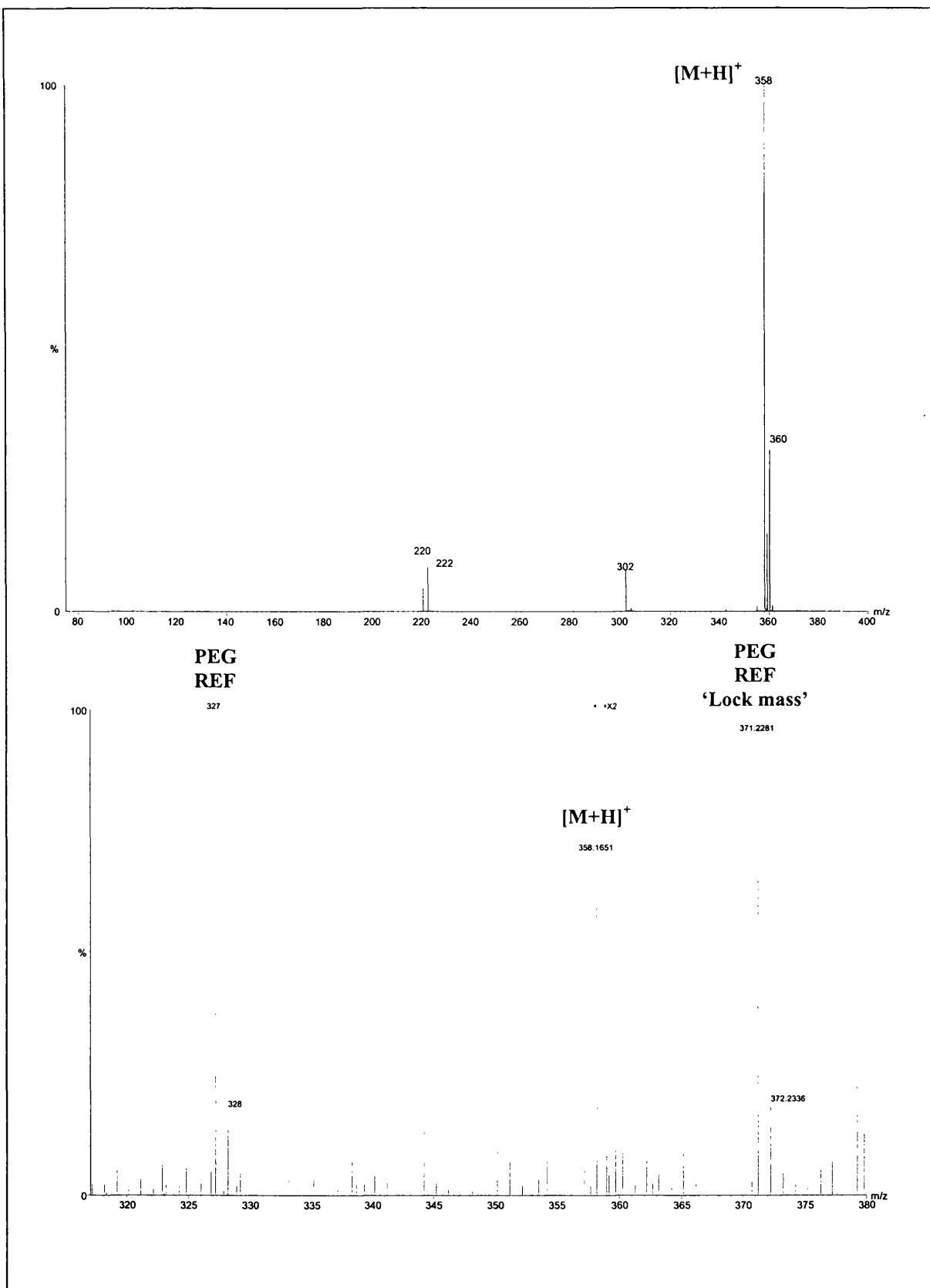


Figure 2.29: Tinuvin 327 mass spectrum (top) and exact mass measurement spectrum (bottom)

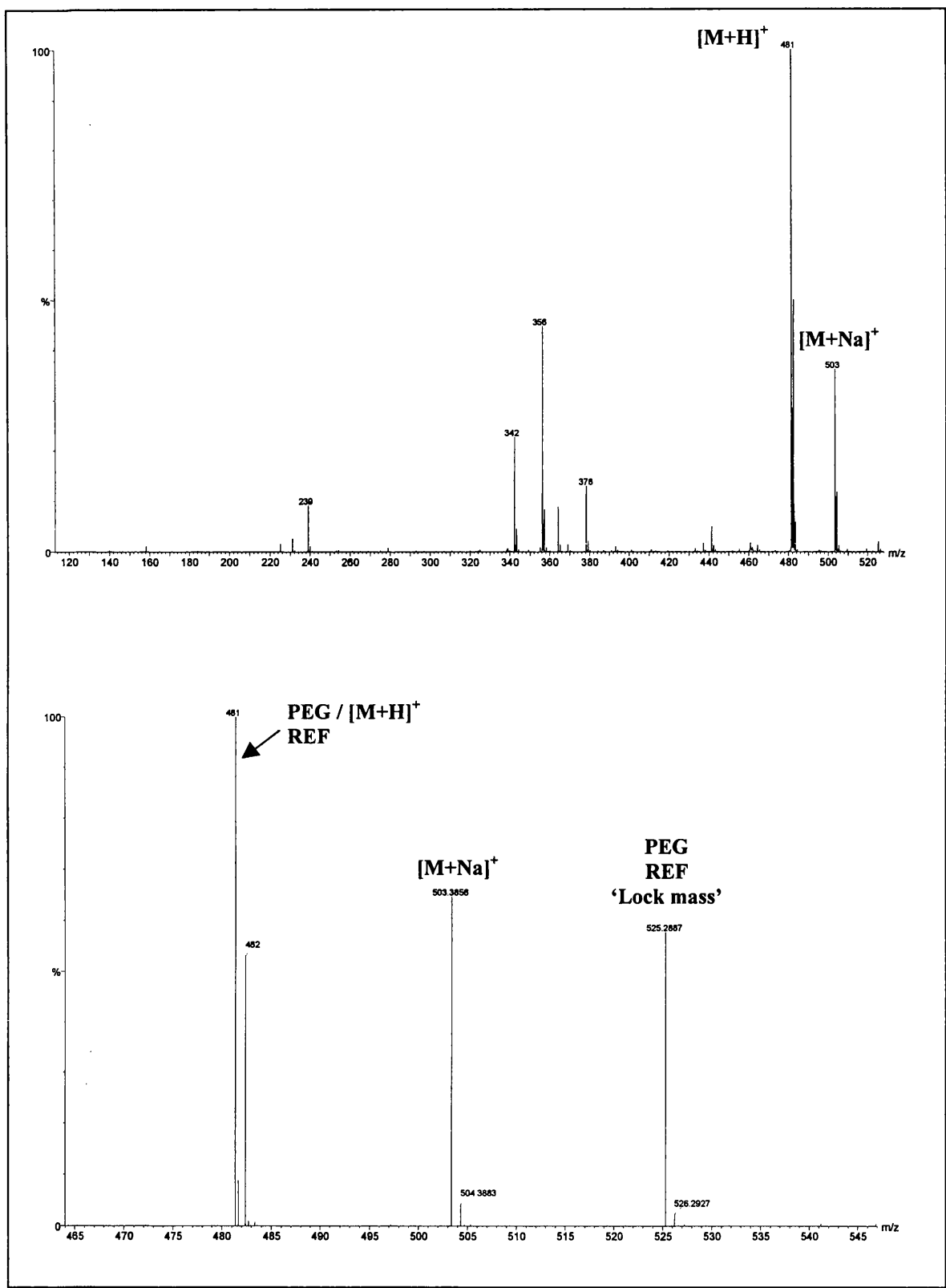


Figure 2.30: Tinuvin 770Df mass spectrum (top) and exact mass measurement spectrum (bottom)

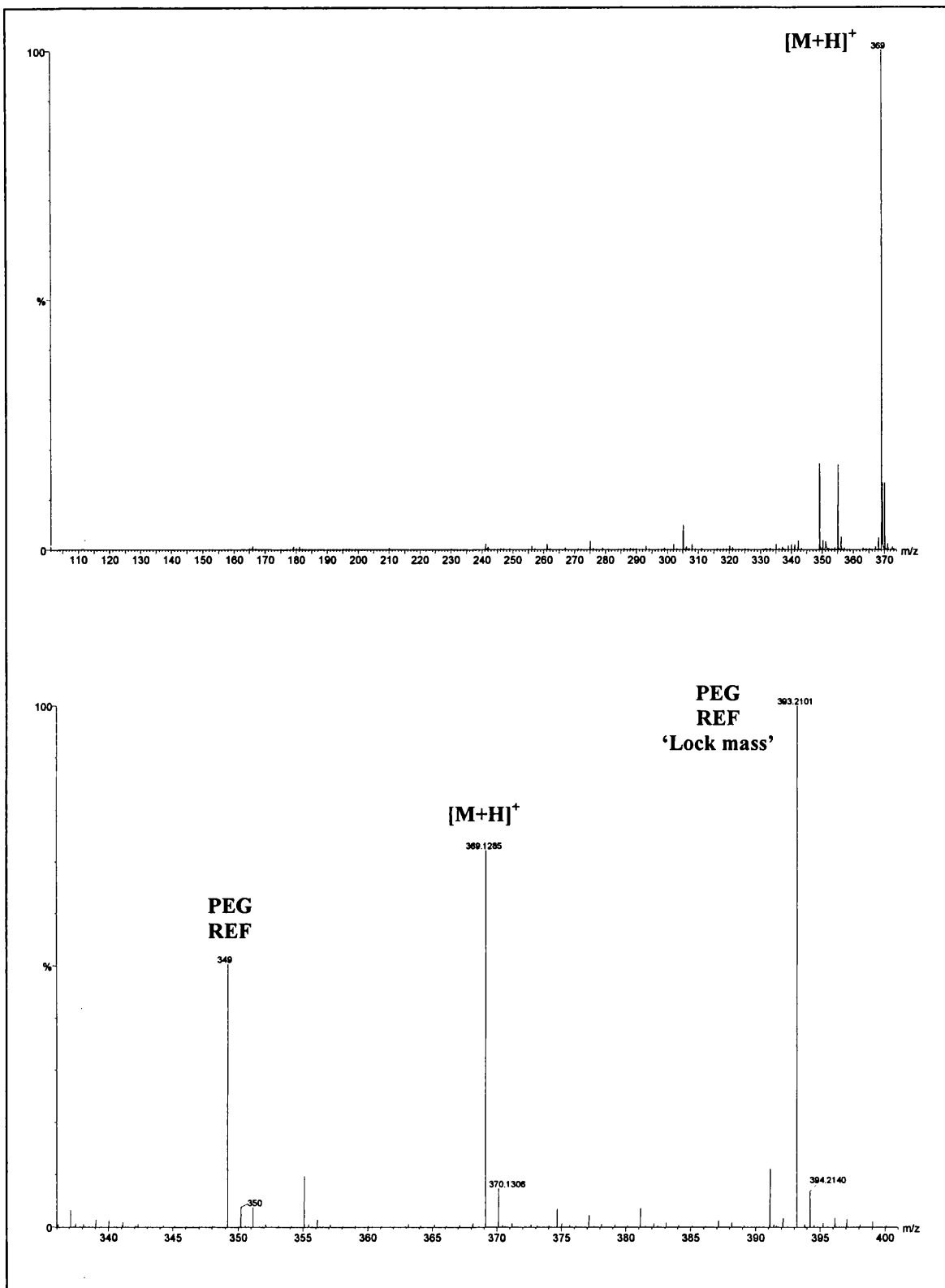


Figure 2.31: TCP mass spectrum (top) and exact mass measurement spectrum (bottom)

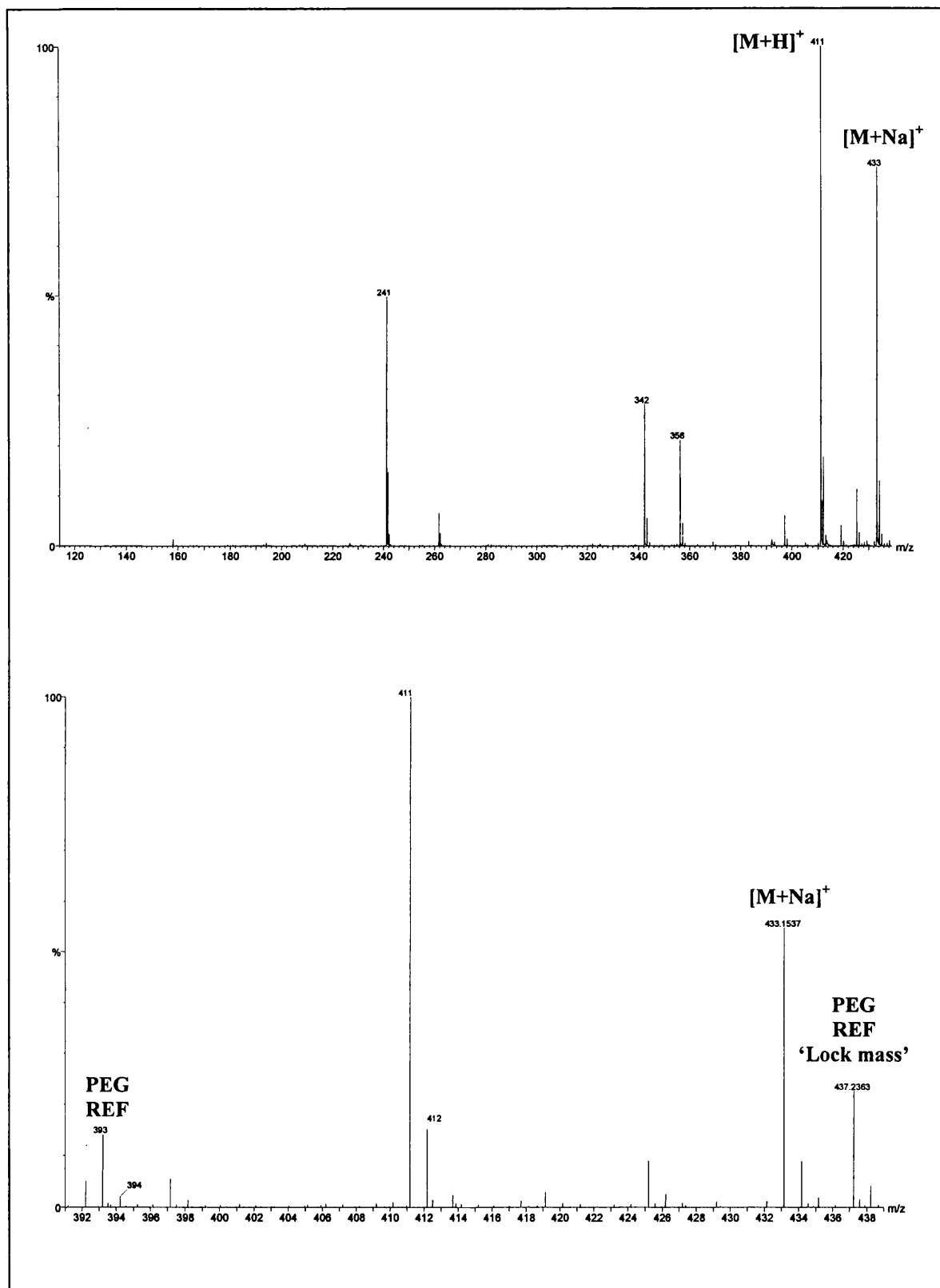


Figure 2.32: TXP mass spectrum (top) and exact mass measurement spectrum (bottom)

Chapter 3

End group determination of some Polystyrene synthetic polymers by means of MALDI-CID orthogonal acceleration- TOFMS

3.1 Aim

The objective of the following chapter was to determine end group information of four polystyrene polymers by means of matrix assisted laser desorption ionisation-collision induced dissociation (MALDI-CID) TOFMS. The investigation was performed in a magnetic sector orthogonal acceleration ToF mass spectrometer. The instrument, commercially known as the Autospec-oa-ToF, was manufactured by Micromass U.K. Ltd.

3.2 Development and principles of MALDI

The ability to determine accurate and sensitive methods for molecular mass determination of biological and polymer macromolecules in the first instance seems rather difficult. Molecules of this type are typically several hundred kilo daltons in mass and need to be converted as intact ionised molecules from the solid phase to the gas phase. This seems problematic due to their large size, their involatility and generally because of their are polarity.

Until MALDI was developed, several earlier methods were adopted to ionise such large molecules. Field desorption (FD) [1] was used by application of an electric field to the sample, plasma desorption (PD) [2] and secondary ionisation mass spectrometry (SIMS) [3], made use of energetic ions or atoms to ionise the sample and laser desorption (LD) [4], where the sample was ionised by bombardment of short intense pulses of laser light.

These earlier methods set the foundation on which the MALDI technique was built. MALDI [5-7] was developed over a decade ago and as since revolutionised modern day mass spectrometric analysis of bio and polymer macromolecules. As a desorption technique MALDI provides improved resolution and mass accuracy compared with PDMS and fast atom bombardment (FAB) [8] (where a beam of ions or high energy atoms are directed at the sample). The latter techniques, also inconveniently use more sample and take a longer time to generate spectra.

Critical to the success of the MALDI process is the matrix solution the analyte sample is mixed with. The analyte sample is mixed with an excess of matrix and the ratio is dependent on the analyte sample. The choice of matrix will depend solely on the molecule being investigated. Desorption occurs by firing a laser, typically N₂ which has a laser wavelength of 337 nm, directly at the sample mixture. The mixture is generally spotted on a steel plate contained in the source region of the mass spectrometer. The matrix serves to absorb light from the laser and isolate analyte molecules. The combination also serves to reduce aggregates being formed from analyte molecules and provides protonated or deprotonated products that ionise analyte molecules. The sample mixture combination expands from the solid phase to the gas phase, where analyte molecules, depending on laser power, remain intact.

The laser delivers an efficient, quick and constant amount of energy to the sample. Molecular ions are generated just above threshold irradiance, whilst too much power will result in fragmentation. The N₂ laser typically produces a 3ns pulse with a fixed energy of 180 μJ [9]. The energy transfer is efficient and the analyte molecules avoid thermal degradation due to the excess presence of the matrix. Ionisation is thought to

be formed by a photoexcitation or photoionisation process followed by protonation or deprotonation from the matrix and sample combination [58].

In summary, MALDI is capable of producing intact molecular ions with molecular weight beyond several hundred kilo daltons. It is a pulsed technique which produces packets of ions from every laser pulse. Thus, MALDI can exploit one of the inherent advantages of TOFMS, its theoretical unlimited mass range.

3.2.1 MALDI TOFMS

The generation of ions from pulsed sources, such as MALDI immediately forms a suitable partnership to ToF mass analysers, since TOFMS requires a well defined starting point in time and space. Ion transmission is high since ToF acquires spectra over the full mass range without scanning. The ‘spotted’ (matrix plus sample) target is set perpendicular to the ToF axis. The ions formed from the desorption process, are extracted in this direction by application of an electric field and the flight time is measured over the linear or reflected flight path. However, a major limitation of early ToF experiments was the relatively poor resolution attained. A resolution of ~ 500 was common in linear mode since the initial spatial and energy spread were not compensated for. The energy spread of the desorbed ions becomes large once they are extracted into the ToF analyser due to collisions with residual gas [10] and can be compensated for by a reflectron [11] but the distribution in time upon ion acceleration cannot be corrected by the reflectron [12].

Significant developments in overcoming the resolution problem were reached in 1994 when Lennon *et al.* [13] applied time-lag focusing, known today as delayed extraction, which provided spatial focusing of the ions. Their results showed an increase in resolution (cytochrome c) up to > 1000 (FWHM). The technique was based on the principles of Wiley and McLaren [14] in which a delay is introduced purposely between ion formation and the extraction of the formed ions. Extraction of the ions cause not only a velocity spread but also a spatial spread which limits resolution. However, if the time delay and careful choice of acceleration potential is applied, ions of the same mass will arrive at the detector at the same time, thus improving the resolving power of the instrument. One shortfall of delayed extraction is that it is mass dependent, this means that the larger the ion the longer the delay.

The combination of delayed extraction with a reflectron yields yet a more significant increase in resolution. Here ions are focused at a plane just beyond the extraction region, called the 'space focus' position. The ions arrive at the space focus with variation in velocity which can then be corrected for by the reflectron. Vestal *et.al* [15] have demonstrated a resolution of > 20000 (FWHM) for bovine insulin with this combination.

The development of TOFMS in the 1990's owes (amongst other things) much to the MALDI technique. Developments in fast digital electronics for recording the vast amount of spectra generated every second, together with the reflectron and delayed extraction has placed TOFMS at the forefront of modern day mass spectrometry.

3.2.2 The application of MALDI TOFMS to Synthetic Polymers

The use of MALDI for the analysis of synthetic polymeric systems has gained widespread use since encouraging results were first reported in the early 1990's. Bahr *et al.* [16] and Danis *et al.* [17] showed that molecular weights up to the order of several hundred kDa could be detected for poly(methylmethacrylate) (PMMA) and poly(styrene) (PS) polymers. ToF mass analysers are coupled to MALDI sources since they form a suitable partnership. Therefore, investigative studies of synthetic polymers by TOFMS owes much to the development of the MALDI technique.

Structural determination and molecular weight distribution are the two main experimentally investigative objectives of synthetic polymers by MALDI TOFMS. End group determination, repeat unit mass, the number average molecular weight (M_n), the weight average molecular weight (M_w) are parameters that can be determined for systematic characterisation of polymeric systems. Many of the above parameters have been determined from low molecular weight polymers (< 20000 Da) to polymers weighing up to 1.5 MDa. Many synthetic polymers have been studied since the introduction of MALDI. Some brief examples are discussed. Low molecular studies have been demonstrated on nylon 6, polycarbonate, polybutylene adipate, polycaprolactone [18] of varying polydispersity, molecular weight distribution of poly(butylmethacrylate) (PBMA) has been studied and compared to size exclusion chromatography (SEC) data [19], polydimethyl siloxane (PDMS), polybutadiene and polyisoprene has been investigated by variation of the matrix sample [20] and the use of time-lag focusing has been applied to polyesters investigating cation influence [21]. However, the majority of studies have involved the characterisation of PMMA

[18,22-32], PS [18-21,25,29,33-35] and poly(ethylene glycol) (PEG) [18,20,21,36-39] over the last decade.

A key aspect of polymer system analysis, is the addition of a metal salt to the sample preparation to aid ionisation. This enables metal-cation attachment called 'cationisation' [22,40,41]. Silver and copper salts are used most frequently with non-polar systems such as polystyrene and polybutadiene, since they have been shown to give better ion signal intensity [42,43]. Alkali metal cations are typically used for more polar, oxygen containing polymers and protonation is used for nitrogen containing polymers. Recent studies have shown that metallocenes such as ferrocene, nickelocene and cobaltocene can be used as cationising agents for PS and PEG samples [44]. Results showed that signal intensity was improved for higher polymer masses.

The acquisition of a MALDI spectrum is influenced by instrumental parameters such as acceleration fields, laser wavelength, laser energy, laser pulse width and incident angle of laser. Some of these effects have been analysed for wide polydisperse polymers [45].

The molecular weight distributions of polymers such as PS, PMMA and PEG with varying polydispersity have been thoroughly investigated and show some fundamental limitations for systems that have a polydispersity > 1.2 obtained by the MALDI technique [18,46,47]. Thus, much attention has been paid concerning this phenomena [18,19,30,48].

[A commonly used technique utilised for the calculation of the molecular weight distribution of synthetic polymers is SEC. This method is routinely used by the polymer manufacturer to yield a most probable molecular weight, which is taken at the apex of the peak obtained by the SEC chromatogram].

For polymers which have a narrow molecular weight distribution, polydispersity < 1.2, data obtained by SEC and MALDI TOFMS are often in close agreement [25,49]. However, for systems with a polydispersity >1.2, the molecular weight distribution data do not agree [18,32,50]. This mass discrimination effect is thought to be due to factors such as sample preparation, salt added, laser intensity and different ToF instrumentation used [51].

Methods have been sought that overcome the conflicting results by fractionating the wide polydispersed polymers by SEC. This results in each fraction having a narrow distribution which can then be reliably mass measured by the MALDI technique, thus becoming a detector for SEC. This procedure has been demonstrated by Nielen *et.al* [51,52]. The technique could open up many avenues for the study of high polydispersed homo- and copolymeric studies in the future.

3.2.3 Molecular weight characterisation of polymers [53]

Polymers are characterised by M_n , M_w and polydispersity values. Polymers are said to be polydisperse. This means that the individual molecules in the polymer have varying mass. Thus, only average values of relative molecular masses can be determined. Consider a polymer that could be fractionated. Each fraction would

consist of N_x molecules of one relative molecular mass (M_x). The total number of molecules in the original polymer is said to be ΣN_x . The relative mass of N_x molecules of relative molecular mass M_x is $N_x M_x$, so that $\Sigma N_x M_x$ is the mass of the original sample. Therefore, the average number relative molecular mass (M_n) is the total mass divided by the total number of molecules:

$$M_n = \frac{\Sigma N_x M_x}{\Sigma N_x}$$

The weight average molecular mass (M_w) can be determined from the weight of each fraction, where $W_x = N_x M_x$, therefore replacing N_x with W_x one obtains a weight average molecular weight where:

$$M_w = \frac{\Sigma N_x M_x^2}{\Sigma N_x M_x}$$

The polydispersity, M_w/M_n , is a measure of the width of the polymer molecular weight distribution.

3.2.4 Size Exclusion Chromatography (SEC) [54]

Briefly, SEC is an analytical method that can yield information about the molecular weight and molecular weight distribution of synthetic polymers. It is different from other chromatographic techniques since separation is based on molecular size and not on chemical interactions or attractions.

The technique itself uses columns that are filled with small porous particles, made typically from PS cross linked with divinylbenzene. The polymer (in solution) under investigation is thus passed through the column. Larger molecules spend less time in the column and elute first compared to smaller molecules, since they cannot gain access to the pores. As the polymer elutes the detector response is measured as a function of time. The technique depends on a suitable calibrant, which should be of the same origin of the polymer under investigation, which has a known molecular weight distribution. [PS proved to be a suitable polymer to investigate since standard calibration samples, covering a large mass range are commercially available]. The calibration curve can then be manipulated to provide molecular weight (not absolute) information.

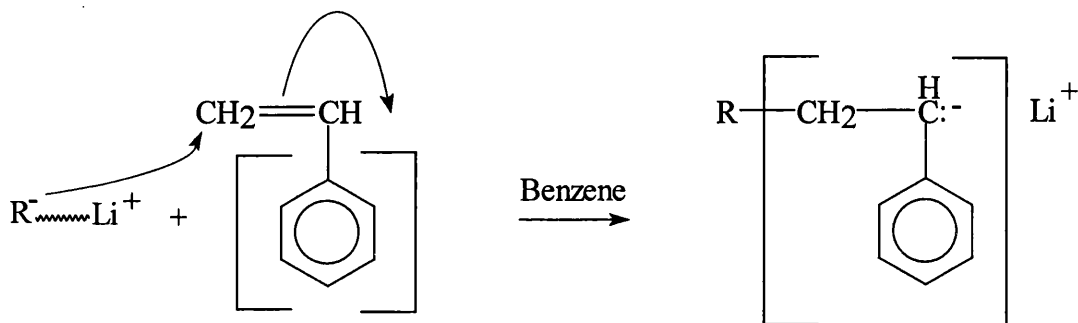
3.2.5 Polystyrene polymerisation

The method by which the four polystyrene samples were synthesised is termed ‘anionic polymerisation’. An example of the synthesis procedure will be shown for Polystyrene A only, since the other samples were also polymerised anionically.

Anionic polymerisation in this instance is initiated by sec-butyl lithium, which results in the formation of an anionic intermediate which is resonance stabilised by the delocalisation of the pi electrons in the aromatic ring.

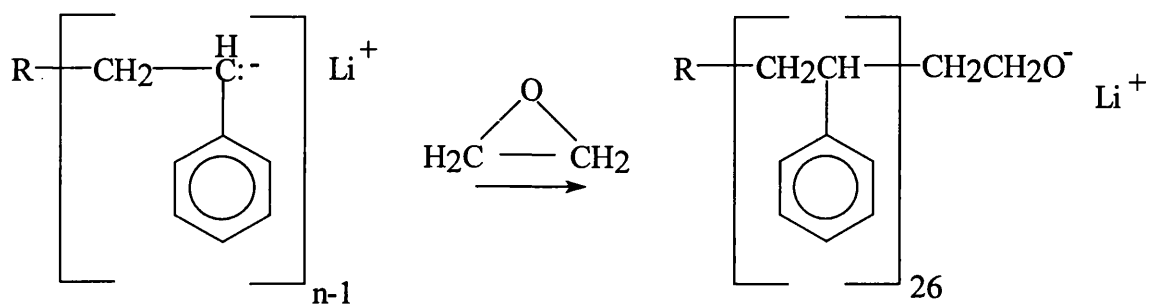
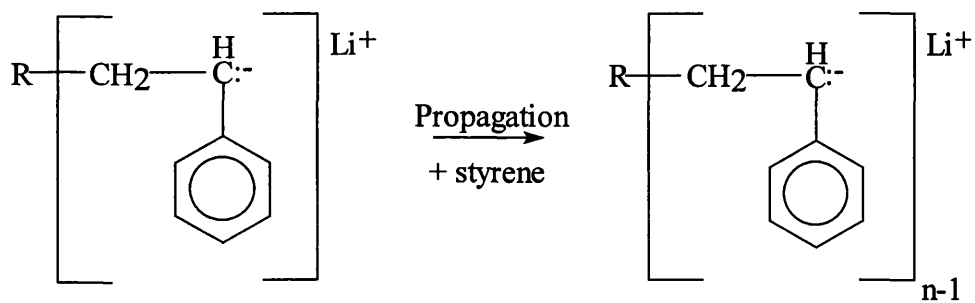
Initiation

Nucleophilic attack on the styrene double bond yields a carbanion (a base, since it has an unshared pair of electrons). The anion thus formed may add additional molecules of the styrene monomer in a suitable solvent environment. Here, R represents C_4H_9 , the attacking nucleophile:



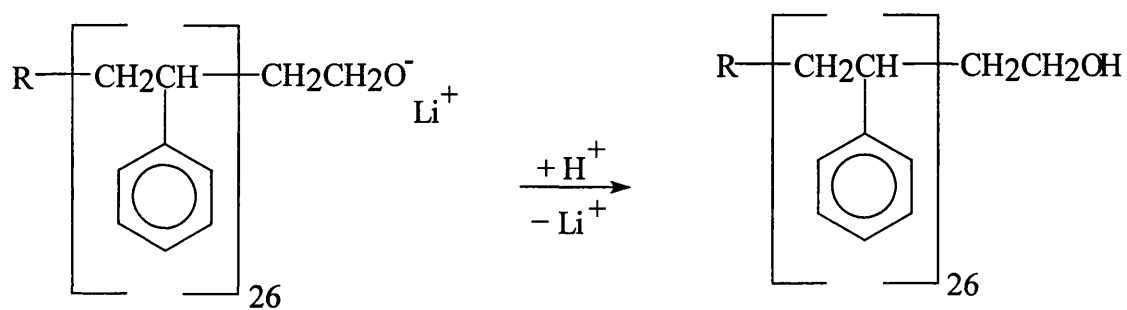
Propagation

For active polymerisation to occur (as above) after the initiation reaction, the chain will want to retain its negative charge. This can be carried out in a suitable 'aprotic' solvent such as benzene, since it will not want to donate a proton to the living polymer. The chain however is stabilised by being capped with ethylene oxide. Ethylene oxide facilitates the addition of a single ethylene oxide unit when lithium is the counter ion. [It should be noted that this procedure is not typical for PS but only for this particular sample].



Termination

The polymerisation is terminated, yielding the required product, Polystyrene A, by a final reaction in methanol. This then yields an alcohol end group.



3.2.6 Ionisation mechanism of synthetic polymers (Polystyrene)

An absolute mechanism of ion formation produced by the MALDI technique, is still after one whole decade of existence, not clearly understood. It is assumed that the formation of ions may be generated in two ways. Ions could be 'pre-formed' in the condensed phase and be freed through irradiation from the laser pulse or that the ions could be formed by ion-molecule reactions, after the onset of the laser pulse, in the gas phase.

Polystyrene is a non-polar synthetic polymer, which has been shown to be efficiently detected by MALDI TOFMS if metal salts are added during the preparation stage. Thus, ionisation is achieved via a cation (metal attachment to the polymer). Polystyrene is cationised by a number of metals, particularly copper and silver, which form intense singly charged adducts in the acquired spectra. This phenomena has been investigated by a number of groups [40,55,56].

It is highly likely that the electrons from the metal d-orbitals form a bond with the pi system of the benzene ring. Experimental investigations by Lehmann *et al.* [57] indicate that the metal-polystyrene complex is formed in the gas-phase and not desorbed from the solid Maldi sample.

Zenobi *et al.* [58] have shown that protonation of polystyrene is highly unlikely since the reaction would be endothermic if a proton was available in the first instance. However, cation attachment in the gas phase is highly favorable since it would

proceed exothermically. Several research groups have also concluded that cationisation of non-polar synthetic polymers takes place in the gas-phase [26,43].

3.3 MALDI-collision induced dissociation (MALDI-CID) of Polystyrene

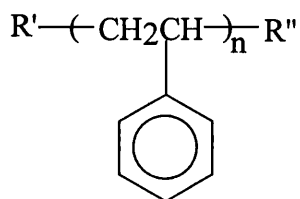
3.3.1 Introduction

The following project concerned itself with the study of four homopolymer PS samples of narrow polydispersity (all < 1.2) and with average molecular weight of up to 5000 Da. CID was utilised to determine end group information from a selected precursor ion. End group information by MALDI TOFMS and MALDI-CID has previously been demonstrated to be a powerful tool for the structural characterisation of some synthetic polymers [59-63].

The combined masses of the end groups may be inferred by subtraction of the cation mass and a number of styrene repeat units from the m/z ratio of the intact oligomer ion peaks observed in the MALDI ToF spectra [60]. The error associated with each $[\text{Oligomer} + \text{cation}]^+$ m/z ratio determines the accuracy in mass calculation of both end groups.

The MALDI CID spectra generated shows two intense series of ion peaks (denoted **A** and **B**), from which the masses of both end groups of the polystyrene can be determined. The experiments were carried out on a hybrid magnetic sector orthogonal acceleration ToF instrument. The magnetic sector facilitates the selection of an oligomeric precursor ion, generated from the polystyrene by MALDI. The selected

ion is then induced to fragment by a collision gas, whose products can yield information on the end groups of the polystyrene. It is proposed that the masses of the end groups, from the polystyrene samples, of structure shown below, could be inferred from the m/z of the two series of fragment ions using the following equations:



$$m/z (\mathbf{A}) = M(R'') + 90 + 104n + M(\text{Cat}) \quad (\text{Equation 1})$$

$$m/z (\mathbf{B}) = M(R') + 104 + 104n + M(\text{Cat}) \quad (\text{Equation 2})$$

where, $m/z (\mathbf{A})$ and $m/z (\mathbf{B})$ are the mass-to-charge ratios of the ion peaks from the two series (denoted **A** and **B** respectively). The mass of the cation is $M(\text{Cat})$ and the masses of the end groups R' and R'' are denoted as $M(R')$ and $M(R'')$ respectively. The fragment ion peaks can be differentiated from other peaks observed in the acquired Maldi-CID spectra since they are observed at low m/z and that:

$$m/z (\text{precursor}) = m/z (\mathbf{A}) + m/z (\mathbf{B}) + 104n - M(\text{Cat}) + 14 \quad (\text{Equation 3})$$

where, $m/z (\text{precursor})$ is the mass-to-charge ratio of the precursor ion selected by the magnetic sector.

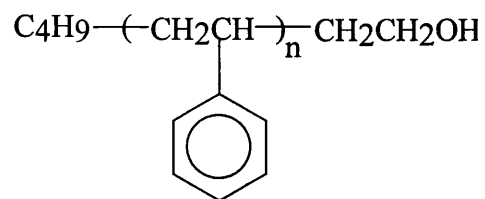
The four polystyrene samples investigated have the following structures, which are shown in Figure 3.01. Each polystyrene sample is shown to have different end groups which is achieved by a variation in the polymer synthesis. The results achieved demonstrate unambiguously how the masses of these end groups can be determined by this technique.

3.4 Experimental

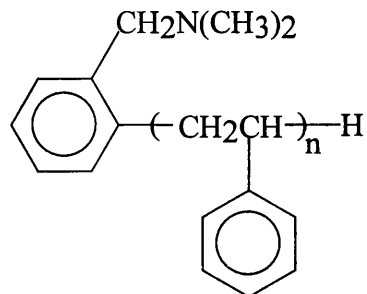
3.4.1 Polymer synthesis

The four polystyrene samples were polymerised using standard high vacuum techniques. Three different lithium initiators were used along with three different terminating agents to introduce a variety of end groups. Polystyrene **A** was initiated with sec-butyl lithium, polymerised in benzene and capped with ethylene oxide, which when lithium is the counterion, results in the addition of a single ethylene oxide unit. Termination with methanol yields the alcohol end group. Polystyrene **B** was initiated using N,N-dimethylbenzylaminolithium (synthesised according to the method of Schadler [64]), polymerised in 70:30 (benzene:ether) mixture and terminated with methanol. Polystyrene **C** and Polystyrene **D** were prepared in the same experiment. Both styrene monomers were initiated with propyllithium (synthesised according to the method of Hadjichristidis *et al.* [65]) and polymerised in benzene which contained 1-2 mL of tetrahydrofuran (THF). The living polymer was then divided into two, one half terminated with methanol, yielding Polystyrene **C** and the other half capped with 1H, 1H, 2H, 2H-perfluorooctyldimethylchlorosilane yielding Polystyrene **D**. Molecular weights were obtained by SEC using a

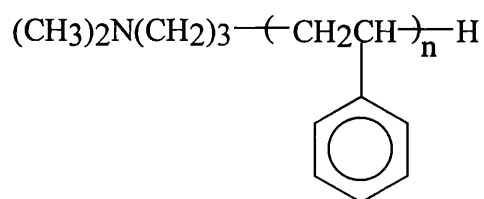
Polystyrene A



Polystyrene B



Polystyrene C



Polystyrene D

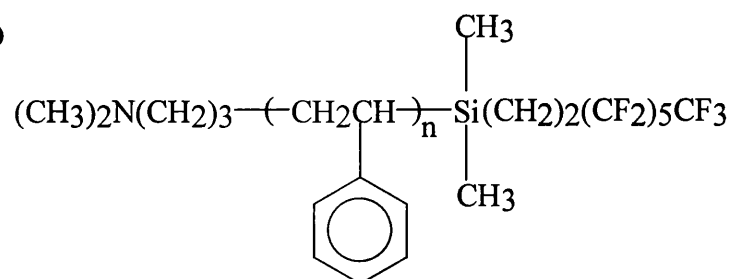


Figure 3.01: Structures of the four Polystyrenes investigated

conventional calibration procedure of polystyrene standards. The data is shown in table 1 below:

Sample	Number average Molecular weight (M_n)	Weight average Molecular weight (M_w)	Polydispersity (M_w/M_n)
Polystyrene A	2600	2800	1.06
Polystyrene B	1600	1800	1.13
Polystyrene C	2400	2500	1.07
Polystyrene D	2800	2900	1.06

Table:1

3.4.2 Instrumentation

3.4.2.1 The 'AutoSpec' oa-ToF tandem mass spectrometer

All experimental work was carried out on the VG Autospec 5000-ToF which is a hybrid tandem mass spectrometer (MS/MS) that combines the power of a magnetic sector instrument (MS-1) for precursor ion selection, with an orthogonal acceleration ToF mass analyser (MS-2) which provides high sensitivity for full product ion spectra. A detailed schematic of the instrument design is shown in Figure 3.02. The instrument has been described in great detail elsewhere [66,67], so only a brief description of its operation will be described here.

The instrument itself is very versatile. It can be equipped with various external ionization sources depending on what method of analysis is preferred. Results for this thesis made use of the instrument equipped with a MALDI source.

The inlet system for the source region is fitted with a probe to which a thin narrow plate can be attached. The samples being investigated are mixed with a suitable matrix

and then spotted on to the plate. The plate is then firmly fixed on to the probe and placed inside the ionization source. Ionization of the sample is achieved by firing a Nitrogen laser ($\lambda = 337 \text{ nm}$) which is operated typically with a pulse rate of 10 Hz in the source, directly at the spotted target. The position of the laser when striking the spotted target is controlled by the computer software. A small camera is also fitted to the instrument to view the target during the acquisition of data.

Depending on the particular application of analysis the instrument can be set up so that the magnet by-pass is optional (see Fig.3.02), this then allows the user to perform either MS or MS/MS analysis.

If MS mode of operation was desirable, the magnet is switched off and the pulsed ion beam from the MALDI source enters a separate by pass flight tube before reaching the oa-ToF region. Once the ion beam enters the oa-region, a 'packet' of ions is sampled orthogonally to the incoming beam axis and full range, high sensitivity MS spectra can be produced.

In MS/MS mode of operation the magnet is switched on and the magnet by pass is switched off. This particular set up allows the magnetic sector to select precursor ions from the pulsed beam.

Precursor ions are accelerated from the source with a voltage typically of 8 kV. After exiting MS-1, these ions are further focussed into a collimated beam by a two stage deceleration electrostatic lens to an energy of 800 eV. The focused precursor ion beam then enters a collision cell, where they collide with xenon collision gas. As a result of this collisional process product ions are formed. On exiting the collision cell both sets of ions, product and precursor, enter the oa-region and get deflected at an

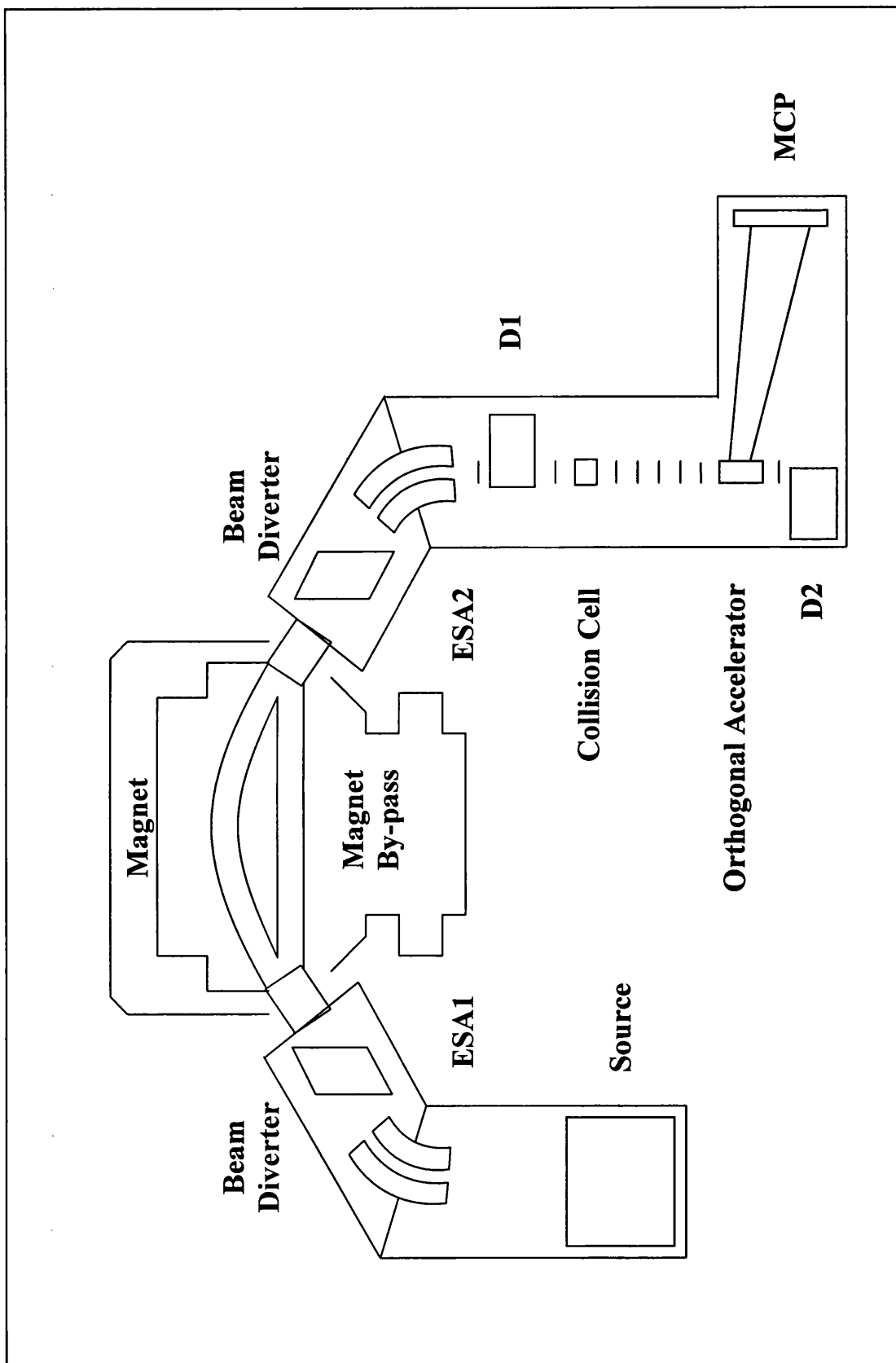


Figure 3.02: Schematic of the 'Autospec 5000' hybrid MS/MS instrument

angle that is perpendicular to their incoming trajectory, into the oa-ToF analyser (MS-2).

Once the oa-region is full both sets of ions experience this 'push-out' pulse, which is automatically timed to coincide with the time at which both sets of ions pass through the orthogonal accelerator. These ions are accelerated to zero potential through a dual stage source and are detected by an MCP detector at the end of the linear ToF analyser which has pathlength of approximately 0.5 metres.

In both MS and MS/MS mode of operation, ions that do not get sampled by the orthogonal accelerator may be detected by a photomultiplier which is positioned at the end of the instrument.

The mass range of the oa-ToF in MS and MS/MS modes is limited by the repetition rate of the pusher. A mass range of m/z 7000 can be obtained with a repetition rate of 30 kHz which corresponds to a flight time of approximately 33 μ s. To observe a lower mass range the repetition rate is increased, thus giving a lower flight time.

In conclusion, the time of flight of the ions is determined from the time of application of the pusher pulse to the time they are detected by the MCP detector of MS-2. This detector comprises of three MCP's which allows detection of full product ion spectra. The maximum repetition rate of the pusher is 100,000 times per second. The MCP is capable of acquiring all of these spectra which is then summed.

When an ion strikes the MCP a count of one is recorded on a TDC. This process is repeated many times over the acquisition time period and the signal output is presented in the form of an histogram. Individual spectra are summed in a histogram

memory and the histogrammed spectrum is then transferred to the host computer. Instrument control and data acquisition is made through the OPUS software. The number of laser shots that were averaged to obtain a mass spectrum ranged from approximately 5000-15000, corresponding to 10-30 minutes acquisition time.

An inherent advantage of a ToF mass analyser is that it simultaneously transmits all the ions that are produced in the mass spectrum. It achieves a 100 % sampling efficiency for pulsed ionisation sources due to its highly compatible partnership. It thus has greater sensitivity in MS and MS/MS mode of operation over conventional scanning mass analysers.

3.4.3 Sample preparation

The metal salts, copper (II) nitrate and silver nitrate (used to cationise the polystyrene samples), *all-trans*-retinoic acid (the matrix) and anhydrous THF were purchased from Aldrich Chemical Company (Gillingham, U.K.). Analytical grade THF was from Fisons Scientific Equipment (Loughborough, U.K.) and HPLC grade ethanol from BDH (Lutterworth, U.K.).

Samples for analysis by MALDI were prepared as follows: Except for silver nitrate in ethanol, each solution was prepared at a concentration of 10 mg mL⁻¹. Anhydrous THF was used to dissolve each polystyrene and matrix. They were then mixed in a 1:20 ratio (v:v) (PS:matrix). Copper (II) nitrate or a saturated solution of silver nitrate in ethanol was then added to the above solution in a 100:1 (v:v) ratio (PS +

matix:salt). Approximately 0.5 μL of this final mixture was then applied to a stainless steel holder for analysis.

3.5 Results and Discussion

(i) *Polystyrene A*

MALDI-CID was performed on the $[\text{PS} + \text{Ag}]^+$ ion with m/z 2914.6, from the 26-mer since this ion produced the most intense peak in the MALDI-ToF data. The MALDI product ion spectrum of the $[\text{PS} + \text{Ag}]^+$ ion obtained by CID from the 26-mer is shown in Figure 3.03 (a).

The product ions are proposed to retain the cation (Ag^+), except for some low intensity ions observed at a lower m/z ratio ($< m/z$ 200). Below m/z 700 the product ion spectrum is dominated by a series of ions that are separated by a m/z ratio which is equivalent in mass of the styrene monomer (104 Da). The series are labelled **A**, **B** and **G** in Figure 3.03 (a). As stated some ions do not retain the cation, two of which are marked with an asterisk. These particular ions could be formed from an ‘intermediate’ of similar structure to that shown later. These ions are also seen in the CID spectra of PS by Derrick *et al.* [68].

End group characterisation of the PS may be inferred from the **A** and **B** product ion series produced from the fragmentation scheme proposed in Figure 3.03 (b). The **A** and **B** series are adduct ions formed with the silver cation. This particular PS is initiated with a butyl group of m/z 57 (represented as R') and terminated with an

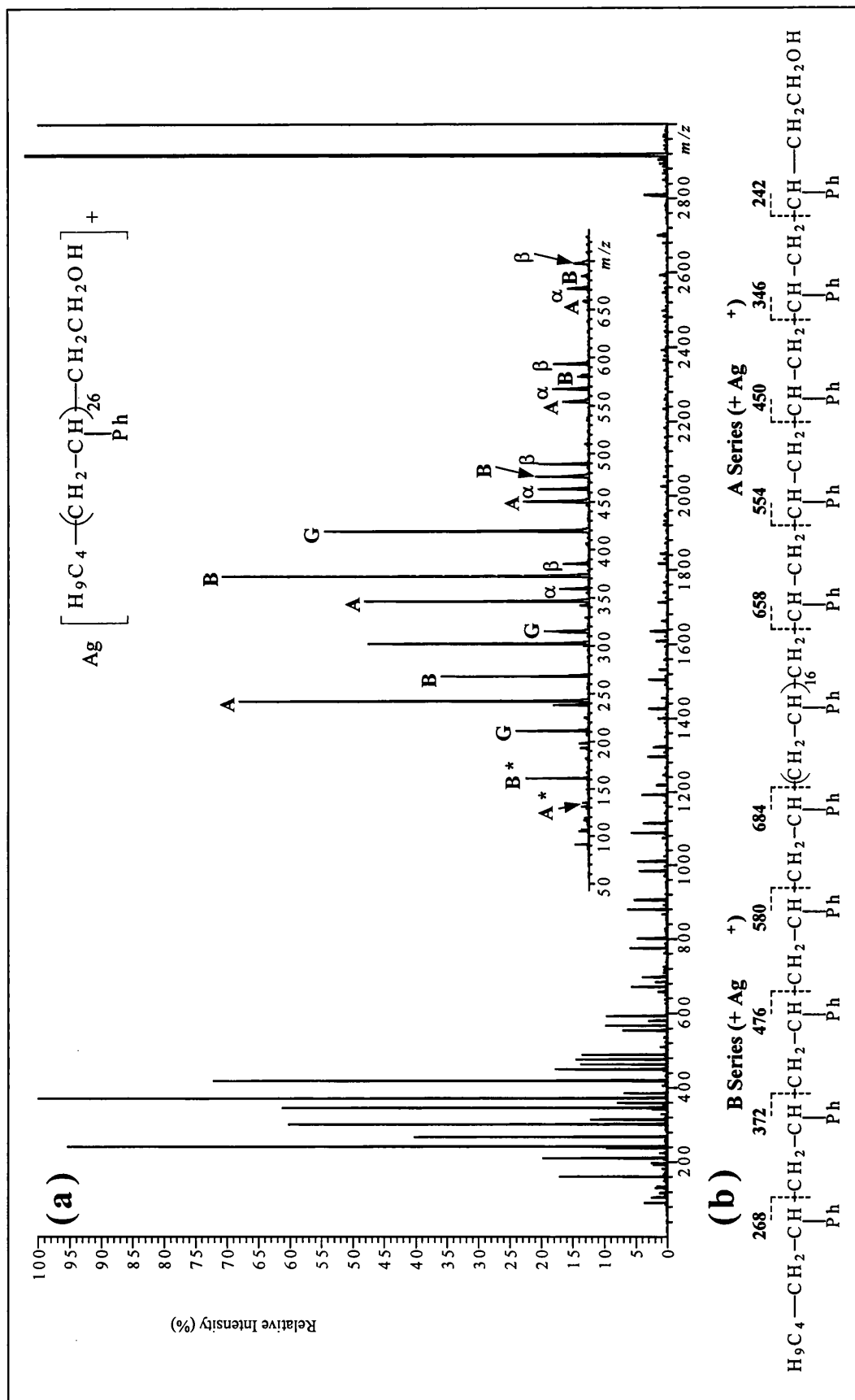


Figure 3.03: (a) Maldi-CID spectrum of [PS + Ag]⁺, m/z 2914.6, of the 26-mer of Polystyrene A (Inset-expansion of m/z 50-730). All fragments retain the cation (Ag⁺) except where denoted by an asterisk. The A and B series are observed at m/z 242 + 104n and 268 + 104n, where n is 0-4. The G series is observed at m/z 211 + 104n, where n is 0-2. The α and β series is seen at m/z 255 + 104n and 281 + 104n, where n is 1-22. The C, D, E, and F series are seen at m/z 267 + 104n, 179 + 104n and 345 + 104n respectively, where n is 5-22.

(b) Proposed fragmentation pathways of [PS + Ag]⁺, m/z 2914.6, of the 26-mer of Polystyrene A showing how the A and B series may be used to infer the masses of the end groups of the polymer

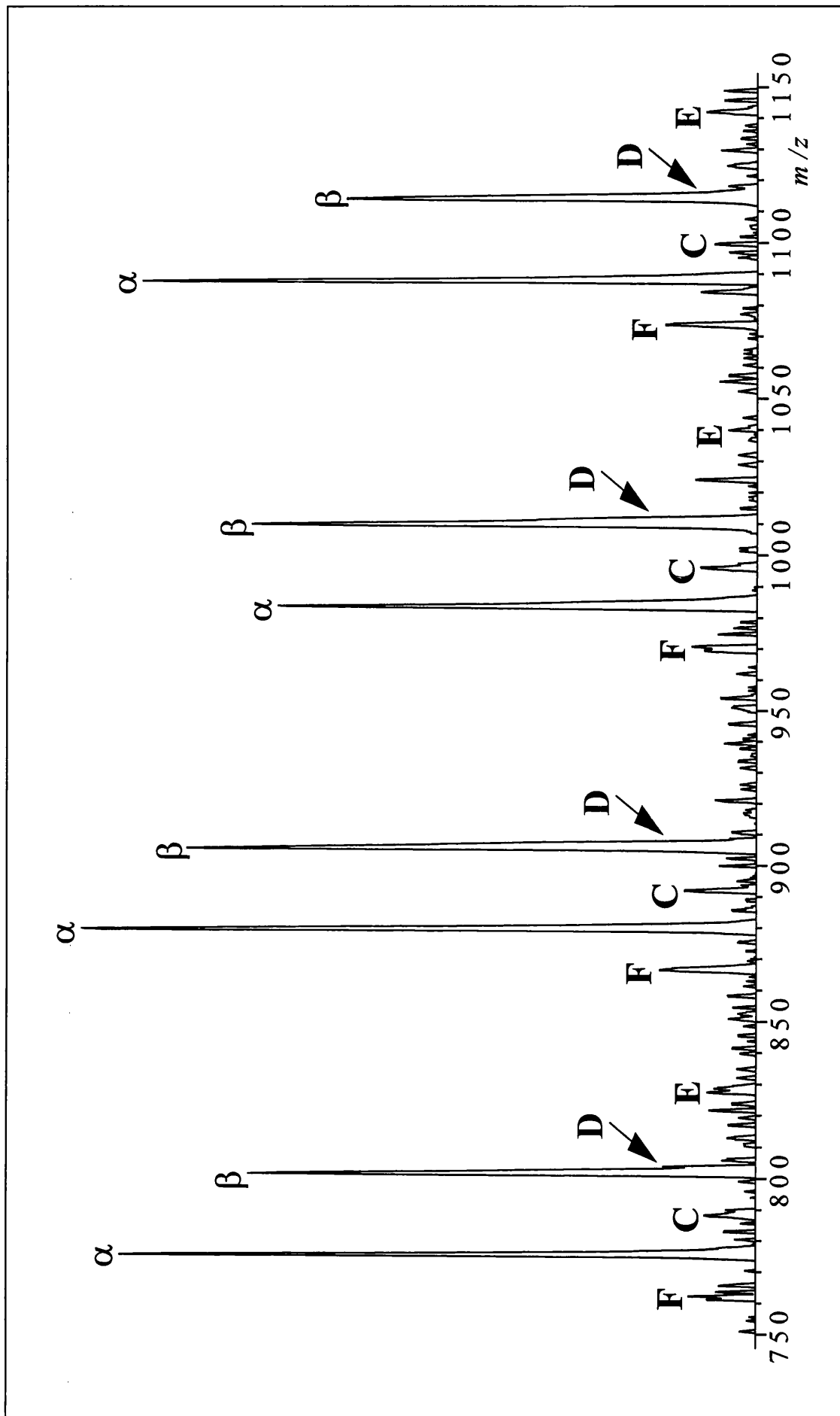


Figure 3.04: Expansion (m/z 750-1150) of the Maldi-CID spectrum of $[\text{PS} + \text{Ag}]^+$, m/z 2914.6, of the 26-mer of Polystyrene A

alcohol group of m/z 45 (represented as R''). The mass of each end group R' and R'' can be derived from the **B** and **A** series respectively, by use of equations 2 and 1. For example, use of equation 2 for calculation of R' from product ion at m/z 476 in the **B** series, where n= 2:

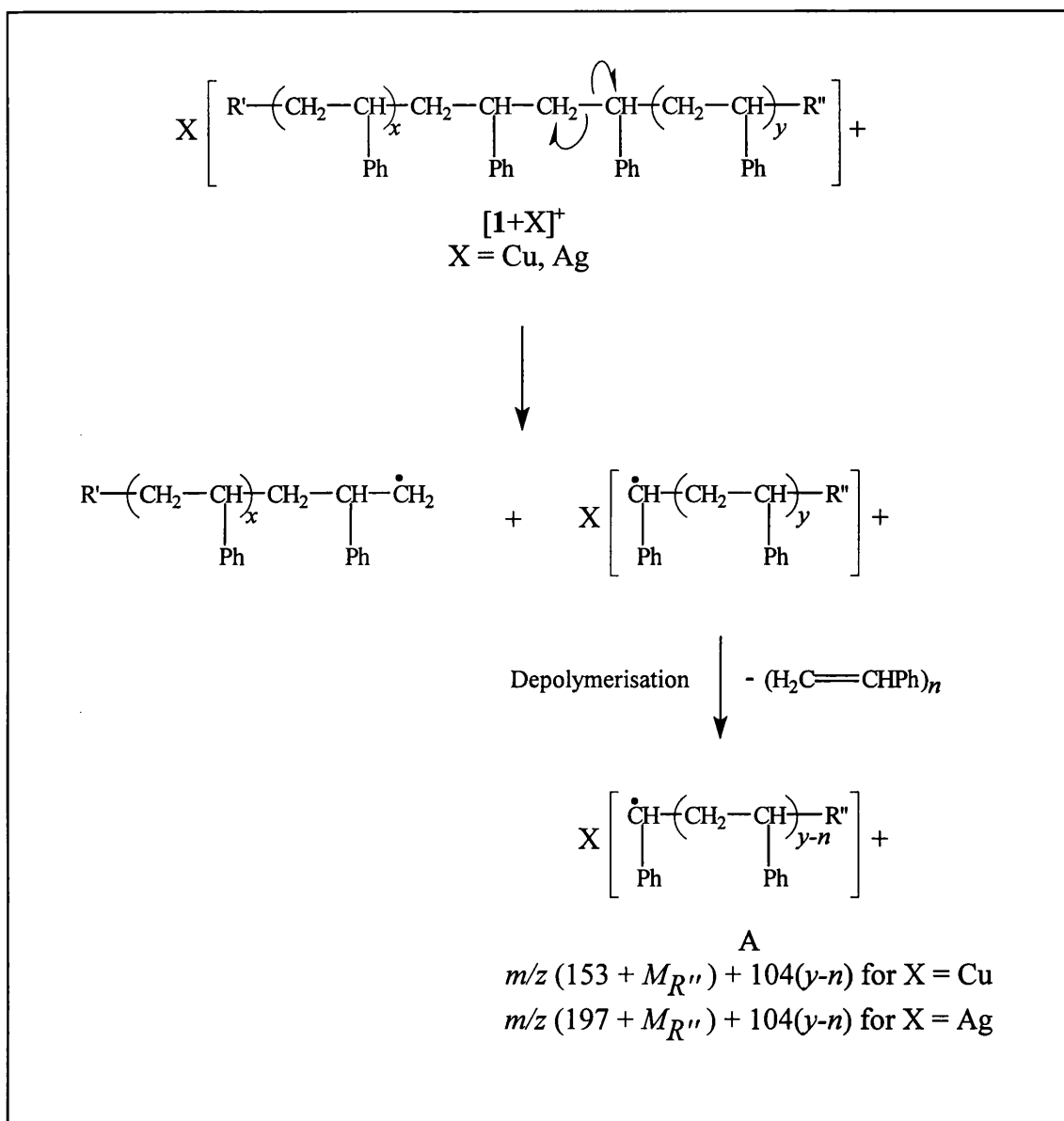
$$\begin{aligned} m/z (\mathbf{B}) &= M(\mathbf{R}') + 104 + 104n + M(\text{Cat}) \\ 476 &= M(\mathbf{R}') + 104 + 208 + 107 \\ \underline{M(\mathbf{R}') = 57} \end{aligned}$$

Endgroup R'' can be calculated for example, from product ion at m/z 450 in the **A** series, where n=2:

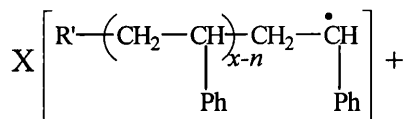
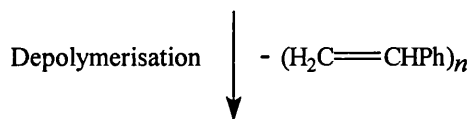
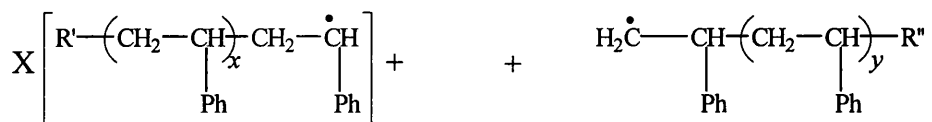
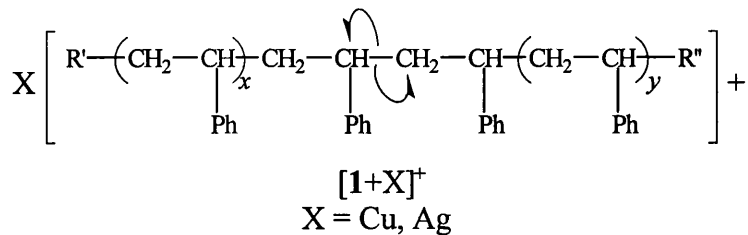
$$\begin{aligned} m/z (\mathbf{A}) &= M(\mathbf{R}'') + 90 + 104n + M(\text{Cat}) \\ 450 &= M(\mathbf{R}'') + 90 + 208 + 107 \\ \underline{M(\mathbf{R}'') = 45} \end{aligned}$$

The structures assumed for the product ion peaks of the **A** and **B** series and mechanistic ion formation are shown in schemes **I** and **II**. It is thought that these ions are radical cations, assumed to be distonic in nature, where the radical site is positioned on a secondary carbon of the PS backbone. (A distonic ion is a radical cation where the charge and radical centres are separated by some distance [69]).

Direct cleavage of the PS backbone (with part of the cleaved backbone retaining the 'picked up' cation) followed by loss of n(styrene monomers) (depolymerisation) leads to the formation of the **A** and **B** series. It can be clearly seen that the only difference in mechanism of both ion series is the site of cleavage, where perhaps the charge is



Scheme I: Proposed mechanism for generation of the A series from Polystyrene



B

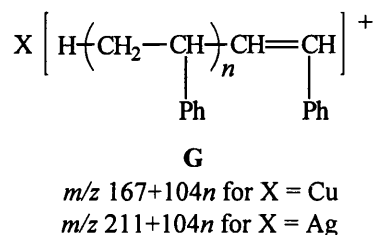
$m/z (167 + M_{R'}) + 104(x-n)$ for $X = \text{Cu}$

$m/z (211 + M_{R'}) + 104(x-n)$ for $X = \text{Ag}$

Scheme II: Proposed mechanism for generation of the **B** series from Polystyrene

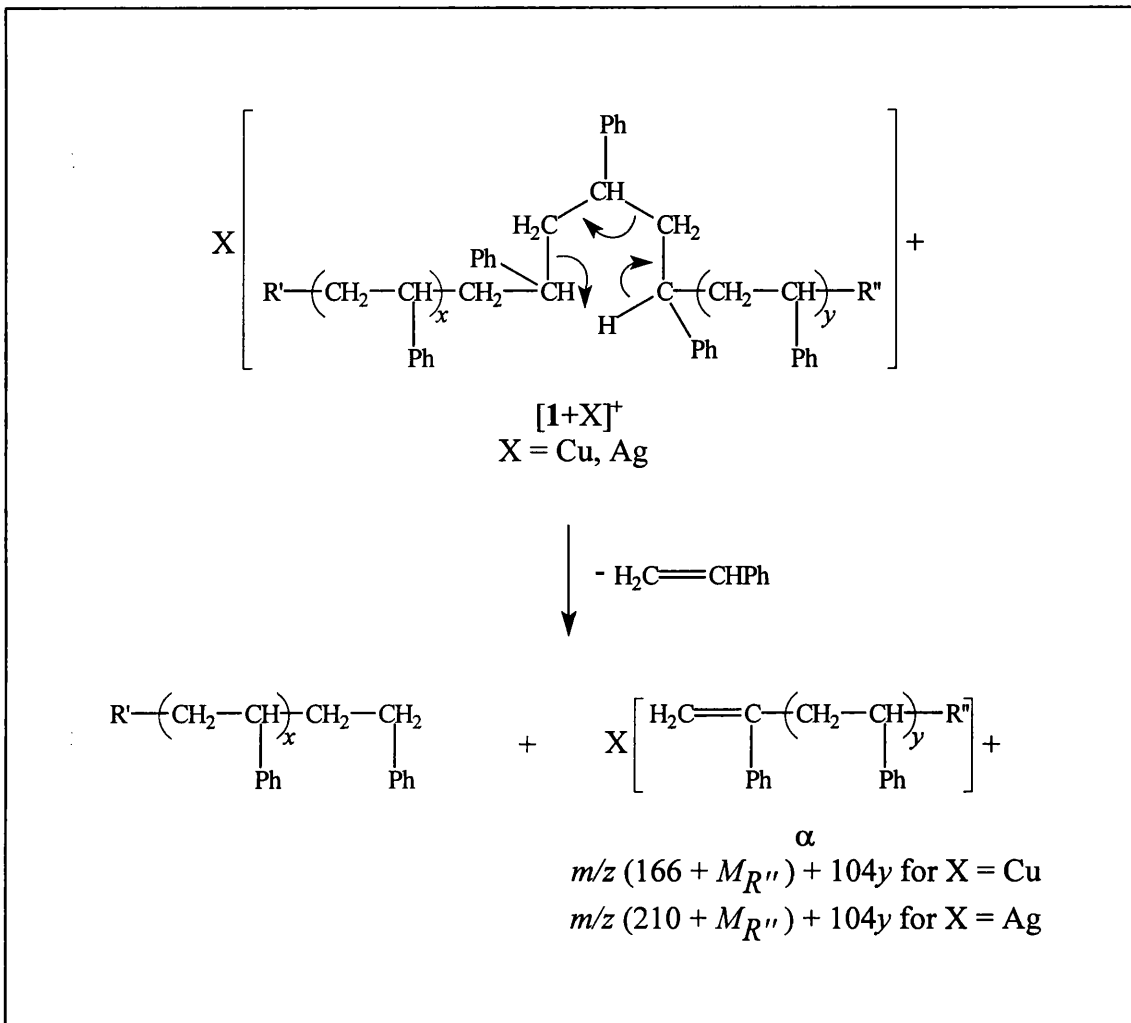
directing the fragmentation. This would explain the peak intensities for the **A** and **B** series.

The other intense product ion series, labelled the **G** series is observed at odd m/z ratios in the mass spectrum. It is postulated that these ions are formed by rearrangement reactions rather than by direct cleavage [63]. A possible structure for the **G** ion series is presented below:

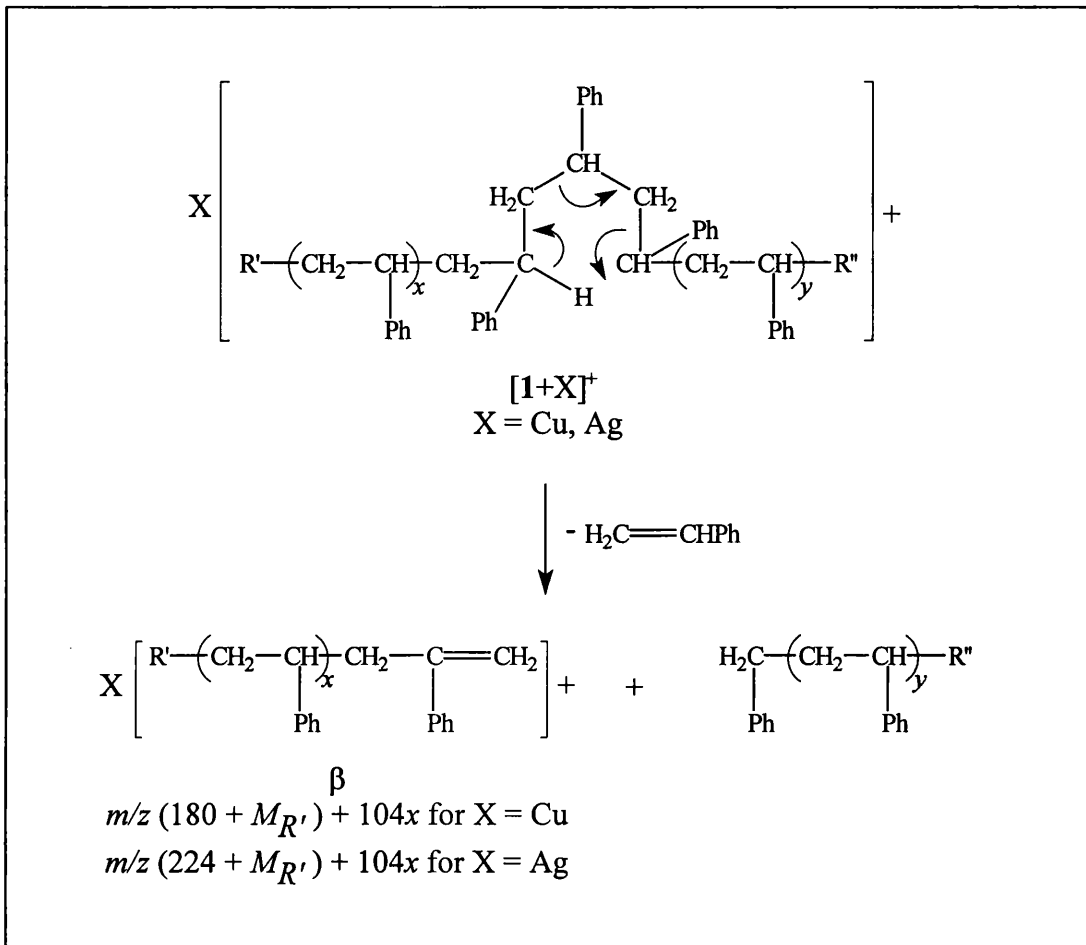


Some ions observed in the mass spectrum are not labelled since they are not formed as part of any of the previously mentioned series. For example, the ion peak situated between **B** ($n=0$) and **A** ($n=1$) series at m/z 302 is proposed to be loss of ethylene oxide (m/z 44) from ion m/z 346 in the **A** series.

Also visible in the mass spectrum are two less intense series of product ion peaks, labelled α and β , which can be seen in the expansion of the product ion spectrum in Figure 3.04. Each successive peak in the spectrum has a mass difference of 104 Da, corresponding to the mass of a styrene monomer. The structures of these ions and possible mechanism of formation is shown in Schemes **III** and **IV**.



Scheme III: Proposed mechanism for generation of the α series from Polystyrene

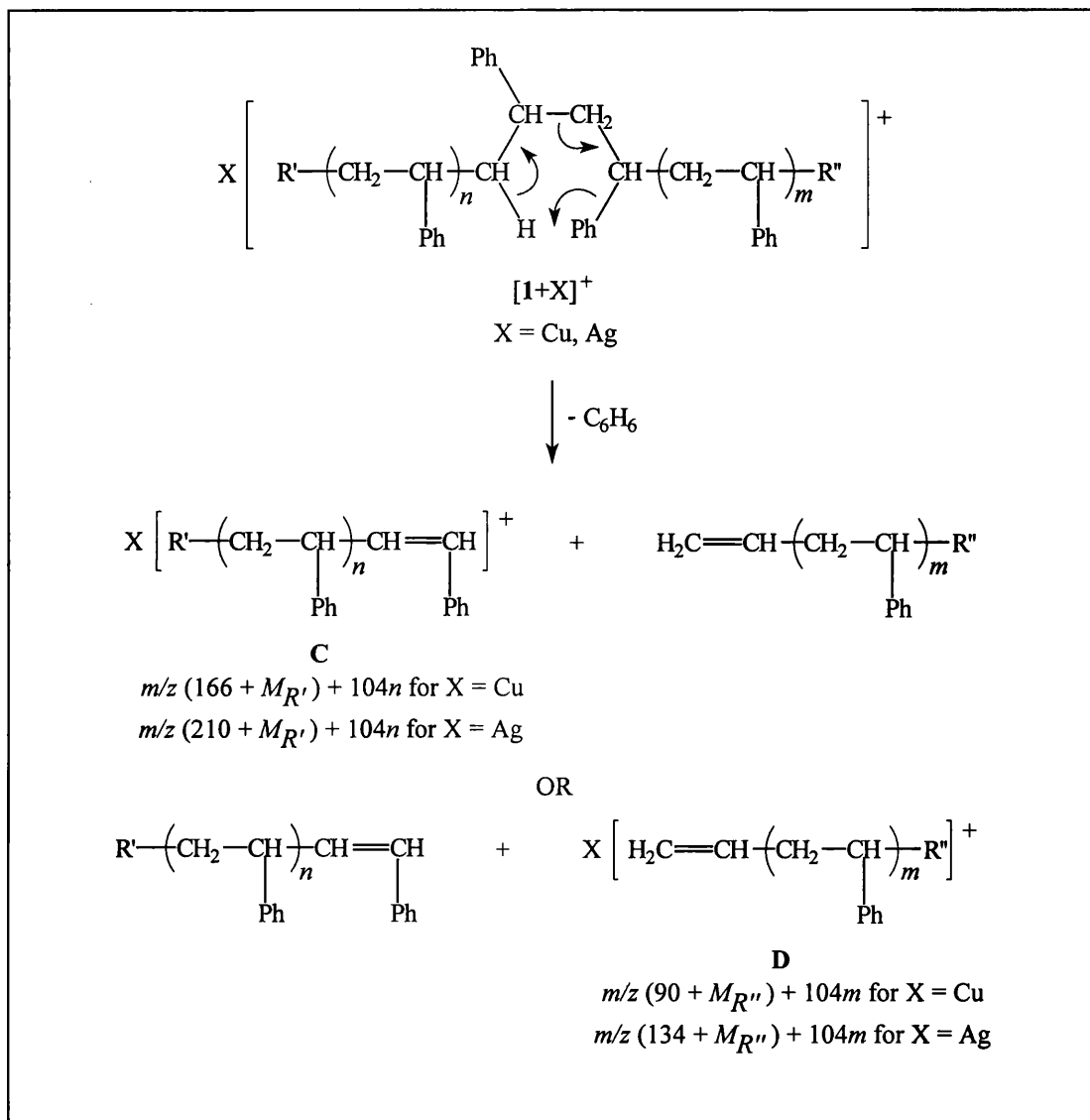


Scheme IV: Proposed mechanism for generation of the β series from Polystyrene

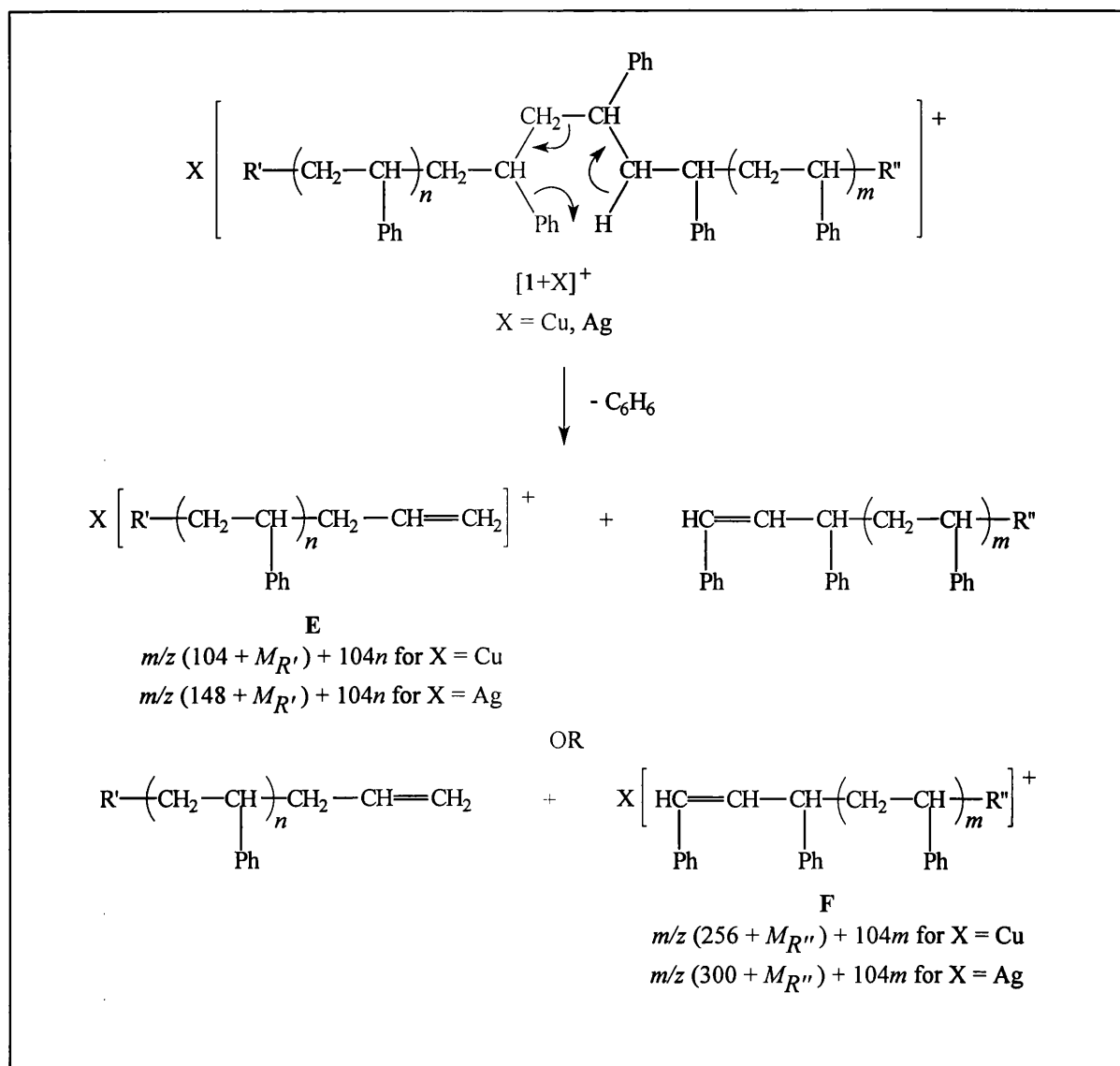
The ions are proposed to be formed by means of 1,5-hydrogen rearrangements with the charge being retained by alternative fragments. The reactions proceed via loss of a styrene monomer and a portion of the oligomer with a saturated chain end. Here, the affinity to 'pick up' a silver ion (see previous text page) is greater with an unsaturated chain end than for a saturated chain end, since the delocalisation of the electron cloud is more pronounced. This phenomena seems very plausible since no product ions are seen in the spectra with cation retention at fragments with two saturated chain ends.

The α series of product ion peaks are generated with cation retention at the oligomer section that contains the alcohol group and the β series with cation retention at the section that contains the butyl group for Polystyrene A.

Four other product ion series, labelled **C**, **D**, **E** and **F** are observed in the mass spectrum. These are clearly seen in the mass spectrum which has been expanded in the y-direction (m/z 750-1150) in Figure 3.04. These ion peaks however, are of lower intensity than the **A**, **B**, **G**, α and β series. These series of peaks are again proposed to be formed by 1,5-hydrogen rearrangements. Their structure and proposed mechanism of formation is shown in Scheme V for the **C** and **D** series and Scheme VI for the **E** and **F** series. Both mechanisms involve cleavage of the PS backbone, followed by the loss of a benzene molecule, resulting in the formation of product ions and neutrals with unsaturated end groups.



Scheme V: Proposed mechanism for generation of **C** and **D** series from Polystyrene



Scheme VI: Proposed mechanism for generation of **E** and **F** series from Polystyrene

(ii) *Polystyrene B*

The $[\text{PS} + \text{Cu}]^+$ ion at m/z 1969.1 from the 17-mer was chosen for study as it generated the most intense peak in the MALDI-ToF data. MALDI-CID was performed on this precursor ion and the acquired spectrum is shown in Figure 3.05 (a).

Intense product ion peaks are observed below m/z 500 and the series labelled as **A**, **B**, **G**, α , and β each of which retain the cation (Cu^+). Ions marked with an asterisk do not retain the cation. Each of the above ion series are separated by a m/z ratio of 104 Da, equivalent to the mass of a styrene monomer.

End group characterisation of the PS is inferred from the **A** and **B** product ion series, produced from fragmentation of the PS backbone as shown in Figure 3.05 (b). The R' and R'' m/z ratios obtained are consistent with those expected from Equations 1 and 2. The mechanism of formation of the **A** and **B** series (shown in Scheme I and II) is also consistent with the obtained m/z ratios.

Product ion peaks from the α and β series are observed up to m/z 1300 in the acquired mass spectrum. Ion peaks representative of the **E** and **F** series are observed in the mass spectrum but show low intensity signals. Product ions of the **C** and **D** series are observed above m/z 1000 but are not sufficiently resolved in the mass spectrum since they only have a mass difference of 1 Da. Mechanistic ion formation is shown in Schemes III, IV, V and VI for α , β , **C**, **D**, **E** and **F** series respectively.

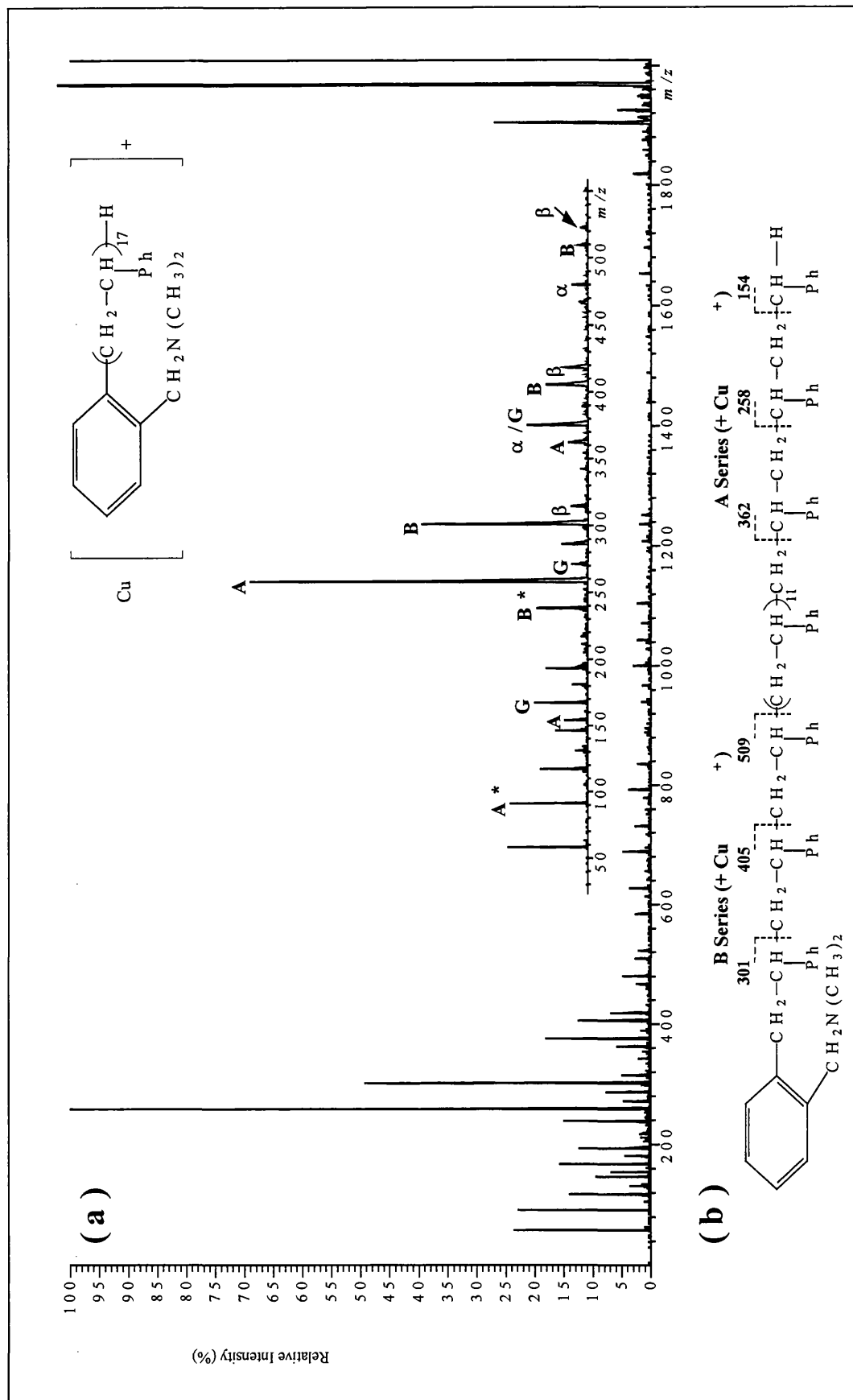


Figure 3.05: (a) Maldi-CID spectrum of $[\text{PS} + \text{Cu}]^+$, m/z 1969.1, of the 17-mer of Polystyrene **B** (inset-expansion 30-550). All fragment ions retain the cation (Cu^+) except where denoted by an asterisk. The **A** and **B** series are observed at m/z $154 + 104n$ and $301 + 104n$, where n is 0-2. The **G** series is seen at m/z $167 + 104n$, where n is 0-2. The α and β series are seen at m/z $167 + 104n$ and $314 + 104n$ respectively, where n is 0-10. The **C**, **D**, **E** and **F** series are observed at m/z $300 + 104n$, $91 + 104n$, $238 + 104n$ and $257 + 104n$ respectively, where n is 3-15. (b) Proposed fragmentation pathways of $[\text{PS} + \text{Cu}]^+$, m/z 1969.1, of the 17-mer of Polystyrene **B** showing how the masses of the end groups may be inferred from the **A** and **B** series

An intense ion at m/z 58 is observed in the mass spectrum. This ion is presumed to be due to loss of ($^+\text{CH}_2\text{N}(\text{CH}_3)_2$) from the phenyl ring.

(iii) *Polystyrene C*

MALDI-CID was performed on the $[\text{PS} + \text{Cu}]^+$ ion from the 22-mer, since this ion generated the most intense ion peak in the MALDI-ToF data. The MALDI product ion spectrum of the $[\text{PS} + \text{Cu}]^+$ ion obtained by CID on the precursor ion at m/z 2439.4 is shown in Figure 3.06 (a).

The most intense product ion peaks are observed below m/z 700. These series are marked **A**, **B** and **G**, in which these ions retain the copper cation. The fragmentation pattern for the **A** and **B** series is shown in Figure 3.06 (b). This series of ions is again separated by 104 Da, the mass of a styrene monomer. The m/z ratios of the **A** and **B** series agree with those predicted from Equations 1 and 2. Their mechanistic scheme of formation has been demonstrated and is consistent with the m/z ratios expected.

Six other ion peak series are also observed again in the acquired mass spectrum, that is α , β , **C**, **D**, **E**, **F** and **G** series. The first five of these produce lower signal-to-noise ratios than all other ions observed. Other product ions are observed whose m/z ratios suggest that cation retainment is absent. These particular ions are again marked with an asterisk. The ion signal at m/z 58 is proposed to be of the same structure as the ion produced from direct cleavage of the substituent on the phenyl ring in *Polystyrene B*.

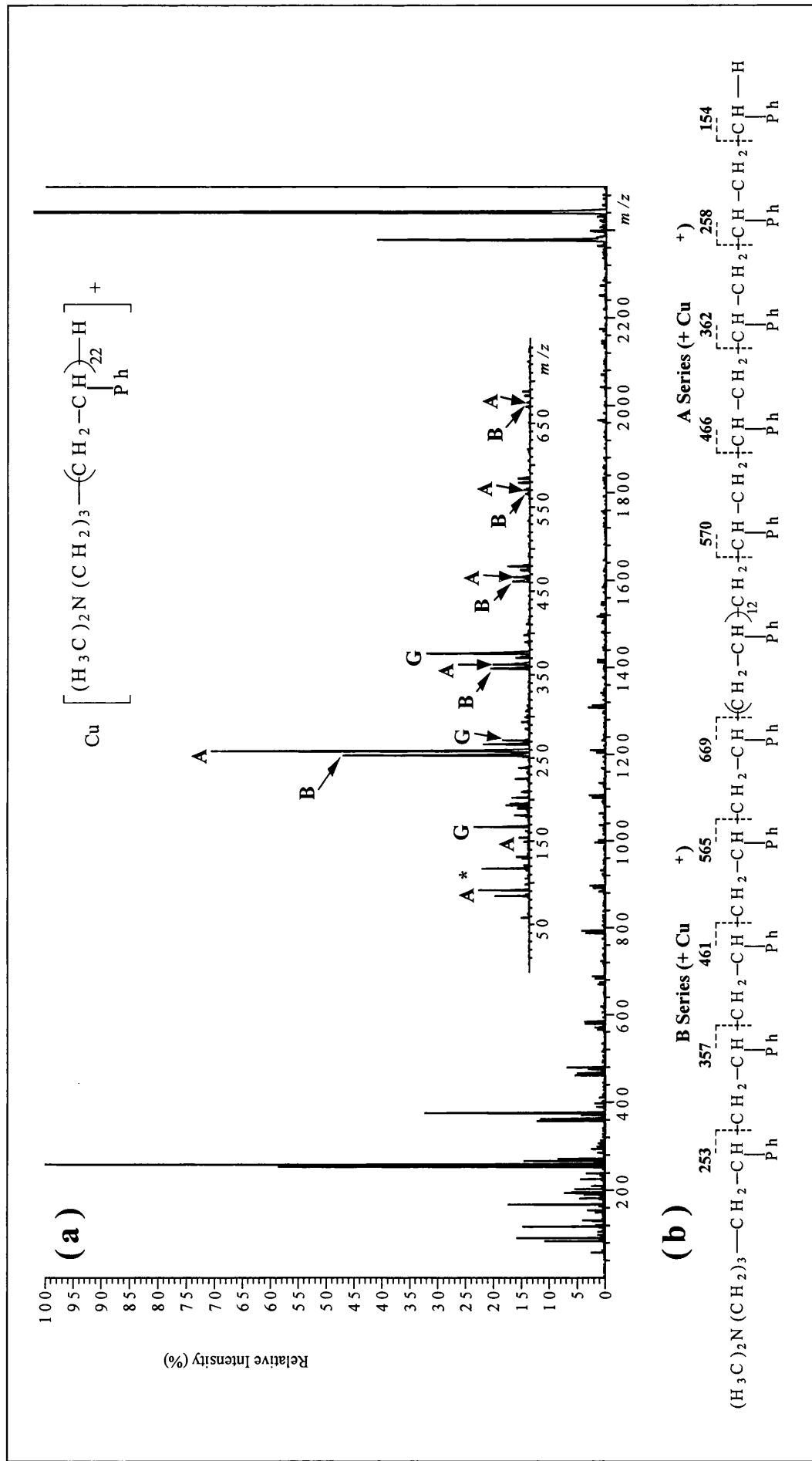
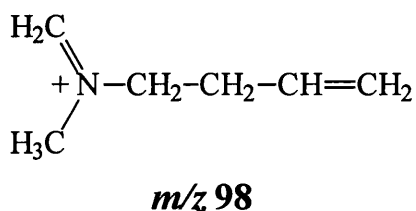
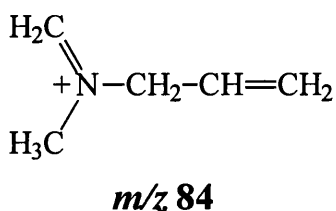


Figure 3.06: (a) Maldi-CID spectrum of [PS + Cu]⁺, m/z 2439.4, of the 22-mer of **Polystyrene C** (Inset-expansion of m/z 30-750). All fragment ions retain the cation (Cu⁺) except where denoted by an asterisk. The **A** and **B** series are observed at m/z 154 + 104n and 253 + 104n, where n is 0-4. The **G** series is seen at 167 + 104n, where n is 0-2. The **α** and **β** series are seen at m/z 167 + 104n and 266 + 104n, where n is 0-20. The **C**, **D**, **E**, and **F** series are observed at m/z 252 + 104n, 91 + 104n, 190 + 104n and 257 + 104n respectively, where n is 4-20.

(b) Proposed fragmentation pathways of [PS + Cu]⁺, m/z 2439.4, of the 22-mer of **Polystyrene C** showing how the **A** and **B** series may be used to infer the masses of the end groups of the polymer

Two other ions are observed at m/z 84 and m/z 98 and are postulated to be formed from two hydrogen rearrangement reactions from the $[\text{PS} + \text{Cu}]^+$ precursor ion. Their structures may take the following form:



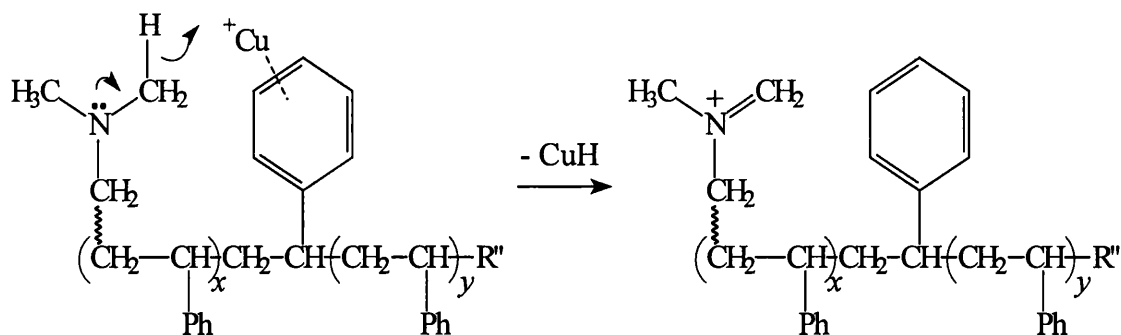
(iv) ***Polystyrene D***

The $[\text{PS} + \text{Cu}]^+$ ion at m/z 2843.4 from the 22-mer was chosen for investigation as it generated the most intense peak in the MALDI-ToF data. MALDI-CID was performed on this ion and the acquired spectrum is shown in Figure 3.07 (a).

Intense product ion peaks are observed in the mass spectrum (expansion m/z 30-950) from the **A** and **B** series produced from fragmentation of the PS backbone, as shown in Figure 3.07 (b). The **A** and **B** series are adducts with copper and their m/z ratios are consistent with the expected m/z ratios from Equations 1 and 2. The product ions are therefore again used to infer end group characterisation of this PS. Other ions observed, **B**, β , **C** and **E** series occur at the same m/z ratios as with *Polystyrene C* since these ions are formed from the same end of the PS with the same end group. The

C and E series of ions are observed at much lower signal intensity than the other series. The product ion peaks of the A, α , D and F series are observed at a m/z difference of 404 Da from data obtained with *Polystyrene C* due to the difference in terminating group at this portion of the PS. The D and F ions have a signal-to-noise ratio that is lower than all other ions observed in the spectrum. Ions are observed at m/z 58, 84 and 98 which do not retain the cation. Their origin is assumed to be the same and structurally the same as with *Polystyrene C*.

A product ion observed in the mass spectrum of **Polystyrenes B, C and D** occurs at a mass difference of 64 Da from the precursor ion. The origin of this ion is postulated to be the loss of $\text{Cu}^{(I)}\text{H}$ from the precursor ion. A possible mechanism could be of the form shown below:



3.6 Conclusion

It has been clearly demonstrated that tandem mass spectrometric studies combined with the MALDI technique on the hybrid sector oa-ToF instrument is a powerful and excellent technique for the end group determination and thus structural characterisation of the Polystyrene samples investigated.

The 'Autospec-oa-ToF' facilitates precursor ion selection through a double focusing MS1 whose CID products can be mass analysed by oa-ToF, situated at the end of the instrument, MS2. Sampling of the product ions orthogonal to the main ion beam axis into the ToF chamber greatly improves the sensitivity of full scan product ion spectra. The instrument takes advantage of MALDI, a pulsed technique, which has shown to provide good sensitivity by achievement of a 100% duty cycle. It should be noted, that a large portion of the ion beam is lost in the orthogonal accelerator, due to the grided extraction region.

The product ions produced, from fragmentation of the polymer backbone by CID, at low m/z ratios (**A** and **B** series), which are adducts with the cation from the metal salt used for cationisation, have proved vital for end group determination. Equations were used which provide unambiguously, efficient characterisation of the end groups from the samples investigated with great accuracy.

The technique of MALDI provides much quicker, efficient, reproducible data over the mass range of interest compared to other desorption techniques, for example FD. Acquiring a decent mass spectrum by FD at times could take as long as several hours

providing the emitter does not fail during an acquisition, due to the low ion currents generated. The MALDI data obtained on the 'Autospec' does not have this problem. A time-to-digital converter (TDC) is employed which records a count of one, if a single ion arrives at the MCP detector. Spectra are produced in the form of a histogram of all ion events over the acquisition time period. Good signal-to-noise is achieved through low background noise provided for by single ion event recording. The histogrammed spectra is then transferred to the host computer.

The technique it is hoped will provide structural identification of unknown mixtures, and co-polymers which was previously unobtainable by other ionisation techniques. The use of MALDI (CID) TOFMS to aid the structural identity of co-polymers is at present still in its infancy but this technique could be exploited to further characterise such complex systems.

3.7 References

1. HD Beckey, 'Principles of Field desorption mass spectrometry', Pergamon Press: Oxford, 1977.
2. RD MacFarlane, DF Torgerson, *Science*, 191 (1976) 920.
3. A Benninghoven, WK Sichtermann, *Anal.Chem.*, 50 (1978) 1180.
4. RJ Cotter, *Anal.Chim.Acta.*, 195 (1987) 45.
5. M Karas, F Hillenkamp, D Bachmann, *Anal.Chem.*, 57 (1985) 2935.
6. M Karas, F Hillenkamp, D Bachmann, U Bahr, *Int.J.Mass Spectrom.Ion Processes*, 78 (1987) 53.
7. M Karas, F Hillenkamp, *Anal.Chem.*, 60 (1988) 2301.
8. M Barber, RS Bordoli, RD Sedgwick, AN Tyler, *Nature*, 293 (1981) 270.
9. AE Ashcroft, 'Ionisation methods in organic mass spectrometry', RSC publishers, 1997.
10. J Zhou, W Ens, KG Standing, AN Verentchikov, *Rapid Commun.Mass Spectrom.*, 6 (1992) 671.
11. BA Mamyrin, VI Karataev, DV Schmikk, VA Zagulin, *Sov.Phys.JETP.* 37 (1973) 45.
12. X Tang, R Beavis, W Ens, F Lafortune, B Schueler, KG Standing, *Int.J.Mass Spectrom.Ion Processes*, 85 (1988) 43.
13. JJ Lennon, RS Brown, *Anal.Chem.*, 67 (1995) 1988.
14. WC Wiley, I McLaren, *Rev.Sci.Inst.*, 26 (1955) 1150.
15. ML Vestal, P Juhasz, SA Martin, *Proceedings of 45th ASMS, 1997*, P.1100.
16. M Karas, U Bahr, A Deppe, B Stahl, F Hillenkamp, *Macromol.Chem.Macromol.Symp.* 61 (1992) 397.
17. PO Danis, DE Karr, F Mayer, A Holle, Ch Watson, *Org.Mass Spectrom.*, 27 (1992) 843.
18. G Montaudo, MS Montaudo, C Puglisi, F Samperi, *Rapid Commun.Mass Spectrom.*, 9 (1995) 453.

19. PO Danis, DE Karr, WJ Simonsick, DT Wu, *Macromolecules*, 28 (1995) 1229.
20. AM Belu, JM DeSimone, RW Linton, GW Lange, RM Friedman, *J.Am.Soc.Mass Spectrom.*, 7 (1996) 11.
21. AT Jackson, HT Yates, WA MacDonald, JH Scrivens, G Critchley, J Brown, MJ Deery, *J.Am.Soc.Mass Spectrom.*, 8 (1997) 132.
22. J Spickermann, K Martin, HJ Rader, K Mullen, H Schlaad, AHE Muller, RP Kruger, *Eur.Mass Spectrom.*, 2 (1996) 161.
23. PO Danis, DE Karr, *Org.Mass Spectrom.*, 28 (1993) 923.
24. H Pasch, F Gores, *Polymer*, 36 (1995) 1999.
25. J Schweer, J Sarnecki, F Mayer-Posner, K Mullen, HJ Rader, J Spickermann, *Macromolecules*, 29 (1996) 4536.
26. B Thomson, K Suddaby, A Rudin, G Lajoie, *Eur.Poly.J.*, 32 (1996) 239.
27. D Dogruel, RW Nelson, P Williams, *Rapid Commun.Mass Spectrom.*, 10 (1996) 801.
28. G Montaudo, *Polym.Prep.*, 37 (1996) 290.
29. PM Lloyd, KG Suddaby, JE Varney, E Scrivner, PJ Derrick, DM Haddleton, *Eur.Mass Spectrom.*, 1 (1995) 293.
30. BS Larsen, WJ Simonsick, CN McEwen, *J.Am.Soc.Mass Spectrom.*, 7 (1996) 287.
31. KG Suddaby, DM Haddleton, JJ Hastings, SN Richards, JP O'Donnell, *Macromolecules*, 29 (1996) 2083.
32. C Jackson, B Larsen, C McEwen, *Anal.Chem.*, 68 (1996) 1303.
33. PO Danis, DE Karr, Y Xiong, KG Owens, *Rapid Commun.Mass Spectrom.*, 10 (1996) 862.
34. DJ Duncalf, HJ Wade, C Waterson, PJ Derrick, DM Haddleton, A McCamely, *Macromolecules*, 29 (1996) 6399.
35. D Schriemer, L Li, *Anal.Chem.*, 68 (1996) 2721.
36. HMD Liu, UP Schlunegger, *Rapid Commun.Mass Spectrom.*, 10 (1996) 483.
37. JC Blais, M Tessier, G Bolbach, B Remaud, L Rozes, J Guitard, A Brunot, E Marechal, JC Tabet, *Int.J.Mass Spectrom.Ion Processes*, 144 (1995) 131.

38. H Pasch, K Rode, *J.Chrom.A.*, 699 (1995) 21.
39. S Lee, MA Winnick, RM Whittal, L Li, *Macromolecules*, 29 (1996) 3060.
40. MJ Deery, KR Jennings, CB Jasieczek, DM Haddleton, AT Jackson, HT Yates, JH Scrivens, *Rapid Commun.Mass Spectrom.*, 11 (1997) 57.
41. U Bahr, A Deppe, M Karas, F Hillenkamp, U Giessman, *Anal.Chem.*, 64 (1992) 2866.
42. H Rashidezadeh, B Guo, *J.Am.Soc.Mass Spectrom.*, 9 (1998) 724.
43. CF LLenes, RM O'Malley, *Rapid Commun.Mass Spectrom.*, 6 (1992) 564.
44. SK Poehlein, SJ Dormady, DR McMillin, FE Regnier, *Rapid Commun.Mass Spectrom.*, 13 (1999) 1349.
45. CN McEwen, C Jackson, BS Larsen, *Int.J.Mass Spectrom.Ion Processes*, 160 (1997) 387.
46. K Martin, J Spickermann, HJ Rader, K Mullen, *Rapid Commun.Mass Spectrom.*, 10 (1996) 1471.
47. J Axelsson, E Scrivener, DM Haddleton, PJ Derrick, *Macromolecules*, 29 (1996) 8875.
48. G Montaudo, MS Montaudo, C Puglisi, F Samperi, *Rapid Commun.Mass Spectrom.*, 8 (1994) 1011.
49. HJ Rader, J Spickermann, K Mullen, *Macromol.Chem.Phys.*, 196 (1995) 3967.
50. CN McEwen, C Jackson, BS Larsen, *Polym.Prepr.*, 17 (1996) 314.
51. MWF Nielen, *Anal.Chem.*, 70 (1998) 1563.
52. MWF Nielen, S Malucha, *Rapid Commun.Mass Spectrom.*, 11 (1997) 1194.
53. IM Campbell, 'Introduction to synthetic polymers', Oxford Science Publications, 1994.
54. PC Painter, MM Coleman, 'Fundamentals of Polymer Science', Technomic Publishing Co.Inc., 1994.
55. AK Chowdhary, G Critchley, A Diaf, EJ Beckmann, AJ Russell, *Macromolecules*, 29 (1996) 2213.
56. IA Mowat, RJ Donovan, RRJ Maier, *Rapid Commun.Mass Spectrom.*, 11 (1997) 89.

57. E Lehmann, R Knochenmuss, R Zenobi, *Rapid Commun.Mass Spectrom.*, 11 (1997) 1483.
58. R Zenobi, R Knochenmuss, *Mass Spectrometry Reviews*, 17 (1998) 337.
59. AT Jackson, HT Yates, JH Scrivens, G Critchley, J Brown, MR Green, RH Bateman, *Rapid Commun.Mass Spectrom.*, 10 (1996) 1668.
60. AT Jackson, HT Yates, CI Lindsay, Y Didier, JA Segal, JH Scrivens, G Critchley, J Brown, *Rapid Commun. Mass Spectrom.*, 11 (1997) 520.
61. AT Jackson, KR Jennings, JH Scrivens, *J.Am.Soc.Mass Spectrom.*, 8 (1997) 76.
62. AT Jackson, HT Yates, JH Scrivens, MR Green, RH Bateman, *J.Am.Soc.Mass Spectrom.*, 8 (1997) 1206.
63. AT Jackson, HT Yates, JH Scrivens, MR Green, RH Bateman, *J.Am.Soc.Mass Spectrom.*, 9 (1998) 269.
64. V Schadler, J Spickermann, HJ Rader, U Wiesner, *Macromolecules*, 29 (1996) 4865.
65. S Pispas, N Hadjichristidis, *Macromolecules*, 27 (1994) 1891.
66. KF Medzihradzky, GW Adams, AL Burlingame, RH Bateman, MR Green, *J.Am.Soc.Mass Spectrometry*, 7 (1996) 1.
67. RH Bateman, MR Green, G Scott, E Clayton, *Rapid Commun.Mass Spectrometry*, 9 (1995) 1227.
68. AG Craig, PJ Derrick, *Aust.J.Chem.*, 39 (1986) 1421.
69. L Radom, WJ Bouma, RH Nobes, BF Yates, *Pure.Appl.Chem.*, 56 (1984) 1831.

Chapter 4

**Studies of consecutive reactions to
distinguish isomeric $C_3H_3^+$ ions formed in
some simple organic molecules**

4.1 Aim

Some metastable reactions yield product ion peaks whose shape is composite in nature. One such reaction involves the formation of $C_3H_3^+$ ions. The composite nature suggests that more than one isomer may be involved either as the precursor or product. Infact, two isomeric $C_3H_3^+$ ions have been observed in the gas phase, the cyclopropenium and propargyl cations. The aim of this study was to investigate a series of precursors and study the isomeric nature of the $C_3H_3^+$ products. Consecutive reaction studies provide an ideal method for differentiating between isomeric ion structures based on their internal energy content, given it is sufficiently difficult to distinguish solely on the basis of their mass-analysed ion kinetic energy (MIKE) spectra.

4.2 Introduction

One of the most important aspects of mass spectrometry is the powerful ability to characterise ionic structures of a wide range of molecules. At first, it seems straight forward, but the confirmation of structural identity of gas phase ions is by no means trivial. To aid the identity of the ions studied during this investigation, two important techniques were utilised. The methods employed were unimolecular (metastable) and collision induced dissociations (CID), whose principles rely heavily upon the internal energy of the sample ion. Without such techniques, the structural identity of ions would be difficult by mass spectrometric detection unless used in conjunction as a combined technique, i.e. GC-MS or LC-MS.

Unimolecular product ion peak shapes are generally classified into the types shown in Figure 4.01. Small energy releases are characterised by a Gaussian shaped curve (I). Large energy releases, for example, the metastable reaction of doubly charged ions, form a dish-topped peak (III) due to instrumental discrimination in the z-direction (the non-focusing direction), other large energy releases are accompanied by flat-topped peaks (II). The final peak shape commonly observed is one that is composite (IV) in nature. It is assumed that this arises when the product ion is formed in one of two different structures, each having different translational energy release distributions, through having different internal energy.

Thus, metastable reactions can yield a tremendous amount of product ion information. However, these reaction types will not solely reveal any definite identifiable characteristics of ion structure since the technique is limited by variations in internal energy of the sample ion. The data obtained by metastable reactions though can be used to aid ion identity by means of CID.

CID analysis is slightly more difficult since the instrument must be capable of performing tandem mass spectrometry experiments (MS/MS). This can be achieved by magnetically selecting a precursor ion of interest, which can be induced to fragment by collision with a neutral gas. The product ions formed upon dissociation will reveal structural information specific of that precursor ion.

Interest arose for this study, from the metastable peak shape obtained from the metastable reaction $C_5H_5^+ \rightarrow C_3H_3^+$ in toluene by Sen-Sharma *et al.* [1]. The peak

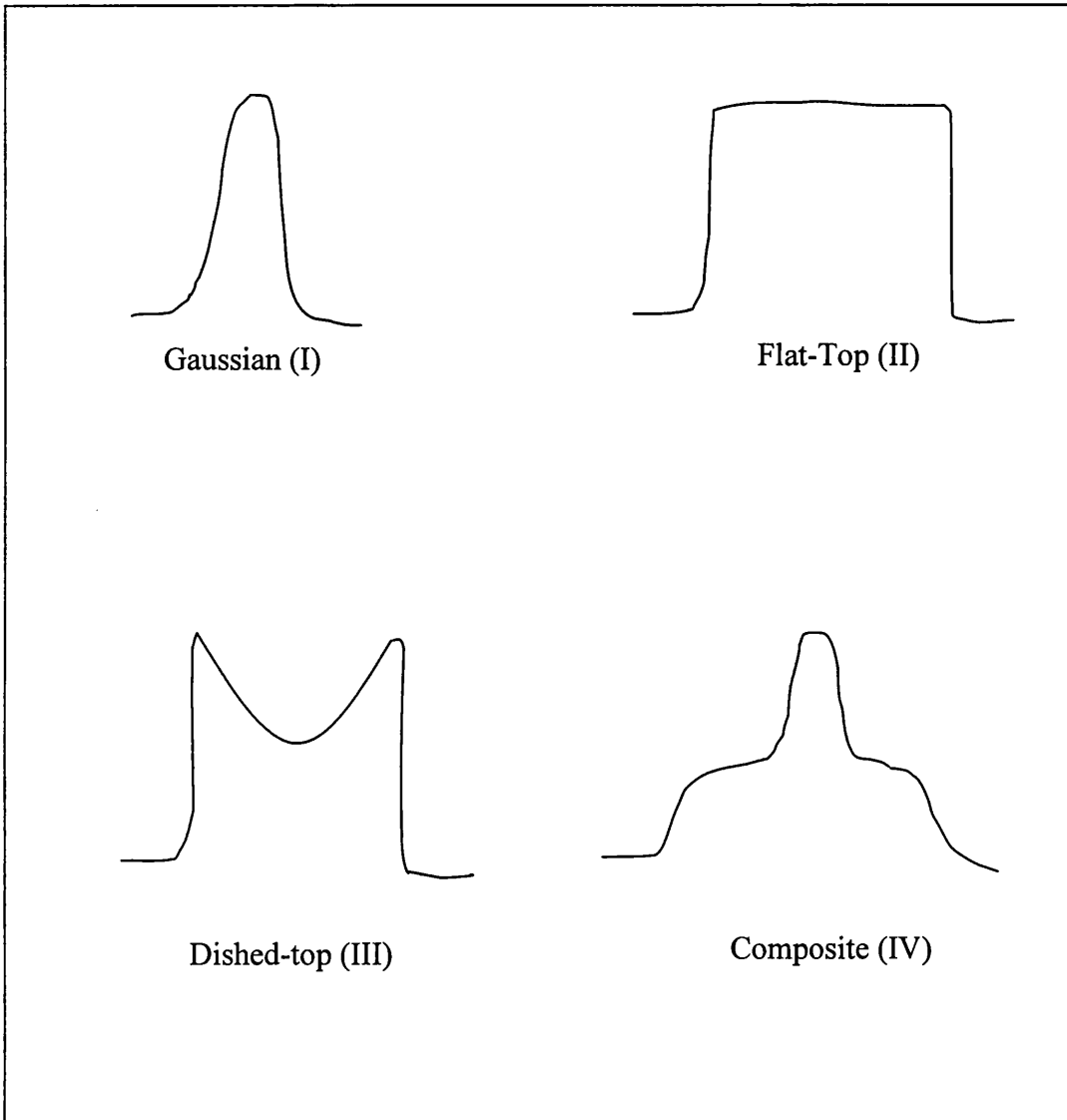


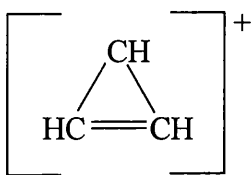
Figure 4.01: Typical peak shapes obtained from metastable dissociations

shape was composite in nature, proposed to be due to the formation of two product ions. A composite peak shape was also observed for the same product ion obtained from *n*-hexane by Goldberg *et al.* [2] and propene by Holmes *et al.* [3]. Holmes *et al.* [4] estimated without showing any mass spectra that the composite nature was due to the formation of two structurally different isomers.

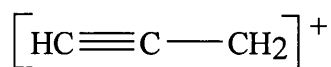
A powerful and extremely reproducible method does exist whereby metastable ions can be selected for CID analysis on the basis of their internal energies. The results achieved from this technique termed ‘consecutive reaction studies’ will demonstrate unambiguously that previous studies [1-3] showing the composite nature of the $C_3H_3^+$ ion peak, formed from some metastable reactions was due to the formation of two structurally different $C_3H_3^+$ ions. The study demonstrates how these different metastable ions will be structurally identified on the basis of their internal energy.

4.2.1 $C_3H_3^+$ ion identification

Two isomeric $C_3H_3^+$ ions have been observed in the gas phase, the cyclopropenium ion (structure A) and the propargyl ion (structure B):



Structure (A)



Structure (B)

This $C_3H_3^+$ ion is observed in the mass spectra of a large number of organic compounds, the structure of which has generated great interest spanning three decades [1,4-9].

Ab initio calculations [7] indicate that the cyclic structure (A) is ~ 60 kcal mol⁻¹ more stable than the linear structure (B). Calculations have also showed that two other isomers are known to be stable below the lowest dissociation limit to $C_3H^+ + H_2$, of structure $[CH_2CH-C:]^+$ and $[H_3CCC]^+$. However, the more stable cyclopropenium and propargyl cations have been the main isomers studied.

Considerable evidence has been concluded from metastable ion dissociation processes and kinetic energy release measurements from toluene [1], simple alkanes [2], allyl halides [11], propargyl halides [9,12] and the 1-halo-1-propynes [9] that the $C_3H_3^+$ ion does to exist in two forms.

Methods other than mass spectrometry have been employed indirectly to aid structural identification of these two more stable isomers.

Coloumb explosion imaging experiments (CEI) [10] have indicated the presence of linear and cyclic ions to be present in 30% (linear) and 70% (cyclic) formed from electron bombardment of allene (C_3H_4). Here, ions impact on a thin foil with MeV energies, which when on impact, electrons from the ions are torn off. Coloumb explosion of the bare nuclei occurs which is detected in coincidence on a spatially resolved analyser plate.

Reaction kinetic studies have been reported for both isomers with various organic compounds including ethyne and benzene on an ICR spectrometer [13]. For instance, results suggested that the linear ion is very reactive with ethyne leading to the formation of $C_5H_5^+$, whereas the cyclic structure is unreactive, which would be expected since the linear isomer has higher internal energy.

$C_3H_3^+$ ions formed from electron impact on methyl acetylene have been used in selected ion flow drift tube (SIFT) experiments [14]. Here, the ions are reacted with gases such as CO and H_2 in the flow tube containing a carrier gas. Results provide rate coefficients and ion product information from ion-molecule reactions. Studies have indicated the presence of both isomers in a 65:35 ratio (cyclic:linear).

The above mentioned techniques however do not provide absolute methods of structural identification. Knowledge gained of this sort together with mass spectrometric information can yield absolute structural identity.

CID developed through Jennings [15] and McLafferty *et al.*[16] aids structural identity unambiguously. Structural ion identity has greatly expanded since the early work of McLafferty [17].

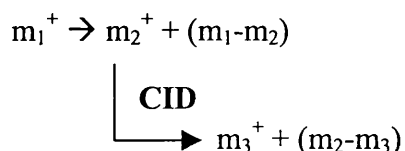
Collision induced product ion spectra has been obtained on various precursor $C_3H_3^+$ ions formed from some simple organic molecules during this investigation and from previous studies [4,8,18]. CID/MIKE spectra obtained show significant differences when propargyl ions are generated at threshold compared to cyclopropenium ions.

4.2.2 Consecutive reaction studies

The first report of a consecutive reaction involving metastable dissociation, was conducted by Jennings [19]. A metastable peak was observed at m/z 16.8 in the mass spectrum of toluene. It was proposed $C_5H_5^+$ ions formed from the dissociation of $C_7H_7^+$ were further dissociated by the consecutive loss of C_2H_2 to form $C_3H_3^+$, resulting in a peak at m/z 16.8 in the spectrum, obtained from a HV scan, which corresponds to a mass of $39^2/91$.

Since these early findings many reports have been cited in the literature involving isomeric ion structure identity and the probing of reaction pathways [20-24]. Metastable ions dissociating in a field free region (FFR) will contain a small distribution of internal energies, just above the critical energy barrier for reacting [25], relating to rate constants between 10^5 - 10^6 s [26]. A range of translational energies can be released upon dissociation [27] resulting in the formation of product ions with a range of internal energies.

A consecutive reaction therefore involves a product ion from a metastable dissociation that is sufficiently capable of further reaction. For this investigation the two-step consecutive reaction process can be represented as:



The first step $m_1^+ \rightarrow m_2^+$ occurs in FFR1, (refer to Figure 4.02). These ions can be successfully transmitted to ESA1 by setting the magnetic field in the magnetic sector to admit ions of m_2^2/m_1 , since the metastable ion obtained from the first step will be observed in the MIKE spectrum at this mass.

Thus, stable m_2^+ ions exiting the magnetic sector will have the correct trajectory to be transmitted to the collision cell by setting the ESA1 voltage to m_2E/m_1 , where E is the electric sector voltage required to accept, without hindrance, the stable ions that have received the full accelerating voltage.

Once the metastable m_2^+ ions have reached the collision cell in FFR3, they are induced to fragment by leaking a neutral gas, typically nitrogen, into the collision cell. The m_3^+ product ions obtained from this collision induced reaction can be detected by scanning around m_3E/m_1 on ESA2.

4.2.2.1 Energetics of consecutive reactions

The energetics for the metastable reaction occurring in a FFR, the first step of the reaction, can be best conceived by considering a potential energy curve for the reaction, as shown in Figure 4.03. Metastable ions which have lifetimes of the order of 10^5 - 10^6 s⁻¹ are denoted by the shaded area. The curve is representative of the two $C_3H_3^+$ product ions formed from the metastable reactions investigated for toluene for example, occurring in FFR3.

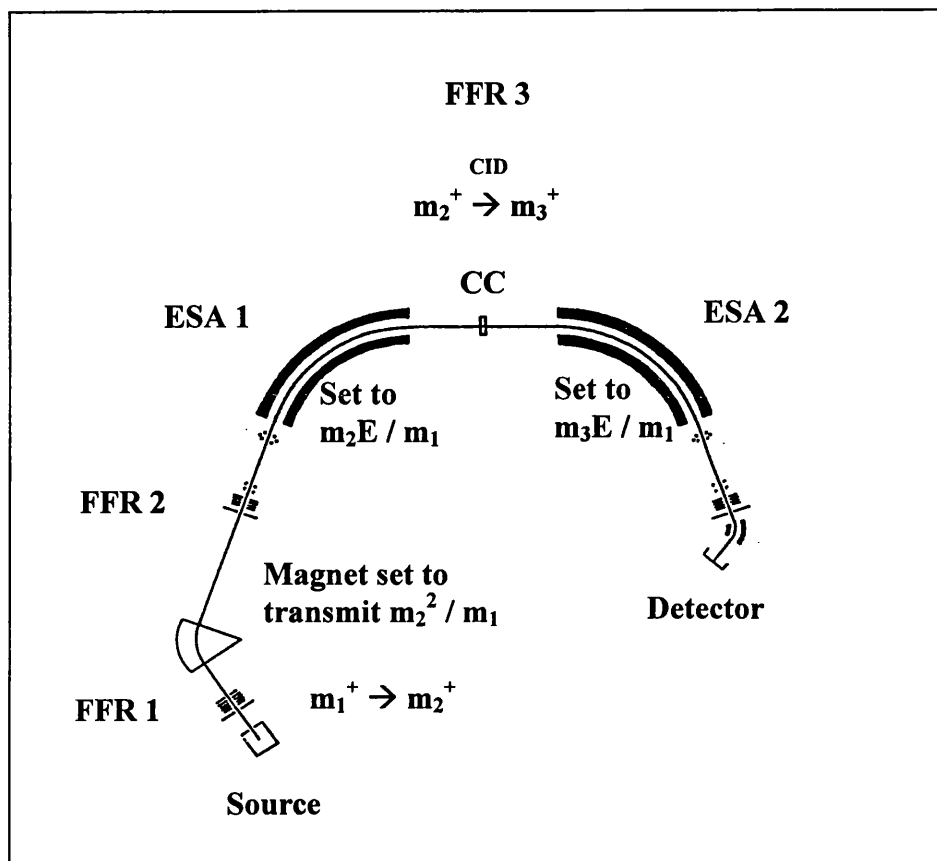


Figure 4.02: Schematic of 'TES II', illustrating the field free regions (FFR) and instrumental settings used for the consecutive reaction studies

The energy the m_1^+ ions contain is sufficient enough to overcome the energy barrier for reaction leading to the formation of m_2^+ product ions. The kinetic energy released in the decomposition of metastable ions can arise from two sources: the excess energy, ε of the activated complex which is available for partitioning between the internal energies of the products and translational energy of their separation and ε_0^\ddagger which is partitioned between internal and translational energy [26].

Thus, for reactions that have a distribution of translational energies the product m_2^+ ions formed will have a distribution of internal energies. Large values of T will represent m_2^+ ions with low internal energy (cyclic structure in this case), represented by the selected portion **II** in Figure 4.04. Small values of T will represent m_2^+ ions with a higher internal energy (linear structure), represented by the selected portion **I**. [ε_0 is the activation energy and ε_0^\ddagger is the reverse activation energy].

Figure 4.04 shows the partial spectrum obtained for the metastable reaction of $C_5H_5^+ \rightarrow C_3H_3^+$ in toluene occurring in FFR3.

This investigation utilised portions of the metastable peaks obtained from reactions occurring in FFR1, which have intensity differences in comparison (see later).

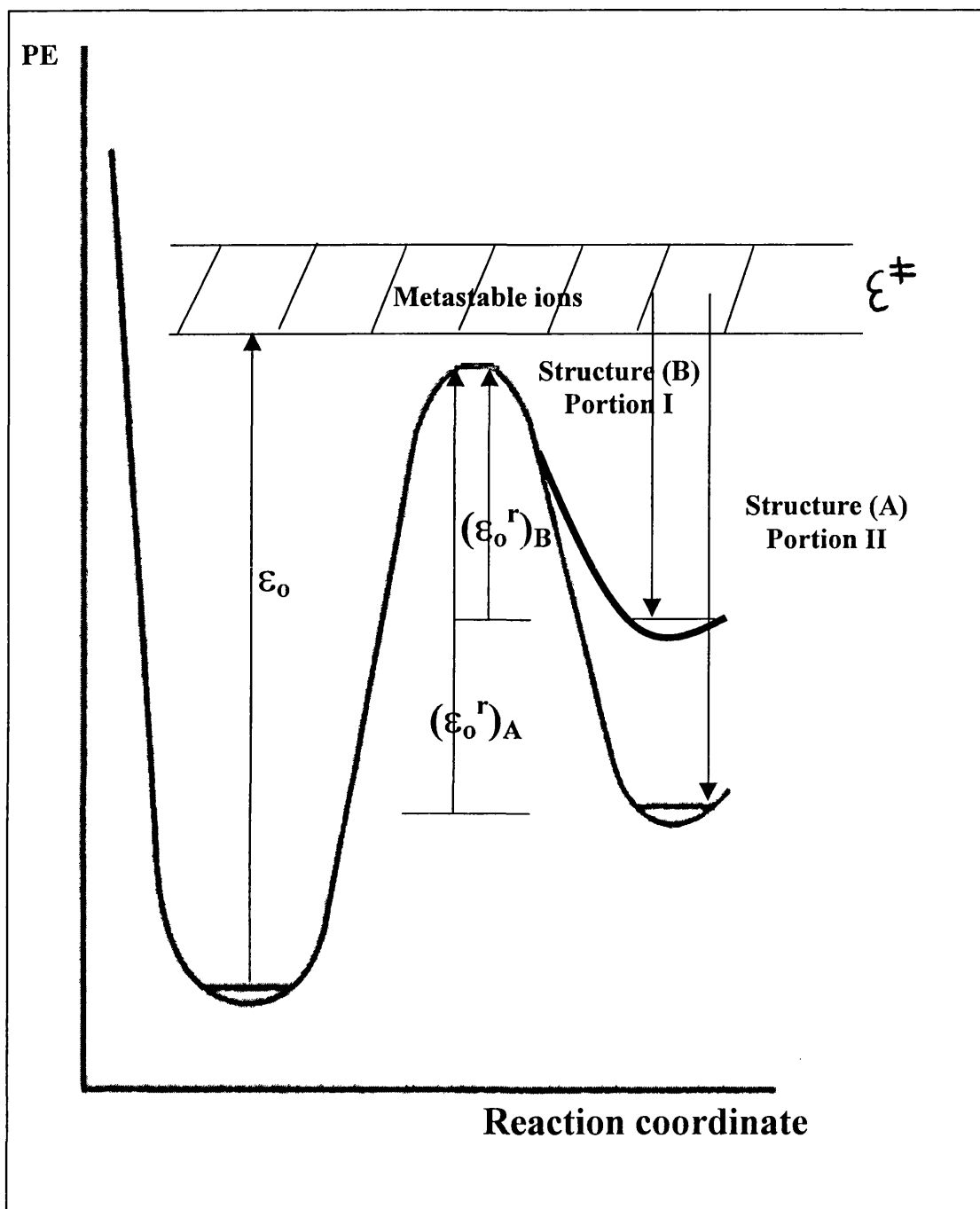


Figure 4.03: Simple PE curve for the metastable reaction $C_5H_5^+ \rightarrow C_3H_3^+$ in toluene occurring in FFR3. The products formed have different energies due to the different translational energy releases

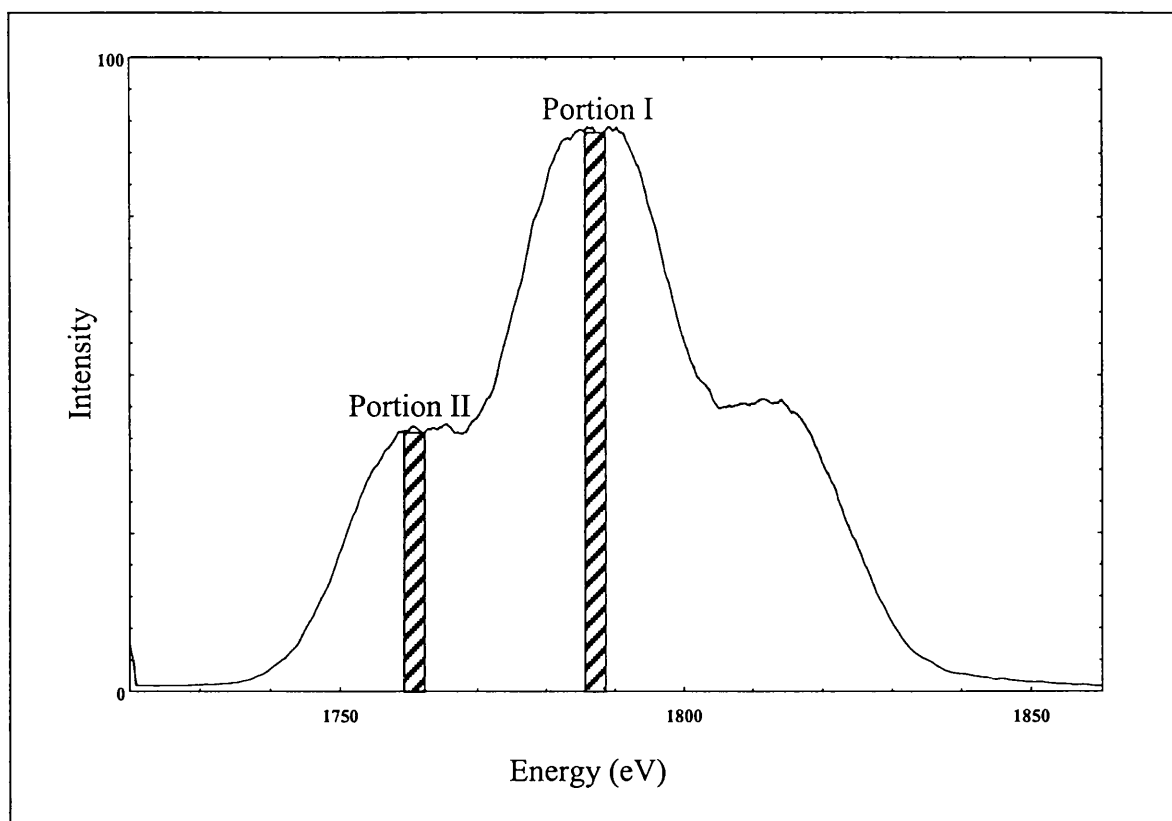


Figure 4.04: Diagram illustrating the selection of different portions of the metastable peak obtained for the metastable reaction of $C_5H_5^+ \rightarrow C_3H_3^+$ in toluene. Portion I corresponds to a small energy release, from ions having a high internal energy (linear). Portion II corresponds to a larger energy release, from ions having a lower internal energy (cyclic)

The use of consecutive reactions will show that by selecting different portions of the metastable peak obtained, that the product ion information gleaned from the collision induced MIKE spectrum provides accurate confirmation of two structurally different $C_3H_3^+$ isomers.

4.3 Experimental

4.3.1 Instrumentation

The instrument used during this study was built in house at Swansea University in 1996. It is a double-focusing mass spectrometer of BEE geometry (B = magnetic sector and E = electric sector) conventionally known as ‘reversed geometry’. Figure 4.05 shows a schematic of the instrument, which is known as TESII. The instrument was designed for high-energy resolution translational energy spectroscopy experiments (~ 20 meV FWHM), where a high energy ion beam is allowed to collide with neutral gas targets. Information regarding the electronic and vibrational structures of both the projectile ion and stationary target can be inferred from the energetics of the collision.

The ‘reverse-geometry’ of the instrument however, is ideal for MIKE mass spectrometry. Here, the magnetic sector is situated before the electric sector, which allows ions of a specific m/z ratio to be isolated from all other ions exiting the source. Any ion that dissociates in one of the field free regions before reaching the detector is called a ‘metastable ion’. Metastable fragmentation occurring in FFR3 can be detected on this instrument by scanning the electric sector voltage on ESA2. The spectrum produced is termed a ‘MIKE spectrum’. Thus, metastable reactions of a precursor ion will reveal energy release data specific to that ion.

Ions are formed in an electron impact source by introducing the sample into this region via an inlet system. This allows stable controllable pressures in the source of the order of $1-5 \times 10^{-5}$ mbar as read on the ion gauge. Electrons emitted from a heated

filament are allowed to collide with molecules of the sample, causing ionisation. Ions are then extracted from the source by application of an acceleration voltage of typically 3kV.

For the consecutive reaction studies, the electron beam used for the formation of the required ions was generated from a rhenium filament. Rhenium was used since they were the only type readily available towards the end of the study, though the lifetime was not as good as the tungsten filaments.

Operating conditions were a trap current of 500 μA and a filament emission current of 3 mA. Electrons were produced with an electron energy of 70 eV throughout the study. The resolving slits labelled S1, S2 and S3 in figure 4.05 were fully open to maximise sensitivity. Nitrogen was leaked into the collision cell, of length 10mm, to a pressure of $\sim 1.5 \times 10^{-6}$ mbar, which was sufficient enough to decrease the precursor ion beam intensity by $\sim 20\%$ in all experiments in order to avoid multiple collisions, since these could have had a serious effect on the product CID MIKE spectrum obtained.

Detection of the ions is achieved by scanning the voltage on ESA2 in tandem with the voltage on ESA3. ESA3 is much smaller than the other two electric sectors and designed solely for the elimination of unwanted ion signals that may arise from ESA2. The ion beam is detected by an off-axis electron multiplier. Here, the ions do not impact directly onto the first dynode of this particular detector. Ions initially strike a deflection dynode, where on impact a shower of electrons is produced. These electrons are then attracted to the first dynode of the electron multiplier where more

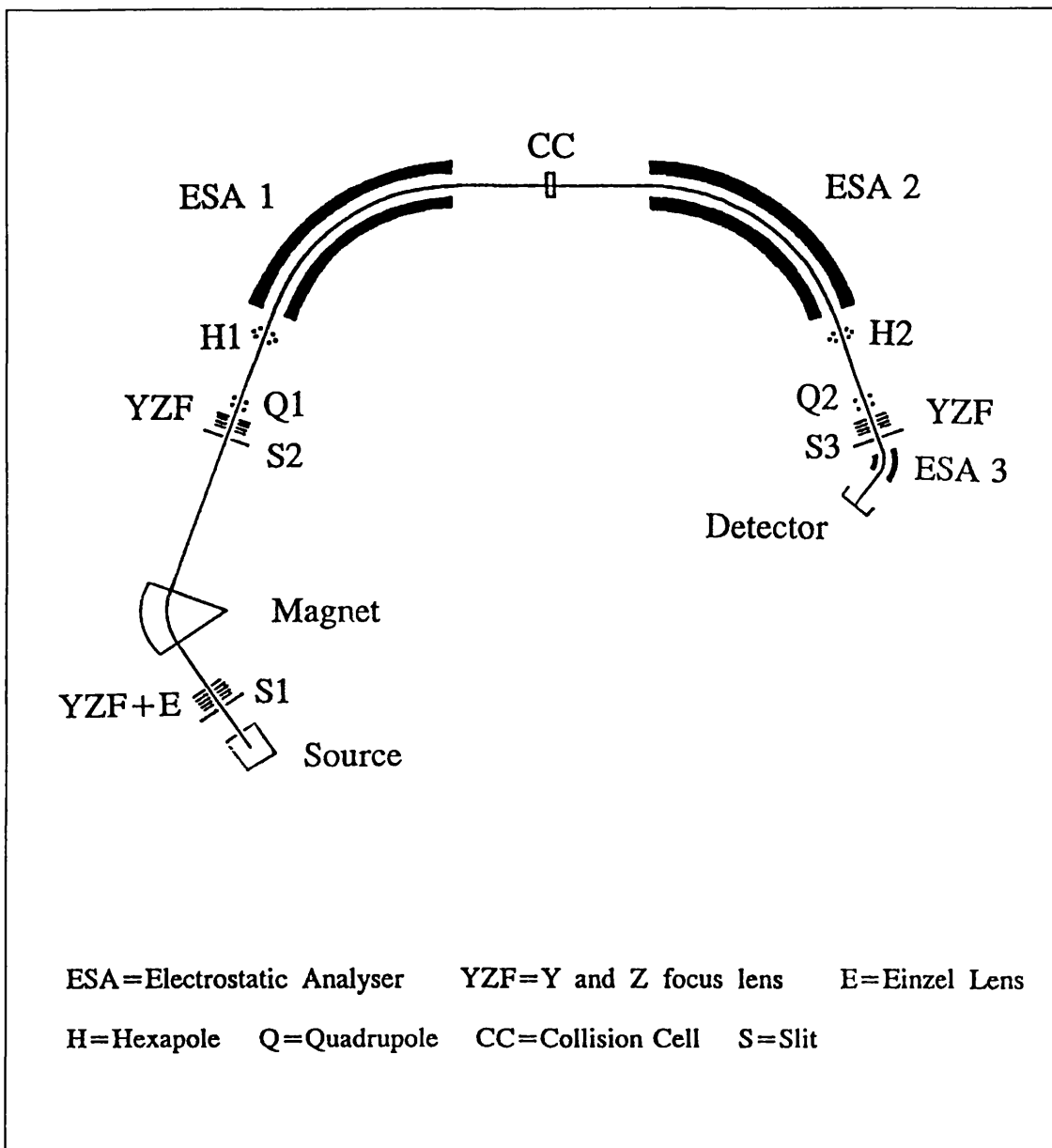


Figure 4.05: Schematic of the instrument employed, 'TES II'

and more electrons are generated on contact with each of the subsequent dynodes along the detector.

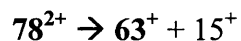
The current thus generated by the electron multiplier is then converted by a pre-amplifier, into an analogue voltage. The voltage generated, determines the gain of the multiplier which can be varied to enable a 10^{-6} A or 10^{-9} A scale to be chosen. This voltage is passed into a 'Chopper Amplifier Unit' with a gain which can also be varied in the range of 1-3000. The signal from the chopper amplifier is displayed on an oscilloscope which is then transferred to a 486 DX2 PC through an analogue-to-digital converter (ADC) operating under Power Basic software (Power Basic Inc, Monterey, CA, USA).

4.3.2 Calibration

The instrument was not initially designed for MIKES mass spectrometry as previously mentioned. Therefore, a method of calibration had to be employed prior to the acquisition of data since the acquisition software had to be substantially modified for this type of analysis.

It was decided to do two experiments involving the charge separation of doubly charged ions formed from benzene and toluene. It is well known that when a doubly charged metastable ion fragments into two separate ions of the same charge, that there is a large energy release associated with the repulsion between the two charges, forming a dish-topped peak.

The first reaction investigated was:



from benzene. The magnet was set to select the $C_6H_6^{2+}$ ion (occurring at m/z 39) and the metastable dissociation, from the charge separation, occurring in FFR3 was observed by scanning ESA2 around $63/39 \times 2996$ eV (2996 eV corresponds to the main beam position for ions accelerated from the source at 3 kV).

Jennings *et al.* [28] had previously shown that the energy release associated with this reaction to be ~ 2.8 eV. The peak shape obtained in the MIKE spectrum for this reaction is shown in Figure 4.06. The energy release for this data can be calculated from the following equation [26]:

$$T = \frac{y^2 m_1^2 eV.}{16 \times m_2 m_3} (\Delta W / W)^2$$

where y is the number of charges on the product ion, eV is the acceleration voltage, x is the number of charges on the precursor ion, ΔW is the width of the metastable peak and W is the main beam position, so:

$$T = \frac{1^2 \times 78^2 \times 3000.}{16 \times 2 \times 63 \times 15} (205 / 2996)^2$$

$$T = 2.82 \text{ eV}$$

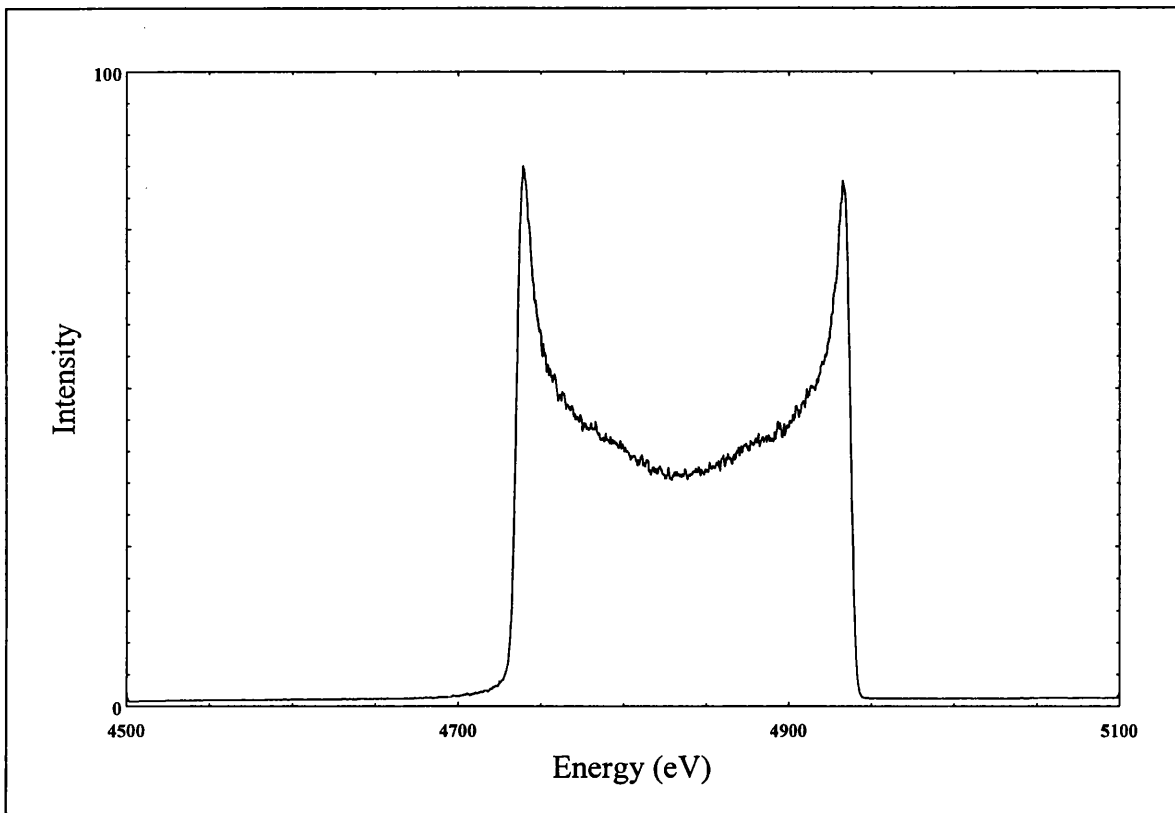


Figure 4.06: Partial MIKE mass spectrum for the reaction $78^{2+} \rightarrow 63^{+}$ in Benzene

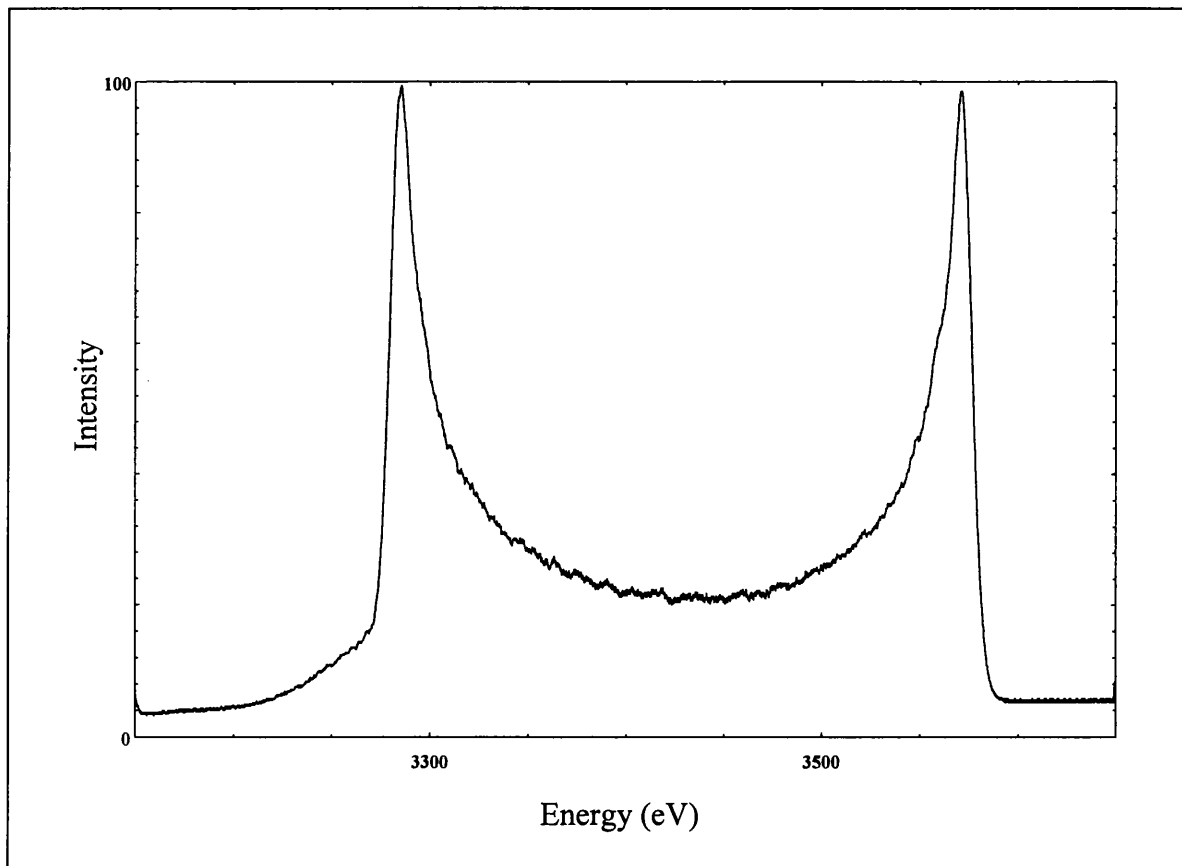
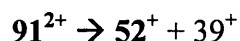


Figure 4.07: Partial MIKE spectrum for the reaction $91^{2+} \rightarrow 52^{+}$ in Toluene

The energy release of ~ 2.82 eV corresponds extremely close to the previous result obtained for this experiment.

The final experiment involved the reaction:



from toluene. The magnet was set to select $C_7H_7^{2+}$ (m/z 45.5) and the charge separation occurring in FFR3 was observed by scanning the electric sector voltage on ESA2 around $52/45.5 \times 2996$ eV. The MIKE spectrum for this reaction is shown in Figure 4.07. Previous results obtained by Beynon *et al.* [29] demonstrated an energy release of ~ 3.8 eV. Results obtained during this study showed the same result.

The experimental results obtained clearly demonstrate that the data acquisition software had been accurately modified for the provision of MIKE mass spectrometry experiments to be carried out.

4.3.3 Sample preparation

Thirteen $C_3H_3^+$ precursor ions were investigated in total, which were formed from a variety of molecules.

Acetophenone, phenylacetylene, benzene, thiophene, 1-hexyne, n-hexane, n-butylbenzene and toluene were purchased from BDH (Poole, U.K.).

2,4-hexadiyne and propargyl alcohol were purchased from Lancaster (Morecambe, U.K.), 1,5-hexadiyne from Alfa Aesar (Hertfordshire, U.K.) and propene from Aldrich (Milwaukee, USA).

Approximately 10 μ L of each sample solution was injected through a septum (as received) into a heated reservoir. The vapor is then leaked into the source, through a heated line via a re-entrant. The temperature applied to the reservoir and re-entrant depended upon the volatility of the liquid injected. Propene was the only gas studied and was leaked into the source via a separate inlet system from a pressurised gas cylinder.

All samples were administered into the source region up to a pressure of $\sim 1-5 \times 10^{-5}$ mbar. For CID analysis, nitrogen was leaked into the collision cell up to a pressure of $\sim 1-5 \times 10^{-6}$ mbar as indicated on the ion gauge. The pressure within the 10mm long cell is estimated to be ~ 300 times higher than this.

4.4 Results and Discussion

Some metastable reactions leading to the formation of the $C_3H_3^+$ ion have been shown to be composite in nature [1-3]. Results obtained suggest that two possible structures for the $C_3H_3^+$ ion exists. To carry out consecutive reaction studies, it was deemed necessary to look at these particular reactions again, since the instrument used in the current study was of different geometry. The following reactions studied initially involved metastable dissociation of the chosen precursor ion in FFR3 of the

instrument. Figure 4.04 shows the reaction $C_5H_5^+ \rightarrow C_3H_3^+$ from toluene, (Figure 4.18 (appendix II) shows the reaction for $C_3H_5^+ \rightarrow C_3H_3^+$ in n-hexane and Figure 4.19 (appendix II) shows the same latter reaction occurring from propene). The metastable MIKE spectrum produced from each clearly shows the formation of two different ion structures. The outer broader distribution is assumed to arise from the formation of the cyclopropenium ion and the inner distribution from the propargyl ion. The major reason the reactions were investigated was to provide the correct portion of ions, (due to difference in energy) to be selected for CID analysis.

Ions selected for consecutive studies were produced in FFR1, it was therefore necessary to look at the metastable peak shape produced for the $m_1^+ \rightarrow m_2^+$ dissociation reaction occurring in FFR1 for each molecule investigated, i.e. toluene, n-hexane and propene.

These experiments proved problematic, since the geometry of the instrument did not facilitate the necessary scan. The ability to observe and detect metastable reactions occurring in FFR1 would be straightforward if the instrument was equipped with a detector positioned after the magnet. The ideal case would be to have one electric sector after the magnet (BE geometry) instead of two as in this case. The BE geometry would allow a B^2/E type scan which permits the fragment ions occurring in FFR1 to be detected with ease. Here, the magnetic sector and electric sector would be scanned simultaneously with the B^2/E ratio kept constant.

An approximate shape of the dissociation occurring in FFR1 was however obtained, by a manual point-by-point method. For example, consider the metastable reaction of

$C_5H_5^+$ (65^+) \rightarrow $C_3H_3^+$ (39^+) occurring in toluene in FFR1. These ions can be transmitted to ESA1 by setting the magnetic field to admit only ions of mass $39^2/65$ (m/z 23.4). The voltage on ESA1 can be varied using an external 10V DC reference supply over different energy ranges, as acquired for the same reaction occurring in FFR3. Thus, once an appropriate voltage has been applied to ESA1, only ions of m/z 23.4 will have the 'correct' energy to be transmitted through FFR3 and on to ESA2. ESA2 can then be scanned over a very small energy range (< 10 eV) which results in the detection of a broad peak on the oscilloscope. The signal intensity at the top of this peak is then measured. This method was carried out approximately twenty times to obtain sufficient data points for the ion intensity falling on the detector as a function of different energies. The final peak shape derived was an average of three determinations.

It is important to mention that the measurements obtained for the metastable dissociation of ions formed in FFR1 were generated from the mid-point energy of the reaction occurring in FFR3 and below. The data finally presented is therefore a reflection of these signal intensities gained. The reason for this was due to the presence of an artefact peak occurring on the high energy side of the beam. A brief explanation will be discussed later, but the presence of such a peak and its full characterisation was beyond the scope of the present investigation.

Prior to performing consecutive reaction studies it was necessary to perform CID analysis on various $C_3H_3^+$ ions generated from different molecules. Thirteen molecules were chosen in total, some of which had previously been studied [8], (to

see if results gained here were in agreement) and on some which had not been previously studied.

Previous studies [4] have shown that when cyclopropenium ions are generated at threshold energy compared to propargyl ions their CID spectra are significantly different when the ions are accelerated with a voltage of 3 kV from the source. Two product ion intensities, m/z 26⁺ (C₂H₂⁺) and m/z 25⁺ (C₂H⁺) in the CID/MIKE are sensitive to change. CID product ions produced from cyclopropenium ions yield ion intensities where m/z 26⁺ > m/z 25⁺ and propargyl ions yield intensities where m/z 25⁺ has approximately the same intensity as 26⁺. The differences can be seen by observing the partial CID/MIKE spectrum of propargyl chloride, shown in Figure 4.08, which is in agreement with Holmes *et al.* [4] and * 1-hexyne shown in Figure 4.09. It should be noted that these spectra do not necessarily correspond to the production of pure cyclopropenium and pure propargyl ions, although propargyl chloride is known to produce cyclopropenium ions at threshold energy [4].

Figure 4.08, for example shows two peaks. The mass of each peak can be calculated as follows; consider the left hand side peak, the mass can be derived from the energy associated with the centre of the peak, for example;

$$\frac{1916 \text{ (Peak centre)}}{2996 \text{ (Main beam position)}} \times 39^+ \text{ (Precursor ion)} = 25^+$$

Other molecules investigated, illustrating clear differences in the m/z 26⁺: m/z 25⁺ ratio have been tabulated below (table 1). The partial CID/MIKE spectra of each can be found in Appendix II.

Precursor molecule	m/z 26 ⁺ : m/z 25 ⁺	Appendix II
Benzene	1.4	Fig.4.20
*Phenylacetylene	1.3	Fig.4.21
*Thiophene	1.3	Fig.4.22
*Acetophenone	1.1	Fig.4.23
2,4-Hexadiyne	1.1	Fig.4.24
Propene	1.1	Fig.4.25
*Butylbenzene	1.0	Fig.4.26
*n-Hexane	0.9	Fig.4.27
Toluene	0.9	Fig.4.28
*Propargyl alcohol	0.9	Fig.4.29
1,5-Hexadiyne	0.9	Fig.4.30

Table 1: * represents those molecules that do not appear to have been previously investigated

The error associated from an average of three readings is +/- 0.1 (arbitrary units) in all cases.

From these highly reproducible differences obtained it is clear that more than one $C_3H_3^+$ ion is being formed in the ion source which does not appear to isomerise to the most stable form (cyclic structure) within the time-scale of these experiments.

The CID of pure cyclopropenium ions can be achieved by selectively transmitting portions of ions that make up the broader distribution of the metastable reactions studied. Pure propargyl ions cannot be analysed since the inner distribution will always contain a small component that makes up the outer distribution.

The expected mass spectra for the CID of cyclopropenium and propargyl ions chosen for consecutive reaction studies, should take the form of the constructed 'stick' mass spectrum shown in Figure 4.10 .

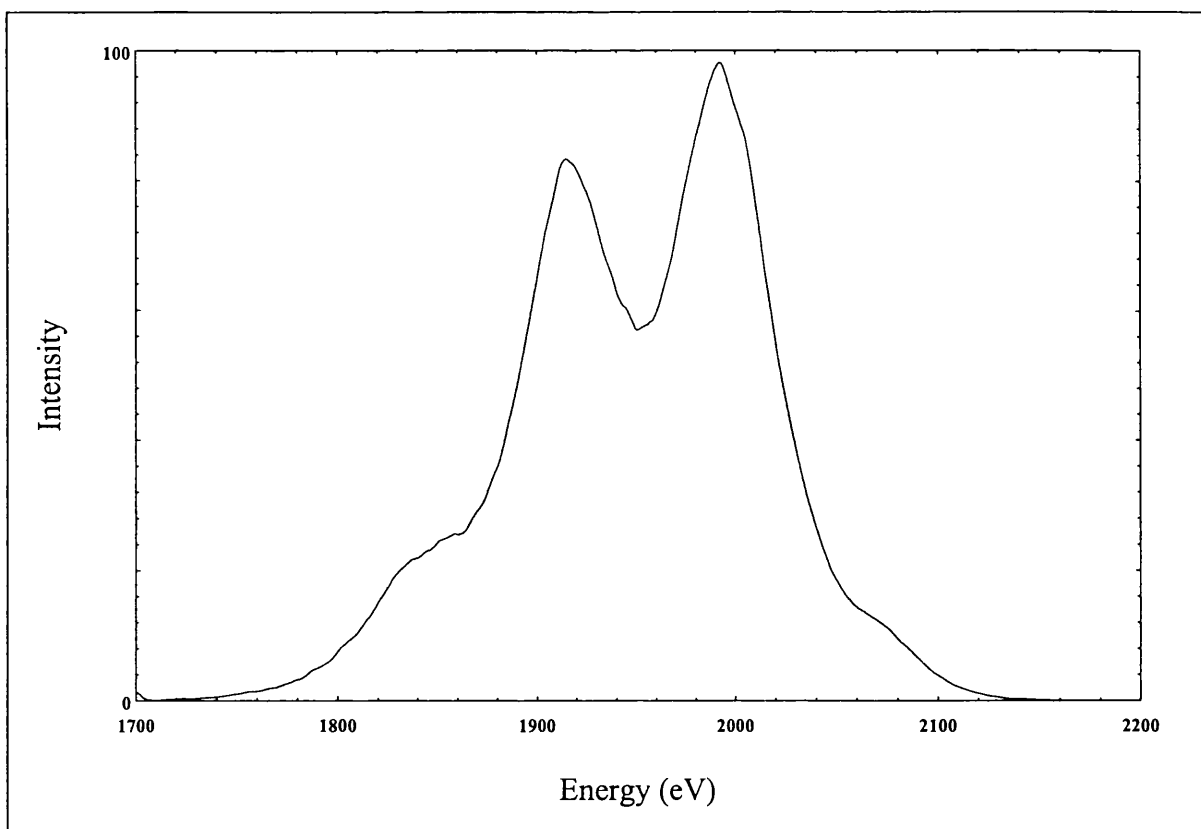


Figure 4.08: Partial CID/MIKE spectrum of $C_3H_3^+$ in Propargyl chloride

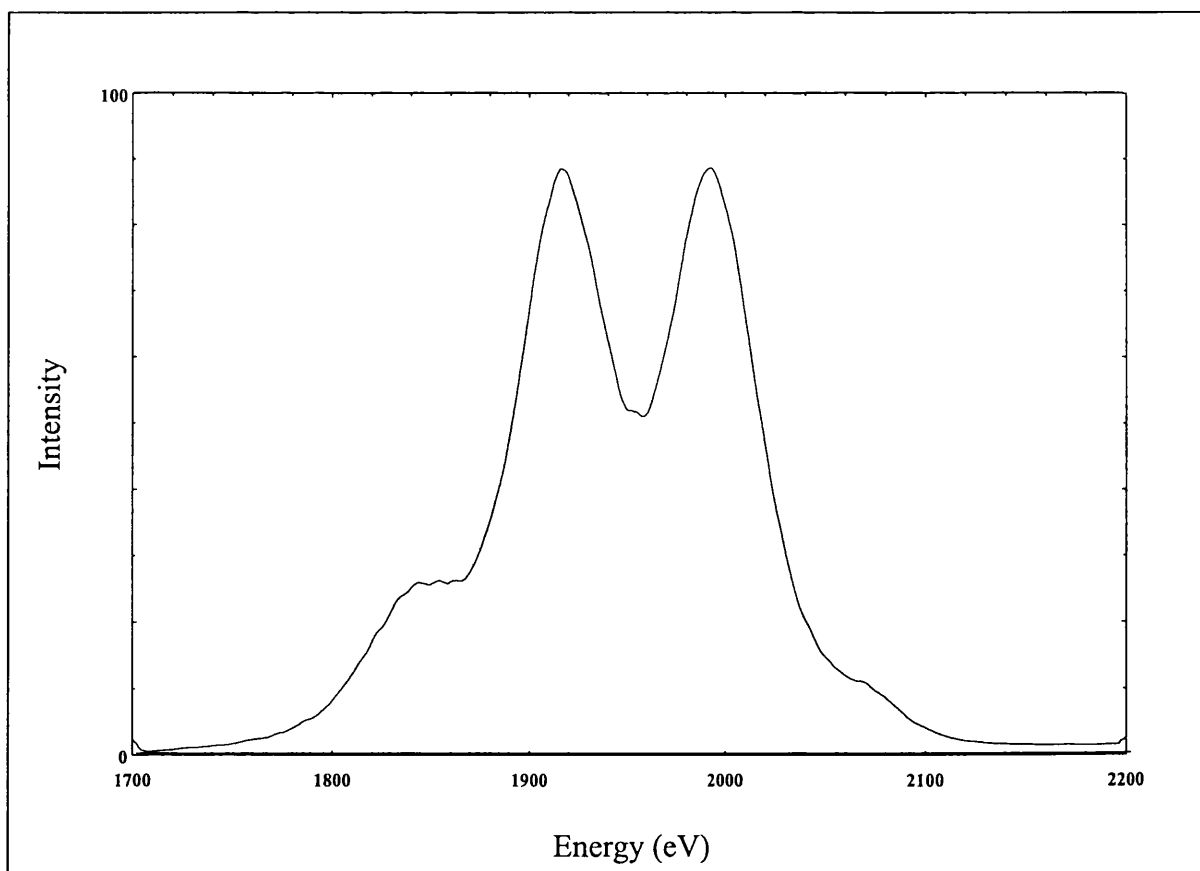


Figure 4.09: Partial CID/MIKE spectrum of $C_3H_3^+$ in 1-Hexyne

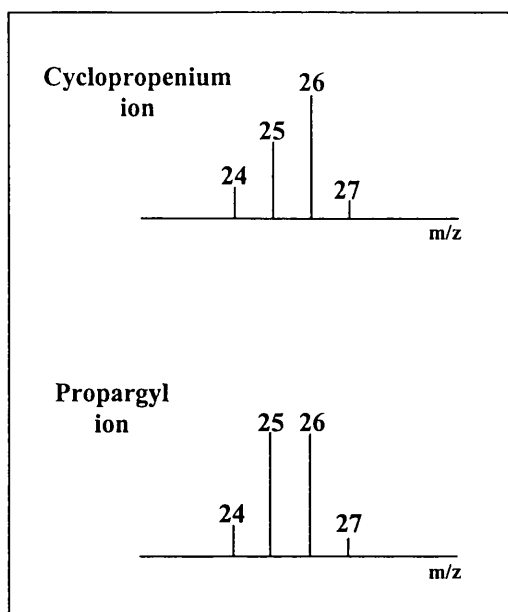


Figure 4.10: Showing expected CID product spectra

A possible energy diagram illustrating the formation of the product ion formed from the CID of two structurally different $C_3H_3^+$ ions could take the form of Figure 4.11

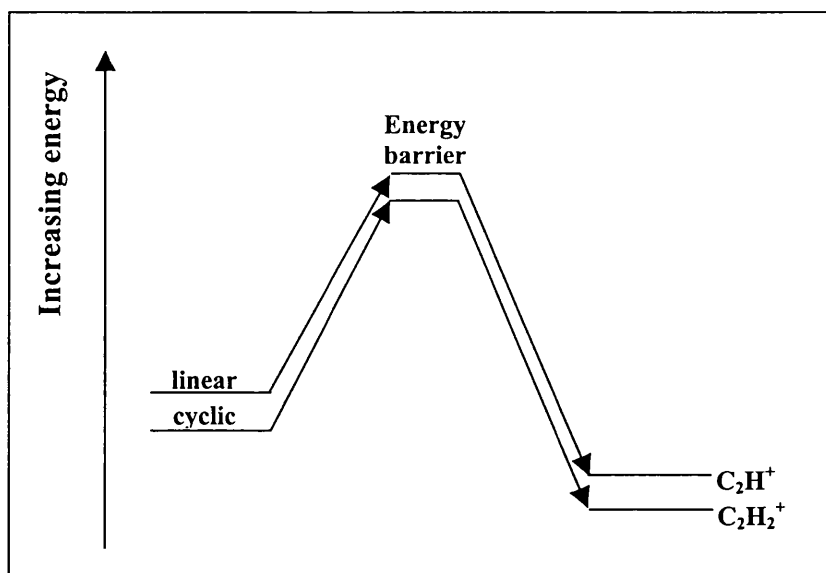


Figure 4.11: Energy diagram showing product ions formed from CID of two structurally different $C_3H_3^+$ ions

4.4.1 Toluene

Different $C_3H_3^+$ ions were chosen for CID analysis on the basis of internal energy. Various portions of the metastable peak occurring in FFR1, see Figure 4.12, were selectively transmitted to FFR3 for CID analysis.

If the assumption by Sen-Sharma *et al.* [1] was correct, i.e. that the central component, portion **I** of the metastable peak was due to the generation of propargyl ions, then it is known from these studies that the CID product ions of interest, m/z 26⁺ and m/z 25⁺, have approximately the same intensities. Thus, by selectively transmitting portion **I** ions, occurring at mass 39²/65 to the collision cell, the results generated should be of the same magnitude.

The outer more broader component of the peak, should yield results where the m/z 26⁺ ion is of greater abundance when ions selected from portion **II** undergo CID if pure cyclopropenium ions are formed.

The partial CID/MIKE spectra obtained is shown in Figure 4.13. The top spectrum obtained from selecting portion **I** and the bottom spectrum obtained from selecting portion **II**. It is clearly evident that by selecting ions from portion **II**, that a more abundant m/z 26⁺ is observed, as would be expected if pure cyclopropenium ions were responsible for the broad component of the metastable peak.

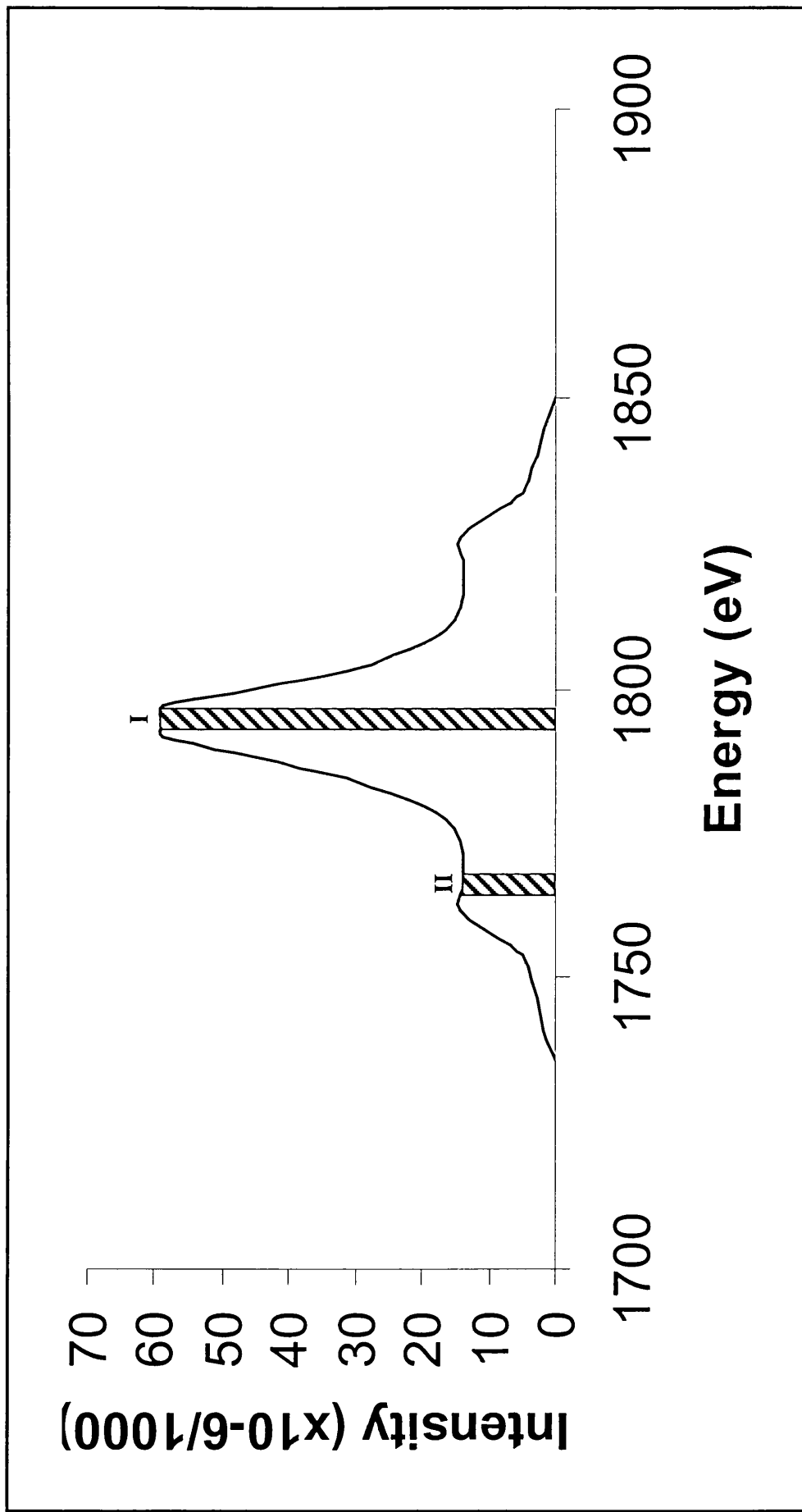


Figure 4.12: Metastable reaction of $C_5H_5^+ \rightarrow C_3H_3^+$ occurring in FFR1 for Toluene. Portion **I** and **II** represent the selected ions used for CID analysis

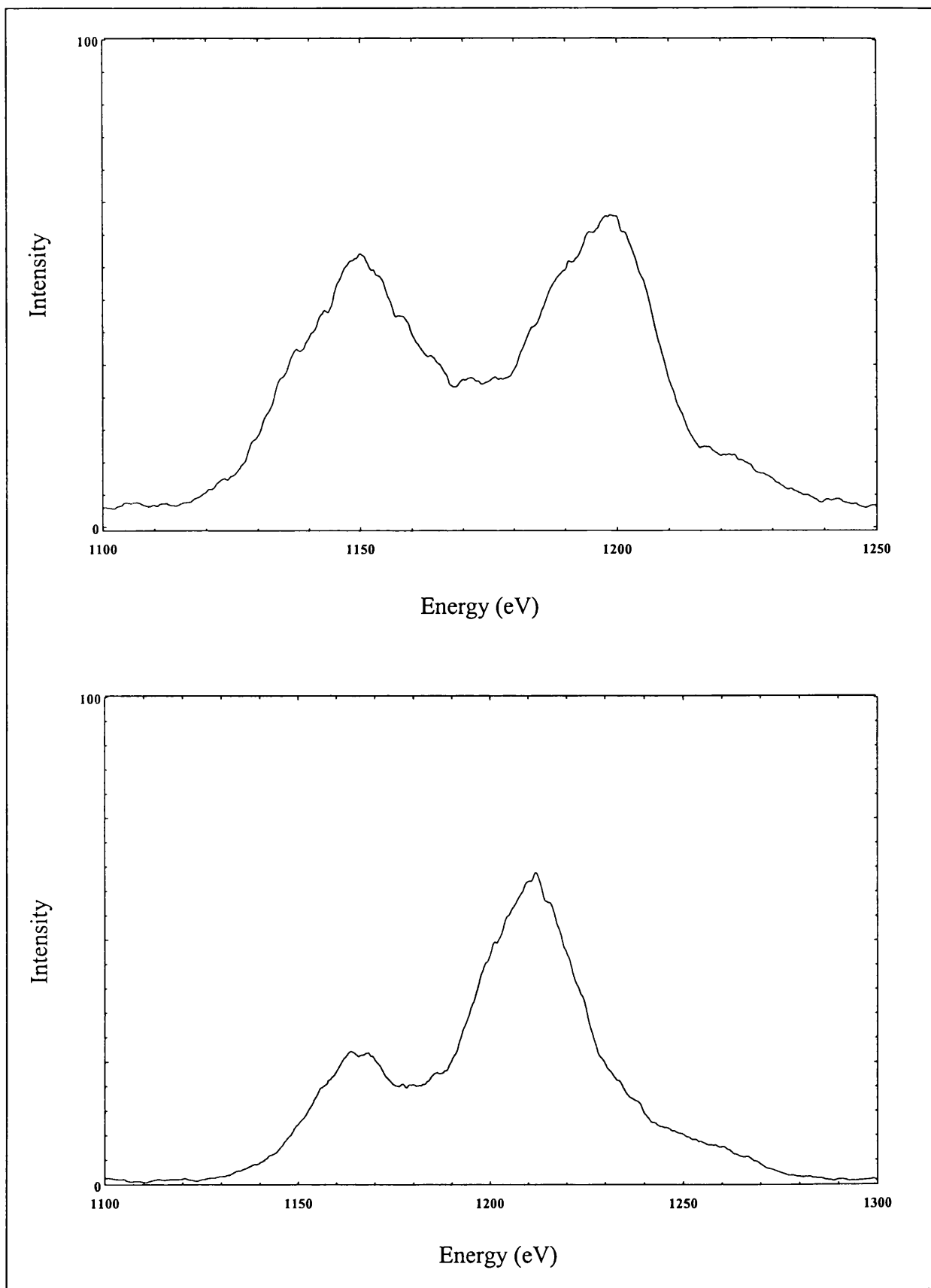


Figure 4.13: Partial CID/MIKE spectrum obtained from consecutive reaction in Toluene. Top spectrum obtained from selecting portion **I** in Figure 4.12 and bottom from selecting portion **II**

The central component of the peak, portion I, does not generate the product ions of interest with the same intensity as would be expected if pure propargyl ions were solely being formed. A reason for this slight indifference could be due to the presence of some cyclopropenium ions. However, the spectrum obtained is significantly different from the CID for ions with lower internal energy.

It is reasonable to assume, from these results, that the composite nature of the peak was due to the formation of two structurally different $C_3H_3^+$ ions.

To confirm these findings it was deemed necessary to study two more consecutive reaction investigations on n-hexane and propene. The following results proved more fruitful since the signal intensity was approximately 3 and 30 times respectively more intense than with toluene.

4.4.2 n-Hexane

The magnetic sector current was set to accept ions of mass $39^2/41$ (m/z 37.1). Ions from portion I of the metastable peak, shown in Figure 4.14 were transmitted to the collision cell by application of an appropriate voltage to ESA1. Selection of ions from portion II meant that the voltage across the ESA1 plates had to be lowered by approximately 1V.

Figure 4.15 shows the partial CID/MIKE spectrum obtained from selecting these different portions on the basis of internal energy. The spectra unambiguously

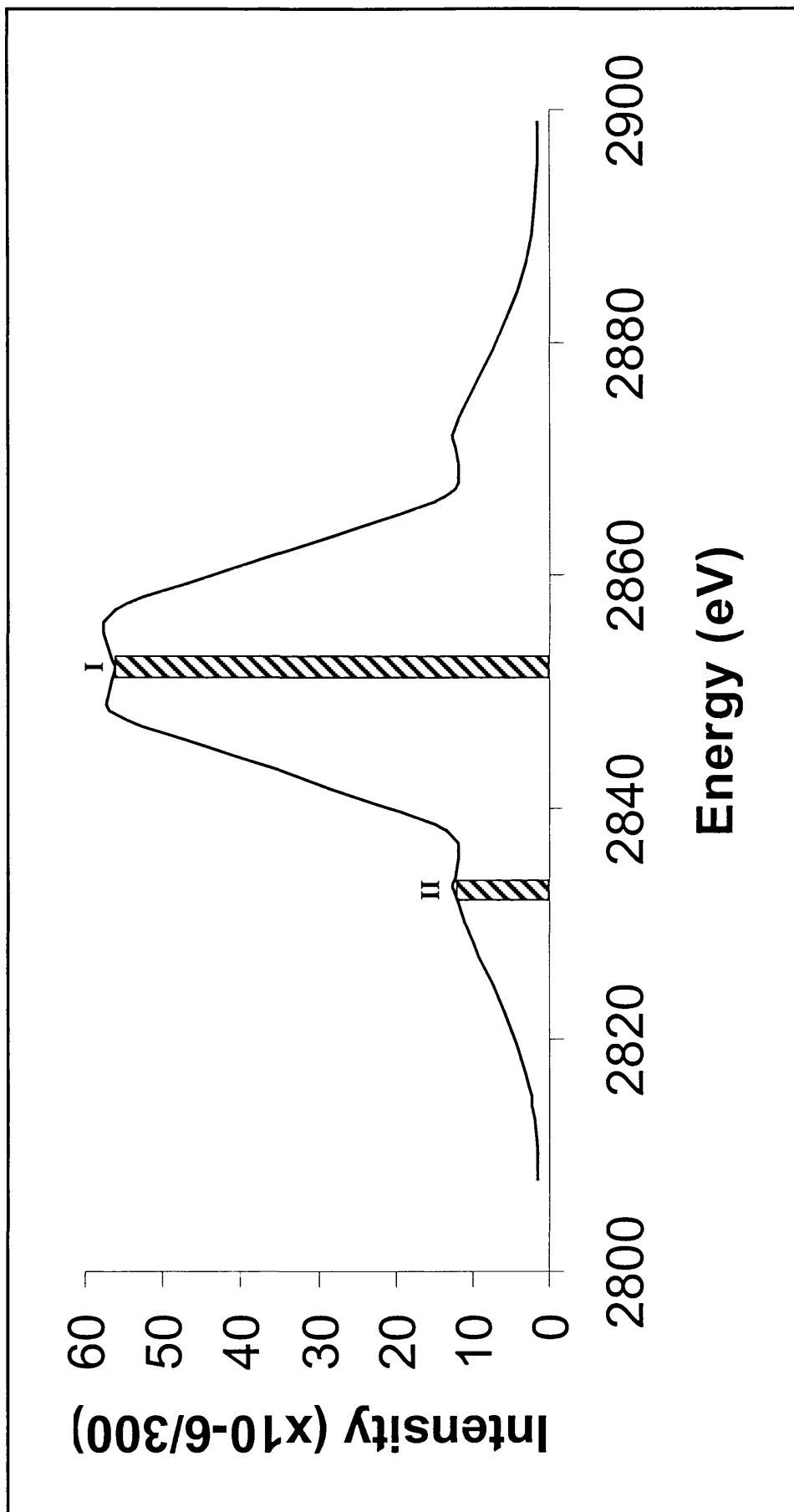


Figure 4.14: Metastable reaction of $C_3H_5^+ \rightarrow C_3H_3^+$ occurring in FFRI for n-Hexane. Portions **I** and **II** represent the selected ions used for CID analysis

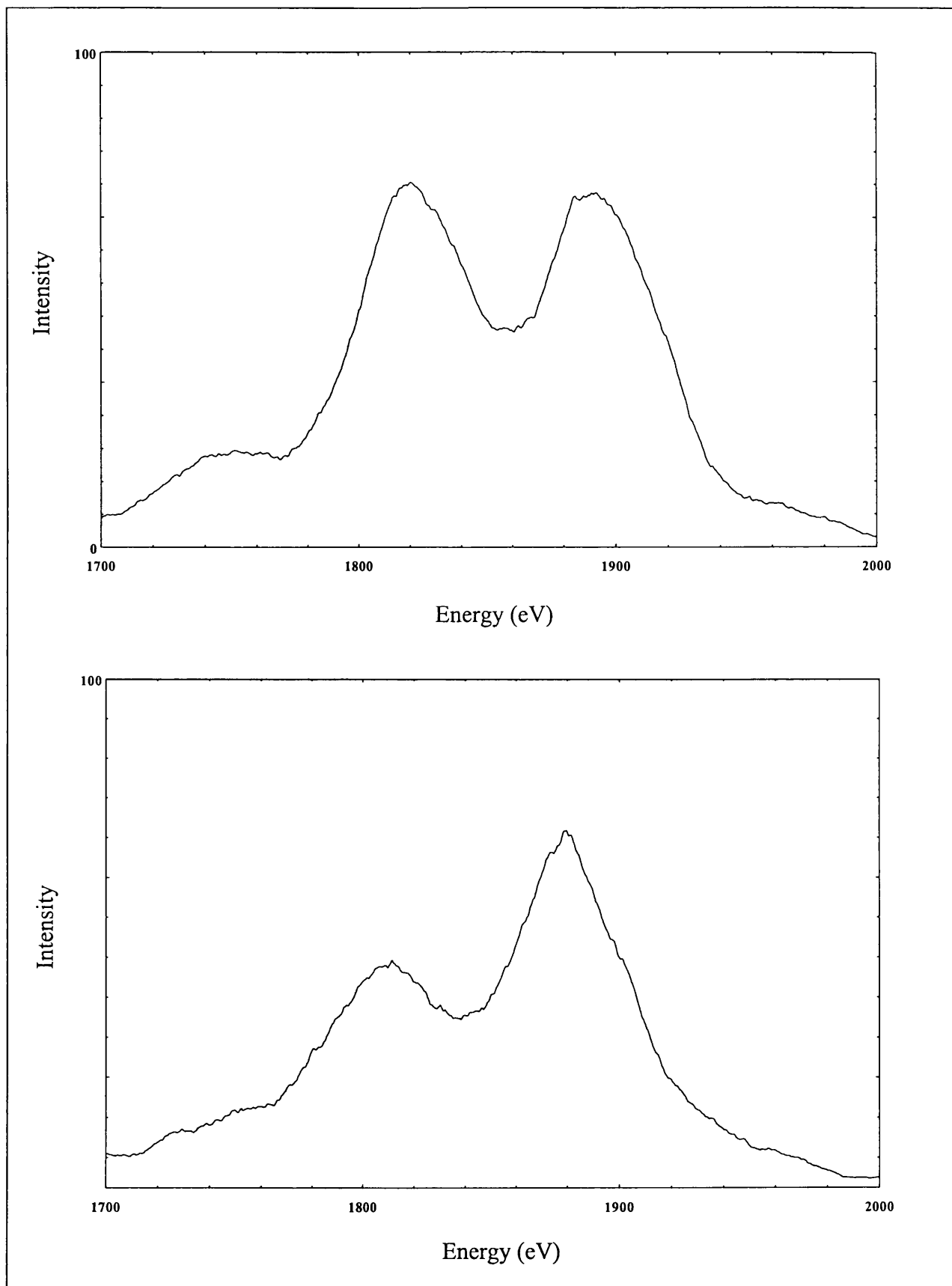


Figure 4.15: Partial CID/MIKE spectra obtained from consecutive reaction in n-Hexane. Top spectrum obtained from selecting portion **I** in Figure 4.14 and bottom spectrum obtained from selecting portion **II**

demonstrate the formation of two structurally different isomers. The ratio of abundances generated for the ions of interest do not remain constant. The selection of ions from portion **II** shows the m/z 26⁺ ion intensity is fairly constant whereas the m/z 25⁺ ion signal dramatically falls off, compared to selecting ions from portion **I**.

This seems to suggest that the inner distribution is composed of a greater proportion of propargyl ions in comparison to toluene.

4.4.3 Propene

As with n-Hexane H₂ loss from the molecular ion generates a metastable composite peak. The intensity of this peak as mentioned was the most intense which allowed three separate portions of the peak to be individually selected for CID analysis, Figure 4.16 shows the three different portions selected.

Figure 4.17, shows the partial CID/MIKE spectrum obtained by from selecting the different C₃H₃⁺ ions on the basis of varying internal energy. It is evident from the spectra, as with the other two molecules, that the product ion abundance does not remain constant. The higher energy ions (propargyl), portion **I**, generate product ions of approximate equal intensity. As the lower energy ions are selected, portions **II** and **III**, the m/z 26⁺ ion intensity remains fairly constant but again the m/z 25⁺ ion intensity significantly decreases, as would be expected for the generation of cyclopropenium ions.

These results ultimately confirm the presence of two C₃H₃⁺ isomers.

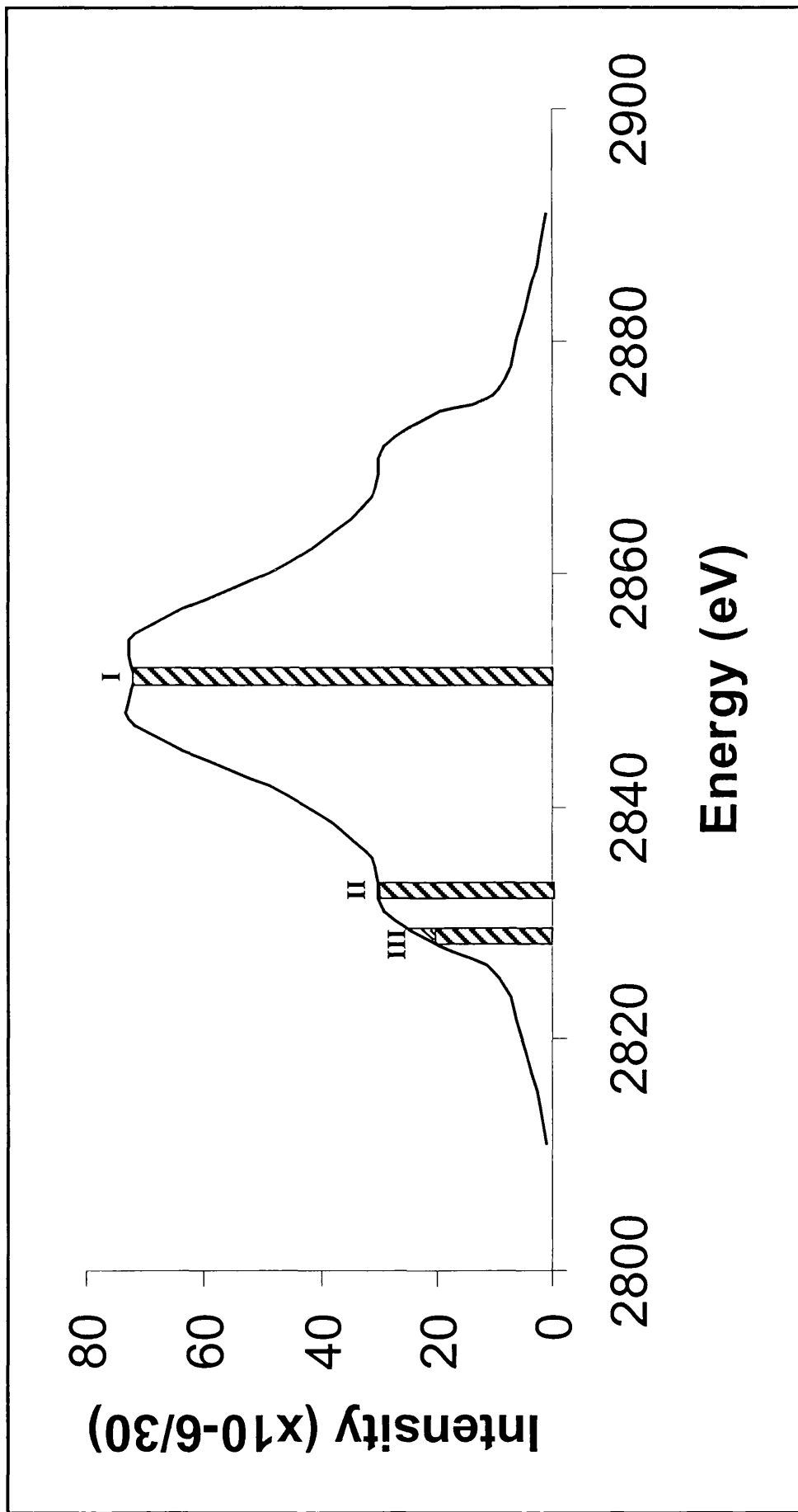


Figure 4.16: Metastable reaction of $C_3H_5^+ \rightarrow C_3H_3^+$ occurring in FFR1 for Propene. Portions I, II and III represent the selected ions used for CID analysis

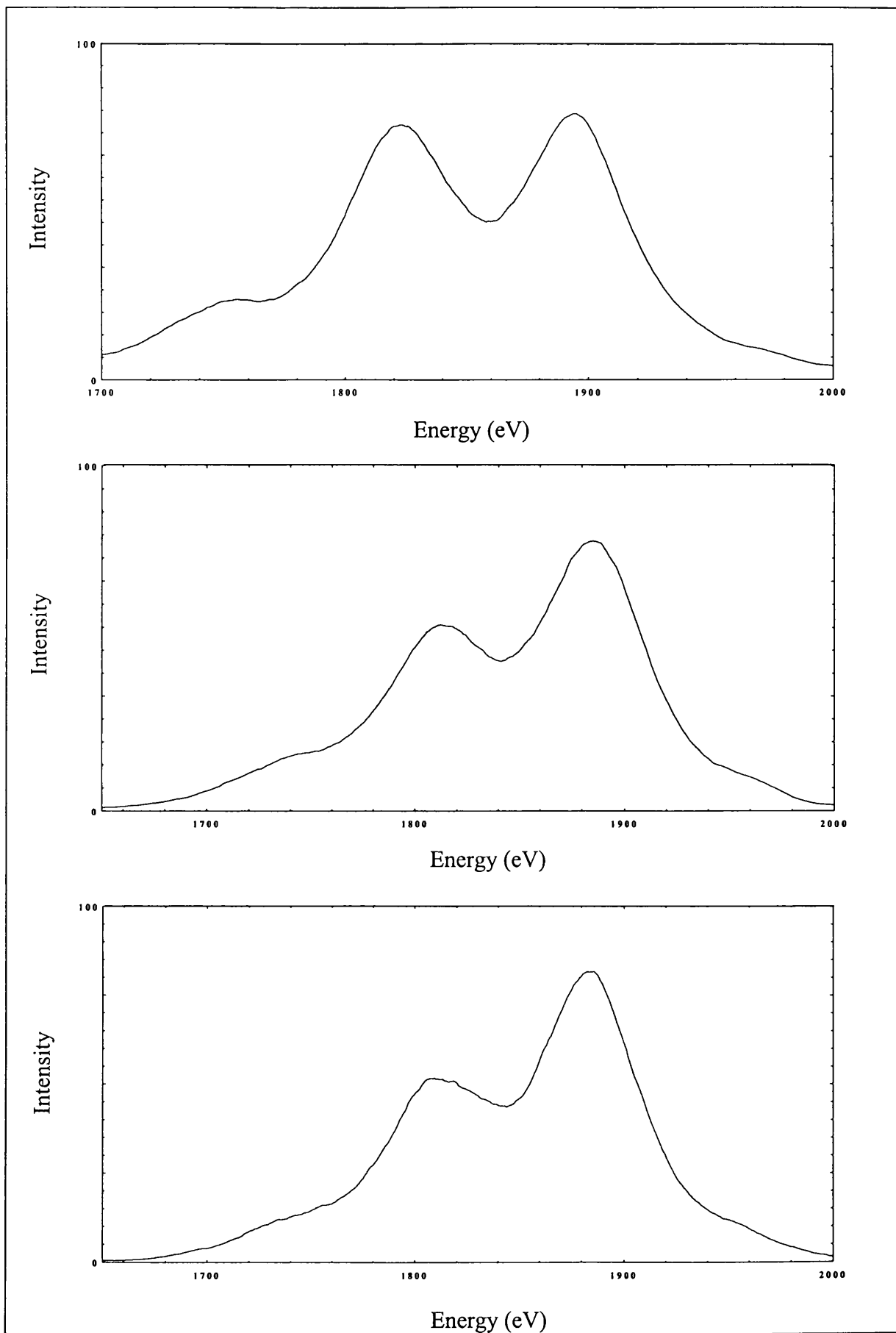


Figure 4.17: Partial CID/MIKE spectra obtained from consecutive reaction in Propene. Top spectrum obtained from selecting portion I in Figure 4.16, middle spectrum obtained from selecting portion II and bottom spectrum obtained from selecting portion III

4.5 Conclusions

Consecutive reaction studies have been used to identify structurally different $C_3H_3^+$ ions, based on internal energy. The main conclusions are as follows:

1. The metastable peak shapes leading to the formation of $C_3H_3^+$ ions formed in toluene, n-hexane and propene are composite in nature. This signifies the proposed formation of two isomeric ion structures.
2. Further characterisation for the above proposal has been performed using consecutive reactions utilising CID MIKE spectrometry. It has been shown unambiguously that the technique used is an excellent method for determining differences in isomeric ion structure on the basis of internal energy of the selected precursor ion.
3. The MIKE technique used for the consecutive reactions is very time consuming, since the acquisition of data is extremely insensitive. The results generated for each consecutive reaction spectrum, meant that ESA 2 had to be scanned very slowly for long periods, typically of the order of 30-100ms/eV, to obtain enough data points for a useable spectrum.
4. The method although very insensitive is extremely reproducible.
5. An artefact peak was observed on the high energy side of the beam for the metastable reactions occurring in FFR1. It is proposed that the selected ions

are fragmenting in one of the sectors, most likely to be within the flight tube of the magnetic sector, leading to a continuum type artefact.

6. Initial proposals [1-3] that the composite nature for the metastable reactions investigated, was due to the formation of two structurally different $C_3H_3^+$ ions has been shown by consecutive reaction studies to be correct.

7. The results estimated by Holmes *et.al* [4] are in slight disagreement since the CID spectra of $C_3H_3^+$ ions derived from $C_5H_5^+$ ions (toluene) and $C_3H_5^+$ ion (n-hexane and propene) in this case, do not give intensity ratios of equal magnitude for C_2H^+ and $C_2H_2^+$ product ions generated from propargyl ions. Two reasons could possibly be due to the fact that; different translational energies were used and that their results were overestimated, since the inner distribution of the metastable peaks contain more cyclopropenium ions than calculated.

4.6 References

1. DK Sen-Sharma, KR Jennings, JH Beynon, *Org.Mass Spectrom.*, 11 (1976) 319.
2. P Goldberg, JA Hopkinson, A Mathias, AE Williams, *Org.Mass Spectrom.*, 3 (1970) 1009.
3. JL Holmes, JK Terlouw, *Org.Mass Spectrom.*, 10 (1975) 787.
4. PC Burgers, JL Holmes, AA Mommers, JE Szulejko, *J.Am.Chem.Soc.*, 106 (1984) 521.
5. FW McLafferty, in '*Determination of organic structures by physical methods*', ed. by FC Nachod and WD Phillips, V2, P.138, Academic Press, New York (1962).
6. AG Harrison, in '*Topics in organic mass spectrometry*', ed. By AL Burlingame, P.144, Wiley-Interscience, New York (1970).
7. L Radom, PC Hariharan, JA Pople, PVR Schleyer, *J.Am.Chem.Soc.*, 98 (1976) 10.
8. C Koppel, FW McLafferty, *Org.Mass Spectrom.*, 19 (1984) 643.
9. JL Holmes, FP Lossing, *Can.J.Chem.*, 57 (1979) 249.
10. Z Vager, R Naaman, EP Kanter, in '*Ion and cluster ion spectroscopy and structure*', ed. by JP Maier, Elsevier, Amsterdam, (1989).
11. JL Holmes, AD Osborne, GM Weese, *Org.Mass Spectrom.*, 10 (1975) 867.
12. BP Tsai, AS Werner, T Baer, *J.Chem.Phys.*, 63 (1975) 4384.
13. PJ Ausloos, SG Lias, *J.Am.Chem.Soc.*, 103 (1981) 6505.
14. D Smith, NG Adams, *Int.J.Mass Spectrom.Ion Processes*, 76 (1987) 307.
15. KR Jennings, *Int.J.Mass Spectrom.Ion Processes*, 1 (1968) 227.
16. WF Haddon, FW McLafferty, *J.Am.Chem.Soc.*, 90 (1968) 4745.
17. FW McLafferty, PF Bente, R Kornfeld, SC Tsai, I Howe, *J.Am.Chem.Soc.*, 95 (1973) 2120.
18. JK Terlouw, Pc Burgers, H Hommes, *Org.Mass Spectrom.*, 14 (1979) 574.

19. KR Jennings, *Chem. Commun.*, (1966) 283.
20. CJ Proctor, JH Beynon, B Kralj, V Kramer, *Vestn.Slov.Kem.Drus.*, 29 (1982) 43.
21. CJ Proctor, B Kralj, *Org.Mass Spectrom.*, 15 (1980) 326.
22. CJ Proctor, B Kralj, EA Larka, CJ Porter, A Maquestiau, JH Beynon, *Org.Mass Spectrom.*, 16 (1981) 312.
23. CJ Proctor, CJ Porter, JH Beynon, *Org.Mass Spectrom.*, 16 (1981) 62.
24. CJ Proctor, B Kralj, AG Brenton, JH Beynon, *Org.Mass Spectrom.*, 15 (1980) 619.
25. FW McLafferty, T Wachs, C Lifshitz, G Innorta, P Irving, *J.Am.Chem.Soc.*, 92 (1970) 6867.
26. RG Cooks, JH Beynon, RM Caprioli, GR Lester, in 'Metastable ions', Elsevier, Amsterdam, (1973).
27. RK Boyd, JH Beynon, *Int.J.Mass Spectrom.Ion Processes*, 23 (1977) 163.
28. W Higgins, KR Jennings, *Chem. Commun.*, (1965) 99.
29. A Mendez Amaya, AG Brenton, JE Szulejko, JH Beynon, *Proc.R.Soc.Lond.*, A373 (1980) 13.

Appendix II (Chapter4)

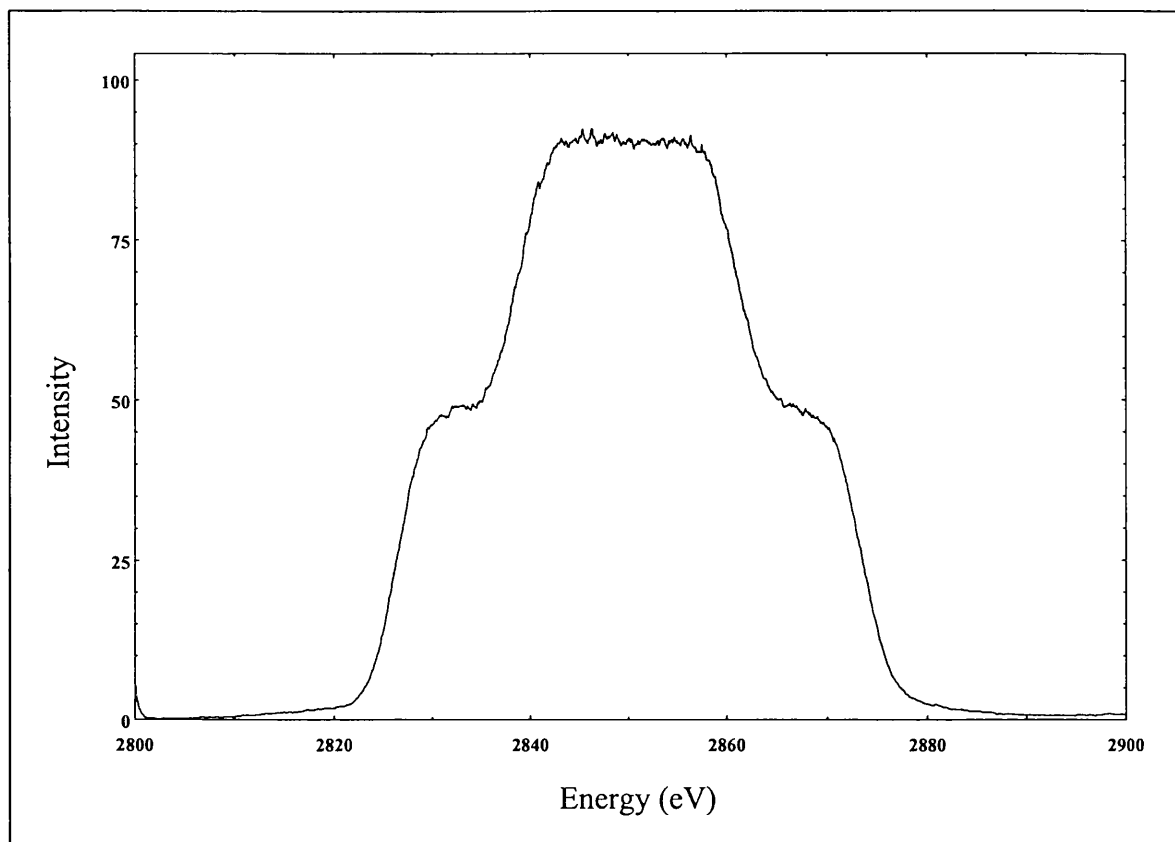


Figure 4.18: Metastable reaction of $C_3H_5^+ \rightarrow C_3H_3^+$ in n-Hexane occurring in FFR3

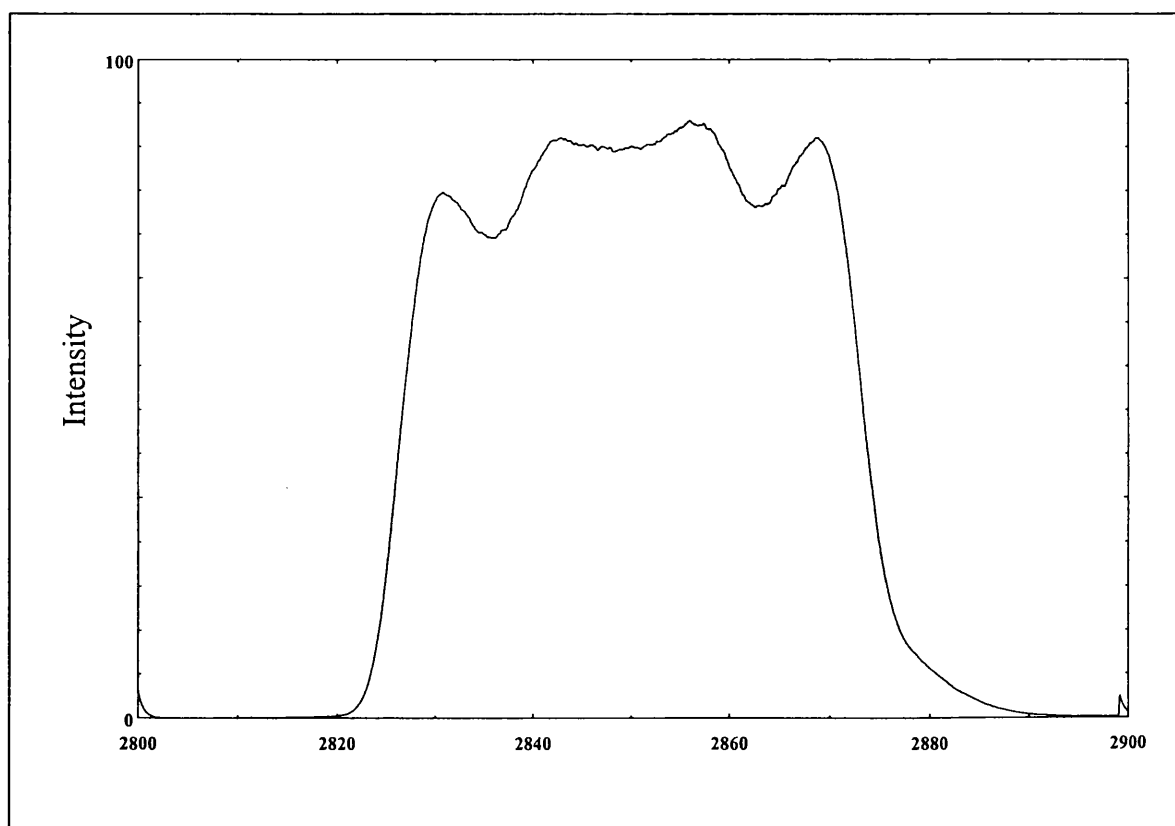


Figure 4.19: Metastable reaction of $C_3H_5^+ \rightarrow C_3H_3^+$ in Propene occurring in FFR3

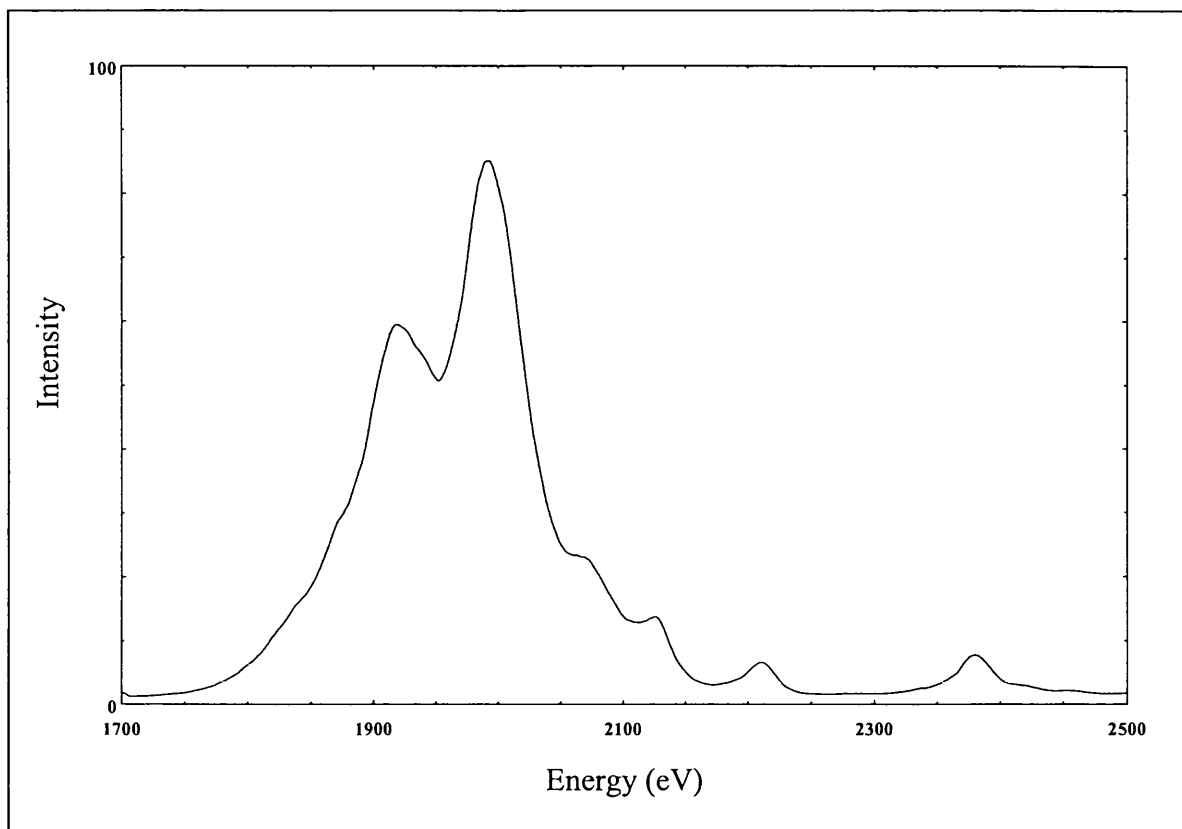


Figure 4.20: Partial CID/MIKE spectrum of $C_3H_3^+$ in Benzene

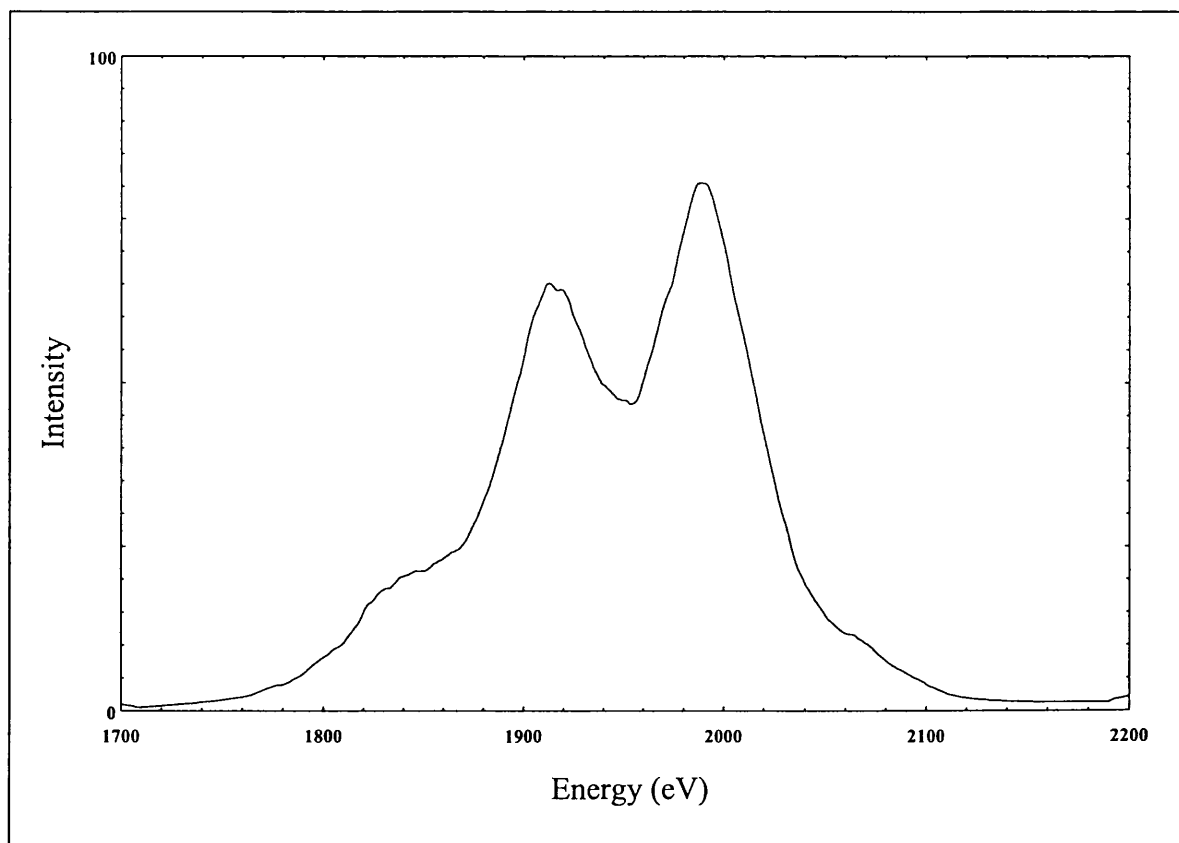


Figure 4.21: Partial CID/MIKE spectrum of $C_3H_3^+$ in Phenylacetylene

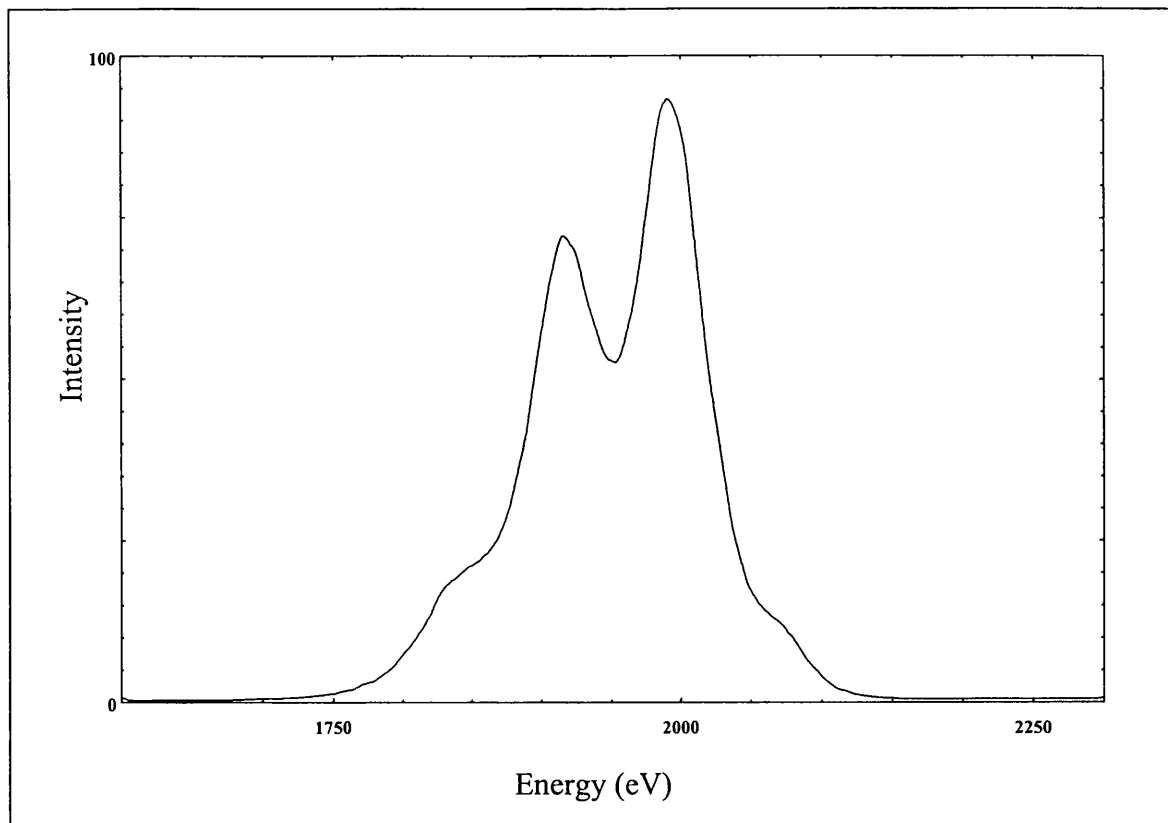


Figure 4.22: Partial CID/MIKE spectrum of $C_3H_3^+$ in Thiophene

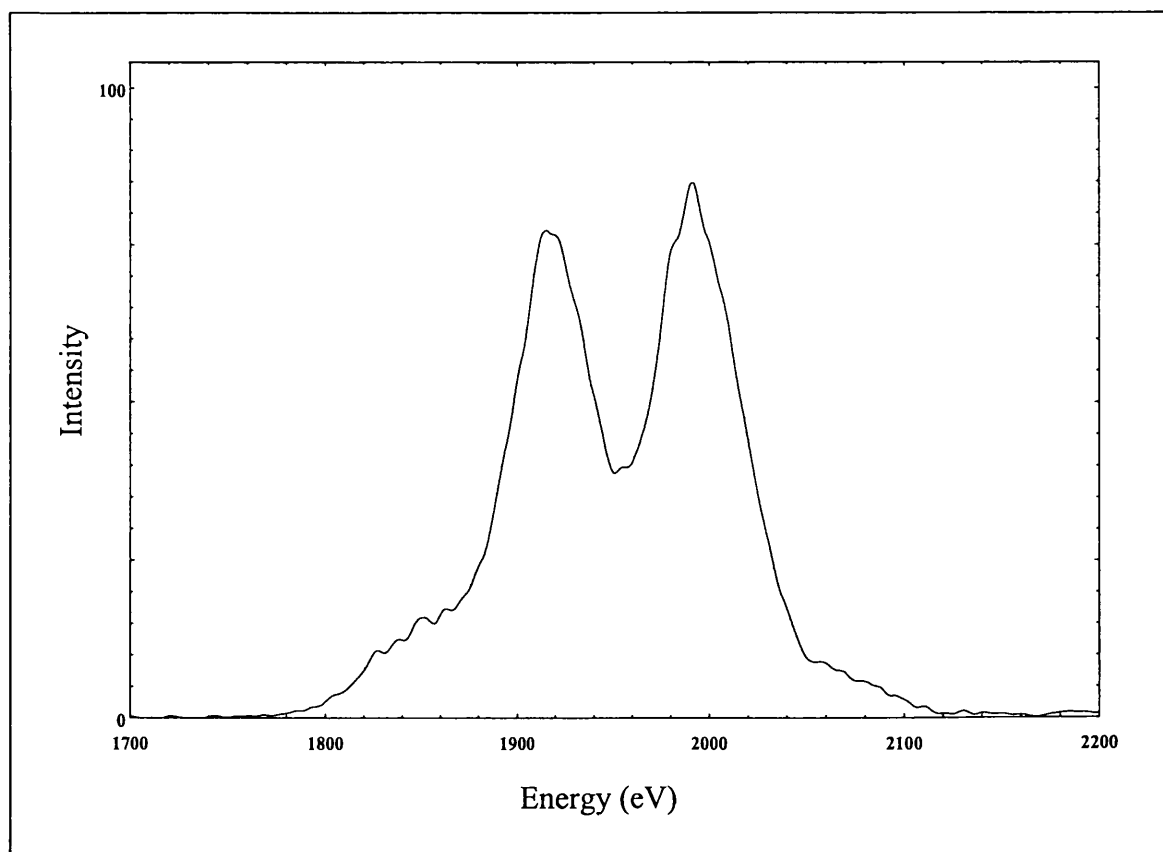


Figure 4.23: Partial CID/MIKE spectrum of $C_3H_3^+$ in Acetophenone

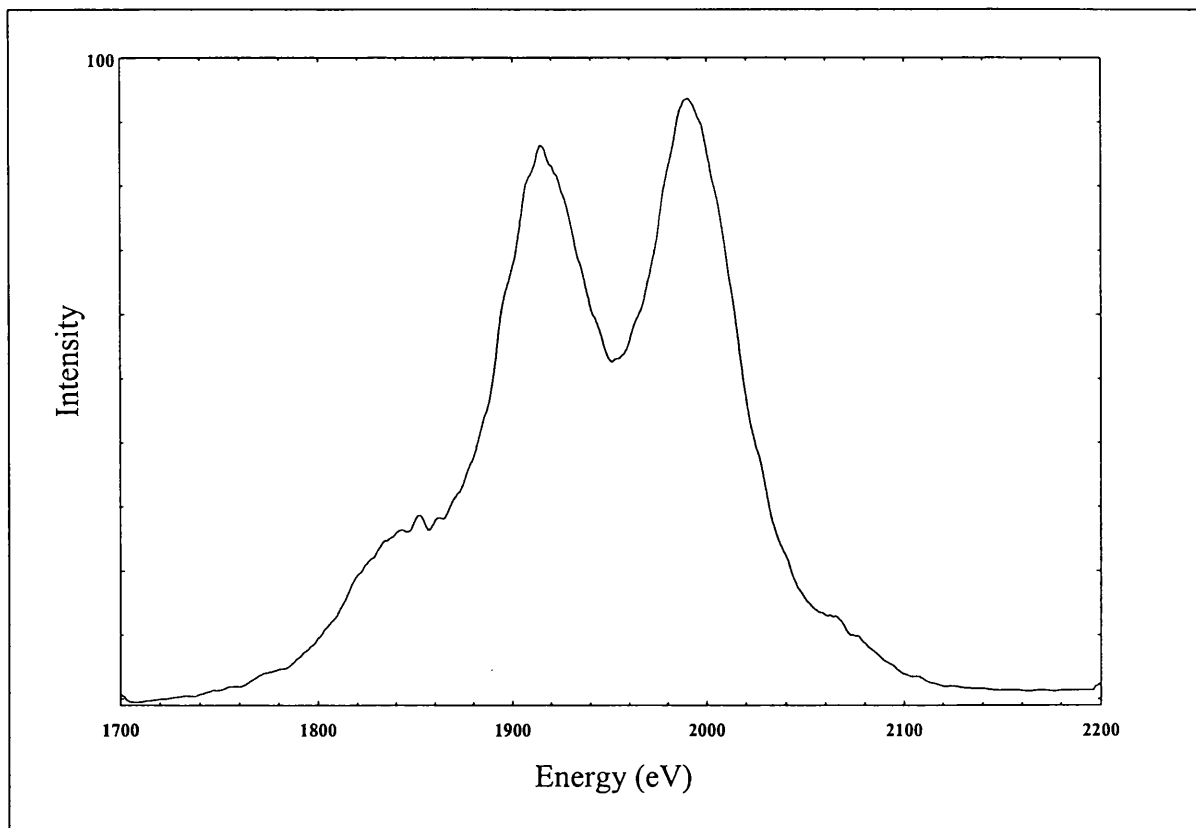


Figure 4.24: Partial CID/MIKE spectrum of $C_3H_3^+$ in 2,4-Hexadiyne

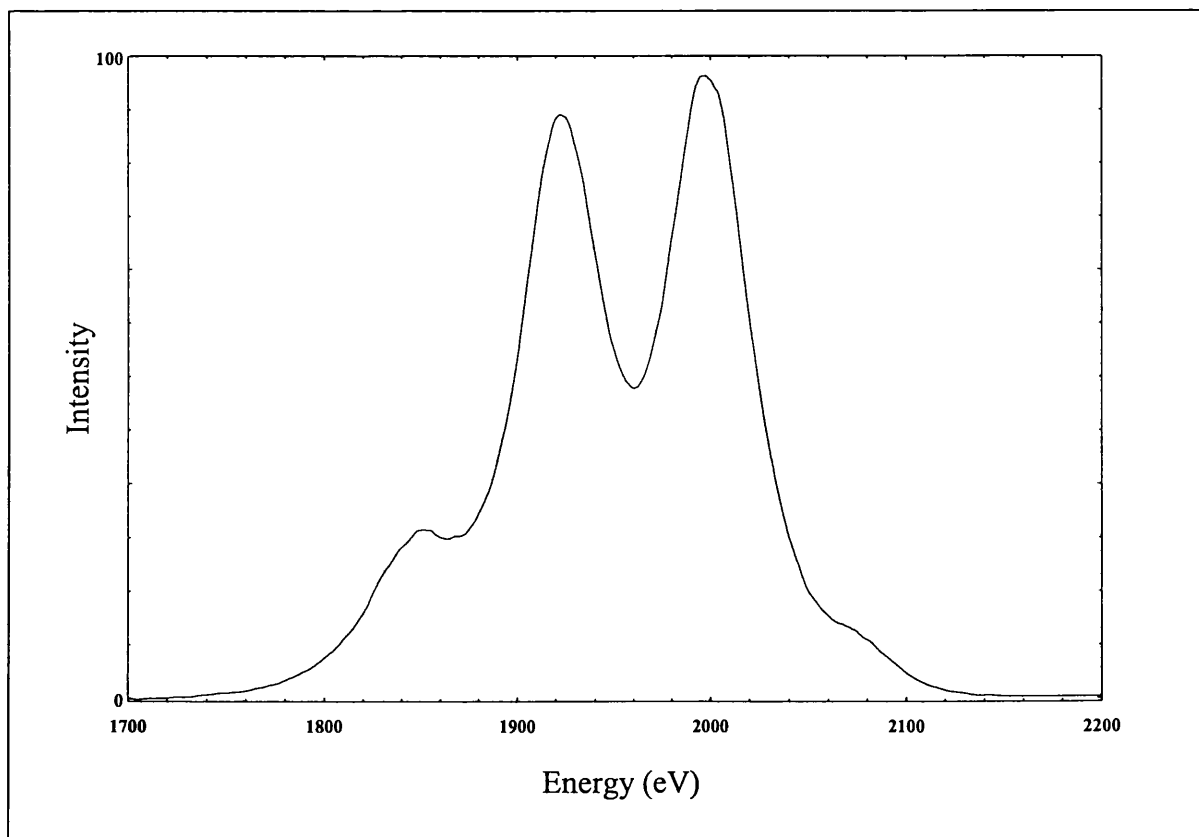


Figure 4.25: Partial CID/MIKE spectrum of $C_3H_3^+$ in Propene

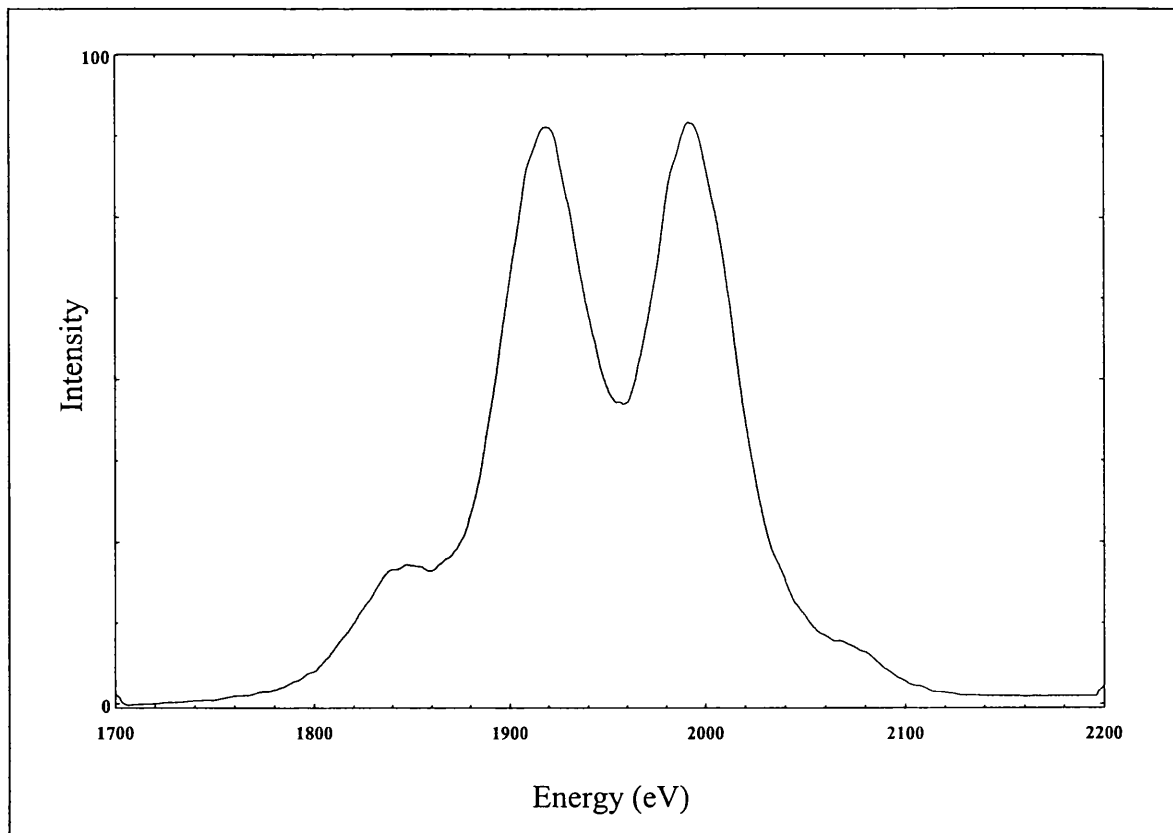


Figure 4.26: Partial CID/MIKE spectrum of $C_3H_3^+$ in Butylbenzene

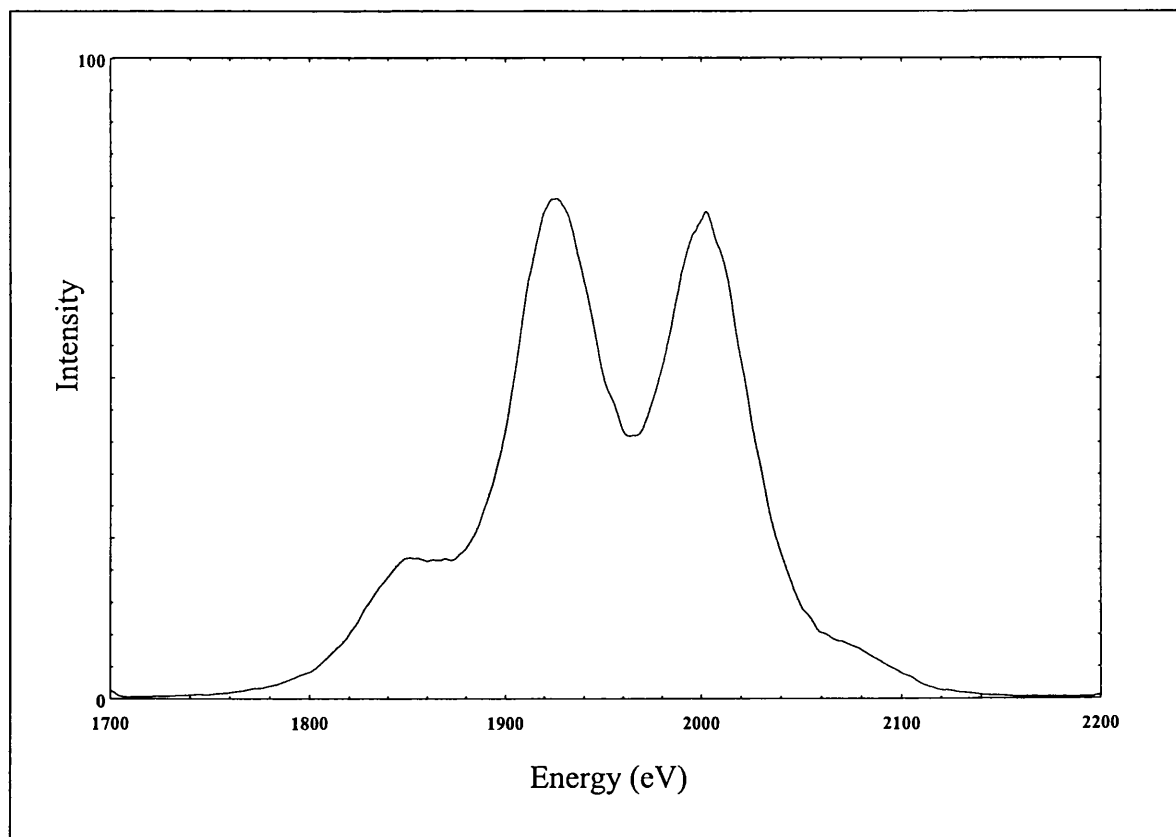


Figure 4.27: Partial CID/MIKE spectrum of $C_3H_3^+$ in n-Hexane

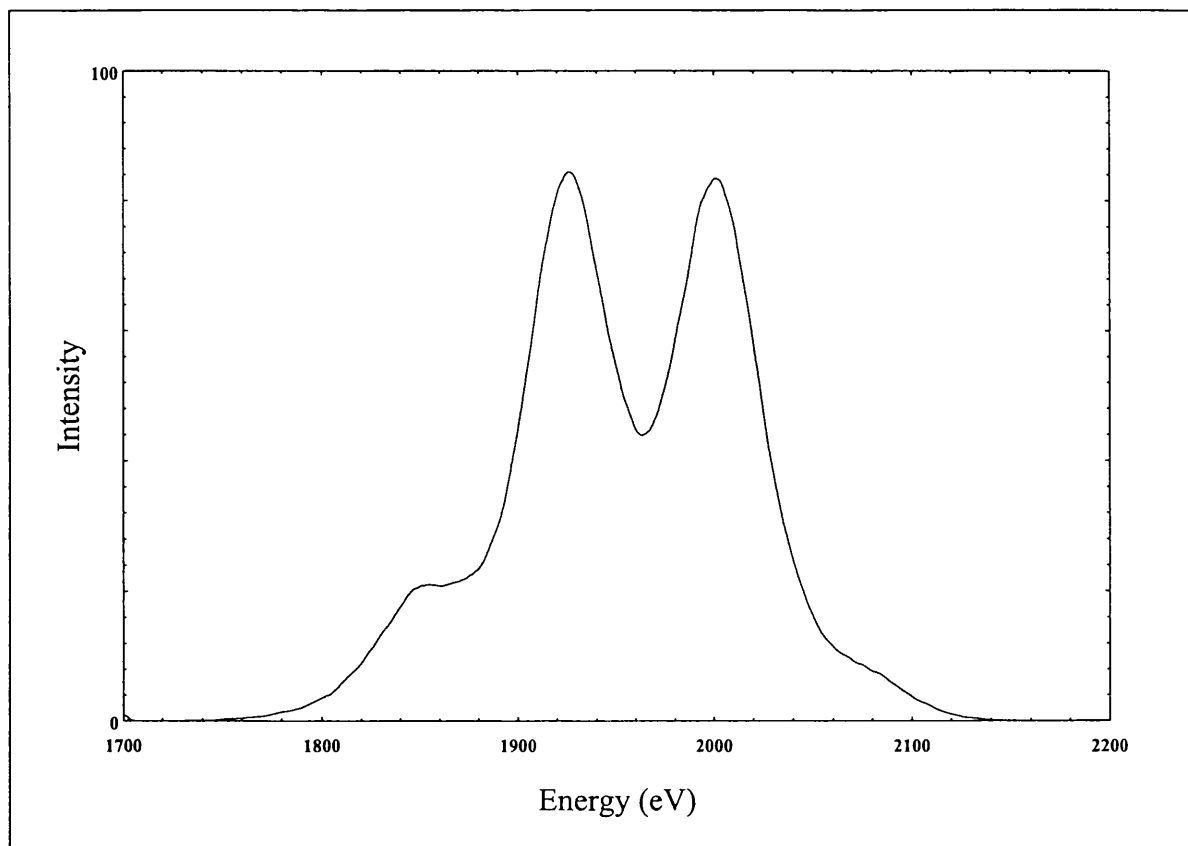


Figure 4.28: Partial CID/MIKE spectrum of $C_3H_3^+$ in Toluene

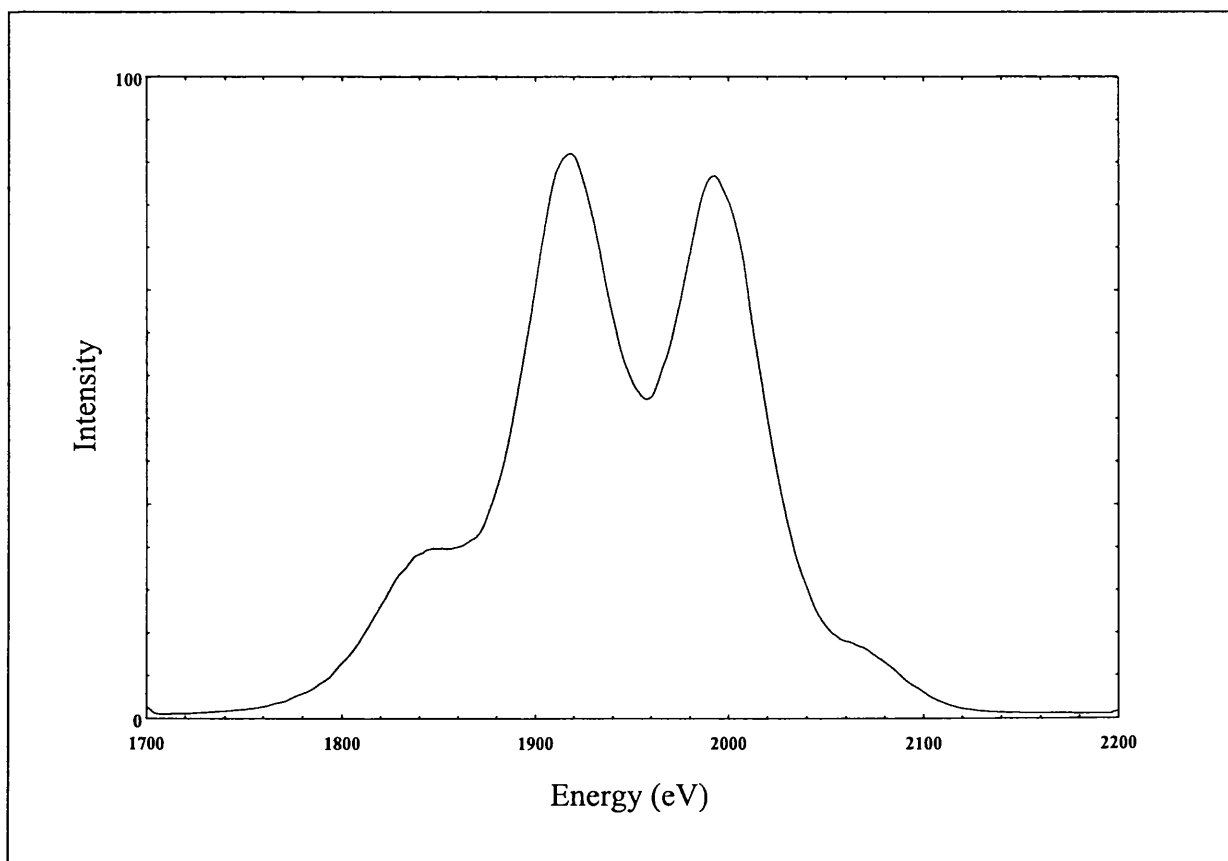


Figure 4.29: Partial CID/MIKE spectrum of $C_3H_3^+$ in Propargyl alcohol

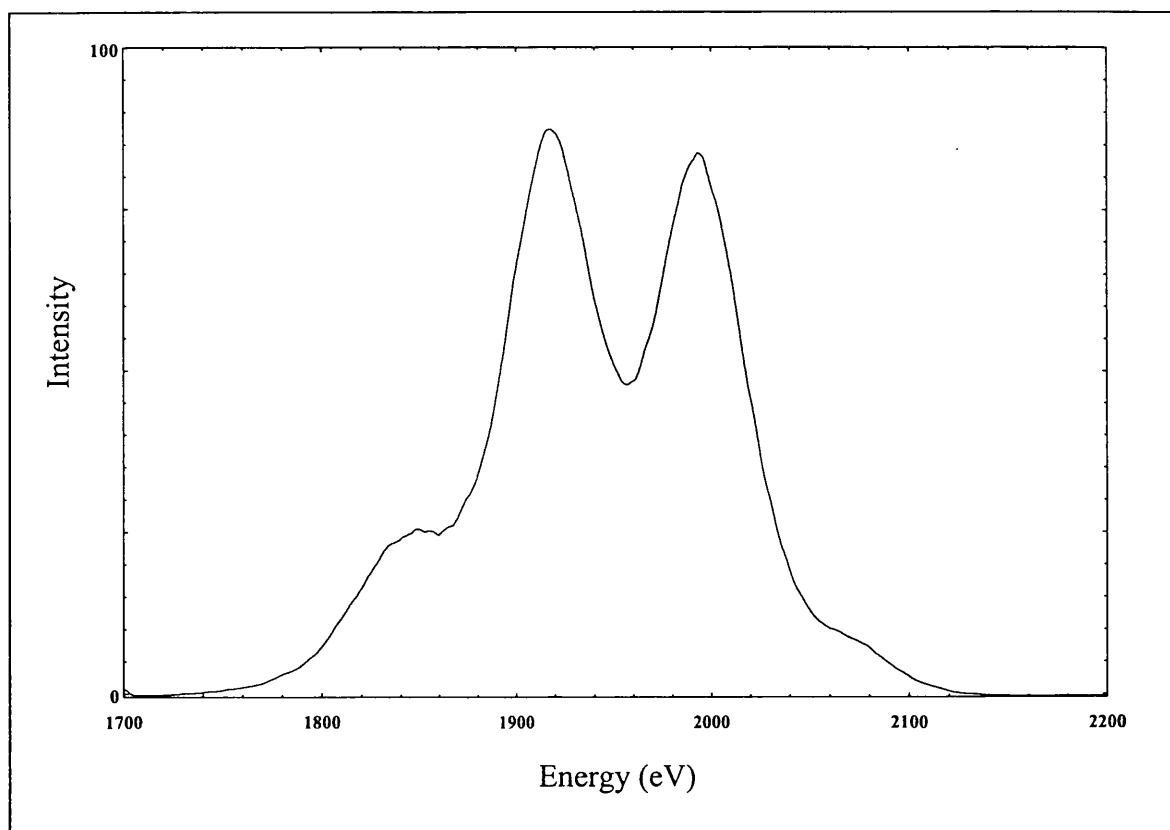


Figure 4.30: Partial CID/MIKE spectrum of $C_3H_3^+$ in 1,5-Hexadiyne